ELECTRIC FIELD MILL

for the
Simultaneous Measurement of Electric Field Strength and Ion Current Density

Department of Electrical Engineering
University of Cape Town

Student Name: Malcolm Sellars

Student Number: SLLMAL001

Supervisor: Mr. J.H. van Nierop

Thesis prepared in partial fulfilment of the requirements for the Degree of MSc. in Electrical Engineering.

Declaration

This thesis is being submitted for the degree of Master of Science in the Department of Electrical Engineering at the University of Cape Town. It has not been submitted before for any degree or examination at this or any other university. The author confirms that it is his own unaided work.

A talk on this thesis was presented by the author at the 35th Annual SAAPMB (South African Association of Physicists in Medicine and Biology) Congress. This Congress was held at Groote Schuur Hospital, Cape Town, from the 9th to the 12th of May, 1995.

Malcolm Sellars

21 September 1995

Acknowledgements

Many thanks are due to the following:

- The Beit Trust (Harare, Zimbabwe), for sponsorship to study for my MSc. at the University of Cape Town.
- Mr. Johan van Nierop (my supervisor), for guidance, encouragement and support.
- Mr. Horst Emrich (Mechanical Engineering, UCT), for precision machine-work on the electric field mill.
- Dr. C. Beardwood (Dept. of Physiology, UCT Medical School), for advice and laboratory time.
- Mr. Tony Britten (ESKOM), for helpful discussions and information.
- Mr. George Tattersfield (UCT).
- Mr. Steven Schrire (UCT).
- Mr. Albert Martin (UCT).
- Mr. Ian de Vries (UCT).
- Mr. Ian Sellars (UCT).

André, Ilona, Ross and Garrick

Terms of Reference

This thesis was put forward by Mr. J.H. van Nierop, Dept. of Electrical Engineering, University of Cape Town. This thesis was set as an MSc. half-thesis in electrical engineering, requiring 6 months of postgraduate work.

Date of Commencement: 1 February 1994

Date due: 30 September 1995

Specific Instructions:

1. Design, construct and test an electric field mill for the simultaneous measurement of electric field strength and ion current density. The required resolutions are:

   Electric field strength of 100V/m
   Ion current density of 100nA/m^2

2. Clearly describe the operating principles of the electric field mill, and the various design considerations.

Synopsis

In the last 20 years, the use of high voltage direct current (HVDC) power transmission has grown considerably. With the increase in the number of HVDC transmission lines and in the transmission voltages, concern has increased as to possible health effects. For research on these health effects to be carried out, it is necessary to measure the electrical environment of HVDC transmission lines accurately.

The electrical environment of HVDC transmission lines is characterised by:

Electric field strength	**E**	[V/m]
Ion current density	**J**	[A/m^2]
Space charge density	ρ	[C/m^3]

Typical values measured under HVDC transmission lines are: **E** = 10kV/m, **J** = 400nA/m^2.

This thesis describes the design, construction and testing of an electric field mill capable of measuring electric field strength from 0 to 25kV/m (resolution = 10V/m), and ion current density from 0 to 1000 nA/m^2 (resolution = 20nA/m^2). The electric field readings have an accuracy of +/-8%. The ion current density readings have an accuracy of +/-12%.

The field mill was tested in the laboratory in a simulated HVDC environment, and found to give good performance. For operation under a HVDC line, the field mill design will need some alterations to make it weatherproof.

The design considerations described in this thesis should be helpful in the design of electric field mills in general.

Table of Contents

List of Illustrations

List of Tables

Glossary

AC	Alternating current. **ac**.
bucking voltage	A d.c. voltage that is applied to either the rotor or stator of the electric field mill in order to "buck" (or null) the spurious electric field signal (which is due to contact potentials).
charged aerosol	Ion comprised of charged particles, solid or liquid, suspended in air.
conduction current	The component of the ion current density caused by the motion of ions in the applied electric field.
contact potential	The d.c. voltage between the stator and rotor surfaces caused by junctions of dissimilar metals in the rotor-stator circuit, and due to different electron work functions between the rotor and stator surfaces. Also known as **Volta Potential**.
convection current	The component of the ion current density caused by the transport of ions and charged aerosols by the wind.
corona	A luminous discharge due to ionisation of the air surrounding an electrode caused by a voltage gradient exceeding a certain critical value.
DC	Direct current. **dc**.
displacement current	The component of the ion current density that is caused by the movement of electric charges above the surface of the field mill stator (or Wilson Plate).
electric field mill	A device in which a conductor is alternately exposed to the electric field to be measured, and then shielded from it. Also known as a **generating voltmeter**.
electric field strength	The electric field produced by dc power lines and space charge. Units [V/m].
electrometer	Very sensitive amplifier, capable of measuring low-level currents in the nA range and below. Electrometers are characterised by very high input impedance.
electrometer op-amp	Operational amplifier optimised for measuring very low currents.
electrometer resistor	Very high value resistor (above 1000MΩ).
electrostatic field	Electric field in which all electric charges are confined to conductor surfaces. No ions are present.
ground plane	Large flat conducting surface at ground potential.
HVDC	High voltage direct current.
HVDC transmission line	High voltage direct current power transmission line.
IC	Integrated circuit.
ion	The isolated atom, molecule or molecular cluster that by loss or gain of one or more electrons has acquired a net electric charge.
ion current density	A vector quantity describing the magnitude and direction of charge flow per unit area. Units [A/m^2]

ion mobility	The speed attained by an ion in a unit electric field.
ionised electric field	Electric field having some electric charges not confined to the conductors. Ions are present in the electric field.
PCB	Printed circuit board.
Phase sensitive detector	The phase sensitive detector uses a reference signal which is in-phase with the sensed signal to demodulate the sensed signal. The output is a d.c. voltage proportional to the magnitude of the sensed signal.
P.S.D.	Phase sensitive detector.
quadrature	90° out-of-phase.
rms	Root-mean-square.
ROW	Right-of -way.
space charge density	The space charge per unit volume. Units [C/m^3].
spurious electric field signal	The electric field signal that is measured at the output of the electric field mill under zero electric field conditions.
synchronous detector	Phase sensitive detector.
Wilson Plate	A conducting plate that is grounded through an ammeter. It is used to collect the ion current, which is measured as it flows through the ammeter. The plate is sensitive to both ion current density and to changes in electric field (displacement current).

1. Introduction

In the last 20 years, advances in solid-state electronics have enabled power transmission using HVDC (high voltage direct current) transmission lines to increase dramatically. Extensive research is being carried out in Canada, the U.S.A., and other countries, on all aspects related to the design of HVDC transmission lines. One area of research is the development of instruments for measuring the electrical environment of HVDC lines [1]. Some of the reasons for measuring the electrical environment of HVDC transmission lines are given below:

Health effects of HVDC lines

For some time, there has been public concern regarding the possible health effects of HVDC transmission lines. Concern over possible health effects includes headaches, respiratory problems and fatigue experienced by people living or working near HVDC transmission lines [2]. In order to conduct research on these health effects, experimental subjects are exposed to the electric fields and ion currents under HVDC lines for a period of time, and then examined for possible effects. The subjects might be linemen working on high voltage equipment, cattle grazing under HVDC lines, or small animals in indoor test apparatus. In these experiments, it is essential to be able to measure accurately the electric fields and ion currents to which the subject is exposed [1].

Electric shocks experienced under HVDC lines

People and animals under an HVDC line often experience mild electric shocks, due to the presence of ions in the air. Measurement of the electrical environment of the HVDC line will enable guidelines for maximum safe electric fields and ion currents to be determined [3].

Safety checking of de-energised HVDC lines

It is necessary to use a non-contact method to check that the HVDC line is de-energised before starting repair work on the line. This involves measuring the electric field strength under the line [3].

The HVDC transmission line from Cahora-Bassa (Mozambique) to Johannesburg (South Africa) is due to be re-commissioned in 1997. Previous operating experience of the Cahora-Bassa line has shown that ESKOM needs a reliable instrument to measure electric field strength and ion current density under the line [3].

This thesis describes the design, construction and testing of an electric field mill capable of measuring the electric field strength and ion current density at ground level under HVDC transmission lines. The theory and design considerations of the electric field mill are discussed in detail.

References

[1] Maruvada, P.S. Dallaire, R.D. Pedneault, R.
"Development of field-mill instruments for ground-level and above-ground electric field measurement under HVDC transmission lines"
IEEE Trans. Power Apparatus & Systems
Vol. 102 March 1983 pg. 738 - 744

[2] Banks, R. Williams, A.
"The Public Health Implications of HVDC Transmission Lines"
IEEE Trans. Power Apparatus & Systems
Vol.102 August 1983 pg.2640-2648

[3] Britten, A.C. (ESKOM)
Private communication to M.Sellars, 1995

2. DC Power Transmission Lines

2.1 Introduction

High voltage DC for the purposes of bulk power transmission is becoming a serious competitor to conventional high voltage AC transmission [1]. Sending power from one place to another by a transmission line, regardless of voltage, is cheaper and more efficient using DC rather than AC (neglecting the costs of terminating equipment). The obstacle to the use of DC has always been the technical difficulties involved in transforming the power from high voltage AC to high voltage DC, and back again, conveniently and economically [2]. Until recently this has prevented high voltage DC from being widely-used for power transmission.

As early as 1881, Marcel Deprez published the first theoretical examination of high voltage DC power transmission. In 1882 he transmitted 1.5 kW of power at 2 kV over a distance of 35 miles. The Swiss engineer, R.Thury, continued this work from 1889 onwards. He installed a high voltage DC line carrying 20 MW of power at 125 kV over a distance of 230 km between Moutiers and Lyon in France [3]. In 1926 a 17 mile HVDC transmission line was installed between Mechanicville and Schenectady in New York, transmitting 5.25 MW at 30 kV.

2.1.1 Mercury-arc valve technology

Among the various switching techniques used in the early DC transmission systems, mercury-arc rectification was found to be most suitable for handling large currents. In 1939, Dr. Uno Lamm in Sweden invented a system of grading electrodes, an important development in mercury valve technology. (Dr. Lamm is regarded as the father of HVDC power transmission). This paved the way for the first commercial application of high voltage DC technology in Sweden in 1954: a 20 MW, 100 kV, 100 km submarine link between Sweden and the Island of Gotland.

The following table lists major high voltage DC transmission schemes which used the mercury-arc valve technology:

Table 2.1 Major HVDC schemes using mercury-arc valves

HVDC Scheme	Year	Countries	Power	Voltage	Distance
Sweden - Gotland	1954	Sweden	20 MW	100 kV	96 km
English Channel	1961	England France	160 MW	+/- 100 kV	64 km
Volgograd - Donbass	1962	Russia	720 MW	+/- 400 kV	470 km
New Zealand North-South	1965	New Zealand	600 MW	+/- 250 kV	610 km
Konti-Skan	1965	Sweden Denmark	250 MW	250 kV	87 km
Sardinia-Italy	1967	Italy	200 MW	200 kV	121 km
Pacific Intertie	1970	U.S.A.	1440 MW	+/- 400 kV	1372 km
Nelson River I	1973	Canada	1620 MW	+/- 450 kV	895 km
Kingsnorth Scheme	1974	England	640 MW	+/- 266 kV	84 km

Although mercury-arc valves were used successfully, they suffered from arc-backs and voltage limitations. Also, the mercury-arc valves were bulky, had high losses, and required considerable maintenance.

2.1.2 Thyristor technology

The invention of the thyristor , or silicon controlled rectifier (SCR) in the late 1950's had a dramatic effect on static converter technology. The thyristor overcame the voltage limitations and arc-back problems of the mercury-arc valve. Thyristors are not only cheaper to manufacture than the mercury-arc valves per se, but they also reduce costs of the power station overall. Even before the commissioning of the last schemes to use mercury-arc valves in the 1970's, experience gained with thyristors was sufficient to discourage any further development of the mercury-arc valve technology [3].

The following table lists major high voltage DC transmission schemes that use thyristor technology:

Table 2.2 Major HVDC schemes using thyristor technology

HVDC Scheme	Year	Countries	Power	Voltage	Distance
Skagerrak	1976	Norway Denmark	500 MW	+/- 250 kV	240 km
Cahora-Bassa	1977	Mozambique South Africa	1920 MW	+/- 533 kV	1414 km
Square Butte	1977	U.S.A.	500 MW	+/- 250 kV	750 km
Nelson River II	1978	Canada	1800 MW	+/- 500 kV	937 km
Coal Creek	1979	U.S.A.	1000 MW	+/- 400 kV	701 km
Inga-Shaba	1981	Zaire	560 MW	+/- 500 kV	1700 km
Itaipu	1983	Brazil Paraguay	788 MW	+/- 600 kV	850 km
Ekibastuz Centre	1985	Russia	6000 MW	+/- 750 kV	2414 km
English Channel	1985	England France	2000 MW	+/- 270 kV	64 km
Intermountain Power Project	1986	U.S.A.	1600 MW	+/- 500 kV	787 km
New England - Hydro-Quebec I	1986	Canada	690 MW	+/- 450 kV	170 km
Fenno - Skan	1994	Sweden Finland	500 MW	400 kV	233 km

DC transmission grew slowly at first. In 16 years, only 6000 MW of DC systems were installed using mercury-arc valves. By 1980, 12 000 MW of high voltage DC transmision shemes had been installed, divided equally between mercury-arc and thyristor technology. By 1992, over 50 000 MW of high voltage DC transmission schemes were installed [3].

2.2 Why use high voltage DC transmission?

2.2.1 Economic considerations

It can be shown that for lines designed with the same insulation level, a DC line can carry as much power with 2 conductors as an AC line with 3 conductors of the same diameter [4]. (This assumes that insulator characteristics are the same for AC and DC, and depends on the peak level of voltage applied with respect to ground). DC transmission requires just one conductor if earth is acceptable as the return path (monopolar transmission). Otherwise it requires two conductors for bipolar transmission. With AC, three conductors are required for a single three-phase circuit, and six conductors for double three-phase. Furthermore, power flow on an AC line is not only the real (active) power, but includes a considerable amount of reactive power. This means that full conductor capacity cannot be used for active power. This implies that for a given power level, the DC line requires less Right of Way (ROW), simpler and cheaper towers, and has lower conductor and insulator costs. ***It can be said with confidence that at any power level or transmission distance, using cable or overhead lines, DC is cheaper than AC, line for line [2].*** However, DC lines have higher terminal equipment costs relative to AC.

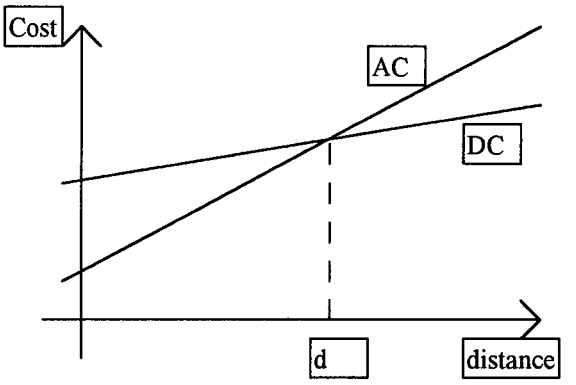

Fig.2.1 Relative costs of AC and DC transmission

The diagram above shows that for distances greater than the 'break-even" distance d, the cost of a DC line is lower than that of an AC line. The 'break-even" distance d varies from 500 km to 800 km depending on the per-unit line costs [4]. A more thorough treatment of economic trade-offs is given in Chapter 9 of [3].

The typical capacities of AC and DC circuits are compared in the table below. It can be seen that one +/-500kV DC line has about the same capacity as one 765kV AC line, or two 500kV AC lines [17].

Table 2.3. Typical capacities of AC and DC lines

AC		DC	
Voltage (kV)	Power (MW)	Voltage (kV)	Power (MW)
230	150	+/- 250	500
345	400	+/- 400	1000
500	1000	+/- 500	2000
765	2500	+/- 600	3000

The diagram below shows typical self-supporting lattice-type transmission line structures for:

(a) One +/-500kV DC line.
(b) One 765kV AC line.
(c) Two 500kV AC lines.

Each of these would have a power-carrying capacity of about 2000 MW.

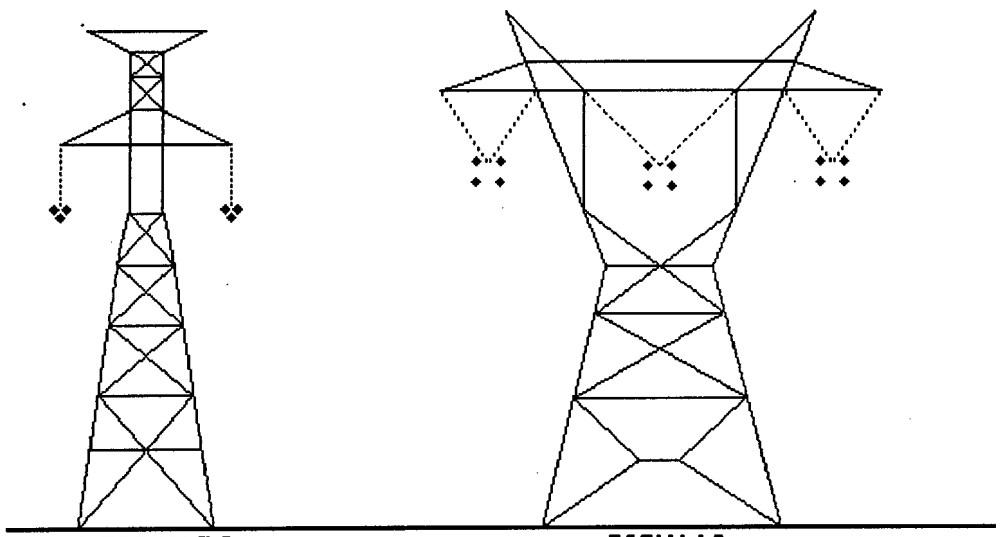

(a) Bipolar HVDC line

(b) Single high-voltage AC line

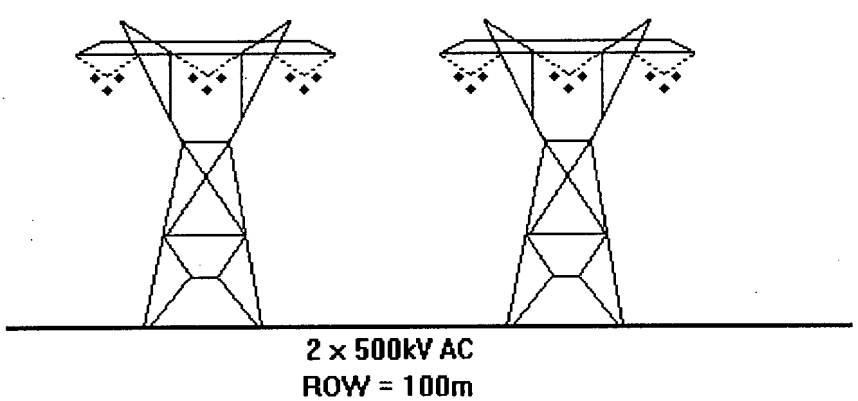

(c) Double high-voltage AC line

Fig. 2.2 Typical DC and AC transmission line structures each carrying 2000 MW

(ROW means Right of Way).

2.2.2. Stability considerations

The power transfer in AC lines is dependent on the angle difference between voltage phasors at the two ends of the line. For a given power level, this angle increases with distance. Maximum power transfer is limited by both steady state and transient stability. The power-carrying capability of DC lines is unaffected by distance.

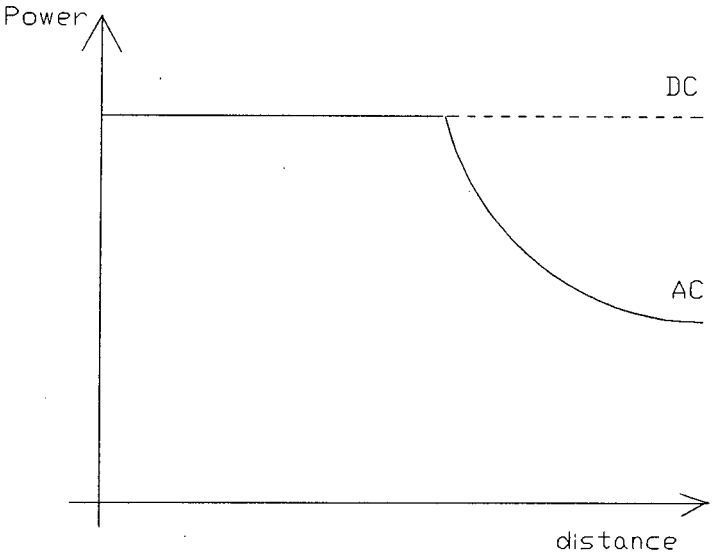

Fig.2.3 Relative power-carrying capability of AC and DC lines

The diagram above shows the reduced power-carrying capability of an AC line above a certain critical distance. The DC line's power-carrying capability is unaffected by distance [4]. A more thorough treatment of stability considerations is given in chapter 9 of [3]. For very long transmission distances, DC lines may be the only viable option, since an AC line would have stability problems. An example is the DC line from Cahora-Bassa (Mozambique) to Johannesburg (South Africa), which is 1414 km long.

2.2.3. Power system interconnections

Two AC power systems may have different frequencies, different frequency controls, or stability problems so that it is not feasible to connect them with an AC line. With DC lines, any level of power can be transmitted asynchronously between the networks. For example, at the Itaipu hydroelectric plant in South America, most of the electricity generated at 50Hz on the Paraguayan side of the plant is transmitted via a 600kV DC link to Sao Paulo in Brazil for use in the Brazilian 60Hz network. In Canada, Hydro-Quebec uses hydropower to generate electricity, which is sent to New England. Connecting the New England and Hydro-Quebec networks with AC ties would have been very difficult since power generated at the hydroplant varies more in frequency than the power generated by steam-fired plants in New England [15].

2.2.4. AC to DC line conversion

Upgrading of existing transmission lines is often the preferred means of providing increased bulk transmission capacity. An alternative to upgrading the capacity of an AC transmission line (using compensation) may be to convert the AC line to DC. Significantly increased transmission line capacity may be achieved by converting existing AC lines to DC. Larger capacity increases, and lower losses may make line conversion to DC economically advantageous compared to upgrading the AC line [17].

2.3 Environmental considerations

The possible environmental effects due to electric fields and space charges (particularly at ground level) are matters of concern, and have to be considered in transmission planning. There are some basic differences in the environmental effects of AC and DC lines:

2.3.1 AC lines

Electric induction effects on people and objects located near the lines are mainly due to capacitive coupling. The alternating electric and magnetic fields induce currents in any conducting object (including people and animals) exposed to these fields. In addition, AC electric fields cause alternating surface charges to appear on a conducting object. Corona-generated space charge oscillates in a small region around the conductors, and so has negligible influence on the induction effects at ground level. Relatively few ions escape from AC transmission lines since ions repelled from the line during the positive half-cycle are attracted back to the line during the negative half-cycle [14].

2.3.2 DC lines

Since the transmission line voltage does not vary with time, capacitive effects are almost non-existent. Induction effects are due to charged ions produced by corona on the conductors. Corona-generated space charge fills the entire space between the transmission line conductors and ground, so creating an ionised electric field. (The term "ionised electric field" is used to describe an electric field that is not purely electrostatic, but rather has electrical charges present). DC electric fields induce charges on the surface of a conducting body (such as a human being) and may therefore be "perceived" by humans as hair stimulation, and sensations felt on the skin. A human being exposed to the DC ionised field experiences both surface charges and conducted ion currents [1].

Note: in this thesis, the HVDC transmission lines considered are all above-ground lines. HVDC underground and submarine cables are not considered.

2.4 Electrical environment of HVDC transmission lines

The electrical environment of HVDC transmission lines is determined by 3 types of electrical charge :

1. Charges on the line conductors
2. Air ions
3. Charged aerosols (solid or liquid particles in the air which are electrically charged)

The combined effect of these charges is quantifiable in terms of:

1.	Electric field	**E**	[V/m]
2.	Ion current density	**J**	[A/m^2]
3.	Space charge density	ρ	[C/m^3]

2.4.1 Electric Field

The electric field has two components:

1. Electrostatic field due to charges on or near the conductor surface
2. Space charge field due to ions produced by corona on the lines

The "total electric field" is the superposition of the electrostatic and space charge fields. This "total electric field" is a DC ionised field.

The unperturbed electric field at ground level is the field which exists in the absence of any perturbing object (such as a person). The presence of an object perturbs the magnitude and direction of the electric field.

2.4.2 Ion current density

The ion current density is defined as the current collected by a flat metal plate of area 1m^2 mounted flush with the ground (see Section 4.1). The ion current density near HVDC lines has 3 components:

1. Displacement current
2. Conduction current
3. Convection current

The displacement current is caused by varying electric fields. Although the electrostatic field under a DC line should be constant, the electric field due to space charge may change as the ions drift with the wind. Thus a random displacement current may be produced.

The conduction current is caused by the motion of ions in the electric field.

The convection current is caused by the transport of ions and charged aerosols by the wind.

2.5 Corona and ionised field of the DC transmission line

Corona is defined as the " luminous discharge due to ionisation of air surrounding a conductor caused by a voltage gradient exceeding a certain value" [4]. The ionisation takes place in a zone which is a thin circumferential layer (not more than 2 cm thick) surrounding the conductor surface. Within this zone, the electric field strength exceeds the dielectric strength of the air. The high field strength causes high velocity particles to collide with the air molecules. Electrons are removed from the atoms of the air molecules and accelerated towards the positive conductor, or away from the negative conductor. These high velocity electrons collide with other air molecules, releasing additional electrons in an avalanche process, and so create ions of both polarities. Ions carrying opposite charge to that of the conductor are drawn towards that conductor, and neutralised on contact. Ions carrying the same charge as the adjacent conductor are repelled from the ionisation zone at initial velocities of :

$$\left.\begin{array}{ll} v \approx 1.4x10^{-4} m/s & \text{(positive ions)} \\ v \approx 1.6x10^{-4} m/s & \text{(negative ions)} \end{array}\right\} \text{per V / m of field strength}$$

Thus a positive conductor in corona acts as a source of positive ions, and a negative conductor as a source of negative ions. Charges can also be generated from corona on objects on the ground (such as at the pointed tips of trees, bushes or grass) if the electric field strength is sufficiently high [18].

Corona should not occur on ideal, smooth, clean conductors at the voltages used on HVDC lines. However, it is not economically feasible to design HVDC lines with conductors of sufficiently large diameter that minor surface defects and adhering foreign particles will not result in measurable corona generation [7]. Corona sources include water droplets, snow particles, ice and dirt. In the U.S.A., it has been found that dead insects deposited on the line are a major source of corona. Insect deposition occurs for conductor potential gradients above 1MV/m [18]. Due to these corona sources, HVDC transmission lines generally operate continuously above corona onset voltage [8].

2.5.1 Unipolar transmission line

For a unipolar positive or negative DC transmission line in corona, ionic space charge with the same polarity as the line fills the entire inter-electrode space between the line conductor and ground. The ions which make up the ionic space charge are subject to drift (characterised by ionic mobility) in the electric field distribution created by the voltage applied to the line.

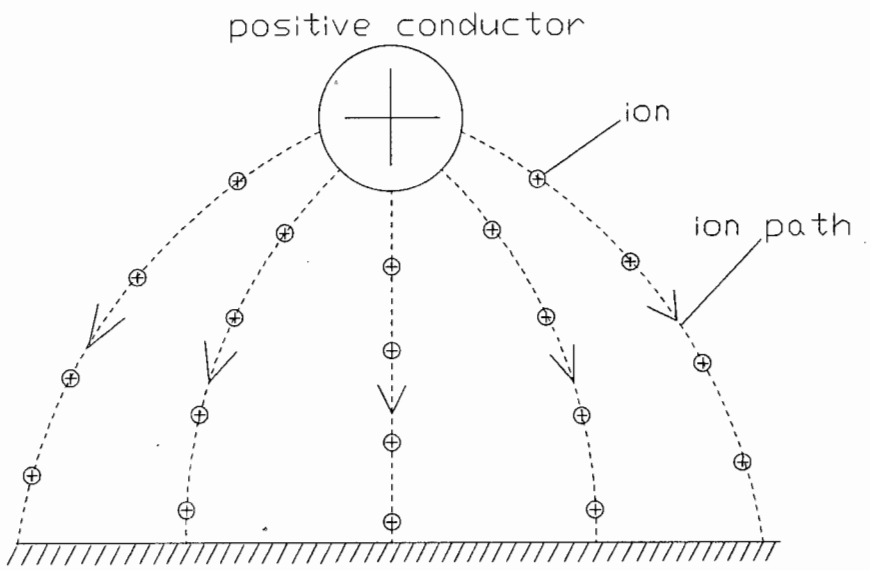

Fig.2.4 Ions drifting to ground from a unipolar DC line

2.5.2 Bipolar transmission line

A bipolar DC transmission line consists of two conductors of opposite polarity. When the line goes into corona, both positive and negative ions are generated by the conductors. The ions generated by each conductor drift either to the conductor of opposite polarity, or to ground. Thus 3 distinct space charge regions exist in the vicinity of a bipolar DC line: one unipolar region between each of the two conductors and ground, and a bipolar region between the two conductors of opposite polarity. In the bipolar region, ions of opposite charges mix, resulting in space charge neutralisation [5].

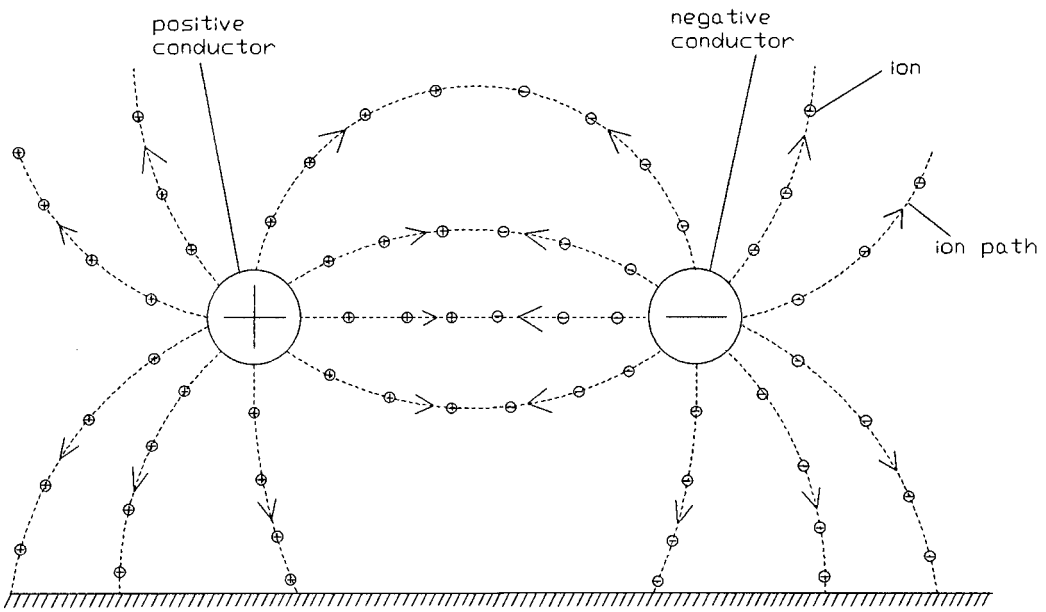

Fig.2.5 Ions drifting to ground and between conductors on a bipolar DC line

2.5.3 Ion characteristics

Ions generated by corona discharge in air are derived from N_2 and O_2 molecules. Mobilities of these ions are:

$$\text{mobility} \approx 1.5 \times 10^{-4} \text{ ms}^{-1} \text{ per Vm}^{-1}$$

(Mobility is the speed that the ion will attain in a unit electric field).

These ions are small air ions and travel at a speed of about 1.5 ms^{-1} in an electric field of 10 kV/m. Whilst near the line, small air ions are moved predominantly by the electric field (rather than by wind) since they have high mobilities. Away from the line, the earth's natural electric field of about 130 V/m has only a slight effect on the small air ions: a force comparable to a wind speed of only 0.02 ms^{-1} . In atmospheric air, these molecular ions may form clusters with water molecules present in the air, giving rise to heavier ions with lower mobilities. Also, aerosols present in the atmosphere may be charged in the ionised fields produced by corona, forming charged aerosols with much lower mobilities than those of smaller ions. Aerosols are solid or liquid particles suspended in the air, (such as smoke, dust and moisture). Charged aerosols have much lower ion mobilities than the small air ions:

$$\text{mobility} \approx 1 \times 10^{-6} \text{ ms}^{-1} \text{ per Vm}^{-1}$$

Charged aerosols are moved predominantly by wind, rather than electric field. (A charged aerosol would travel at a speed of only 0.01 ms^{-1} in an electric field of 10 kV/m. The presence of heavy ions or charged aerosols will influence the characteristics of the DC ionised field [13].

2.5.4 Effect of weather on ions

Corona generated on the conductors, and the resulting ionised fields are greatly influenced by the prevailing atmospheric and weather conditions. Rain or snow increases the corona activity on the conductors, with a corresponding increase in ion current and space charge densities in the vicinity of the line. The increased corona activity is due to the increased number of water-drop corona sources. Mean electric field and ion current density values measured in rain may be 1.5 to 2 times greater than those measured in fair weather [10]. The ambient temperature and pressure, as well as wind direction, also influence corona generation. More importantly, wind speed and direction influence the drift of ions, and thus affect the ionised field distribution, especially if heavy ions or charged aerosols are present. Aerodynamic forces dominate over electrical forces for the larger ions with lower mobilities. Thus, large amounts of space charge may be carried downwind away from the line. Space charge effects have been reported downwind 10 km or more from corona line sources [8]. At very high transmission voltages, (above 1000 kV) the influence of wind on ion drift is reduced, since the electric field is high enough to dominate ion drift. Relative humidity (RH) also affects the corona generation. For values of RH < 70% there is little observed variation of electric field strength **E** and ion current density **J**. For values of RH > 70%, values of **J** increase significantly. It is conjectured that at high values of RH, small objects in the air (particles of dust and vegetation, small insects, etc.) become more conducting, and so more likely to go into corona [10].

2.5.5 Space charge clouds

The ions moving into the inter-electrode region (between pole-pole, or between pole-earth) recombine with oppositely-charged ions or neutral molecules. To maintain the net charge in this region, a corona current flows from the conductor by movement of electrons in the ionisation zone, and by ions beyond this zone. The ion velocities at the ground level are about 3m/s for typical voltage gradients. The ion movement in perfectly still air is restricted to the electric field direction. Due to air motion, localised space charge "clouds" may drift out of the influence of the electrical field. In fair weather, effects of corona-generated space charge may be observed at distances over 100m from the transmission line [8]. With wind movement, the ions are randomly dispersed downwind from the DC line.

2.5.6 Transmission line geometry

DC electric fields and ion currents also depend on the geometry of the transmission line. Both the spacing between conductors (for a bipolar line) and the height above ground influences **E** and **J**. The transmission voltage also plays a part since negative corona current starts to flow at a lower voltage than positive corona current. This causes an asymmetry in ion currents under bipolar lines: measured values of **J** are significantly different underneath the positive and negative conductors [11]. For a particular conductor, the higher the voltage, the higher the electric field at the surface of the conductor, and the more intense is the corona. The smaller the radius of curvature of a conductor, the higher the electric field at the surface for a given voltage. Thus smaller conductors go into corona at lower voltages than larger conductors [14].

2.6 Theoretical modelling of the HVDC transmission line environment

Due to the presence of space charge, theoretical calculations of electric field and ion currents are very difficult. In the conventional methods of describing DC ionised fields, the following simplifying assumptions are made:

1. Ionic mobilities are constant (independent of electric field magnitude)
2. Positive and negative ion mobilities are equal.
3. Diffusion of ions is neglected.
4. The effect of humidity, wind and aerosols is neglected.

With these assumptions there are two ways to proceed with calculations:

a) Unipolar DC ionised fields are described by the following equations:

$$\text{a) } \nabla.\vec{E} = \frac{\rho}{\varepsilon_o} \qquad \text{Poisson's equation}$$

$$\text{b) } \vec{J} = k\rho\vec{E} \qquad \text{interdependence of } \vec{J} \text{ and } \vec{E}$$

$$\text{c) } \nabla.\vec{J} = 0 \qquad \text{continuity equation for ions}$$

k = ion mobility (1.6×10^{-4} m / s per V / m for negative ions)

ρ = charge density (C / m^3)

$\vec{E}$ = electric field (V / m)

$\vec{J}$ = ion current density (A / m^2)

ε_o = electric permittivity (F / m)

The above equations must be solved with appropriate boundary conditions, derived from known potentials applied to the conductors. The computation of ion flow fields is complex as non-linear partial differential equations are involved. Computations are simplified by Deutsch's Assumption which assumes that the space charge affects only the magnitude (and not the direction) of the electric field, so reducing the two-dimensional problem to one-dimension [6].

b) Another approach to estimating the values of electric field and ion currents uses limiting conditions to establish upper and lower bounds on space charge generation [18]. The limiting conditions used are:

1. Electrostatic case: All charges are confined to the transmission line conductors
2. Corona saturated: Conductors are in extreme electrical corona so that they cannot hold any charges on their surface. The space between conductors and ground becomes saturated with ions.

Results for these limiting conditions have been obtained with tests on models of HVDC lines [18]. From knowledge of the limit conditions, the maximum possible variations of electric field and ion current may be predicted. The engineering problem is then reduced to characterising the corona properties of the conductors. Unfortunately, the presence of wind and aerosols limits the application of the "corona saturated" condition to the region in the immediate vicinity of the line. Away from the line, it is necessary to know the wind strength and direction, concentration of aerosols in the air, mechanisms for aerosol charging and transport by wind.

2.7 Effects Experienced by People and Animals near HVDC lines

2.7.1 Electric induction effects

Ions drifting in the inter-electrode space not only cause corona power loss, but are also responsible for electric induction effects on people and animals in the vicinity of the lines [5]. Any object located under a DC line intercepts the ion flow between the conductors and ground. If the object is perfectly insulated from ground, its potential difference with respect to ground will increase until it reaches the equilibrium space potential (or until the insulation breaks down). In practice, the potential to which an object is raised will be limited by its insulation resistance to ground. If a grounded person touches the object, he/she may receive an initial carpet-type shock of extremely short duration, followed by a small steady current. Similar induction effects are also produced when a well-insulated person located under the line touches a grounded object. Electrical induction effects on persons or objects located under DC transmission lines are characterised by:

1. Open circuit induced voltage
2. Short circuit current

The only noticeable effects under a DC line may be due to micro-shocks (similar to carpet shocks) when a reasonably-grounded person touches a large, well-insulated object located under the line. This is due to the open circuit induced voltage [12]. In operating experience with the Cahora-Bassa HVDC line, it is reported that technicians working near the line sometimes experience painful electrical shocks [20].

2.7.2 Currents experienced in a DC ionised field

A well-grounded person under a DC line will also experience a steady small flow of current. This current is due to the flow of ions. Under a HVDC transmission line the ion current density:

$$\vec{J} = k\rho\vec{E}$$

The charge density at ground level:

$$\rho = \varepsilon_0 \nabla . \vec{E} \qquad \varepsilon_0 = \text{electric permittivity}$$

These equations may be used to estimate values for the total current flowing through a person to ground, when he or she is standing under a HVDC line. Electrical induction measurements under DC transmission lines show that under worst conditions the induced currents in a person are of the order of a few microamps, which is several orders of magnitude smaller than perception levels for direct currents [12]. Total current density intercepted by a person at ground level = (current density) x (equivalent area). (Equivalent area is related to height). For a person of height 1.73m the maximum current intercepted is:

$$\text{Current} \approx 3\mu A \text{ under a line operating at } \pm 600 \text{ kV}$$

The threshold levels of perception are [4]:

5.2 mA for men
3.5 mA for women

2.7.3 Health effects of HVDC transmission lines

Electric field strength, ion currents and ion concentrations are significantly higher underneath DC lines than under AC lines of similar power capacity. In particular, air ions are a source of public health concern. Since both electric field and ion densities from HVDC lines may be significantly above ambient levels even at locations several hundred metres from the line, a large number of people are exposed to the effects. Away from the DC line, the space charge consists mainly of aerosols, which researchers believe may penetrate further into the human respiratory tract than small air ions [18].

In the U.S.A. there has been considerable public opposition to the installation of high voltage DC lines, due to fears of the possible health effects on people and animals. The construction of Coal Creek HVDC power line in Minnesota, U.S.A., caused disputes, protests and demonstrations over a four-year period. One of the largest demonstrations, in 1978, drew several thousand protestors from Minnesota and neighbouring states. During the disputes, 15 transmission towers were knocked over, and 7600 insulators shot out by angry farmers [16]. Researchers say that not enough work has been done so far to conclusively identify or disprove any such health effects. Research projects on the biological effects of air ions are described in the book "Air Ions: Physical and Biological Effects" [14]. Some of the possible health effects experienced by people living or working near HVDC transmission lines include [19]:

1. Headaches
2. Respiratory problems
3. Fatigue
4. "Tingling sensations"

In a simulated HVDC transmission line environment, the following biological responses have been recorded in humans [14]:

1. Change in EEG waves (electrical signals of the brain).
2. Change in ECG waves (electrical signals of the heart).
3. Change in serotonin levels in the urine.

2.7.4 Safety Precautions for Transmission Line Maintenance

In servicing high voltage lines, it is normal practice to use a 'liveline", or 'hotline" detector to determine if the line is energized. This is an essential safety precaution for technicians carrying out repairs on HVDC lines. Such instruments are available for use on AC lines, but a prototype instrument for DC lines has only recently been developed [21]. A non-contact measurement of the line voltage is required, and this is accomplished using an electric field mill. Mr. Britten has indicated that ESKOM is particularly interested in the development of such an instrument [20].

2.8 The Need for Physical Measurement of Electric Field and Ion Current Density

The presence of corona-generated space charge makes the electrical environment of HVDC lines complex and dynamic [14]. Calculations of electric field, ion current density and space charge density offer insight into field and ion phenomena, but provide only approximate estimates of their values [8]. The dependence of space charge distribution on wind and meteorological conditions results in time-varying electric fields and ion current densities that can only be adequately characterised by long term physical measurements. Results are best represented statistically, and measurements made in differing weather conditions are usually presented separately [18]. Corona depends not only on conductor voltage, but also on humidity, weather, conductor size and transmission line geometry. Under certain conditions, the load current carried by the transmission conductors has a measurable effect on corona generation due to the variation in temperature of the conductors [9]. Not only do **E** and **J** show temporal variation due to variations in wind, weather, corona, etc., but there is also spatial variation depending on the lateral position underneath the transmission line conductors. All this means that for the electrical environment of high voltage DC transmission lines to be characterised accurately, a means of physically measuring electric field strength **E**, ion current density **J**, and space charge density ρ underneath HVDC transmission lines is needed.

Mr. Tony Britten of ESKOM has expressed interest in the electric field mill developed for this thesis. He has said that ESKOM needs a reliable instrument for the measurement of electric field strength and ion current density underneath the Cahora-Bassa HVDC line. Work was started some years ago by ESKOM on an electric field mill for this purpose, but the project was never completed [20]. Mr. Britten also said that at the present time, ESKOM has a lack of expertise in the instrumentation needed for such measurements.

With the imminent re-commissioning of the Cahora-Bassa HVDC line in 1997, it is considered that research in instrumentation for measuring the electrical environment of HVDC transmission lines is appropriate at this time.

2.8.1 Instrumentation for measuring the electrical environment of HVDC lines

Some of the instruments needed to characterise the electrical environment of HVDC lines are listed in the table below.

Table 2.4 List of instruments used to measure the electrical environment of HVDC lines

Instrument	Quantity
Electric field mill	Electric field
Wilson Plate	Ion current density
Space charge cage	Ion density
Ion mobility chamber	Ion mobility
Optical particle counters	Aerosol size distribution
Wind sensors	Wind speed and direction

2.9 References

[1] Maruvada, P.S. Nguyen, D.H.
"An exposure chamber for studies on human perception of DC fields and ions"
IEEE Trans. Power Delivery
Vol. 9 No. 4 October 1994
pg. 2037 - 2045

[2] Hingorani, N.G.
"DC Power Transmission, High Voltage"
Ency. Physical Science and Technology
Academic Press 1985
pg. 4 - 325

[3] Arrilaga, J.
"High Voltage DC Transmission"
Peter Peregrinus 1983

[4] Padiyar, K.R.
"HVDC Power Transmission Systems"
John Wiley 1991

[5] Maruvada, P.S.
"Corona-generated space charge environment in the vicinity of HVDC transmission lines"
IEEE Trans. Electrical Insulation
Vol. 17 No. 2 April 1982
pg. 125 - 130

[6] Bouziane, A. Waters, R.T.
"Assessment of corona models based on the Deutsch approximation"
J. Phys. D Vol. 27 (1994)
pg. 320 - 329

[7] McKnight, R.H. Kotter, F.R. Misakian, M.
"Measurement of ion current density at ground level in the vicinity of HVDC lines"
IEEE Trans. Power Apparatus & Sys.
Vol. 102 April 1983 pg. 934 - 941

[8] Bracken, T.D. Capon, A.S.
"Ground level electric fields and ion currents on the Celilo-Sylmar +/-400 kV DC Intertie"
IEEE Trans. Power Apparatus & Sys.
Vol. 97 Mar/Apr 1978 pg. 370 - 378

[9] Pedrow, P.D. Qin, B.L. Wang, Q.Y.
"Influence of load current on bipolar DC corona"
IEEE Trans. Power Delivery
Vol. 8 July 1993
pg. 1443 - 1449

[10] Comber, M.G. Johnson, G.B.
"HVDC field and ion effects research at Project UHV"
IEEE Trans. Power Apparatus and Systems Vol. 101 July 1982
pg. 1998 - 2007

[11] Hara, M. Hayashi, N.
"Influence of wind and conductor potential on distributions of electric field and ion current density"
IEEE Trans. Power Apparatus & Sys.
Vol. 101 April 1982 pg. 803 - 814

[12] Maruvada, P.S. Goodman, J.S.
"Environmental effects of the Nelson River HVDC transmission lines"
IEEE Trans. Power Apparatus & Sys.
Vol. 101 April 1982 pg. 951 - 959

[13] Carter, P.J. Johnson, G.B.
"Space charge measurements downwind fron a monopolar 500 kV DC test line"
IEEE Trans. Power Delivery
Vol. 3 October 1988
pg. 2056 - 2063

[14] Charry, J.M. Kavet, R.
"Air Ions: Physical and Biological Aspects"
CRC Press 1987

[15] Zorpette, G.
"HVDC: wheeling lots of power"
IEEE Spectrum
June 1985 pg. 30 - 36

[16] Mains, S.
"The Minnesota Power-line Wars"
IEEE Spectrum
July 1983 pg. 56 - 62

[17] Wu, C.T.
"AC - DC economics and alternatives 1987 Panel Session Report"
IEEE Trans. Power Delivery
November 1990 pg. 1956 - 1968

[18] Johnson, G.B. Zaffanella, L.E.
"Study of electric field and ion effects on HVDC lines"
DOE Report DOE/RA/50153-T1
October 1984

[19] Banks, R. Williams, A.
"The Public Health Implications of
HVDC transmission lines"
IEEE Trans. Power Apparatus & Systems
Vol.102 No.8 August 1983 pg.2640-2648

[20] Britten, A.C. (ESKOM)
Private communication to M.Sellars
1995

[21] Feldman, J. Reinhardt, N. Kuehn, K.
"A Hotstick Instrument for Estimation of
the Potential of an HVDC Conductor"
IEEE Trans. Power Delivery
Vol.7 No.3 July 1992 pg.1533-1541

3. Electric Field Mill Theory

There are two commonly-used types of electric field strength meters for measuring DC electric field strength:

1. Electric field mill (or "generating voltmeter").
2. Vibrating-plate electric field meter.

This chapter describes the basic theory of operation of electric field mills in general. The specific details of the electric field mill that was built for this thesis will be discussed in Chapters 6 and 7. The vibrating-plate electric field meter will not be discussed.

3.1 Basic components of the electric field mill

The diagram below shows the basic components of an electric field mill:

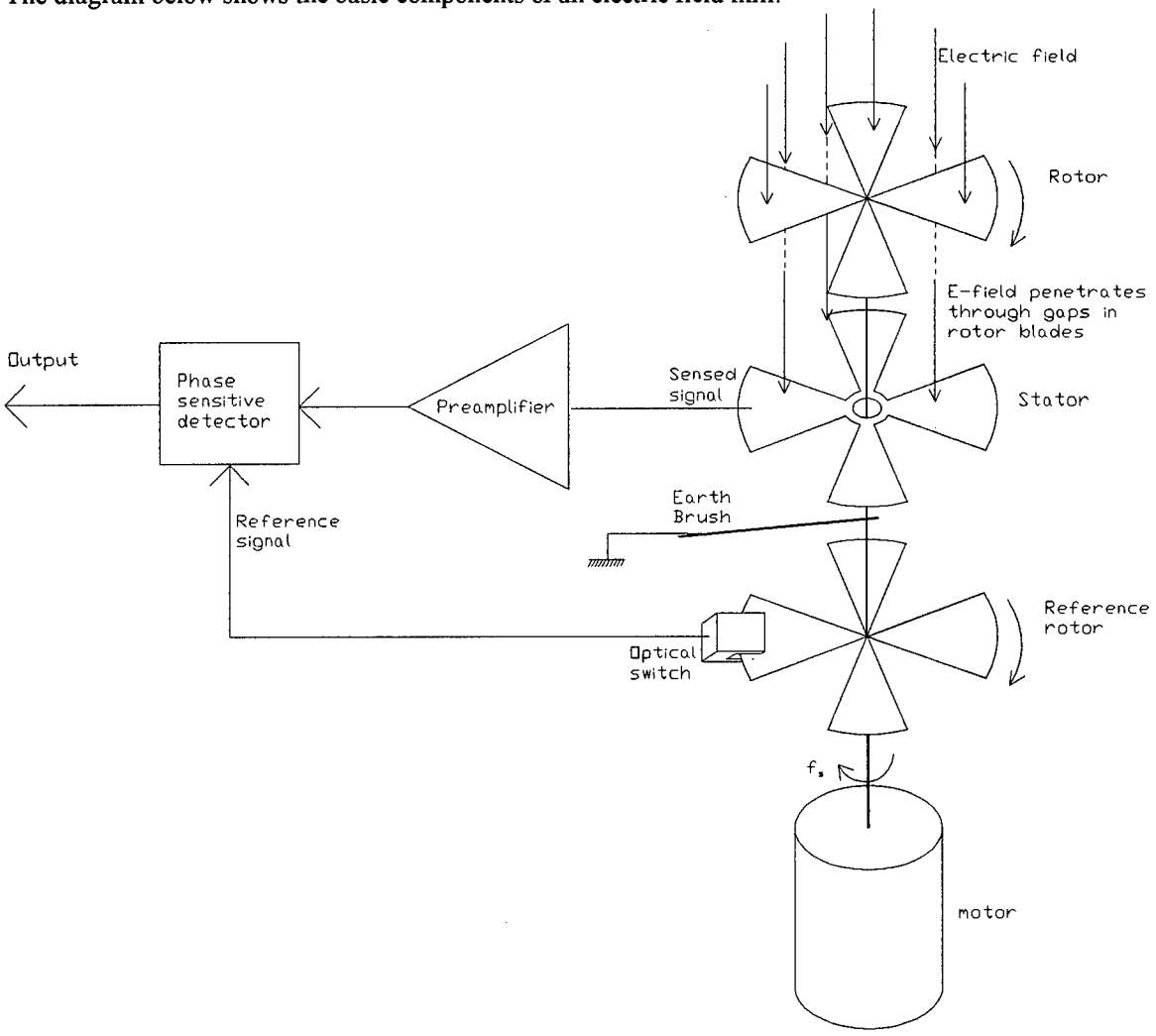

Fig. 3.1 Basic components of an electric field mill

In the diagram above:

$n = 4$	= number of rotor and stator blades
f_s	= rotational frequency of shaft
$f = 1/T = nf_s$	= frequency of modulation of stator signal
A_s	= surface area of one stator blade
$A_{max} = nA_s$	= maximum exposed area of stator

All field mill instruments have a multiblade rotor spinning in front of a multiblade sensor plate, which is stationary. (This sensor plate is the stator). As the rotor spins, so each blade (or "vane") of the stator is alternately exposed to, and shielded from, the ambient electric field. Charge is induced on each blade of the stator when exposed to the electric field, and expelled (conducted away) when the rotor blade covers the stator blade. The induced current signal is sensed at the stator, and is passed into a preamplifier, and then into a synchronous detector (phase-sensitive detector). The rotor is kept at earth potential by a conducting metal brush that rubs against the shaft of the field mill. A reference rotor lower down on the field mill shaft is aligned with the top rotor, and passes through a slotted optical switch. The signal from the optical switch provides a reference signal, which is used for synchronous detection of the stator signal.

The electric field mill is operated flush with the ground plane, so that the incident electric field is perpendicular to the surface of the sensing plate (stator blades). The ground plane is a large flat conducting surface at ground potential. This is shown in the diagram below:

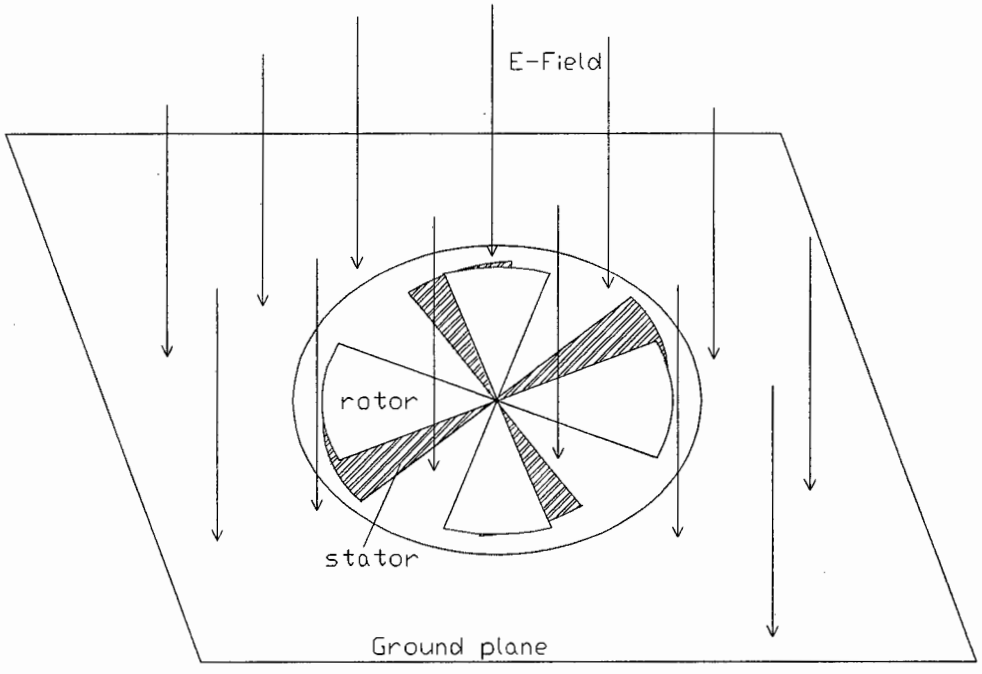

Fig. 3.2 Field mill mounted in the ground plane

3.2 Equivalent circuit of the electric field mill

The electric field mill acts as a varying capacitance between the high voltage source (which may be a power line, thundercloud or charged object) and the preamplifier. This is shown in the diagram below:

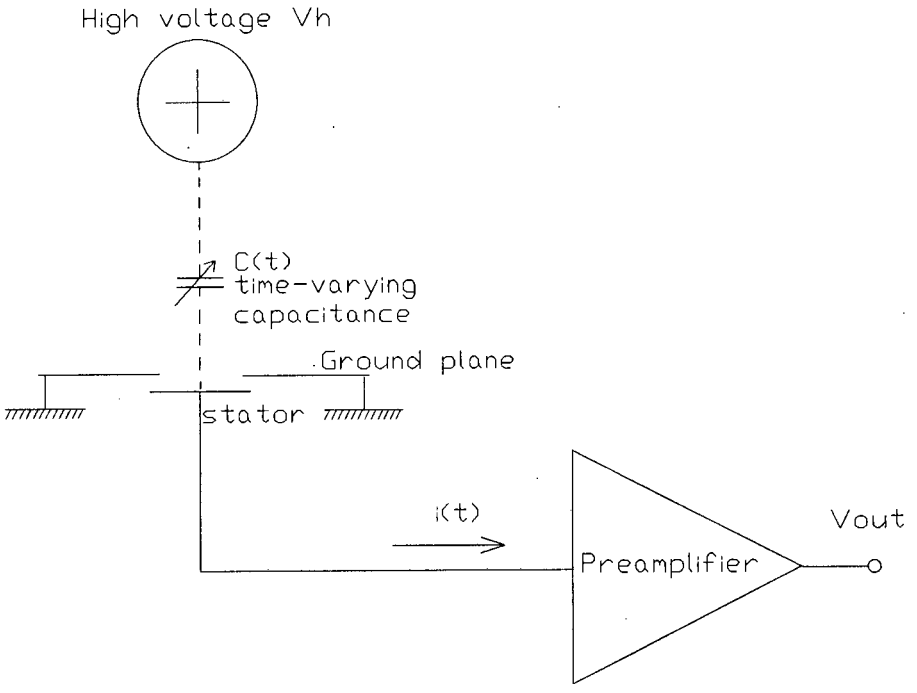

Fig. 3.3 Field mill is effectively a varying capacitor between the high voltage source and preamplifier

The time-varying capacitance C(t) is formed by the changing effective area of the stator vanes as they are periodically exposed to, and shielded from, the high voltage source by the spinning rotor. In the diagram above, this is represented as a time-varying capacitance C(t) and a stator with constant effective area.

The time-varying capacitance causes an alternating current i(t) to flow through the stator to ground:

$$i(t) = \frac{d\,q(t)}{dt} = \frac{d\,(CV)}{dt}$$

In our case, the voltage is constant, and the capacitance is time-varying so that:

$$i(t) = \frac{d\,V_h C(t)}{dt} \qquad \text{..... (3.1)}$$

3.3 Field Mill Preamplifier

The preamplifier is a current to voltage converter, which may take several forms. The simplest is an impedance Z to ground, through which the current from the stator flows, so producing a voltage. The voltage is sensed with a high impedance voltmeter. This is shown in Fig.3.4 (a) below. A more recent method is to use an operational amplifier (opamp) configured as a current-to- voltage converter, with the same impedance Z in the feedback loop (this configuration is also known as a voltage-shunt amplifier). This is shown in Fig.3.4 (b) below:

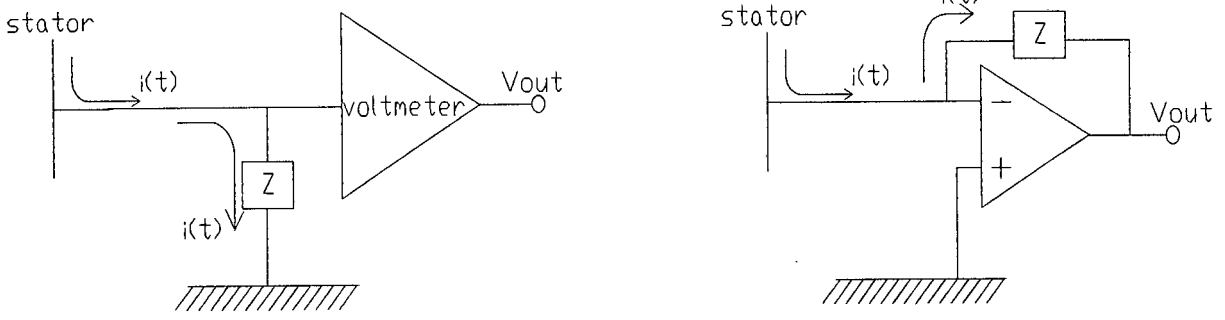

(a) Stator current flows through Z to ground

(b) Opamp used as current-to-voltage converter (voltage-shunt amplifier)

Fig. 3.4 Two forms of preamplifier

For both preamplifier circuits, the output voltage:

$$v_{out}(t) = i(t)Z \quad \text{..... (3.2)}$$

The impedance Z is usually a parallel RC network, as shown in the diagram below:

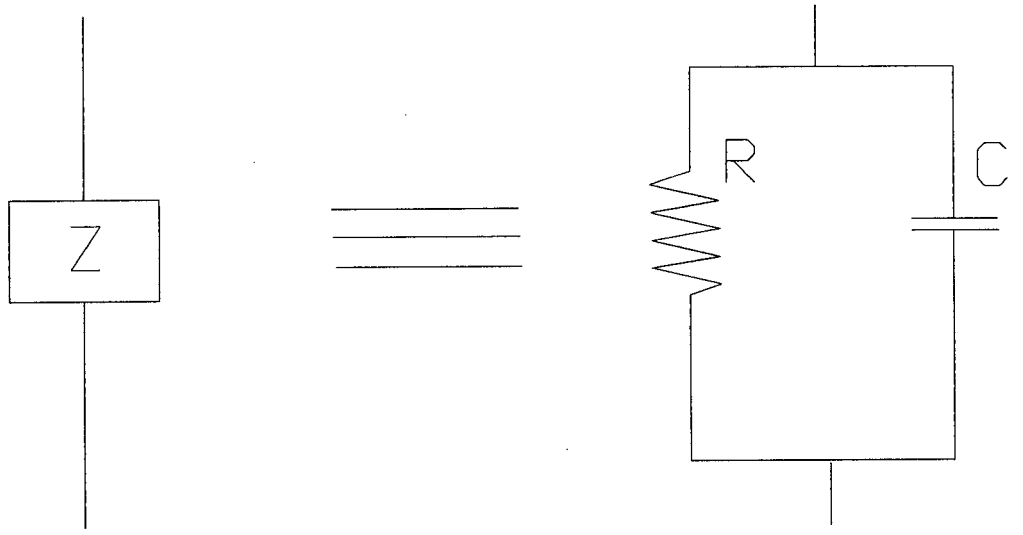

Fig. 3.5 Impedance Z is a parallel RC network

3.4 Electrical signal of the field mill

Assuming the blades of both the stator and rotor are sector-shaped, then the exposed area of the stator blades (vanes) will vary linearly as the rotor spins. This variation is shown below [1]:

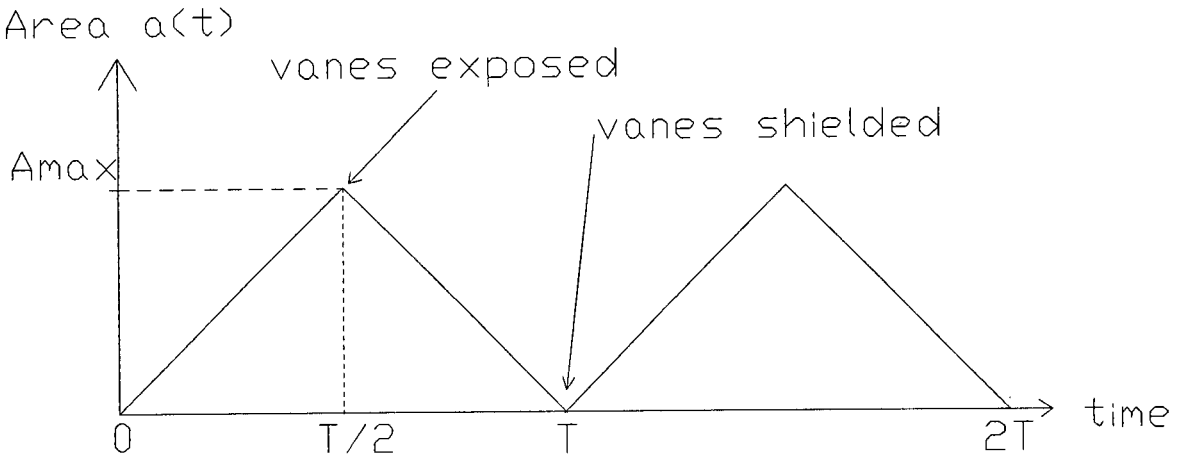

Fig. 3.6 Variation of exposed area of stator vanes as rotor spins

Note: Frequency of modulation $f = 1/T = nf_s$ (f_s = rotational frequency of the shaft, n = number of blades).
Maximum exposed area of the stator $A_{max} = nA_s$ (A_s = surface area of one stator blade).

The charge induced on the exposed stator vanes is directly proportional to the exposed area:

$$q(t) = \varepsilon_o E a(t) \quad \text{where } q = \text{charge } [C], \ \varepsilon_o = \text{permittivity } [Fm^{-1}], \ E = \text{electric field } [Vm^{-1}], \ a(t) = \text{exposed area } [m^2] \qquad \text{..... (3.2)}$$

The peak charge induced is: $Q = \varepsilon_o E A_{max}$ ..... **(3.3)**

(where A_{max} is the maximum exposed area).

The current that is sensed at the stator due to the induced charge is found by differentiating:

$$i(t) = \frac{d\,q(t)}{dt}$$

The waveform of induced charge is triangular in shape, so when differentiating this a square wave is obtained for the current sensed at the stator.

The peak current is:

$$I_{max} = \frac{Q}{(T/2)} = 2fQ = 2f\varepsilon_o E A_{max} \qquad \text{..... (3.4)}$$

(where $f = 1/T$ = frequency of modulation).

The waveforms of the charge q(t) induced on the stator, and of the sensed current i(t), are shown below:

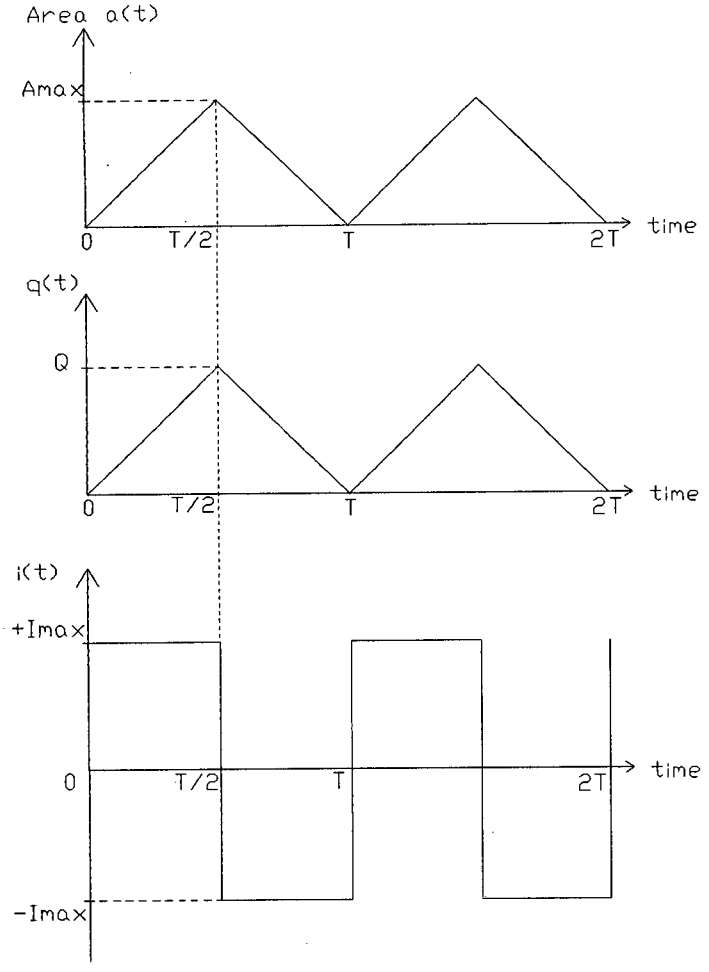

(a) Variation of exposed area of stator

(b) Charge induced on stator

(c) Current sensed at the stator

Fig. 3.7 Waveforms of the field mill stator

3.5 Preamplifier waveforms and design

The current sensed at the stator is then passed through the preamplifier, which is a current-to-voltage converter. Let us consider the voltage $v_{out}(t)$ measured at the preamplifier output when the current i(t) passes through the impedance Z (which is a parallel RC network):

The following mathematical derivation is adapted from the paper by Mapleson & Whitlock [2]. Consider the stator plate to be completely shielded at time t=0, and exposed at time t=T/2. During this time:

$$\begin{cases} \text{area} \quad a = \dfrac{At}{(T/2)} \\ \text{charge} \quad q = q_o + \dfrac{Qt}{(T/2)} \\ \text{current} \quad i = \dfrac{dq}{dt} = \dfrac{Q}{(T/2)} \end{cases}$$

where: q_o = charge on the stator at time t=0
$A = A_{max}$

Referring to Fig.3.4 and Fig.3.5, let v(t) be the instantaneous voltage developed across the impedance Z, then:

$$C\frac{d\,v(t)}{dt} = i(t) - \frac{v(t)}{R}$$

$$\therefore v(t) = I_{max}R + \beta e^{-t/RC} \qquad \text{(where } I = I_{max} \text{ and } \beta \text{ is a constant to be found)}$$

This differential equation is now solved for the first half-cycle of the specific waveforms shown in Fig.3.7. The boundary conditions are:

$v(t) = q_o/C$ at $t = 0$
$v(t) = V$ at $t = T/2$

therefore: $\beta = q_o/C - IR$

and so: $$V = IR\left(1 - e^{-\frac{T}{2RC}}\right) + \frac{q_o}{C}e^{-\frac{T}{2RC}}$$

Assuming that the voltage at the beginning of the half-cycle v(0) = -V then:

$$V = \frac{IR\left(1 - e^{-\frac{T}{2RC}}\right)}{1 + e^{-\frac{T}{2RC}}} = \frac{IR\left(1 - e^{-\frac{\pi}{\omega RC}}\right)}{\left(1 + e^{-\frac{\pi}{\omega RC}}\right)} \qquad \text{..... (3.5)}$$

The above expression is for the peak voltage measured at the preamplifier output. There are two limiting cases as follows:

1. Choose $\omega RC >> 1$

Impedance is predominantly capacitive. This is the case of a "charge amplifier", where the charge induced on the stator oscillates backwards and forwards between the stator and the capacitor of the preamplifier.

$$\text{Peak voltage } V \approx \frac{IR\left(\frac{\pi}{\omega RC}\right)}{2} = \frac{\pi I}{2\omega C} \quad (\text{where } I = I_{max})$$

$$\therefore V = \frac{\varepsilon_o E A_{max}}{2C} = \frac{k_1}{C} \quad (\text{where } k_1 \text{ is a constant}) \qquad \text{..... (3.6)}$$

From this last equation, we can see that the peak voltage V is proportional to 1/C. Thus for maximum sensitivity, we would like to choose the smallest value for C possible, that will not violate the condition $\omega RC >> 1$. Preamplifier waveforms are shown below:

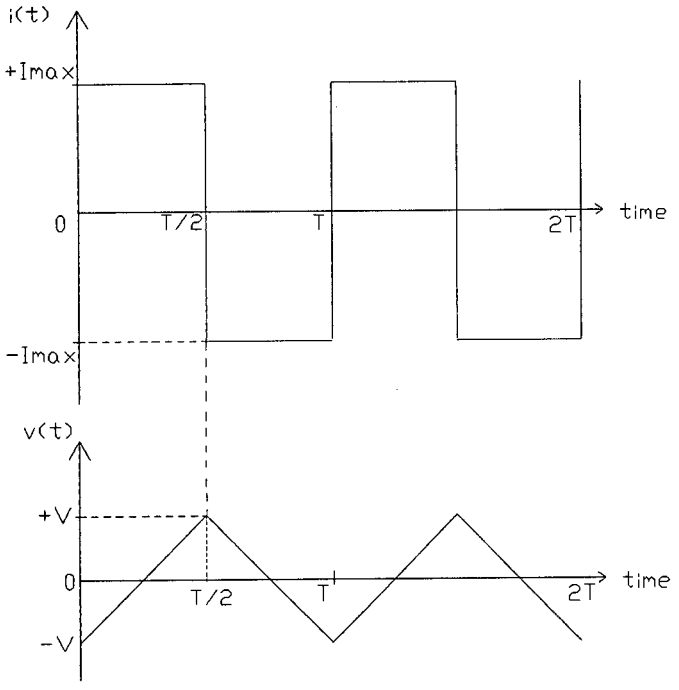

(a) Stator current

(b) Preamplifier output voltage

Fig. 3.8 Preamplifier waveforms for Z mainly capacitive

2. Choose $\omega RC << 1$

Impedance is predominantly resistive. This is the case of a simple resistive element, which converts the current flowing through it into a voltage. Peak voltage $V \approx IR$.

$$\therefore V = 2f\varepsilon_0 EAR = k_2 fR \quad \text{..... (3.7)}$$

(Where $I = I_{max}$ $A = A_{max}$ k_2 = constant).

From this equation we can see that the peak voltage V is directly proportional to frequency f, and resistance R. Thus the higher the resistance R, the greater the sensitivity. We would therefore like to choose the highest value of resistor R that does not violate the condition: $\omega RC << 1$. Preamplifier waveforms are shown below:

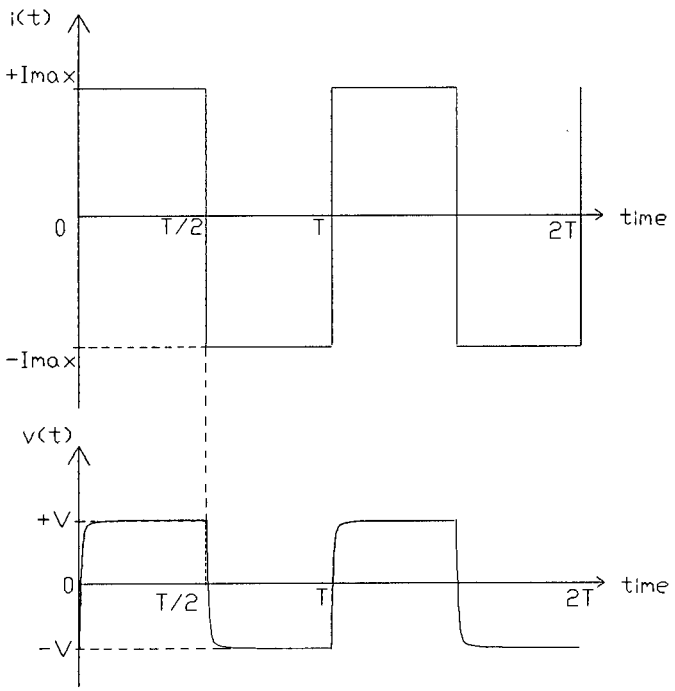

(a) Stator current

(b) Preamplifier output voltage

Fig. 3.9 Preamplifier waveforms for Z predominantly resistive

3. No clear choice: ωRC ≈ 1

It is necessary to make a definite choice between the two cases shown above. If a clear-cut choice is NOT made (ie. $\omega RC \approx 1$) then it is difficult to simplify the complicated expression for the output voltage v(t) in equation 3.5, and the value of the peak output voltage now becomes dependent on all 3 variables: R, C and frequency f. This is undesirable, since we would like to simplify the expression for v(t) as much as possible, and reduce the number of variables which affect the reading. A sample waveform is shown below for $\omega RC \approx 1$:

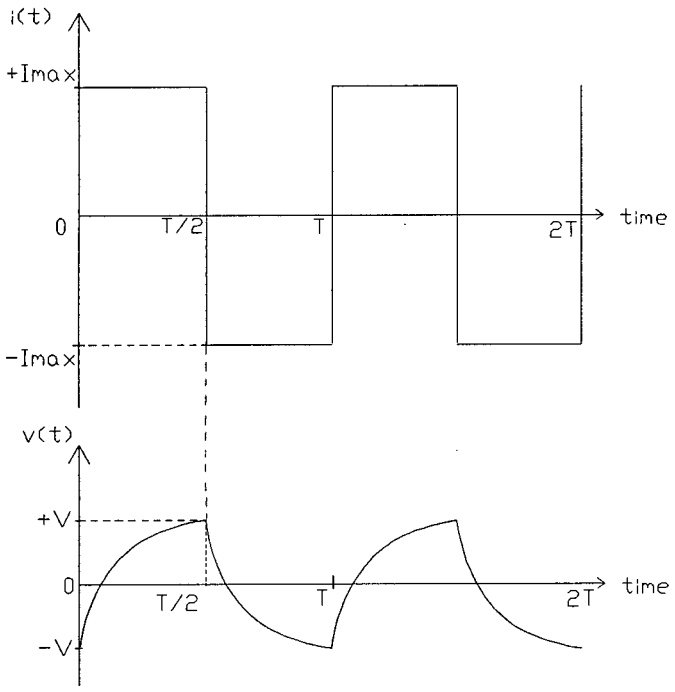

(a) Stator current

(b) Preamplifier output voltage

Fig. 3.10 Preamplifier waveforms for Z both resistive and capacitive

3.6 Sensitivities of the two preamplifier circuits

In order to give an example of the sensitivities that we may expect, let us make some assumptions about the electric field mill apparatus:

(a) Assume that the maximum exposed area of the stator plates is:	$A = 0.0025 m^2$
(b) Assume frequency of modulation	$f = 150$ Hz
(c) Assume the minimum value of capacitance	$C = 4$pF
(d) Assume that the largest resistor available	$R = 100$ Mega-ohms

1. $\omega RC >> 1$ (impedance mainly capacitive)

In this case: peak voltage $V = \frac{\varepsilon_o EA}{2C}$

Choose $\omega RC = 5$ (at least).

$C_{min} = \frac{5}{\omega R}$, so this gives us $C_{min} = 53$pF

Therefore the peak voltage V = 210μV per Vm^{-1}.

2. $\omega RC << 1$ (impedance mainly resistive)

In this case: peak voltage $V = 2\varepsilon_o EAfR$

Choose $\omega RC = 0.2$ (at most).

$R_{max} = \frac{0.2}{\omega C}$, so this gives $R_{max} = 53$Mega-ohms (since $C_{min} = 4$pF).

Therefore the peak voltage V = 350μV per Vm^{-1}.

From this simple comparison, we see that the maximum sensitivity is of the same order of magnitude in both cases. The sensitivity in case 1 may be increased using a high quality electrometer resistor (R=1000 MΩ or higher) [16], but these resistors are expensive and unavailable in South Africa. The maximum sensitivity in case 2 is effectively limited by the minimum input capacitance C of the preamplifier. The input capacitance of commonly-available operational amplifiers is about 4pF or higher. For practical reasons, it is not possible to achieve an input capacitance much lower than 4pF.

Conclusions

In the example above, the sensitivities are the same order of magnitude. A capacitive impedance has the advantage that the electric field reading is independent of variations in modulating frequency, f, which is an important factor when the speed of the motor may not be constant (for example in battery-powered instruments) [3].

3.7 Calibration of electric field mills

Due to the presence of space charge in the vicinity of HVDC transmission lines, a known DC electric field with space charge is desirable for calibration purposes. However, producing a known electric field with space charge present is difficult. The paper by Martin Misakian [6] describes a calibration apparatus that generates a DC electric field with space charge, which may be necessary if the ion current densities to be measured are significantly higher than 1000 nA/m^2. Note that this apparatus and the associated electric field calculations are considerably more complicated than the purely electrostatic calibration apparatus which is described in this section.

It is usually more convenient to calibrate the electric field mill in a purely electrostatic field. An electrostatic field is easily produced by applying a known voltage across two parallel plates which are a known distance apart. This method has been used for calibrating a wide range of electric field mills for use under HVDC transmission lines [8]. A parallel-plate apparatus for producing an electrostatic field (electric field **E** that has no ions or space charge present) is shown below:

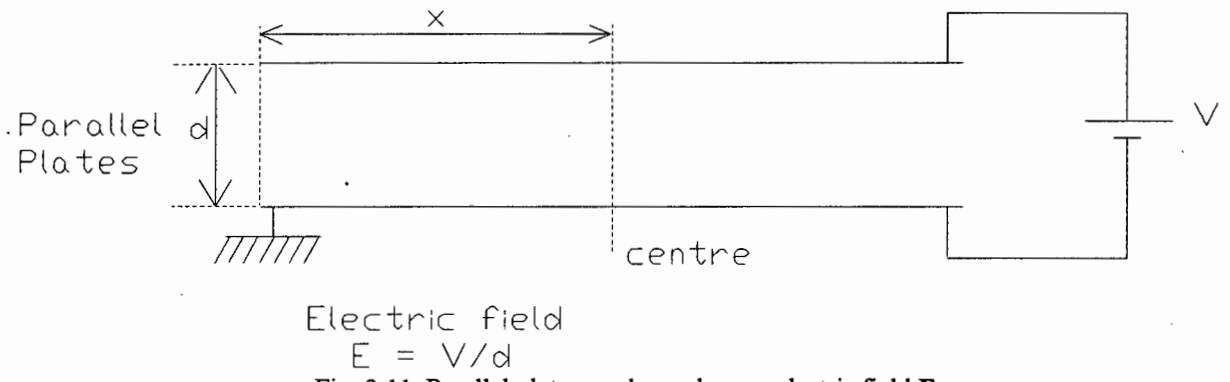

Fig. 3.11 Parallel plates produce a known electric field **E**

The electric field mill that is to be calibrated is mounted flush with the ground plane (the lower plate in the diagram above), by making an aperture in the ground plane. The field mill output is then compared with the calculated value for electric field. The diagram below shows the field mill mounted in an aperture in the lower plate of a parallel plate calibrator. The aperture has radius r.

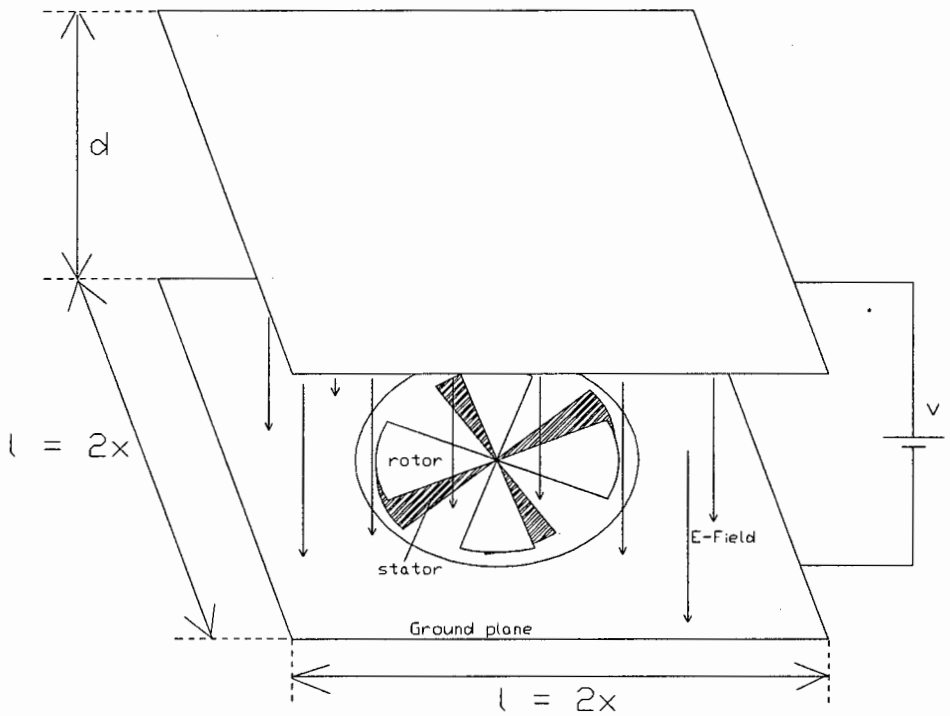

Fig.3.12 Field mill mounted in the ground plane of a parallel-plate calibrator

There are a number of sources of error that must be avoided in the parallel-plate calibrator:

1. Field perturbation due to aperture in ground plane

The plates must be placed sufficiently far apart that perturbation of the field by the sensing aperture of the field mill is localised to the vicinity of the aperture. The electric field perturbation due to a circular aperture in the ground plane decreases to less than 1% at a distance of 3 aperture radii above the aperture. Thus a parallel plate spacing d that is 3 times the radius of the sensing aperture will conservatively eliminate significant perturbations of the electric field by the presence of the aperture.

Use d = 3r (minimum)

(d = plate separation, x = plate radius, r = aperture radius)

2. Fringing fields at plate boundaries

The plates must be sufficiently large that the electric field in the calibration region is not influenced by fringing fields from the plate boundaries. The IEEE Standard [7] recommends that the plate radius, x, should be at least as large as the plate spacing, d, for the effect of fringing fields from the plate boundaries to be negligible.

Use x = d (minimum)

(d = plate separation, x = plate radius)

3. Stray fields from external sources

The plates must be sufficiently large compared to their spacing that the electric field in the calibration region is not influenced by external charged surfaces. The IEEE Standard [7] recommends that the outer edge of the sensing aperture should be at least twice the plate spacing, d, from the edge of the grounded lower plate. Chubb [9] recommends a plate radius, x, of at least four times the plate separation, d.

Use x = 2d+r (minimum)

(d = plate separation, x = plate radius, r = aperture radius)

Discussion

The dimensions given above are used for highly accurate calibration of electric field mills. If very high accuracy is not critical, the following dimensions are the minimum requirements for the size of the calibration plates [17]. An estimate of the calibration error involved in using these dimensions is 5%.

x = d

(d = plate separation, x = plate radius)

Conclusion

If the following dimensions are used for the size of the calibration plates, a 1% calibration accuracy may be achieved [7].

plate separation d = 3r
plate radius x = 7r
(d = plate separation, x = plate radius, r = aperture radius)

If smaller dimensions are used for the calibration plates, the accuracy will be reduced. Reasonable accuracy is still achieved if the plate radius, x, is not less than the plate separation, d:

plate separation $x \geq d$
(d = plate separation, x = plate radius)

3.8 Sources of Measurement Error in Electric Field Mills

There are a number of sources of error in electric field mill systems [10]. The important sources of error are:

1. Noise due to the preamplifier, and due to contact potential variations.
2. Errors in electric field strength if field mill is not flush with the ground plane.
3. Contamination of field mill sensing surfaces due to dirt, insects and rain.

Preamplifier noise is specific to the design of the preamplifier, and will be discussed in a later chapter. Contact potential variations cause a spurious electric field signal at the field mill output, and this will be discussed in detail in section 3.8.1.

3.8.1 Spurious signals from the electric field mill

It is well known that an anomalous output from a field mill instrument operating under nominal zero-field conditions can be obtained due to the contact potential differences in the rotor-stator electrical circuit [3]. Contact potential differences are formed in two ways:

1. Contact potential difference between rotor and stator surfaces.
2. Contact potential differences between dissimilar metals in the wiring which connects the earthing brush to ground potential.

3.8.1.1 Contact potential differences between rotor and stator surfaces

Contact potentials (or "Volta potentials") exist between the surfaces of any two different metals (which are in close proximity but not touching), due to different electron work functions in the two surfaces. In the case of the field mill, this occurs between the upper surface of the stator and the lower surface of the rotor. If the surfaces are made from the same material, contact potentials still exist due to small variations in surface structure, oxidation or contamination [4]. Attempts to equalise the work function are almost futile, since even small changes in the crystalline structure influence the contact potential difference [5].

3.8.1.2 Contact potential differences between dissimilar metals in the rotor-stator circuit

The junction of any two dissimilar metals will generate a small voltage or contact potential difference. An example of such a junction would be the region where the earthing brush (which might be gold wire) rubs on the field mill shaft (which might be stainless steel).

The different contact potential differences are lumped together and considered as the "contact potentials". The rotor and sensor plate are normally separated by only a small gap so as to maximise the field mill sensitivity. Under these conditions, the contact potentials create a significant electric field at the sensor plate segments. This introduces a spurious electric field signal which is in phase with the signal due to the external electric field, and is indistinguishable from it. The diagram below illustrates the effect of contact potentials.

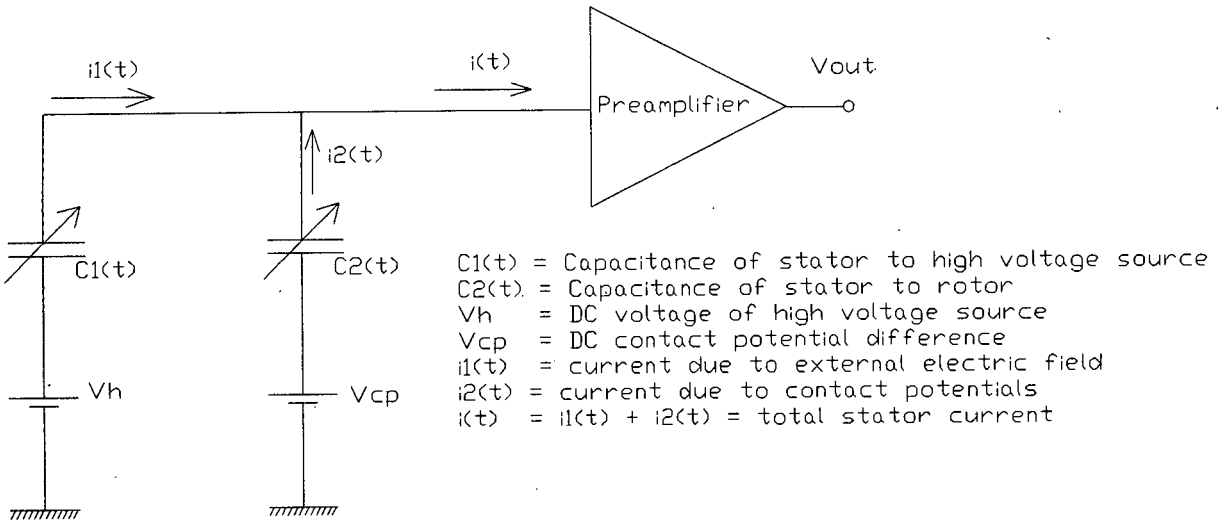

Fig. 3.13 Field mill circuit showing contact potentials adding to the stator signal

In Fig. 3.13, it is seen that the contact potential difference V_{cp} adds to the sensed stator signal via the changing rotor-stator capacitance $C_2(t)$. Although the high voltage source V_h has a very much larger magnitude than V_{cp} (V_{cp} may be of the order of 100mV, and V_h may be of the order of 100kV), the capacitance between the stator and high voltage source $C_1(t)$ is very much smaller than the capacitance between the rotor and stator $C_2(t)$. Thus the overall effect of the contact potential difference becomes significant at low values of electric field, and at zero external field it appears as a spurious electric field signal.

In practice, this difficulty is overcome by making the rotor potential variable with respect to ground, and adjusting this potential under zero impressed field conditions to give zero output from the circuit [3]. This is illustrated in the diagram below:

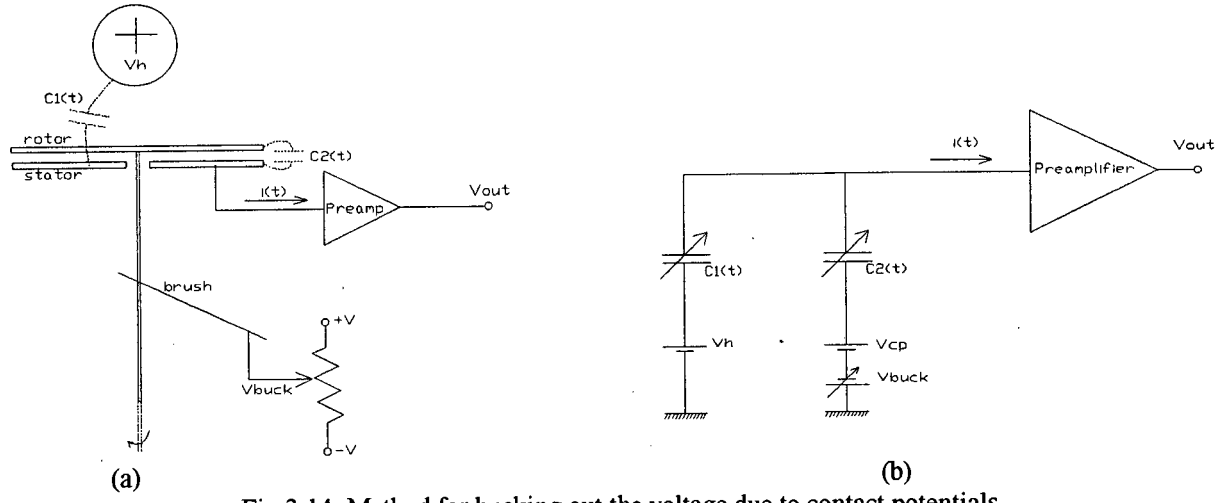

Fig.3.14 Method for bucking out the voltage due to contact potentials

In Fig.3.14 (a), the earth brush is no longer earthed, but rather is connected to a bucking voltage V_{buck} which is used to null or "buck" out the contact potential difference V_{cp}. This is shown in Fig.3.14(b).

3.8.2 Errors in electric field due to field mill not being flush with ground plane

If the field mill protrudes above the surface of the ground plane, then recalibration is necessary to take into account the enhancement of the electric field [8], [12]. In some cases, it may be necessary to mount the field mill a significant height above the ground to avoid problems with rain, dirt and insects. This enhances the electric field readings, and the values will need to be corrected [11].

If the field mill is below the ground plane then the electric field incident on the sensing surface will be attenuated relative to the field at the plane of the ground. It is usual that the rotor of the field mill is mounted flush with the ground plane, and that the stator is therefore slightly recessed below the ground plane. This means that there is some attenuation of the electric field that reaches the stator. This is a problem which is not easy to solve since the design of the rotating vane electric field mill dictates that the stator should be physically below the plane of the rotor. This problem is illustrated below:

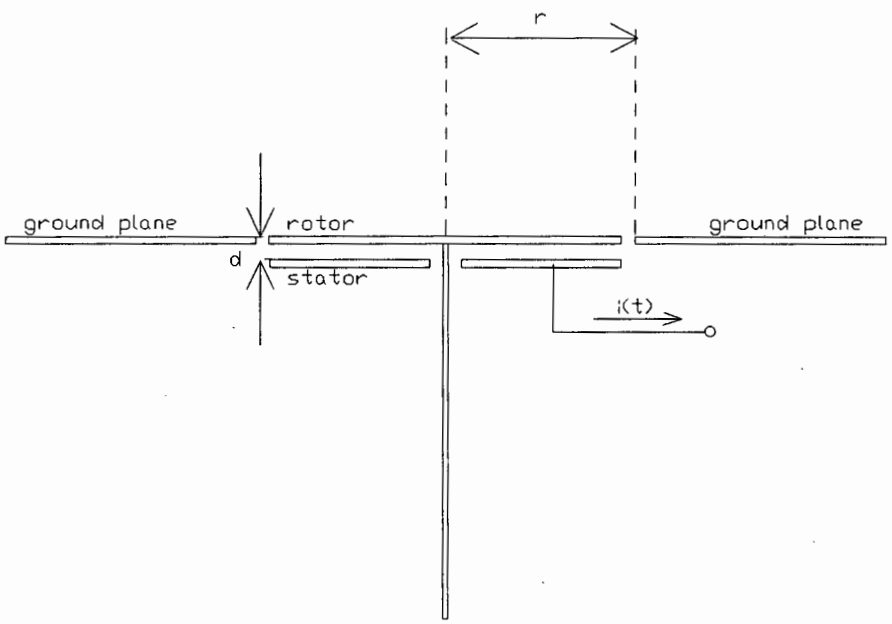

Fig.3.15 Stator of field mill recessed some depth d below the ground plane

This recessed stator position results in attenuation of the electric field at the sensing surface, which introduces a constant loss factor into the readings. It is possible to calculate this loss factor using 3D computer modelling, but Chubb recommends that this loss factor should just be calibrated out [11].

3.8.3 Contamination of field mill sensing surfaces

In many applications, electric field mills are required to operate outdoors without any shelter. Continuous operation over periods as long as a year may be necessary [13]. In these conditions, it is important that the field mill is resistant to contamination by dust and dirt, water, ice and snow, vegetation and insects. Any contamination of the sensing surface may result in a spurious electric field signal (as discussed in Section 3.7.1), as well as reduced effective stator area. Water, ice and snow may also clog the rotating vanes, causing fluctuations in rotational speed. Insects, and even frogs have been known to cause failure of electric field mills operated outdoors. Fortunately, the rotating vanes of the electric field mill have the tendency to eject water droplets and snow, although in heavy rain the field mill may become swamped. The field mill designed by IREQ [14] featured heating elements to melt any accumulated ice and snow. Yeboah-Amankwah used heated stator studs that prevented water vapour from condensing on the stator surfaces [15]. Chubb suggests that if dirt, rain and insects are a problem, then the field mill may be mounted on a slender pole 1 to 2 metres above the ground, pointing downwards. This reduces the requirements for preventing contamination, but requires different calibration procedures [11]. Zero drift in the electric field mill readings may be caused by dust being blown onto the sensing surfaces [12]. In dirty conditions or in situations where charged dust particles may be present, clean gas may be used to purge the sensing surfaces [10].

3.9 References

[1] Dahl, H.
"On the sensitivity of generating electrostatic D.C. voltmeters"
Christian Michelsen Institutt,
Beretninger XIV, 3 (1951)
Available free of charge from:
Christian Michelsen Research
P.O. Box 3 N-5036 Fantoft
Bergen, Norway

[2] Mapleson, W. Whitlock, W.
"Apparatus for the accurate and continuous measurement of the earth's electric field"
J. Atmospheric and Terrestrial Physics
Vol. 7 (1955) pg.61-72

[3] Secker, P.E.
"The use of field-mill instruments for charge density and voltage measurement"
Inst. Physics Conf. Series
No.27 (1975) pg.173-181

[4] Israel, H.
"Atmospheric Electricity"
pg. 594 - 601

[5] Knott, K.
"Elimination of Volta-Potential Noise from Plate Field Mills"
Review of Scientific Instruments
Vol.38 No.5 (1967) pg.602-604

[6] Misakian, M.
"Generation and measurement of dc electric fields with space charge"
J. Applied Physics
Vol.52 No.5 (1981) pg.3135-3144

[7] IEEE Standard 1227-1990
IEEE Guide for the Measurement of DC Electric-Field Strength and Ion Related Quantities
December 1990

[8] Comber, M. Kotter, R.
"Experimental evaluation of instruments for measuring DC transmission line electric fields and ion currents"
IEEE Trans. Power Apparatus & Systems
Vol.102 No.11 (1983) pg.3549-3557

[9] Chubb, J.
"The calibration of electrostatic fieldmeters and the interpretation of their observations"
Electrostatics '87, Inst. Phys. Conf. Series
Vol.85 (1987) pg.261-266

[10] Chubb, J.
"The performance capabilities of electrostatic fieldmeters"
SEE Conference, Nice Section C2
October 1986 pg.93-96

[11] Chubb, J.
Private communication to M.Sellars
March 1995
See Appendix D

[12] Bracken, T. Capon, A.
Montgomery, D.
"Ground level electric fields and ion currents on the Celilo-Sylmar +/- 400kV DC Intertie"
IEEE Trans. Power Apparatus & Systems
Vol.97 April 1978 pg.370-378

[13] Chartier, V.
"Performance of a long-term unattended station for measuring DC fields and air ions from an operating HVDC line"
IEEE Trans. Power Delivery
Vol.4 No.2 April 1989 pg.1318-1328

[14] Maruvada, P.S. Dallaire, R.D.
Pedneault, R.
"Development of field-mill instruments for ground-level and above-ground electric field measurement under HVDC transmission lines"
IEEE Trans. Power Apparatus & Systems
Vol. 102 March 1983 pg. 738 - 744

[15] Yeboah-Amankwah, D. V.d.Made, P.
"Sign discriminating field mill"
J. of Atmospheric and Terrestrial Physics
Vol. 54 1992 pg. 851 - 861

[16] Dostal, J.
"Operational Amplifiers"
Elsevier 1981
Chapter 5

[17] Kirkham, H. Johnston, A.
"AC and DC Electric Field Meters"
JPL Publication 87-20 (1987)
Jet Propulsion Laboratory, CalTech

4. Measurement of ion current density

4.1 Wilson Plate

The vertical component, J, of the ion current density (**J**) is measured at ground level using a Wilson Plate [1], [2], [3]. This is simply a flat metal plate which is mounted flush with the ground plane, but insulated from it. The Wilson Plate is effectively an insulated portion of the earth's surface, and so absorbs the vertical current flowing into this portion of the surface. An electrometer is used to measure the current I that flows from the Wilson Plate to ground. The Wilson Plate is isolated from ground, but is held at ground potential by the electrometer circuitry. A grounded guard band surrounds the Wilson Plate, and reduces fringing fields. A diagram of a Wilson Plate is shown below:

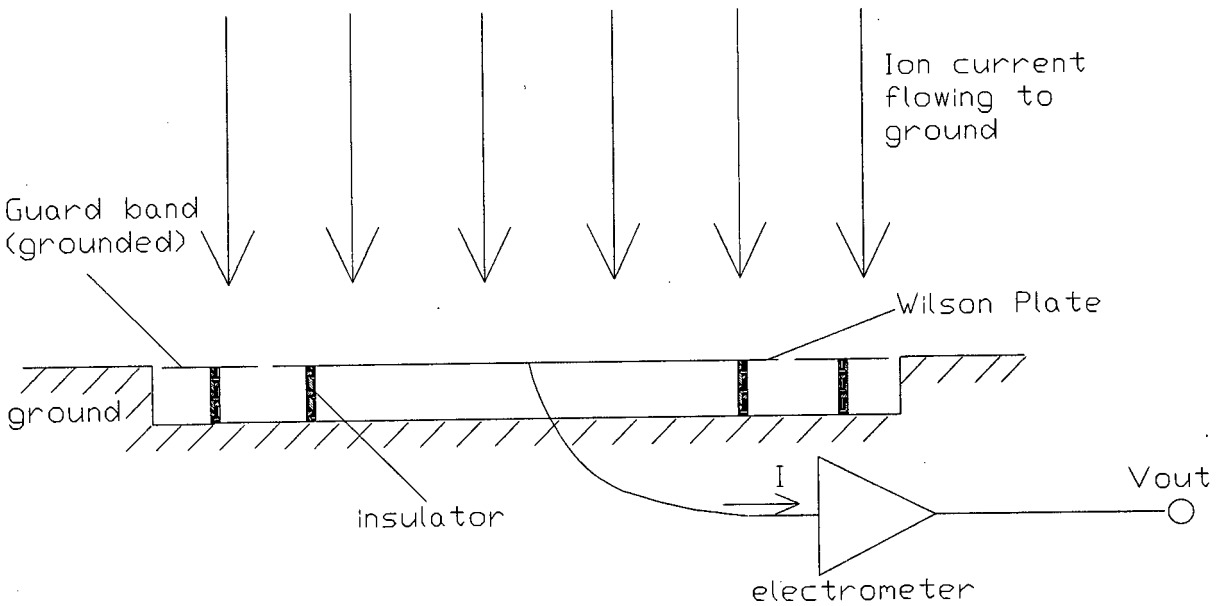

Fig.4.1 Wilson Plate mounted flush with the ground plane

The current density is:

$$J = I/A \quad \text{..... (4.1)}$$

where J = ion current density [A/m^2]
I = measured current [A]
A = surface area of Wilson Plate [m^2]

If necessary, the sensitivity of the current measurements may be increased by increasing the area of the Wilson Plate. Ion current densities under HVDC power lines are typically several orders of magnitude higher than the ambient air-earth current. This means that the sensitivity requirements for current measurements under HVDC power lines are lower than the requirements for atmospheric electricity research [4].

4.2 Calibration of the Wilson Plate

Calibration of a Wilson Plate measurement system requires knowledge of the uncertainties in the measurement of the sensed current, I, and the Wilson Plate area, A. The uncertainty in the area of the Wilson Plate can be lessened by reducing the gap spacing beween the plate and the guard band, and by assuming that the effective ion collecting area of the plate extends to the midpoint of the gap [2]. This assumption is necessary since fringing fields at the edges of the Wilson Plate tend to concentrate onto the plate those ions which would otherwise fall into the air gap.

The electrometer may be calibrated with a current injection circuit consisting of a high-standard resistor, a DC power supply, and an accurate voltmeter. (An electrometer is a highly sensitive current-measuring amplifier). An example of this circuit is shown below:

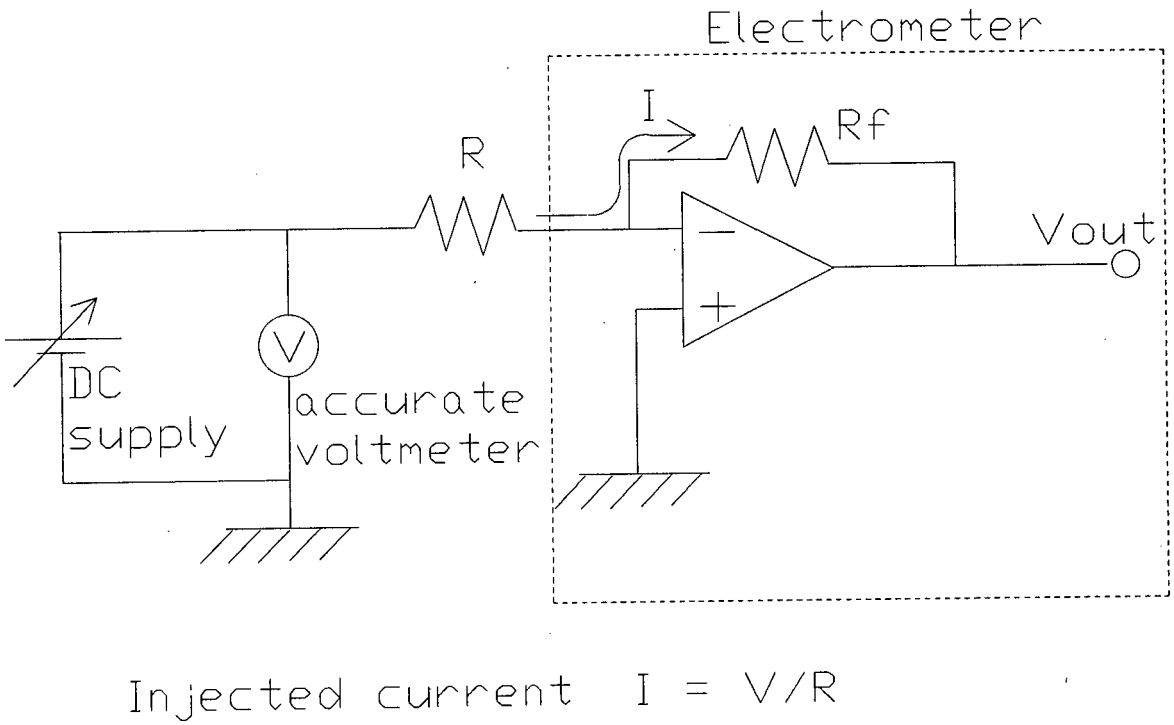

Fig.4.2 Current injection circuit for calibrating electrometer used with Wilson Plate

The current injection circuit for calibrating the electrometer is recommended by the IEEE Standard 1227-1990 [2]. This circuit was also used by Chartier [6] for calibrating his Wilson Plate circuitry. His current injection circuit was capable of injecting currents ranging from 0.1nA up to 10nA. Chartier stated that, in 1989, no ion-generating-source standard existed for producing a standard ion density for field-type installations. Thus the best that can be done is to calibrate the electrometer circuitry accurately, and to use a guard ring that fits as close to the edge of the Wilson Plate as possible, in order to reduce uncertainties in the surface area.

4.3 Sources of error in current density measurements

The main causes of error in current density measurements with a Wilson Plate are:

1. Displacement current due to movement of charge
2. Errors if the Wilson Plate is not flush with the ground plane
3. Leakage currents

4.3.1 Displacement current

If the electric field at the surface of the Wilson Plate changes due to the sudden shift of a cloud of charge overhead, then a displacement current is induced in the Wilson Plate that is indistinguishable from the conduction current (ion current density that is being measured) [2], [7]. This causes intermittent fluctuations in the level of the current measured in the Wilson Plate. Some researchers have used averaging techniques to smooth out these fluctuations [5].

4.3.2 Enhancement of ion current above the ground plane

For a variety of reasons, (such as the presence of thick ground vegetation), it may not be feasible to mount the Wilson Plate flush with the ground plane. This introduces errors since the ion current is enhanced by the presence of the Wilson Plate, due to fringing fields at the plate edge.

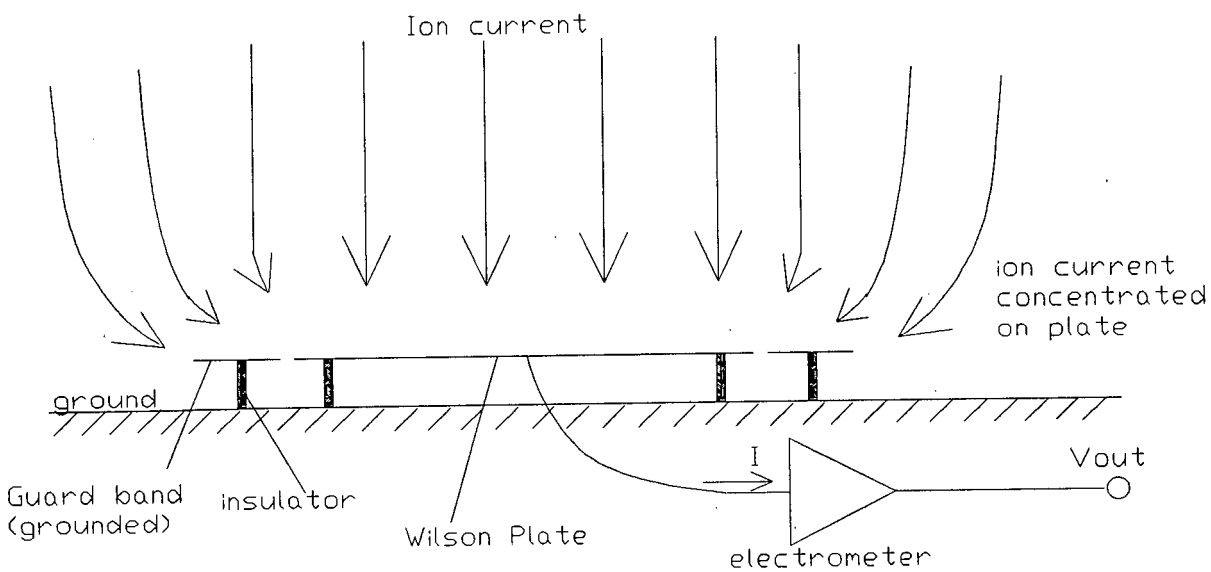

Fig.4.3 Enhancement of ion current for Wilson Plate above the ground plane

As shown in Fig.4.3 above, the ion current is enhanced by the presence of the Wilson Plate above the ground plane. Should it be necessary to mount the Wilson Plate above the ground, it is necessary to use a correction factor in measurements of ion current density. This is discussed in detail by McKnight [4].

4.3.3 Leakage currents

For measurements under HVDC transmission lines, the Wilson Plate apparatus may be required to operate outdoors for long periods of time. The Wilson Plate cannot be shielded, and it must face vertically upwards, which means that contamination is difficult to avoid. Leakage currents may occur from the Wilson Plate to ground if the insulators should become contaminated. Water vapour condensing on the insulators may degrade their performance, so allowing leakage currents to ground. This problem has been observed during heavy fog [6].

If the gap between the grounded guard band and the Wilson Plate should become bridged, then a leakage current will also flow. This has been observed during heavy rain and snow, or if loose pieces of vegetation are blown by the wind onto the Wilson Plate. In warm weather, spider webs may also bridge the gap and cause leakage currents. These leakage current errors are difficult to avoid in outdoor measurement systems, but regular cleaning of the Wilson Plate allows continuous operation [6]. Heating elements built into the Wilson Plate may help to reduce contamination from rain, ice and snow [2].

4.4 References

[1] Wilson, C.
"On the Measurement of the Air-Earth Current and on the Origin of Atmospheric Electricity"
Proc. Camb. Phil. Society
Vol.13 (1906) pg.363-382

[2] IEEE Standard 1227-1990
IEEE Guide for the Measurement of DC Electric-Field and Ion Related Quantities
December 1990

[3] Israel, H.
"Atmospheric Electricity"
pg. 594 - 601

[4] McKnight, R. Kotter, F. Misakian, M.
"Measurement of Ion Current Density at Ground Level in the vicinity of HVDC transmission lines"
IEEE Trans. Power Apparatus & Systems
Vol.102 April 1983 pg.934-941

[5] Bracken, T. Capon, A.
Montgomery, D.
"Ground level electric fields and ion currents on the Celilo-Sylmar +/- 400kV DC Intertie"
IEEE Trans. Power Apparatus & Systems
Vol.97 April 1978 pg.370-378

[6] Chartier, V.
"Performance of a long-term unattended station for measuring DC fields and air ions from an operating HVDC line"
IEEE Trans. Power Delivery
Vol.4 No.2 April 1989 pg.1318-1328

[7] Charry, J. Kavet, R.
"Air ions: Physical and Biological Aspects"
CRC Press 1987 Chapter 3

5. Simultaneous Measurement of Electric Field and Ion Current Density

5.1 Introduction

Any rotating vane electric field mill is sensitive not only to electric field **E**, but also to ion current density, **J**. This is because the stator of the field mill is effectively a Wilson Plate, and so any ion current incident on the stator surface will produce a current flowing in the stator. The spinning rotor will also modulate the incident ion current, so producing a signal that is at the same frequency as the electric field signal [1].

5.1.1 Currents Induced in the Stator

The waveforms induced on the stator are illustrated below, for a rotor-stator pair having sector vanes:

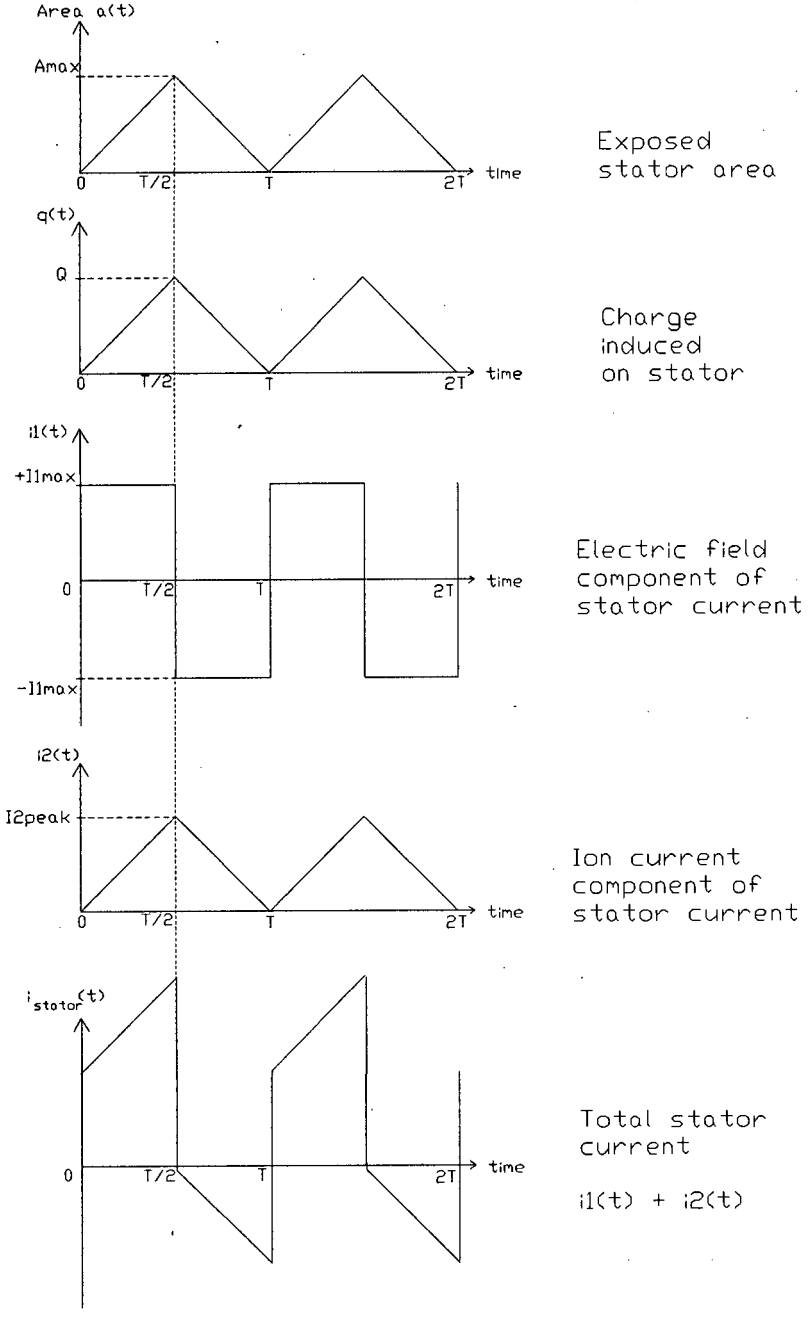

Fig.5.1 Stator waveforms due to electric field and ion current

The two waveforms, $i_1(t)$ due to electric field, and $i_2(t)$ due to the ion current, sum to produce the total current that is induced on the stator:

$$i_{stator} = i_1(t) + i_2(t) \quad \text{..... (5.1)}$$

The phase relationship of the individual components of the stator current is shown in the diagram below:

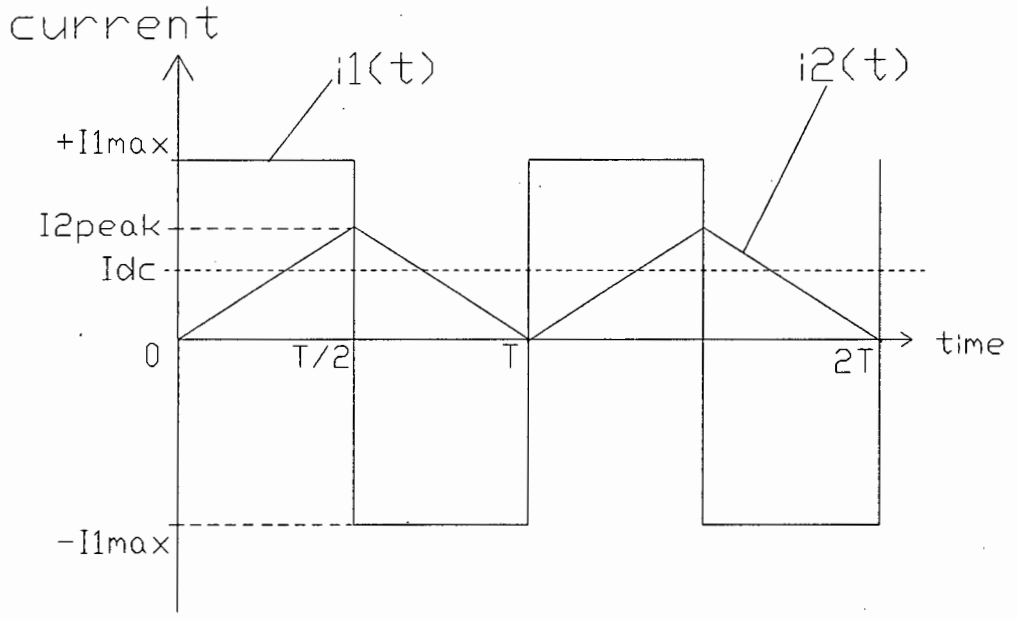

Fig.5.2 Phase relationship of the two currents induced in the stator

As shown in Fig.5.2, the two components of the stator current, $i_1(t)$ and $i_2(t)$ are in quadrature. The ion current component, $i_2(t)$ has a DC component, so that the final output from the stator has a DC offset, I_{dc}. If synchronous detection is not used for detection of the electric field signal, then this DC offset may introduce errors in the electric field measurement. Synchronous detection theoretically rejects all the components of $i_2(t)$ in measurement of the electric field, so that if synchronous detection is used, then the errors due to ion currents should be negligible [2].

By way of example, let us assume that the exposed area of the stator can be approximated as a sinusoidal variation. (This is the case of stator vanes shaped as Bernoulli lemniscates [8]).

Note: $i_1(t) = i_e(t)$, and $i_2(t) = i_j(t)$.

Stator area: $a(t) = A_{max} (1 - \cos \omega t)$ ..... **(5.2)**

A_{max} = maximum exposed stator area
ω = modulating frequency = $2\pi f$

Induced charge: $q(t) = \varepsilon_o E a(t)$ ..... **(5.3)**

ε_o = permittivity
E = vertical component of electric field

Current: $i_e(t) = dq/dt = \varepsilon_o E A_{max} \omega \sin \omega t$ ..... **(5.4)**

$i_e(t)$ = current due to electric field only

$i_j(t) = Ja(t) = JA_{max} (1 - \cos \omega t)$ ..... **(5.5)**

$i_j(t)$ = current due to ion currents only
J = vertical component of ion current density

The diagram below illustrates the stator currents (Eqn.5.5 and Eqn.5.6). Note: $i_e(t) = i_1(t)$ and $i_j(t) = i_2(t)$.

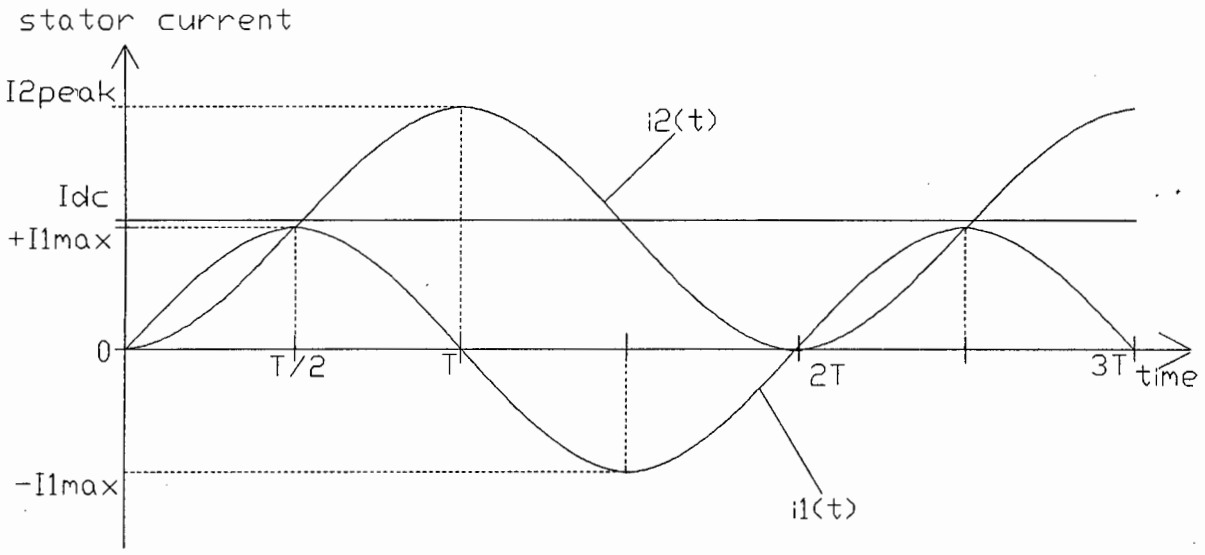

Fig.5.3 Stator current components

The phase relationship of the two components of the stator current are clearly shown in Fig.5.3, and also the DC offset of the ion current component $i_2(t)$. This DC offset is: $I_{dc} = I2_{peak}/2$. Also, $I2_{max} = I2_{peak}/2$.

Note: in Fig.5.3, the magnitudes of $i_1(t)$ and $i_2(t)$ have been shown as being of the same order of magnitude, for purposes of illustration. In the case of HVDC transmission lines, however, the ion current component $i_2(t)$ is very much smaller than the electric field component $i_1(t)$. An example is given below:

Example. Typical values for the electrical environment under HVDC power lines.

$\mathbf{J} = 100$ nA/m^2 $\quad \mathbf{E} = 10$ kV/m $\quad f = 200$ Hz $\quad A_{max} = 1$m^2	
$i_e(t) = i_1(t) = \varepsilon_o E A_{max} \omega \sin \omega t$	$I1_{max} = 111$ μA
$i_j(t) = i_2(t) = J A_{max} (1 - \cos \omega t)$	$I2_{max} = 0.1$ μA

From this example, we can see that the magnitude of the ion current component $i_j(t)$ may be as much as 1000 times smaller than the electric field component $i_e(t)$.

5.2 Simultaneous detection of electric field and ion current

In the classical field mill literature, the ion current is treated as an unwanted interference. In systems not using synchronous detection for electric field measurement, the ion current signal may introduce significant errors if the field to be measured is very low [2].

In the measurement of the environment of HVDC transmission lines, it is necessary to measure both electric field strength and ion current density. This has been accomplished in a number of long-term tests using an electric field mill for electric field measurement, and a Wilson Plate to measure ion current density [4], [5]. The question is asked, why not use the electric field mill to measure both quantities simultaneously? Since the field mill responds to both electric field and ion current, it should not be too difficult to adapt it slightly to measure the ion current instead of rejecting it as an unwanted signal. Some advantages to be gained from a single field mill capable of measuring both electric field and ion current density simultaneously are:

1. Convenience - It is easier to set up a single instrument than two different instruments in the field.

2. Size - A single instrument has advantages in situations where space is limited, such as in exposure chambers for biological experiments.

3. Uncertainties - Measurements of electric field and ion current densities are subject to fluctuations due to wind and weather conditions. A single field mill is able to measure electric field and ion current density at exactly the same physical position, at exactly the same instant in time. This means that uncertainties due to different physical and temporal positioning of the electric field and ion current density measurements are avoided.

5.3 Methods for extracting electric field and ion current signals

The stator current $i_{stator}(t) = i_e(t) + i_j(t)$. This means that it is necessary to extract the components $i_e(t)$ and $i_j(t)$ from the total stator current. There are three obvious ways in which this can be done:

5.3.1 Measuring at different frequencies — METHOD I

The equations for the two current components at the stator are:

$$i_e(t) = \varepsilon_o E A_{max} \omega \sin \omega t \quad \text{..... (5.4)}$$

$$i_j(t) = J A_{max} (1 - \cos \omega t) \quad \text{..... (5.5)}$$

It can be seen that the magnitude of the electric field component $i_e(t)$ is dependent on frequency ω, while the magnitude of $i_j(t)$ is independent of ω. If measurements at a number of different frequencies are made, the magnitude of $i_e(t)$ should vary, while the magnitude of $i_j(t)$ should remain constant. Numerical analysis of the results should then allow the two components $i_e(t)$ and $i_j(t)$ to be separated.

5.3.2 Quadrature detection

METHOD II

The two alternating components of $i_e(t)$ and $i_j(t)$ are 90° out of phase (they are in quadrature), and so can theoretically be separated using two phase-sensitive detectors, one with a 0° reference signal, the other with a 90° reference signal. A diagram of this method is shown below:

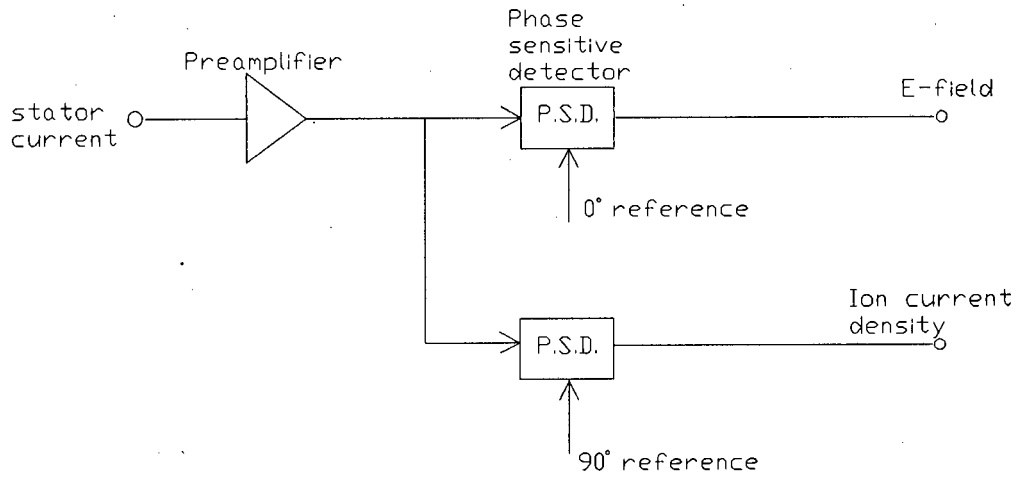

Fig.5.4 Quadrature detection method for separation of $i_e(t)$ and $i_i(t)$

Note: we assume that the 0° reference signal is in-phase with $i_e(t)$, in the diagram above.

5.3.3 Low pass filter

METHOD III

The ion current component of the stator current, $i_j(t)$, is made up of a DC component, I_{dc}, and an alternating component. A low pass filter is used to extract I_{dc}, and phase-sensitive detection with a 0^0 reference signal is used to extract the electric field signal $i_e(t)$.

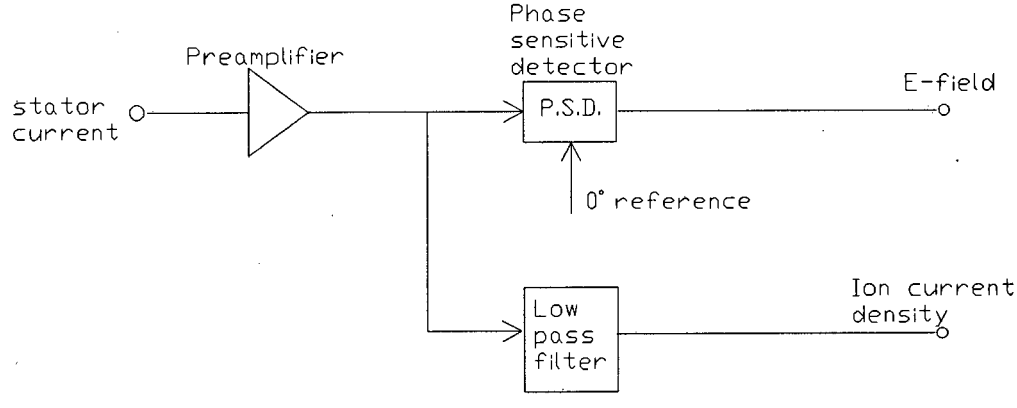

Fig.5.5 Low pass filter used to extract $i_i(t)$

5.4 Simultaneous measurement of electric field and ion current density in the literature

The idea of measuring both quantities simultaneously with a single field mill is not new, and has been mentioned by three authors at least:

5.4.1 Wildman [6] — METHOD I

Wildman constructed an electric field mill to measure electric fields, for use on a rocket or satellite at altitudes of 30km and above. In the upper atmosphere, the ion currents reaching the stator of the field mill are much higher than those normally measured at ground level. Wildman did not use synchronous detection, so that the ion current was a significant source of error in the electric field measurement. Measurements at two different modulating frequencies were used to extract $i_e(t)$ and $i_j(t)$. In order to make measurements at two different frequencies, Wildman used two separate stators: each stator was a set of circular discs mounted around the circumference of a circle. The two circles were concentric, so that there was an inner ring of stator discs and also an outer ring, both lying in the same plane. The outer set of stator discs had a greater number of discs, so that the modulating frequency was higher for the outer stator set. This arrangement enabled simultaneous measurement of the stator current signal at two different frequencies, and this was followed by numerical analysis of the readings.

5.4.2 Sheahen [7] — METHOD II

Sheahen used an electric field mill to measure the electric field at the base of a series of space vehicles as they passed through the ionosphere and re-entered the atmosphere. The range of altitudes was from 70 to 100km. Synchronous detection with both an in-phase and a quadrature reference signal was used to separate the components $i_e(t)$ and $i_j(t)$ of the stator current. As with the apparatus of Wildman, Sheahen was experiencing much larger ion currents in the upper atmosphere than are generally found in ground-level measurements.

5.4.3 Maruvada [8] — METHOD III

For measurements of electric field and ion current density under HVDC transmission lines, Maruvada used a low pass filter to separate the ion current signal, and synchronous detection to separate the electric field signal.

It is interesting to note that in a more recent paper describing electric field and ion current density measurement, Maruvada did not use the single field mill that could measure both quantities simultaneously [9]. Instead, he used an electric field mill to measure electric field strength, and a Wilson Plate to measure ion current density. This arouses some curiosity about the single field mill, developed earlier by Dr. Maruvada [8]. Why was this single field mill, capable of measuring both electric field strength and ion current density simultaneously, not used in recent measurements? This question was discussed in a private communication with Dr. Nguyen, (a colleague of Dr. Maruvada). It was explained that the single field mill was more expensive to manufacture, required more delicate insulation, and required more maintenance than the combination of a conventional field mill and Wilson Plate. The final comment was "In summary, the single field mill is very challenging in terms of design and construction, but not economically justified" [10].

5.5 Conclusion

The construction of a single field mill capable of measuring both electric field and ion current density simultaneously was seen as a challenge for this thesis. Many electric field mills have been developed for measuring electric fields alone, but few for the measurement of both quantities.

5.6 References

[1] Chubb, J.
"Developments in electrostatic fieldmeter instrumentation"
Journal of Electrostatics Vol.14 (1983) pg.349-358

[2] IEEE Standard 1227-1990
IEEE Guide for the Measurement of DC Electric-Field Strength and Ion Related Quantities
December 1990

[3] Israel, H.
"Atmospheric Electricity"
pg. 594 - 601

[4] Bracken, T. Capon, A. Montgomery, D.
"Ground level electric fields and ion currents on the Celilo-Sylmar +/- 400kV DC Intertie"
IEEE Trans. Power Apparatus & Systems
Vol.97 April 1978 pg.370-378

[5] Chartier, V.
"Performance of a long-term unattended station for measuring DC fields and air ions from an operating HVDC line"
IEEE Trans. Power Delivery
Vol.4 No.2 April 1989 pg.1318-1328

[6] Wildman, P.J.L.
"A device for measuring electric field in the presence of ionisation"
J. Atmospheric and Terrestrial Physics
Vol. 27 1965 pg. 417 - 423

[7] Sheahen, T.P.
"Model of response of an electric field mill operating during suborbital flight"
Review of Scientific Instruments
Vol. 45 February 1974 pg. 171 - 177

[8] Maruvada, P.S. Dallaire, R.D. Pedneault, R.
"Development of field-mill instruments for ground-level and above-ground electric field measurement under HVDC transmission lines"
IEEE Trans. Power Apparatus & Systems
Vol. 102March 1983 pg. 738 - 744

[9] Maruvada, P.S. Nguyen, D.H.
"An exposure chamber for studies on human perception of DC electric fields and ions"
IEEE Trans. Power Delivery
Vol.9 No.4 1994 pg.2037-2045

[10] Nguyen, D.H.
Private communication to M.Sellars
February 1995
See Appendix D

6. Construction and Design of an Electric Field Mill

6.1 Physical Construction of the Electric Field Mill

The diagram below is a scale drawing of the physical construction of the electric field mill that was built for this thesis. See Appendix E for photographs of the electric field mill.

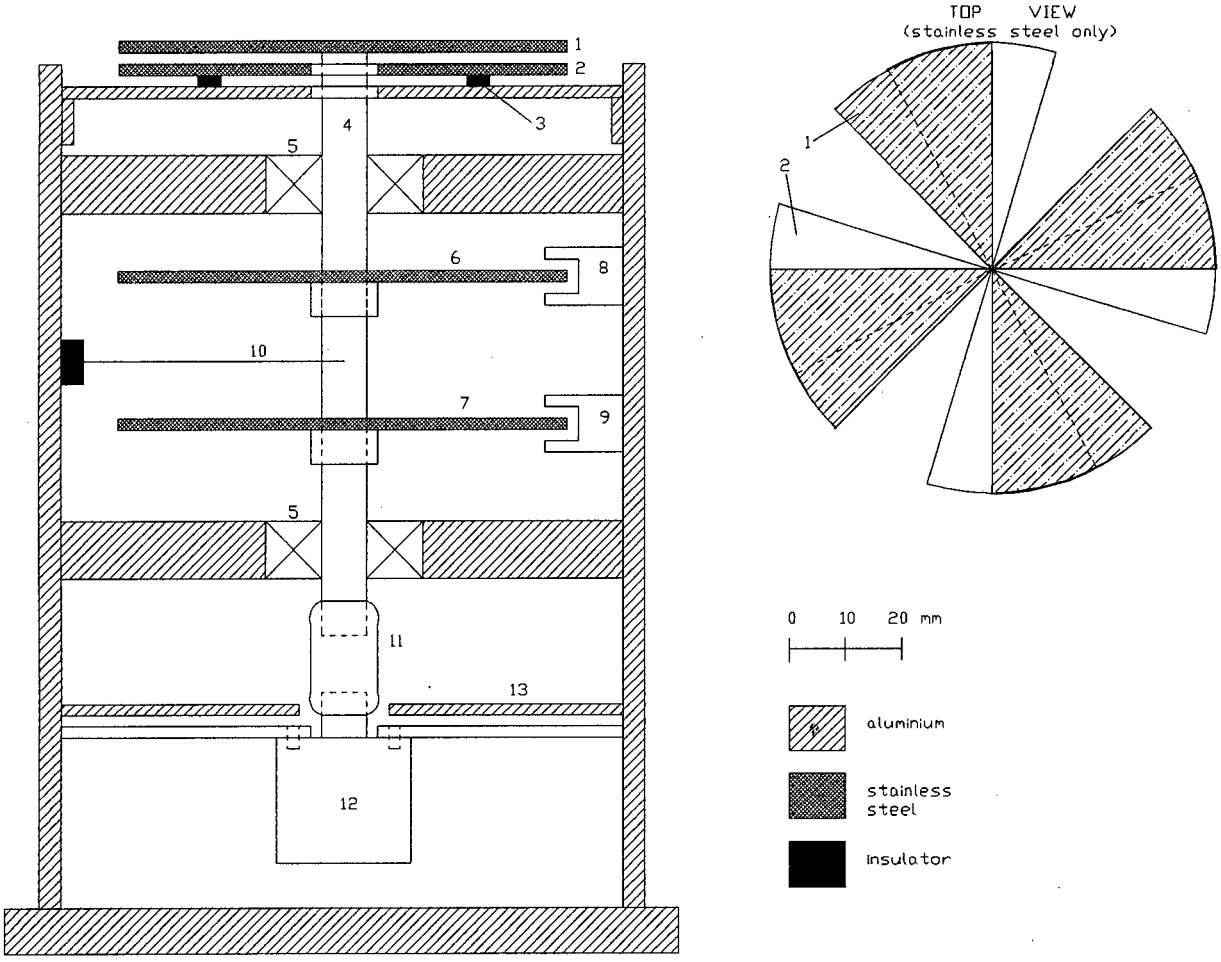

Fig.6.1 Construction of an electric field mill

KEY	
1. Rotor	(stainless steel)
2. Stator	(stainless steel)
3. Insulator	(Teflon)
4. Shaft	(silver steel)
5. Ball bearings	
6. Reference rotor (1)	(stainless steel)
7. Reference rotor (2)	(stainless steel)
8. Optical switch (1)	
9. Optical switch (2)	
10. Earthing brush	(gold wire)
11. Drive coupling	(rubber)
12. D.C. motor	
13. Motor screen	(aluminium)

6.2 Design of stator and rotor

6.2.1 Shape of vanes

The vanes (or blades) of the rotor and stator may have a number of different shapes. The three main shapes discussed in the literature are:

(a) Sector stator, with sector rotor
(b) Bernoulli lemniscate stator, with sector rotor
(c) Stator made from circular plates, rotor has circular holes

These three main types are illustrated below:

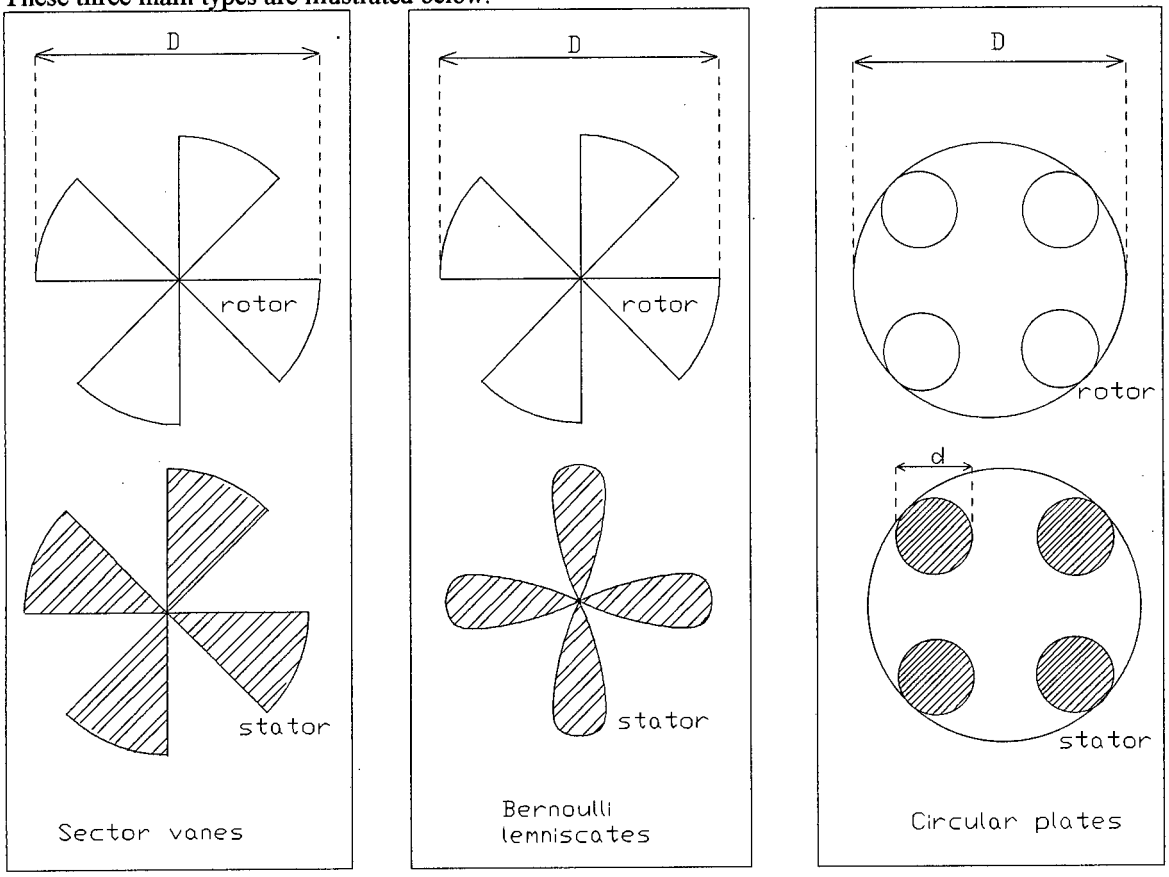

(a) (b) (c)

Fig.6.2 Rotor-stator pairs of different shapes

There are several considerations to bear in mind when examining different shapes of stator and rotor:

1. Harmonic content of the stator signal.
2. Effective stator area should be maximised, to maximise signal magnitude.
3. Vanes should be reasonably easy to manufacture from metal plate.

6.2.1.1 Harmonic content of stator signal

With a sector stator and sector rotor, as in Fig.6.2(a), the exposed area of the stator varies as a triangular waveform as the rotor spins [1]. This means that there is considerable harmonic content in the stator signal. With the stator made from Bernoulli lemniscates, as in Fig.6.2(b), the exposed area of the stator varies as a sinusoidal wave. This means that there are theoretically no harmonics above the fundamental frequency [2]. Schwab [4] says that shaping the vanes in the form of Bernoulli lemniscates should theoretically give a perfectly sinusoidal signal. He also states that in practice, there is still some harmonic content from minor fringing fields, since the rotor and stator are located in different planes. With the stator made from circular plates, as in Fig.6.2(c), the exposed stator area varies only approximately as a sinusoidal wave, so that some harmonics will be present [3].

When using synchronous detection to narrow the measurement bandwidth, odd harmonics of the signal frequency will also be detected. This is because the synchronous detector effectively multiplies the stator signal by a square wave, which contains odd harmonics of the signal frequency, and so any signal components which lie at frequencies that are odd harmonics of the signal fundamental frequency will pass into the synchronous detector passband [32]. Thus, if synchronous detection is to be used for signal recovery, then any harmonic content in the stator signal will increase the signal-to-noise ratio.

To give some idea of the harmonic content of the stator signal with sector rotor and stator, the field mill was set up in an electrostatic field of 10kV/m, and the preamplifier output displayed on a spectrum analyser. The spectrum analyser trace below illustrates the presence of harmonics in the preamplifier output signal:

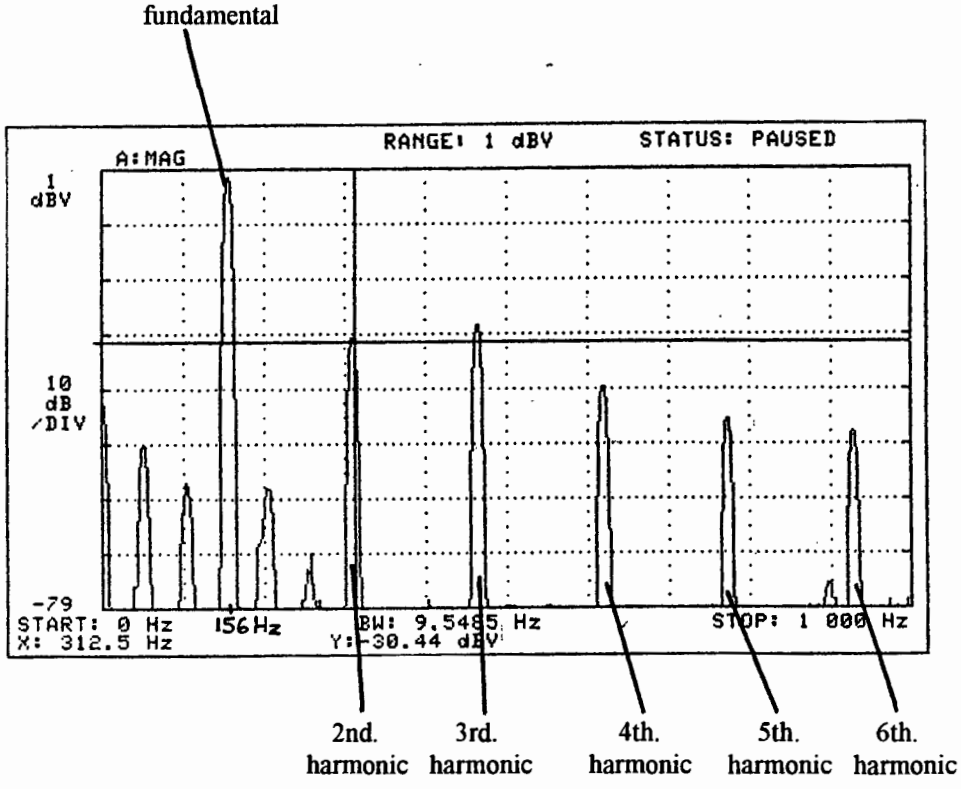

Fig. 6.3 Spectrum Analyser Trace of Preamplifier Output Signal

From the spectrum analyser trace, it is seen that the second and third harmonics are relatively large (being about 30dB below the fundamental at f=156Hz). Higher harmonics are 40dB and lower below the fundamental, so that they can be neglected.

6.2.1.2 Exposed stator area

The maximum exposed stator area determines the magnitude of the peak stator current (see chapter 3). Thus the greater the exposed area, the larger the signal-to-noise ratio. For a given diameter of field mill aperture (shown as D in Fig.6.2), it can be shown that the maximum exposed stator areas are:

(a) Sector vanes: $Area_{max} = {}^1/_2\pi R^2$ ..... **(6.1)**

(b) Bernoulli lemniscate vanes: $Area_{max} = R^2$ ..... **(6.2)**

(c) Circular stator plates: $Area_{max} = 4\pi r^2$ ..... **(6.3)**

where: R = D/2 = radius of large stator plate (field mill aperture) as in Fig.6.2(a) and in Fig.6.2(b).
r = d/2 = radius of each small circular stator plate as in Fig.6.2(c).

A simple program was written using Turbo C++ to plot the variation in exposed stator area as the rotor spins, for the different rotor-stator pairs. (The program source code is given in Appendix B). For the rotor-stator pairs (a), (b), (c) shown in Fig.6.2, the variations in exposed stator area at constant rotational frequency are plotted in Fig.6.4 below. It can be seen from this graph that the maximum exposed area for a sector stator (a) is greater than that of both a lemniscate stator (b), and a stator made of circular plates (c).

Note that for purposes of comparison:

d = 1.00cm = diameter of circular stator plate
D = 7.23cm = diameter of field mill aperture
ω = 1 $rads^{-1}$ = rotational frequency

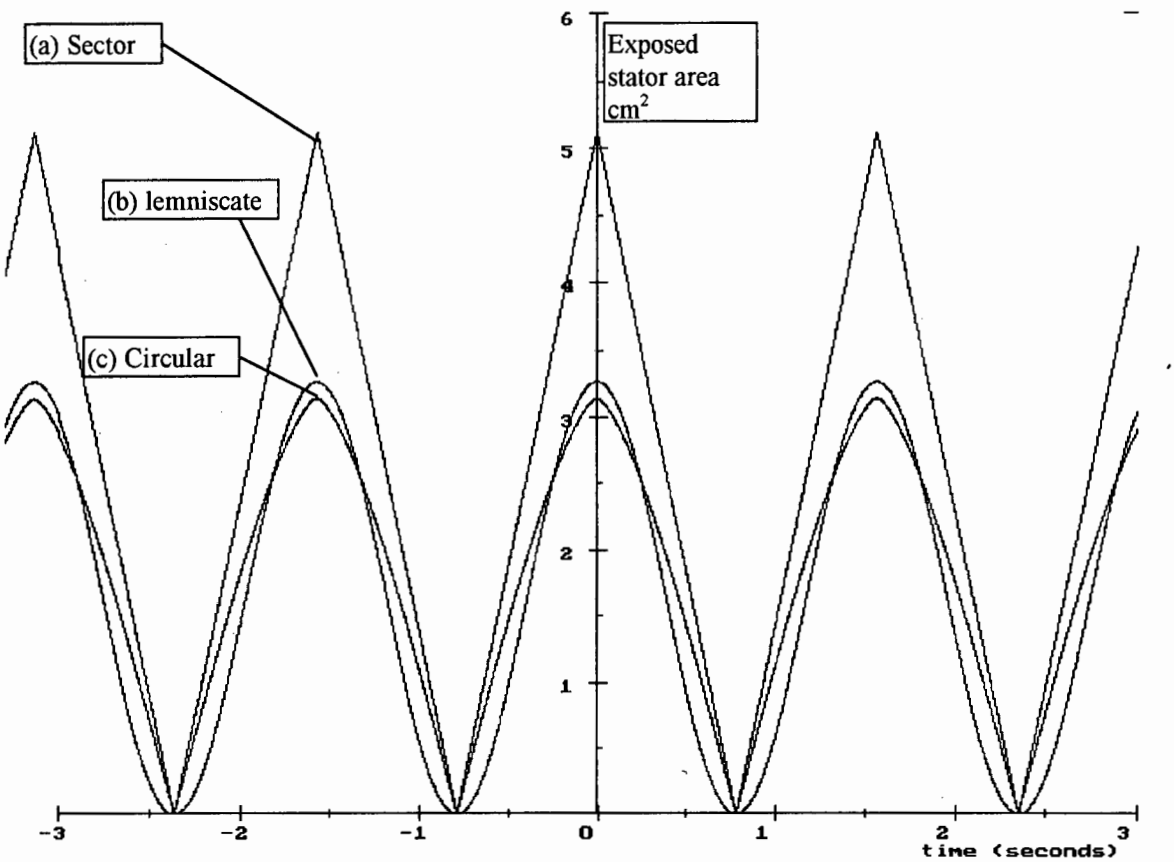

Fig.6.4 Variation of exposed stator area as rotor spins for rotor-stator pairs of Fig.6.2

Van Atta [5] used Bernoulli lemniscates to reduce harmonics of the fundamental frequency, but admitted that this reduced the effective area of the stator by $\pi/2$ compared to using a sector shape, as shown in Fig.6.4(b). Castle [21] used circular stator plates for simplicity and ease of construction. He states that this gives a waveform that is approximately sinusoidal, as shown in Fig.6.4(c).

6.2.1.3 Ease of manufacture

Both the sector blades and the circular stator plates are reasonably easy to manufacture from metal plate. The Bernoulli lemniscates are somewhat more difficult to manufacture due to their complex shape. (Here the aim was to achieve precision machining of the rotor and stator at a reasonably low cost). Dahl [1] states that "a sector-shaped rotor-stator pair is the simplest solution from a design point of view", and that "little can be gained by other shapes".

6.2.1.4 Conclusion

If synchronous detection is to be used, then harmonics of the signal frequency are not a significant problem (in fact harmonics may actually improve the signal-to-noise ratio). Sector vanes are preferred to other shapes because they are easy to manufacture, and also because they maximise the exposed area of the stator.

6.2.2 Flutter of rotor vanes

It has been observed by Sheahen that the blades of the rotor may flutter at the outer edges as the rotor spins [22]. This will produce noise since the distance between the rotor and stator will vary. Smith [23] recommends that the rotor blades should have an outer ring, so that flutter is avoided. This design of rotor is shown in the diagram below:

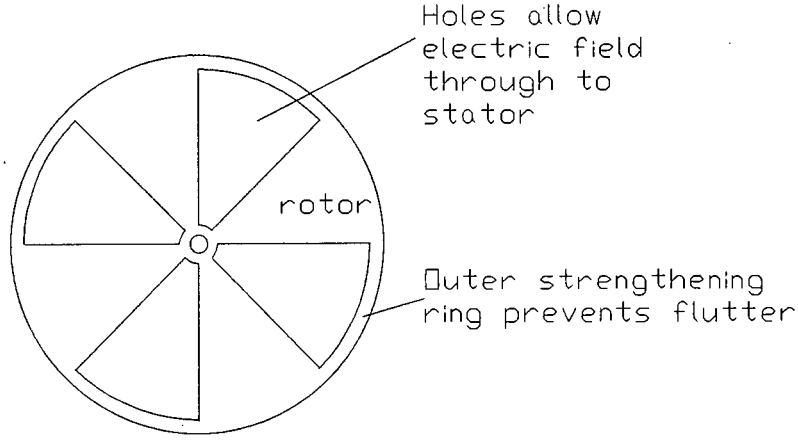

Fig.6.5 Outer ring on the rotor prevents flutter of vanes

For the purposes of this thesis, ease of manufacture of the vanes was an important consideration. The rotor design in the diagram above is not easy to machine from metal plate, unless a special cutting tool is made. Thus the above rotor design was not considered to be feasible for this thesis. The final rotor was machined from 2mm-thick stainless steel plate, which was considered to have sufficient rigidity so that flutter of the blades would not be a significant source of error.

6.2.3 Materials used for stator and rotor

A major source of noise in the field mill instrument is caused by contact potential differences between the rotor and stator surfaces (discussed in Chapter 3.8.1). This produces a signal which is at the same frequency as the signal that is due to the external electrical field, and which makes up part of the stator signal. The choice of materials for the rotor and stator is primarily based on contact potential considerations.

Kessler [6] notes that it is preferable to use the same metal for both stator and rotor, in order to reduce the contact potential difference between the rotor and stator surfaces.

In order to reduce fluctuations in contact potential difference between the rotor and stator surfaces, these metal surfaces must not become contaminated. (This may occur due to oxidation of the metal, or due to particles of dirt settling on the metal surface). Chubb [7] recommends gold-plating of all sensing surfaces in order to keep them chemically stable and clean. Should gold-plating be too expensive, Chubb suggests the use of either stainless steel or nickel plate for the rotor and stator [8]. In his 1994 patent, Stewart uses Type 316 stainless steel for both rotor and stator [9]. Also, the stainless steel surfaces are highly polished and buffed, in order to produce a smooth, mirror-like finish. This prevents dust particles from adhering to the stator and rotor surfaces. Yeboah-Amankwah used a rotor-stator pair made from aluminium plate, but states that uneven aging and oxidation of different parts of the aluminium surfaces could produce contact potential differences which might interfere with the field mill signal. He recommends stainless steel in place of aluminium for more reliable field mill performance over long periods of operation [10]. Mapleson and Whitlock [13] experienced problems with varying contact potentials when using rotor-stator pairs made from brass and aluminium. They found that the use of nickel-plated and also of chrome-plated surfaces reduced the contact potential noise significantly.

The first prototype field mill constructed for this thesis had a rotor-stator pair made from aluminium plate. The aluminium plate was used mainly because of its easy machinability (the stator and rotor were cut out using a bandsaw). These plates functioned well, but the tolerance of the vanes was only +/- 1mm. It was difficult to predict how much error these variations in the shape of the vanes would introduce into the field mill measurements. Also the aluminium vanes were easily bent when working on the mill (due to the low tensile strength of the aluminium). Another problem was the difficulty of soldering the pickup wire onto the aluminium stator surface. Standard electrical solder does not adhere to the aluminium, and it was necessary to use specialised solder wire and flux [14]. This specialised solder is relatively expensive (about R100 for 250g). Accordingly, it was decided to manufacture a new rotor-stator pair out of stainless steel, and to ensure much tighter tolerances on the shape of the vanes. The final field mill prototype had vanes machined from 2mm-thick stainless steel plate (Type K460) using a computerised milling machine. The tolerance of the vanes was +/- 0.05mm.

6.2.4 Number of blades on the rotor and stator

The number of blades (vanes), n, on the rotor and stator determines the frequency of the field mill output signal, f. By increasing the number of blades, n, the frequency may be increased:

$$f = nf_{motor} \quad \text{(6.4)}$$

where: f = signal frequency or "chopping frequency"
n = number of blades on rotor and stator
f_{motor} = rotational frequency of motor shaft

Thus, increasing the signal frequency may be accomplished either by increasing the rotational speed of the motor, or by increasing the number of blades on the rotor-stator pair. (Note: the phrase "n blades on the rotor-stator pair", means n blades on the rotor and n blades on the stator).

When measuring very low-strength electric fields, there may be significant 50Hz pickup. Where this is a problem, it may be necessary to shift the signal frequency well above the frequency of the interfering noise (a frequency of 2kHz is sufficiently high above the 50Hz noise frequency in most cases) [11]. Also, if the field mill is required to have a fast response time (say a few milliseconds), then it is necessary to use a higher signal frequency than the 200Hz maximum usually used for electric field mill systems.

It is not advisable to run the mill at very high speeds (shaft frequencies above 100 Hz, or above 6000 rpm) as this causes the earthing brush to bounce on the shaft, so increasing electrical noise. Furthermore, the earthing brush wears more quickly at high speeds [7]. In battery-powered field mills, brush drag limits the motor speed. Thus, increasing the number of blades on the rotor and stator provides a convenient method of increasing the signal frequency, should this be necessary. The table below shows different signal frequencies obtained in some commercial field mill instruments [7].

Table 6.1 Different signal frequencies obtained by varying the number of rotor blades

Electric field mill type	Number of rotor blades (n)	Motor speed (f_{motor})	Signal frequency (f)
Standard field mill	4	50 Hz	200 Hz
Fast response field mill	20	100 Hz	2000 Hz

For this thesis, only DC electric fields were to be measured, and 50Hz pickup was not found to be a significant source of noise. A rotor-stator pair having 4 blades, and producing a signal frequency of 150 Hz, was found to be satisfactory. (Actually, the frequency ranged from 145 - 155 Hz due to variations in motor speed). Due to time constraints, and limited access to the computerised lathe, it was not possible to experiment with different numbers of blades on the rotor-stator pair.

6.2.5 The use of grounded guard vanes

In some papers written on electric field mills, the authors show a set of grounded guard vanes which are inserted in-between the stator vanes [11], [12]. (The guard vanes do not touch the stator vanes). The purpose of these guard vanes is to reduce fringing fields at the edges of the stator vanes [24], but very little is said in the literature on this point. An example of guard vanes inserted between the stator vanes is shown below:

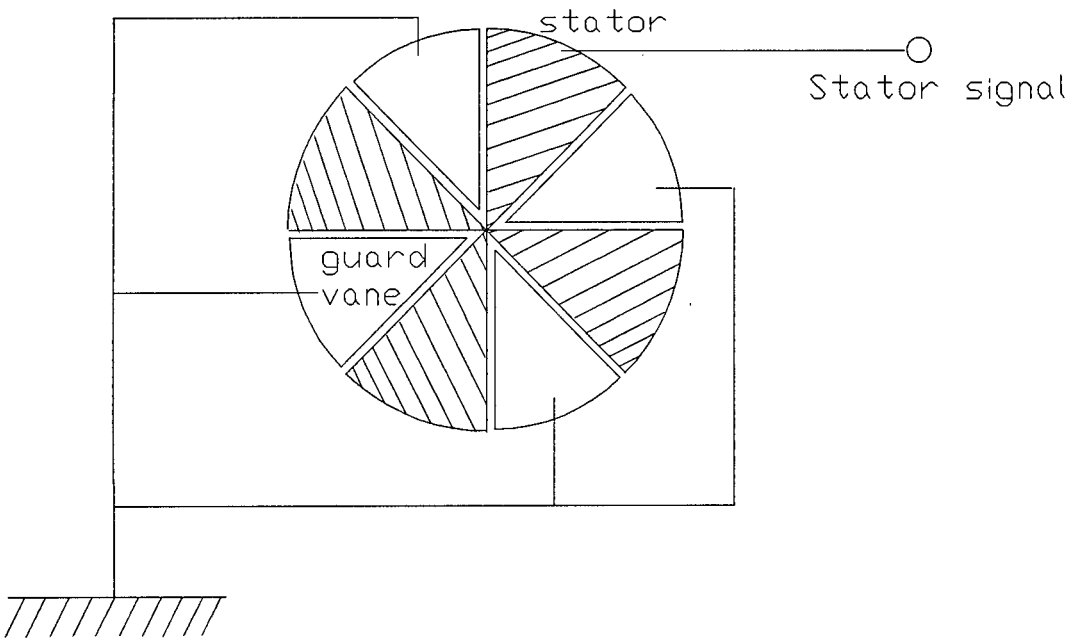

Fig.6.6 Grounded guard vanes inserted in-between the stator vanes

6.2.5.1 Investigating the effect of grounded guard vanes

To investigate the effect of the grounded guard vanes on the fringing fields, the following experiment was conducted. The field mill was set up in the ground-plane aperture of a parallel-plate apparatus (as for electric field calibration in Chapter 3.7). A 1kHz sine-wave of amplitude 10V (peak-peak) was applied to the top plate. Instead of using the motor to turn the field mill rotor, the rotor was turned by hand. The preamplifier output voltage was taken at different positions of the rotor in its path over the stator. The experiment was conducted for two field mill configurations:

(a) Stator without grounded guard vanes.
(b) Stator with grounded guard vanes.

A schematic diagram of the apparatus is shown below:

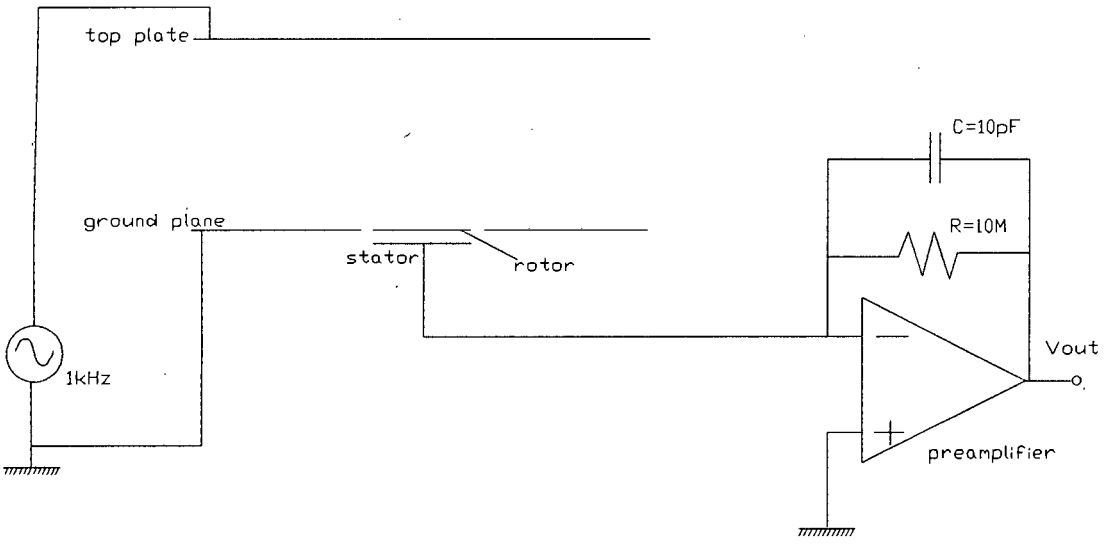

Fig.6.7 Apparatus for investigating the effect of fringing fields

The results of the experiment are displayed in the graph below. The graph shows the peak-peak output voltage (V_{out}) measured at the preamplifier output for different rotation angles of the rotor.

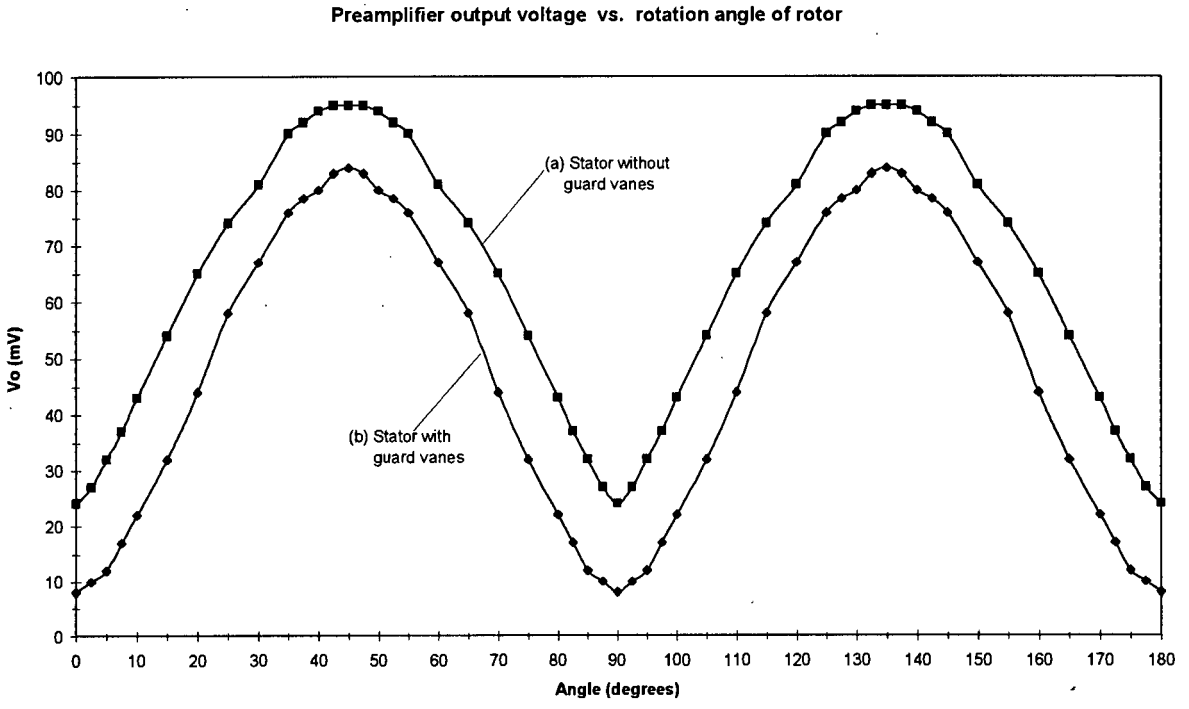

Fig.6.8 Graph showing output voltage vs. rotation angle of stator

The graph shown above is effectively a plot of the variation of effective stator area with time, as the rotor spins. The curve (a) for the stator without guard vanes shows a flat portion at the peak of the curve only. The curve (b) for the stator with guard vanes shows a flat portion at both the peak and trough of the curve.

6.2.5.2 Effect of the guard vanes on the stator signal

The variation in the effective stator area as the rotor spins will determine the waveform of the current that flows in the stator. The diagram below illustrates these effects, using waveforms similar to those observed in Fig.6.8(a) and Fig.6.8(b) for the effective exposed stator area.

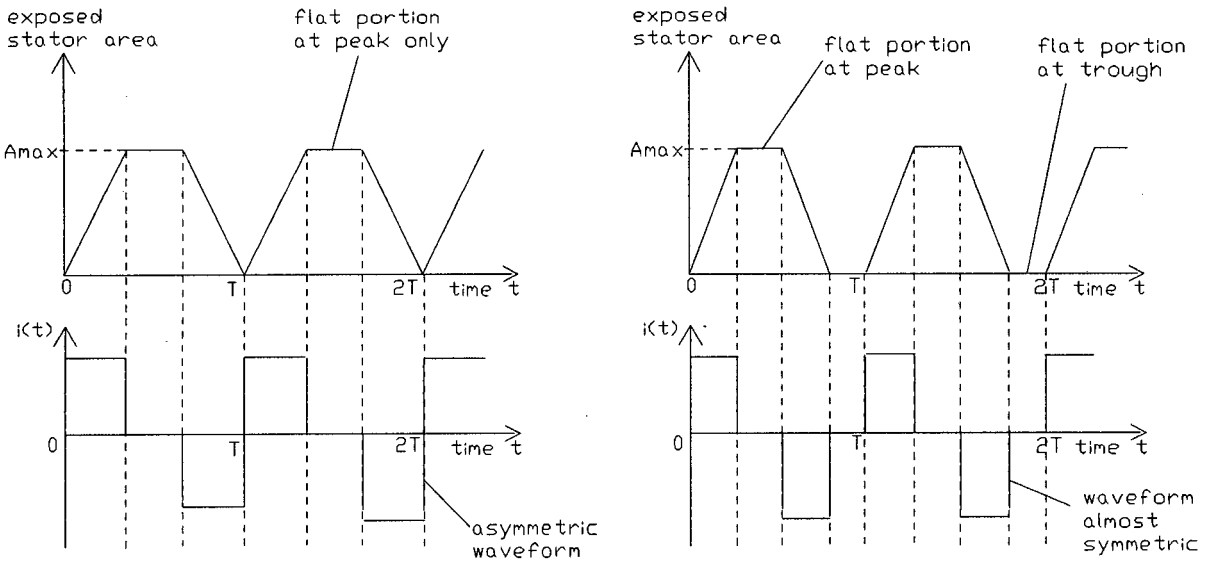

(a) Stator waveform without guard vanes (b) Stator waveforms with guard vanes

Fig.6.9 The effect of grounded guard vanes on the stator signal

As shown in Fig.6.9(a), the stator without guard vanes has a stator current i(t) that has odd symmetry. (By this we mean that the rise-time of the waveform is more rapid than the fall-time). The stator current i(t) with guard vanes, shown in Fig.6.9(b), is more symmetric than that of Fig.6.9(a). This is because of the reduction in fringing fields by the guard vanes, so that the effective stator area has a flat portion at both the peaks and troughs of the waveform.

6.2.5.3 Observations of the effect of the guard vanes

The effect of using grounded guard vanes was investigated by running the field mill in an applied electric field of 15kV/m. The first trace, Fig.6.10(a), shows the field mill ouput without the grounded guard vanes attached. The output waveform is asymmetric (the rise-time is shorter than the fall-time). The second trace, Fig.6.10(b), shows the field mill output with grounded guard vanes attached. The output waveform is markedly more symmetric.

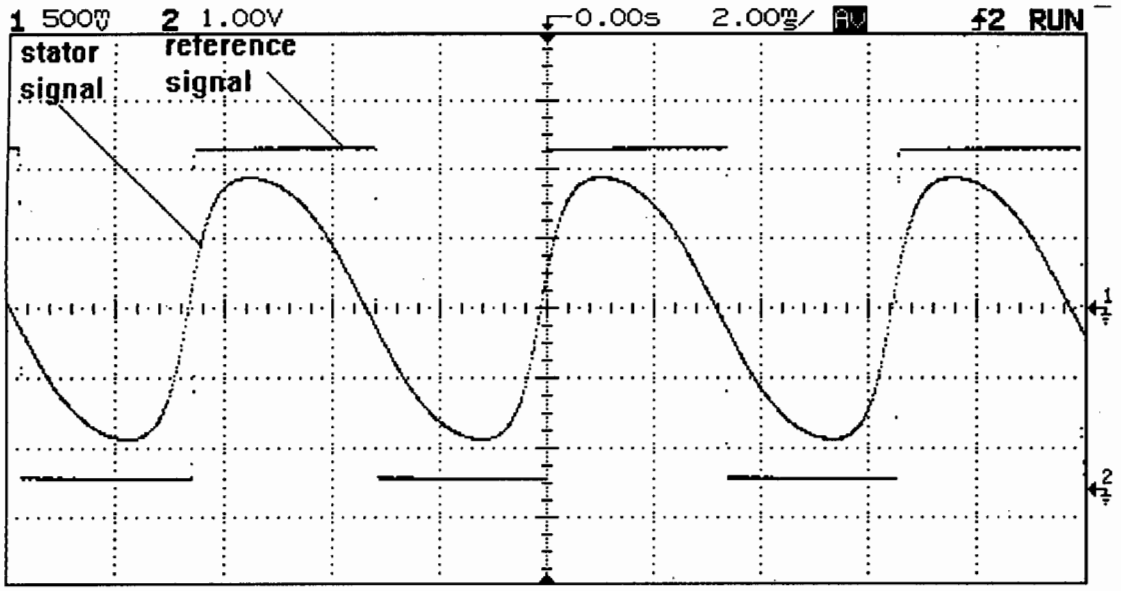

Fig.6.10(a) Field mill output with no grounded guard vanes

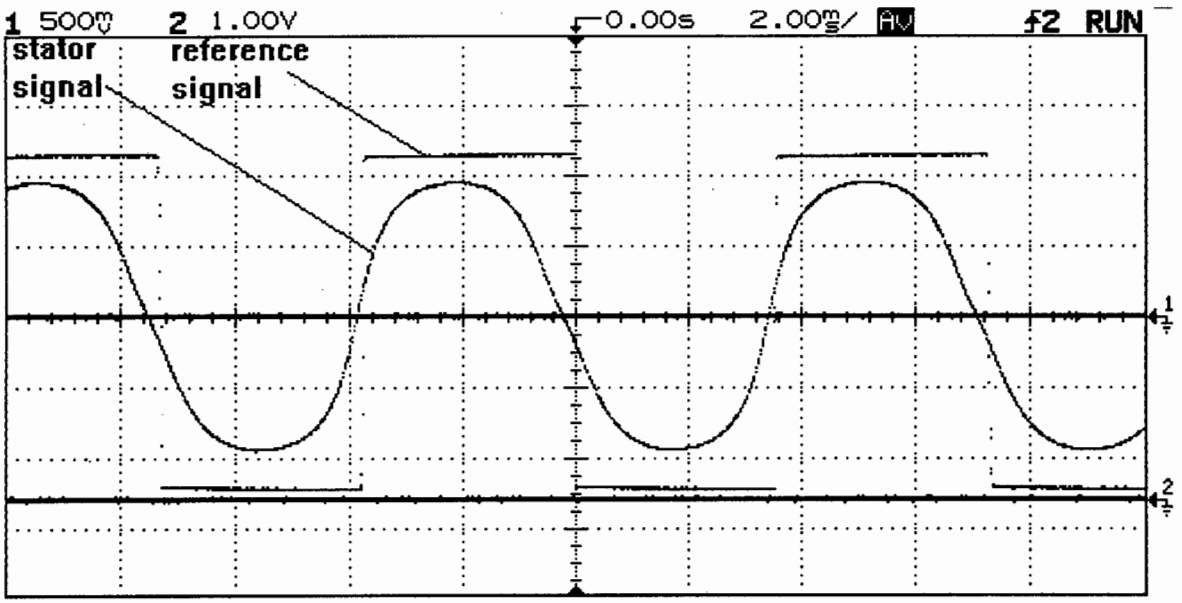

Fig.6.10(b) Field mill output with grounded guard vanes attached

It is postulated that without the grounded guard vanes, fringing fields have the effect of reducing the effective area of the rotor blades, so that the stator blades are continuously exposed to the external field for short periods during the rotor's path across the stator. This would then cause the field mill output to be asymmetric. Yeboah-Amankwah [10] shows an asymmetric waveform almost identical to that of Fig.6.10(a) in his electric field mill documentation, but he does not comment on the asymmetry. (His field mill does not have grounded guard vanes). The grounded guard vanes reduce the fringing fields, and so the waveform in Fig.6.10(b) is more symmetric than that of Fig.6.10(a). Similar results are shown by two other researchers [24], [25].

6.2.6 Rotor-stator gap

The separation between the rotor and the stator influences both the field mill sensitivity, and the spurious electric field signal. (The spurious signal is due to contact potential differences). The diagram below illustrates the separation gap, d, between the rotor and stator:

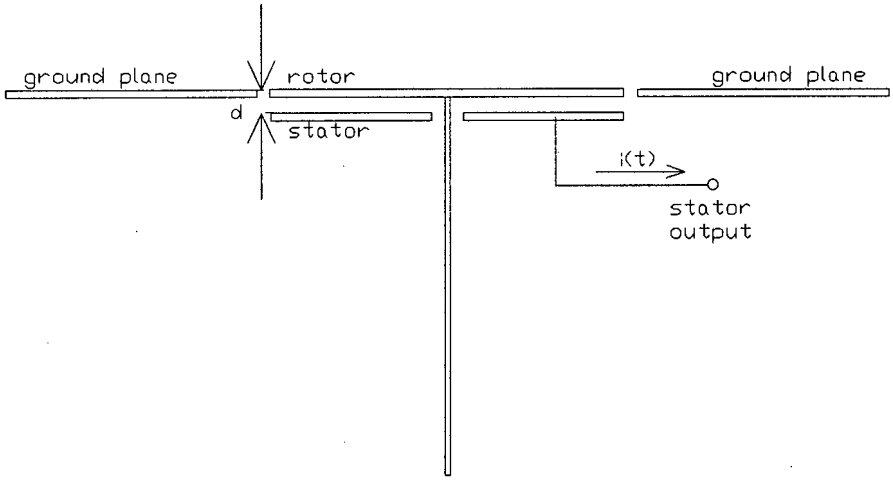

Fig.6.11 Rotor-stator gap, d

As shown in Fig.6.11, by increasing the rotor-stator gap (d), the depth of recession of the stator behind the ground plane is also increased. This means that increasing the gap d:

1. Reduces the magnitude of the spurious signal, since the rotor-stator capacitance is now reduced.

2. Reduces the sensitivity of the field mill to the external electric field, since the electric field lines start to diverge as they progress further below the ground plane. [17]

To investigate this effect further, a series of measurements was taken for different values of the rotor-stator gap, d. Results of these measurements are shown in the following graphs. The first graph shows the peak-peak magnitude of the spurious electric field signal at the preamplifier output:

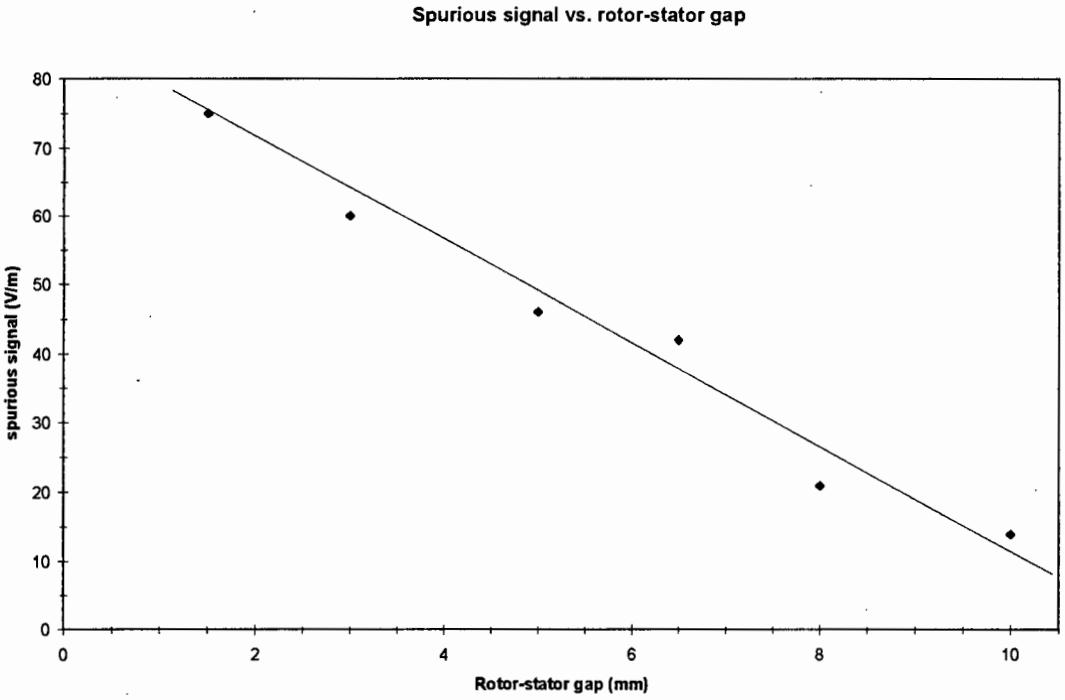

Fig.6.12 Effect of rotor-stator gap, d, on the spurious signal

In Fig.6.12, the spurious signal is expressed as an equivalent spurious electric field for different values of the rotor-stator gap, in a zero electric field. (Note that for these measurements, no nulling or bucking of the contact potential difference was used). From this graph, it is seen that if steps are not taken to null out the spurious electric field signal, then it becomes a significant source of error, particularly for small values of the rotor-stator gap.

Rossi has made numerous measurements of contact potential differences between the surfaces of two metals in close proximity. He notes that as the gap between the metal surfaces increases, the contact potential remains roughly constant. This is to be expected since the contact potential difference is given simply by the difference in the work functions of the two surfaces. In his measurements of contact potential, Rossi used gap distances from 0.1mm up to 1mm [34].

Chubb [15] recommends that in order to reduce the effects of spurious electric field signals due to contact potentials, the stator and rotor should be separated by a relatively large gap (so reducing the rotor-stator capacitance). Chubb does not use any nulling method to reduce the contact potential difference, and so this is the only option left available to him. His justification for not nulling the contact potential difference is that in some industrial applications, where there are large amounts of charged particles and dust present, the contact potentials may vary significantly with time (due to surface contamination of the rotor and stator), so that nulling of the contact potential difference is not feasible. This occurs, for example, when studying electrostatic effects in the transport and handling of highly-insulating powders, such as high density polyethylene. Wildman [26] notes that it is more usual to null out any spurious electric field signal with a bucking voltage.

The graph below shows the electric field mill output for different values of applied electric field strength using different rotor-stator gaps. The measurements represent the peak-peak magnitude of the electric field signal at the output of the preamplifier.

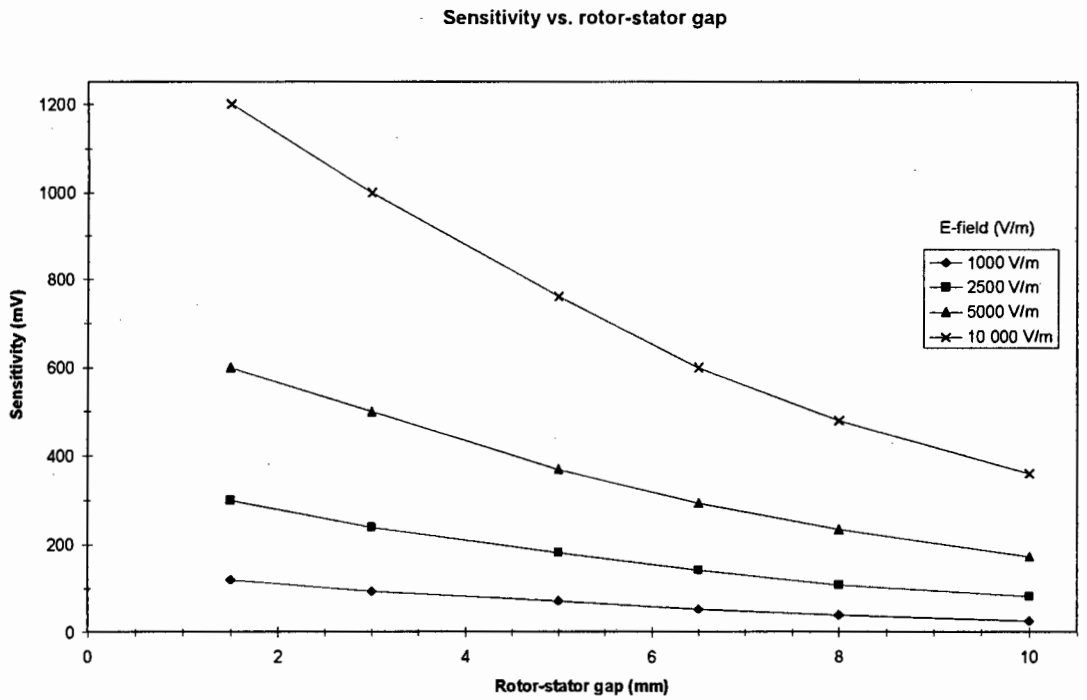

Fig.6.13 Relative sensitivities for different rotor-stator gaps

Fig.6.13 shows how increasing the rotor-stator gap causes a reduction in sensitivity of the field mill output signal. Note that the sensitivities are expressed in mV only and not as electric field strength values. From this graph it can be seen that for maximum sensitivity, the rotor-stator gap must be made as small as possible.

Knott [16] used an elaborate field mill which had a stator plate that was made to shift alternately between two different settings of rotor-stator gap. Readings of electric field strength were taken at each position, and the spurious electric field signal removed using numerical analysis of the results. It was felt that the added complexity of the apparatus needed to shift the stator plate backwards and forwards was not justified as the spurious electrical field signal may be nulled simply and conveniently with a bucking voltage applied to either the rotor or to the stator. This is described in Chapter 7.2.

Many of the papers on electric field mills described the rotor-stator gap as being only a few millimetres wide. The smallest gap used was 1mm (Mapleson & Whitlock [13]). The largest gap used was 18mm (Gathman [17]). See Appendix A for a listing of the rotor-stator gaps used in the literature.

Discussion

For the purposes of this thesis, it is assumed that the contact potentials do not vary significantly with time, so that the contact potentials may be nulled out using a bucking voltage. This means that the smallest convenient rotor-stator gap should be used, so as to maximise the field mill sensitivity. The rotor-stator gap used for calibration purposes was 1.5mm. However, the field mill was designed with an adjustable rotor-stator spacing, so that the spacing may easily be increased, should this be necessary. If the rotor-stator spacing were to be adjusted, the field mill would need to be recalibrated.

6.2.7 Stator insulators

It is necessary for the stator to be supported on insulators, so that it is not in electrical contact with the body of the field mill. In the design of electric field mills, it is necessary that all insulating materials should be screened from external electric fields by conducting surfaces. If insulating surfaces are exposed to external electric fields, they may become charged, and so affect the field mill readings [13]. Wildman used stators mounted on a large sheet of Kel-F insulator, but found that charge trapped on the surface of the Kel-F produced a large zero-error. This was greatly reduced by covering the exposed Kel-F with a metal sheet [26]. Bob Pease notes that Teflon surfaces used in sensitive charge-measurement circuits should be kept as small as possible, and shielded by conducting surfaces, to prevent charge buildup on the Teflon [33]. In the field mill built for this thesis, small insulating Teflon squares were placed below the stator vanes, in such a way that they were completely covered by the vanes. The diagram below shows the positioning of the stator insulators:

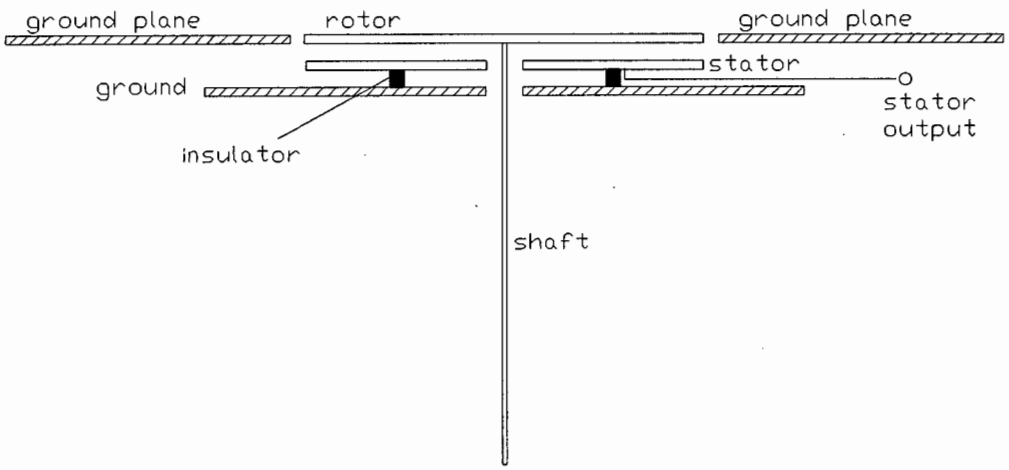

Fig.6.14 Diagram of field mill showing insulators supporting the stator

Ideally, insulators used in systems where very small currents are to be measured should have a high volume resistivity in order to prevent leakage currents. The insulators should also be resistant to water absorption, so that humid conditions do not degrade their insulating properties. There are a number of possible materials that may be used for the insulators. These are listed in Table 6.2 below.

Table 6.2 Properties of various insulating materials [18]

Material	Volume resistivity (Ohm-cm)	Resistance to water absorption	Price and availability
Teflon PTFE	$> 10^{18}$	Very good	Expensive Readily available
Kel-F	$> 10^{18}$	Very good	Very expensive Difficult to obtain
Polystyrene	$> 10^{16}$	Reasonable	Cheap Readily available
Polyethylene	10^{16}	Reasonable	Cheap Readily available
Nylon	10^{13} to 10^{14}	Poor	Cheap Readily available

Teflon PTFE is the most satisfactory insulator for low-level current measurements above 10^{-14} A. It has a high volume resistivity, and water vapour films do not readily form on its surface [18]. Teflon insulators were used for the field mill built for this thesis. The stator was supported by four Teflon insulators, one underneath each vane. Each of these insulators was a small Teflon square measuring 5mm x 5mm x 3mm. These squares were small enough to be completely shielded by the stator vanes above them. Although Teflon is more expensive than polystyrene or polyethylene, it was considered that its superior insulating properties justified the extra cost. A sheet of Teflon measuring 200mm x 300mm x 3mm was purchased for R35 from Cape Plastics [19].

6.3 Earthing Brush

Effective earthing of the rotor is an important factor in achieving low noise and good long-term zero stability of electric field mills. For good noise performance, it is necessary to use a good-quality earthing brush to keep the rotor at earth potential. Both Cross [27] and Layton [28] state that earthing of the field mill shaft and rotor through the ball-bearings gives poor noise performance. The design of earthing brushes is a balance between earthing effectiveness, motor power, and long-term wear [29]. It has been found that simple cantilever spring wires of a precious metal alloy resting lightly on the metal shaft provide effective earthing [7]. It has been found by Chubb that phosphor-bronze earthing brushes produce high noise levels. Rhodium plating gives good noise performance, but unfortunately wears very quickly. Chubb recommends using hard gold spring wire of about 0.5mm diameter with 5g to 10g of spring pressure rubbing on the shaft. These spring wires usually last for about 4 months of continuous operation [8].

The first field mill prototype used a phosphor-bronze earthing brush. This was found to be satisfactory for preliminary experiments, but for measuring low electric fields the noise performance was poor. The final field mill prototype had an earthing brush made from 9-carat gold spring wire, with a diameter of 0.6mm, and length of 100mm. Although made of gold, the spring wire cost only R15 from a manufacturing jeweller [30]. Noise comparisons between the gold wire brush and phosphor-bronze earthing brush are described below.

6.3.1 Noise comparisons

This noise comparison is intended to be a qualitative guide to the choice of earthing brush material, and not a rigorous investigation. The field mill was operated with zero applied field for two periods of 5 hours each. In the first period, a phosphor-bronze earthing brush was used, and in the second period, a gold wire was used as the earthing brush. At intervals during the 5-hour periods, measurements were made of the electric field output of the mill. The field mill was placed between the parallel calibration plates with the top plate grounded, so as to prevent any external fields from influencing the measurements. The field mill was set to run with a modulation frequency of 150Hz (+/- 5Hz). The graph below illustrates the drift of the zero-electric-field-level over the 5-hour periods.

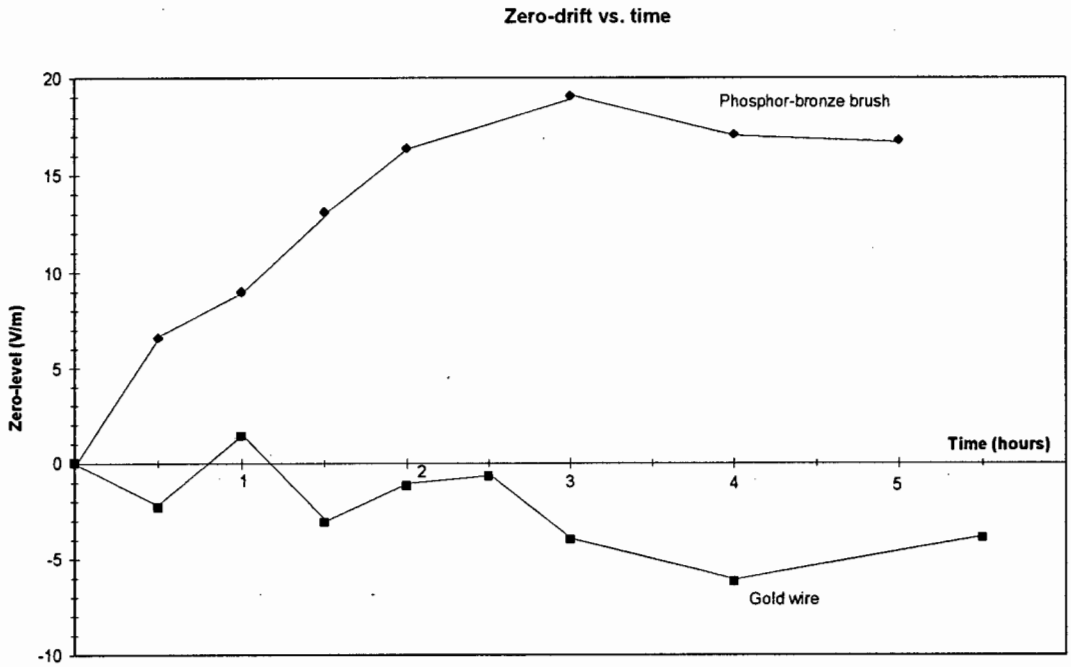

Fig.6.15 Drift of zero electric field with time

Note: each point on the graph in Fig.6.15 represents the average of 100 consecutive readings of the DC output voltage after synchronous detection (at the final output of the field mill), taken with an HP 34401A Multimeter. From the graph above, it can be seen that there is some zero-drift with both earthing brushes. However, the peak drift experienced with the phosphor-bronze brush was approximately double the drift observed with the gold wire. These results are meant to be qualitative only, since the noise produced by the brush will also depend on:

1. Spring pressure (how strongly the brush presses against the shaft).
2. Area of contact (surface area of the earthing brush in contact with the shaft).
3. Ambient temperature and humidity.
4. Condition of the air (presence and concentration of pollutants).

Observations of the earthing brushes

The phosphor-bronze brush quickly developed a black oxide layer in the region where it rubbed against the steel shaft. It was noted that as this oxide layer thickened, so the zero-drift increased, and the brush started to vibrate. At times, the vibrations become large enough in amplitude to cause the brush to bounce as the shaft rotated. A harsh rattling noise could be heard as the brush bounced on the shaft. This increased the drag on the motor, and the modulating frequency dropped significantly. The vibrations could be reduced by removing the brush and cleaning it.

The gold wire ran smoothly on the steel shaft, and at no time was brush bounce found to be a problem. Also, the drag on the motor was less than with the phosphor-bronze brush, (this was apparent from the more constant motor speed).

Conclusions

In general, the phosphor-bronze brush was found to be unsatisfactory for precision work. The gold wire earthing brush ran smoothly on the shaft, and caused less zero-drift of the field mill. Gold wire was therefore preferred for the earthing brush, and this view is supported by the great experience of Chubb [8].

Discussion

Reliable earthing of the rotor presents problems in instruments that are used for long-term electric field measurements, and in fast-response instruments having high rotor speeds. Chubb [7] has developed several new designs of field mill that do not require earthing of the rotor. These designs are more elaborate, requiring an extra rotor, and are unsuitable for ion current measurements. Also, the noise performance of these new designs is no better than the noise performance of the field mill with earthing brush. Thus it was considered that these designs, whilst useful in some applications, were not worth implementing for this thesis.

6.4 Type of motor used for the field mill

Most of the field mills described in the literature use either a synchronous motor or a DC motor to turn the field mill shaft (see Appendix A). If very high speed is required, an air turbine may be used.

For the purposes of this thesis, a 15-Watt, 12-Volt D.C. motor salvaged from a tape-recorder was used to drive the field mill shaft. The motor gave a satisfactory speed of 2500 rpm, which was reasonably constant (+/-5%). Provided that the preamplifier feedback impedance was mainly capacitive, so that the output signal was independent of frequency, small speed variations were not a significant source of error. However, the motor suffered from brush drag when the phosphor-bronze earthing brush was used, and at times this caused drops of up to 50% in motor speed. Fortunately these fluctuations were only intermittent, and the motor worked back up to full speed within about 20 seconds. For continuous monitoring of electric fields over long time periods, this would give unsatisfactory results. The drag of the gold wire earthing brush was much less than that of the phosphor-bronze brush, but even so, the motor suffered from variations in speed (+/-5Hz). High quality D.C. motors were available from Kopp Electronics at prices ranging from R500 up to R700 [31]. However, it was felt that for this thesis the cost was not justified.

6.5 References

[1] Dahl, H.
"On the sensitivity of generating electrostatic D.C. voltmeters"
Christian Michelsen Institutt,
Beretninger XIV, 3 (1951)
Christian Michelsen Research
P.O. Box 3 N-5036 Fantoft
Bergen, Norway

[2] Maruvada, P.S. Dallaire, R.D. Pedneault, R.
"Development of field-mill instruments for ground-level and above-ground electric field measurement under HVDC transmission lines"
IEEE Trans. Power Apparatus & Systems
Vol. 102March 1983 pg. 738 - 744

[3] Malan, D.J. Schonland, B.F.J.
"An electrostatic fluxmeter of short response-time"
Proc. Phys. Society
Vol. 63 1950 pg. 402 - 408

[4] Schwab
"High voltage measurement techniques"
pg.140 - 146

[5] Van Atta Northrup
"Round Hill electrostatic generator"
Phys. Rev. Vol. 49 (1936)
pg. 761 - 776

[6] Kessler, E.
"Instruments and Techniques for Thunderstorm Observation and Analysis"
University of Oklahoma Press
Chapter 8.

[7] Chubb, J.N.
"Two new designs of "field mill" type fieldmeters"
IEEE Trans. Industry Applications
Vol. 26 Nov/Dec 1990 pg. 1178-1181

[8] Chubb, J.N.
Personal Communication to M.Sellars,
University of Cape Town, 1995
See Appendix I

[9] Stewart, M.
United States Patent No. 05315232
1994

[10] Yeboah-Amankwah, D. v.d. Made, P.
"Sign discriminating field mill"
J. of Atmospheric and Terrestrial Physics
Vol. 54 1992 pg. 851 - 861

[11] Secker, P.E.
"The use of field mill instruments for charge density and voltage measurement"
Inst. Physics Conference Series
Vol. 27 1975 pg. 173 - 181

[12] IEEE Standard 1227 - 1990
"IEEE Guide for the Measurement of DC Electric-Field Strength and Ion Related Quantities"

[13] Mapleson, W.W. Whitlock, W.S.
"Apparatus for the accurate and continuous measurement of the earth's electric field"
J. of Atmospheric and Terrestrial Physics
Vol. 7 1955 pg. 61 - 72

[14] Magna 88C White Metal Solder
Magna 51 Flux
Available from:
Maintenance Welding Supplies cc
P.O.Box 14 Pinelands 7430
Tel. 021 - 531 2886

[15] Chubb, J.N.
"Developments in electrostatic fieldmeter instrumentation"
J. of Electrostatics Vol.14 (1983)
pg.349-358

[16] Knott, K.
"Elimination of Volta-Potential noise from plate field mills"
Review of Scientific Instruments
Vol.38 No.5 (1967) pg.602-604

[17] Gathman, S. Anderson, R.V.
"Improved fieldmeter for electrostatic measurements"
Review of Scientific Instruments
Vol.36 No.10 (1965) pg.1490-1493

[18] Keithley Instruments Inc.
"Low level measurements" 1992
Available from:
Protea Test & Measurement
P.O.Box 23694
Claremont 7735, Cape Town
Tel. 021 - 457104

[20] Cape Plastics
25 Carlisle St.
Paardeneiland, Cape Town
Tel. 021 - 5118128

[21] Castle, G. Inculet, I.
"Measurement of the Particle Space Charge in the Outlet of an Electrostatic Precipitator using an Electric Field Mill"
IEEE Trans. Industry Applications
Vol.24 No.4 (1988) pg.702-707

[22] Sheahen, T.P.
"Model of response of an electric field mill operating during suborbital flight"
Review of Scientific Instruments
Vol. 45 February 1974 pg. 171 - 177

[23] Smith, L.G.
"An electric field meter with extended frequency range"
Review of Scientific Instruments
Vol. 25 May 1954 pg. 510 - 513

[24] Lane-Smith, D.R.
"A new design of sign-discriminating field mill"
J. of Atmospheric and Terrestrial Physics
Vol. 29 1967 pg. 687 - 699

[25] Takahashi, Y. Chiba, M.
"Polarity-sensing methods for field mills without phase-sensitive detection"
J.Phys. E: Sci. Instrum. Vol.19 (1986) pg.705-707

[26] Wildman, P.J.L.
"A device for measuring electric field in the presence of ionisation"
J. of Atmospheric and Terrestrial Physics
Vol. 27 1965 pg. 417 - 423

[27] Cross, A.S.
"Two electrostatic field meters"
British Journal of Applied Physics
Vol. S2 1953 pg. S47 - S50

[28] Layton, R. O'Dell, K.
"Student field mill"
American Journal of Physics
Vol.43 No.11 1975 pg.942-943

[29] Chubb, J.
"The performance capabilities of electrostatic fieldmeters"
SEE Conference, Nice
Section C2 October 1986 pg.93-96

[30] Precious Innovations
Manufacturing Jewellers
Murray House, 25 Hout St., Cape Town
Tel. 021 - 235991

[31] Kopp Electronics
P.O.Box 3853, Rivonia 2128
Tel. 021 - 6894141

[32] Meade, M.L.
"Lock-in amplifiers: principles and applications"
Peter Peregrinus 1983
Chapter 3.3

[33] Pease, R.A.
"What's All this Teflon Stuff, Anyhow?"
Electronic Design February 14, 1991
pg.115-117

[34] Rossi, F.
"Contact Potential Measurement: Spacing-dependence errors"
Review of Scientific Instruments
Vol.63 No.9 (1992) pg.4174-4181

7. Electronic circuits

7.1 Design of preamplifier

The preamplifier design has already been discussed briefly in Section 3.2. The preamplifier is based on an operational amplifier (op-amp), configured to measure current. There are a number of considerations in the preamplifier design, which are discussed below:

7.1.1 Type of op-amp

The signal measured from the field mill stator is a low-level current signal in the nA range. This means that the op-amp should be selected to have low input bias currents, and low input current noise. A FET-input op-amp is needed to meet these specifications. (A FET-input op-amp is an op-amp having either JFET or MOSFET transistors in its input stage). The table below shows some of the op-amps available in South Africa that were considered for the preamplifier:

Table 7.1 Available preamplifier op-amps

Op-amp	Manufacturer	Cost (1995 prices)	Input bias current pA @25°C	Input noise current $fA/\sqrt{Hz}$ @25° C f = 1kHz	Op-amp specification
AD 515	Analog Devices	R 45	0.3	0.1	Precision electrometer op-amp
AD 546	Analog Devices	R 15	1	0.4	Low cost electrometer op-amp
AD 549	Analog Devices	R 45	0.06	0.2	Ultra-low input bias current op-amp
CA 3140	Harris	R 3	40	10	General-purpose MOSFET op-amp
LT 1169	Linear Technology	R 32	1.5	0.8	Low noise, picoamp JFET op-amp
TLC 2201	Texas Instruments	R 10	1	0.6	Low noise precision op-amp

For preliminary experiments, the cheap CA 3140 op-amp was found to be satisfactory. More rigorous noise comparisons (see Section 7.1.2) showed that a high quality op-amp with lower noise would improve performance. In the final electronic circuit, the AD546 low cost electrometer op-amp was used for the preamplifier.

7.1.2 Noise comparisons

This section sets out to address two questions regarding the preamplifier:

1. Is it better to use a voltage-shunt amplifier circuit or a voltage follower circuit ?
2. Is there a solid argument for choosing a high quality electrometer op-amp ?

7.1.2.1 Theoretical noise comparisons

The diagram below illustrates the action of the intrinsic amplifier noise sources e_n and i_n.

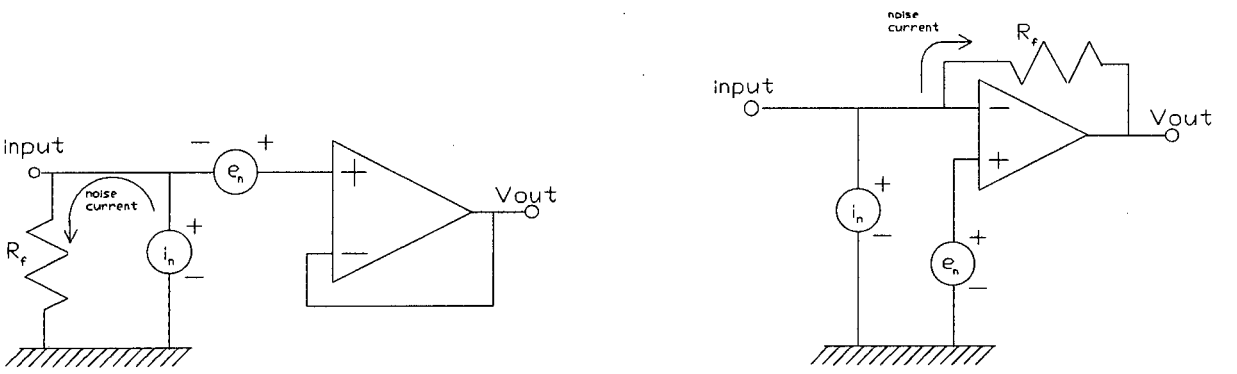

(a) Voltage follower (b) Voltage-shunt amplifier

Fig.7.1 Action of intrinsic op-amp noise sources

For both the voltage follower configuration (a), and the current-to-voltage converter configuration (b), the noise current due to the internal op-amp noise source i_n, flows through the resistor R_f. Thus the contribution of the preamplifier circuit to the total noise will be:

$$e^2 = (i_n R_f)^2 + e_n^2 + 4kTR_f \quad \text{.....(7.1)}$$

where e^2 = equivalent noise voltage density at the output [V^2/Hz]
k = Boltzmann constant
T = absolute temperature (Kelvin)

Note: Eqn.7.1 above is the same for both voltage follower and voltage-shunt amplifier configurations. This is supported by Dostal [4].

The noise performance of the AD546 and CA3140 op-amps is compared in a circuit similar to the preamplifier circuit used in the field mill. A circuit diagram is shown below:

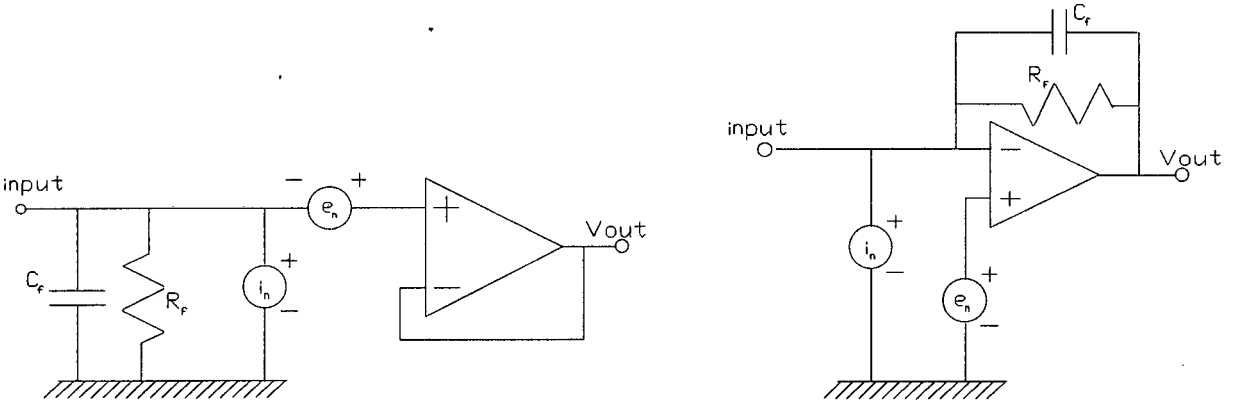

(a) Voltage follower (b) Voltage-shunt amplifier

Fig.7.2 Circuit used for calculations

The presence of the feedback capacitor C_f is necessary to limit wide-band noise in most practical applications. This must be accounted for by rolling-off the noise response at high frequencies. The equation for the equivalent noise voltage now becomes [4]:

$$e^2 = e_n^2 + \frac{(i_n R_f)^2 + 4kTR_f}{1+(f/f_o)^2} \quad \text{.....(7.2)}$$

where: $f_o = 1/2\pi R_f C_f$

Note: we assume that Eqn.7.2 is valid for both the voltage follower and voltage-shunt amplifier circuits, following the work of Dostal [4].

7.1.2.1.1 Noise at high frequency and at low frequency

We wish to find the equivalent noise in a 1Hz measurement bandwidth at low frequency, and at high frequency, in order to gain some idea of the noise levels introduced by the preamplifier itself. (Low frequency here means $f << f_o$, while high frequency means $f >> f_o$). In the quadrature method for ion current detection, (see Chapter 7.5), the modulation frequency $f << f_o$. In the final version of the preamplifier circuit (see Chapter 7.6), the modulation frequency $f >> f_o$. Thus it is of interest to examine the noise both at high frequency and at low frequency.

1. At low frequencies, ($f << f_o$)

$$e^2 \approx (i_n R_f)^2 + e_n^2 + 4kTR_f \quad \text{.....(7.3)}$$

2. At high frequencies, ($f >> f_o$)

$$e^2 \approx e_n^2 \quad \text{.....(7.4)}$$

The following values (obtained from manufacturers' data sheets) are used for calculations, together with equations (7.3) and (7.4):

CA3140 op-amp $\begin{cases} e_n = 100nV/\sqrt{Hz} \\ i_n = 10fA/\sqrt{Hz} \end{cases}$ AD546 op-amp $\begin{cases} e_n = 35nV/\sqrt{Hz} \\ i_n = 0.1fA/\sqrt{Hz} \end{cases}$

Note: we take the values e_n and i_n to be constant over the frequency range of 10kHz. The values used are average values that give a reasonable approximation to the noise over the entire bandwidth.

The specific values assumed for this circuit example are: R_f = 10Mega-ohms, C_f = 47pF, T = 300K
$B_{noise} = 1/4R_fC_f = 532$ Hz B_{eff} = 10kHz

The results of these calculations are summarised in Table 7.2 below:

Table 7.2 Theoretical calculations of equivalent preamplifier noise

Op-amp	Low frequency noise $nV/\sqrt{Hz}$	High frequency noise $nV/\sqrt{Hz}$
AD 546	408	35
CA 3140	431	100

From these simple calculations, it would appear that the higher quality AD546 op-amp should give better noise performance than the CA3140 op-amp, in this application. Note that the noise sources e_n and i_n of the op-amps vary continuously over the frequency range, so that a rigorous theoretical comparison is difficult. However, it does give some idea of the magnitude of the noise introduced by the preamplifier alone. For a more useful noise comparison, it is necessary to evaluate noise performance of the different op-amps and circuit configurations experimentally. This is described in Section 7.1.2.2. Both of the circuits in Fig.7.2 were simulated on PSpice. PSpice gave identical outputs for the voltage follower and voltage-shunt amplifier circuits, so only the results for the voltage-shunt amplifier circuit are shown. This supports the assumption that the noise equations are the same for both voltage follower and voltage-shunt amplifier circuits. The PSpice outputs are shown in Fig.7.3 below. (See Appendix C for the PSpice source code). The PSpice values for equivalent output noise agree with the calculated values in Table 7.2 above.

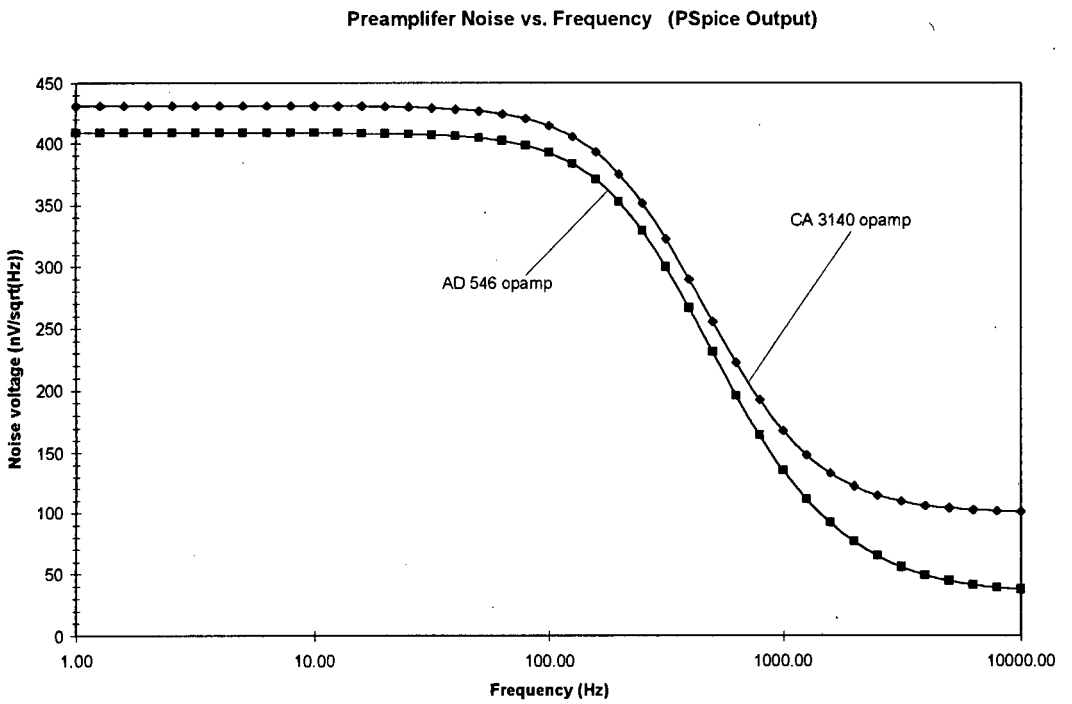

Fig.7.3 PSpice plot of output noise voltage for both op-amps

7.1.2.1.2 Total noise output over measurement bandwidth

In order to calculate the total output noise of the circuit (as used for the experimental noise measurements in the next section), we assume that the noise in the resistor R_f has a bandwidth of:

$$1/4R_fC_f = B_{noise} \quad \text{(7.5)}$$

We also assume that the voltage noise has an effective bandwidth B_{eff} = 10kHz. The bandwidth B_{eff} is set by the external filter that follows the preamplifier, and so is somewhat arbitrary, since it does not depend on the design of the preamplifier per se [6]. We assume B_{eff} =10kHz as a reasonable value for post-filtering of the preamplifier output signal. Total noise due to the preamplifier may be calculated as:

$$E_n = \sqrt{\left((e_n^2)(B_{eff}) + \left((i_nR_f)^2 + 4kTR_f\right)(B_{noise})\right)} \quad \text{(7.6)}$$

where E_n = rms output noise voltage in measurement bandwidth [V]

Again, we assume:

$$\text{CA3140} \begin{cases} e_n = 100nV/\sqrt{Hz} \\ i_n = 10fA/\sqrt{Hz} \end{cases} \qquad \text{AD546} \begin{cases} e_n = 35nV/\sqrt{Hz} \\ i_n = 0.1fA/\sqrt{Hz} \end{cases}$$

C_f = 47pF B_{eff} = 10kHz B_{noise} = $1/4R_fC_f$ T = 300K

Total rms noise calculated for voltage-shunt amplifier circuit with R_f =10MΩ and R_f =100MΩ.

Note: again we take the values e_n and i_n to be constant over the frequency range of 10kHz. The values used are average values that give a reasonable approximation to the noise over the entire bandwidth.

Table 7.3 Output noise voltage for AD546 and CA3140 op-amps

Op-amp	R_f	B_{noise} (Hz)	Dominant noise components	Output noise voltage (calculated) μV rms	Output noise voltage (PSpice) μV rms
AD 546	10MΩ	532	$4kTR_fB_{noise}$	10.0	10.0
AD 546	100MΩ	53.2	$4kTR_fB_{noise}$	10.0	10.0
CA 3140	10MΩ	532	$(e_n)^2B_{eff}$ and $(i_nR_f)^2B_{noise}$	13.9	13.9
CA 3140	100MΩ	53.2	$(e_n)^2B_{eff}$ and $(i_nR_f)^2B_{noise}$	15.5	15.5

These theoretical calculations show that with the AD546 op-amp, the dominant noise source is thermal noise in the feedback resistor R_f. This is the ideal case for a low-level-signal preamplifier, since the intrinsic noise sources are sufficiently low that their noise contributions are below the thermal noise of R_f. This design criterion is recommended by Jiri Dostal [4], and by Analog Devices in their data sheets [5] and Amplifier Applications Guide [6]. The CA3140 op-amp, however, has dominant noise components due to its intrinsic noise sources e_n and i_n. Thus it is a poor choice of op-amp for use in this application. However, its low cost may make it a reasonable choice if high accuracy is not important.

7.1.2.2 Experimental Noise Comparisons

The following noise measurements were made to further investigate the preamplifier design, and the selection of the op-amp. The theoretical calculations show that the two configurations (voltage follower and voltage-shunt amplifier) are identical in terms of noise performance. The calculations also show that the noise performance of the AD546 op-amp is significantly better than that of the CA 3140 op-amp. The purpose of this experimental noise comparison is to see how the theoretical noise performances agree with noise measured in a working circuit. We would also like to see if there is some difference between the voltage follower and voltage-shunt amplifier configurations in a working circuit (although theoretically their noise performance is identical).

Horowitz and Hill recommend that a "true RMS" voltmeter is the best way to measure noise accurately [1]. They say that measuring the noise on an oscilloscope is somewhat subjective, but another paper describes a way to measure noise accurately with an oscilloscope, using the "tangential method" [2]. Both methods were used in this experiment. In order to amplify the noise so that it could be measured more easily, the output of the device under test was amplified by 1000 using the LT1028 ultra-low-noise op-amp. This method of amplifying the noise has been used in a recent paper to verify, by experiment, theoretical noise calculations [3].

Experimental details

The circuit shown below was constructed on double-sided PC board, and enclosed in a metal box. The metal box was connected to the circuit ground. Supply voltage to the circuit is +/- 12V (through 12V voltage regulators mounted on the circuit board). A coaxial cable was used to connect the circuit output to the digital multimeter. The digital multimeter used was an HP 34401A high performance "true RMS" multimeter. It was set to read AC volts with a bandwidth of 3Hz - 300kHz. (Note that the low-pass filter formed by the LT1028 noise amplifier limits the effective bandwidth to approximately 10kHz). The oscilloscope probes used were both on 10:1 setting, and the oscilloscope timebase was set at 100 microseconds per division. The oscilloscope was used to obtain an estimate of the rms noise using the "tangential method" outlined in [2].

The components R=10MΩ and C=47pF were selected from a box of nominal-value components by measuring them on a digital LCR meter until two components with measured values within 2% were found. (This was necessary since 10MΩ resistors were not available in 1% rating). The precision of the LCR meter is better than 2%. The same physical op-amp was used for both IC1 (voltage-shunt amplifier) and IC2 (voltage follower) to ensure that component variation did not affect the results. (This means that the op-amp was plugged into the socket of IC1, noise measurements were made, and then the op-amp was removed and plugged into the socket of IC2, and the noise measurements repeated). The lid of the metal box containing the circuit was secured before each set of noise measurements was made.

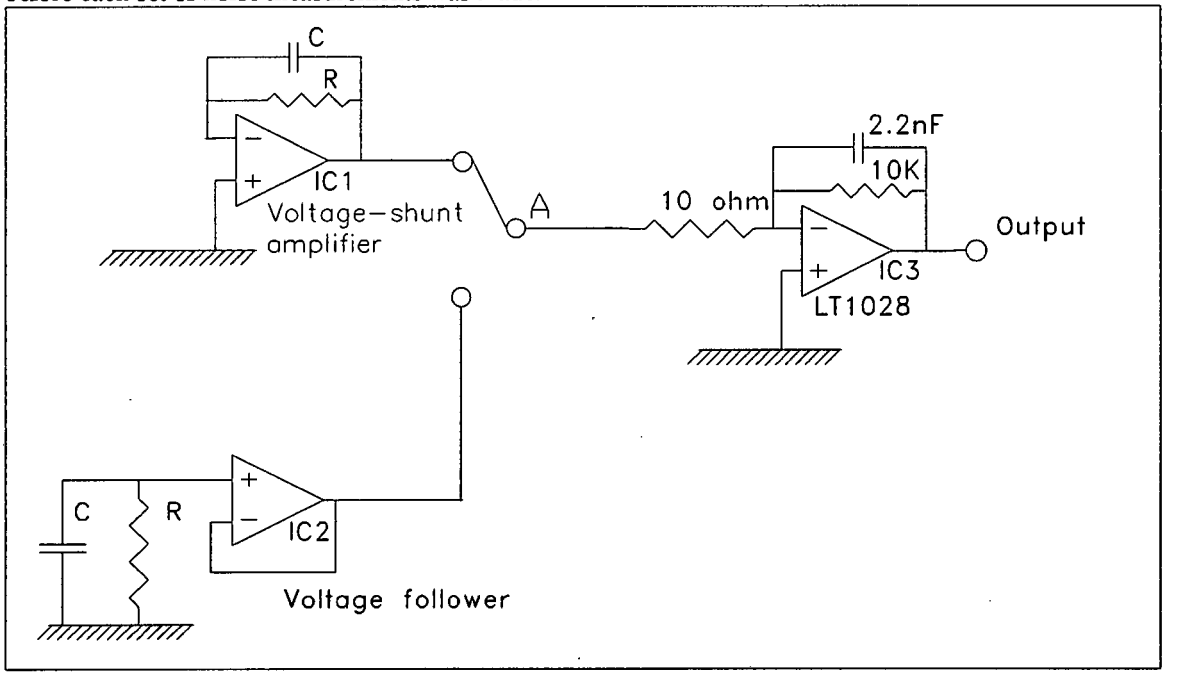

Fig.7.4 Circuit used for experimental noise comparisons

Experimental Results

Table 7.4 Results of noise measurements R=10M C=47pF

Preamp No.	Op-amp	Circuit	Minimum noise mV rms	Average noise mV rms	Maximum noise mV rms	Expected noise * mV rms	Scope mV rms	Bkgd noise mV rms
1	CA 3140	voltage-shunt amp	11.76	12.49	13.33	13.9	12.5	0.43
2	CA 3140	voltage follower	12.49	13.56	14.47	13.9	15.0	0.44
3	AD 546	voltage-shunt amp	7.46	7.84	8.62	10.0	10.0	0.48
4	AD 546	voltage follower	8.52	8.79	9.10	10.0	10.0	0.61

* Expected values are obtained from values of rms output noise voltage in Table 7.3 multiplied by 1000

The values for average noise in mV rms in Table 7.4 are about 1000 times the values for rms noise calculated theoretically in Table 7.3. This gives confidence that the noise voltages being measured are indeed representative of preamplifier noise, and that gross experimental errors have been avoided.

Table 7.5 Results of noise measurements R=100M C=47pF

Preamp No.	Op-amp	Circuit	Minimum noise mV rms	Average noise mV rms	Maximum noise mV rms	Expected noise * mV rms	Scope mV rms	Bkgd noise mV rms
1	CA 3140	voltage-shunt amp	14.56	18.57	20.81	15.5	15.0	0.19
2	CA 3140	voltage follower	13.89	16.91	19.32	15.5	12.5	0.18
3	AD 546	voltage-shunt amp	8.88	10.13	11.21	10.0	10.0	0.28
4	AD 546	voltage follower	8.74	9.54	10.61	10.0	10.0	0.18

* Expected values are obtained from values of rms output noise voltage in Table 7.3 multiplied by 1000

Notes

1. Background noise "Bkgd noise" means the noise measured with the power supply to the circuit switched off.

2. The same physical op-amp was used for both voltage-shunt amplifier and voltage follower measurements.

3. With the connection at point A in the circuit grounded (ie. measuring the noise of the noise amplifier op-amp LT1028 alone) the noise measured by the HP multimeter was consistently below 100μV (rms). This indicates that the noise amplifier op-amp IC3 does not contribute any significant noise to the total noise from either IC1 or IC2. Thus we can say that the noise measured at the circuit output is a reasonable indication of the noise due to IC1 and IC2 (amplified by 1000).

The results shown in Table 7.4 and Table 7.5 are plotted in the two graphs below. Note that in these graphs, the minimum, average and maximum readings for each preamplifier are shown connected by a solid line (error bar). This enables the spread of noise values for each preamplifier to be taken into consideration. In all measurements, the spread of values was much lower for the AD546 op-amp than for the CA3140 op-amp.

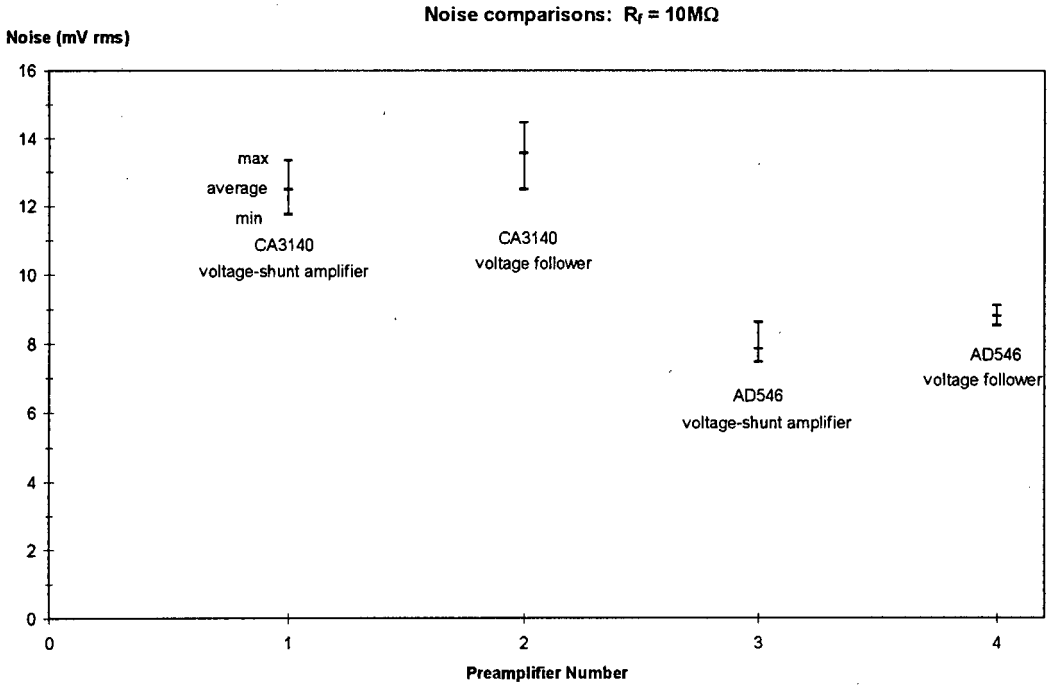

Fig.7.5 Noise comparisons of Table 7.4

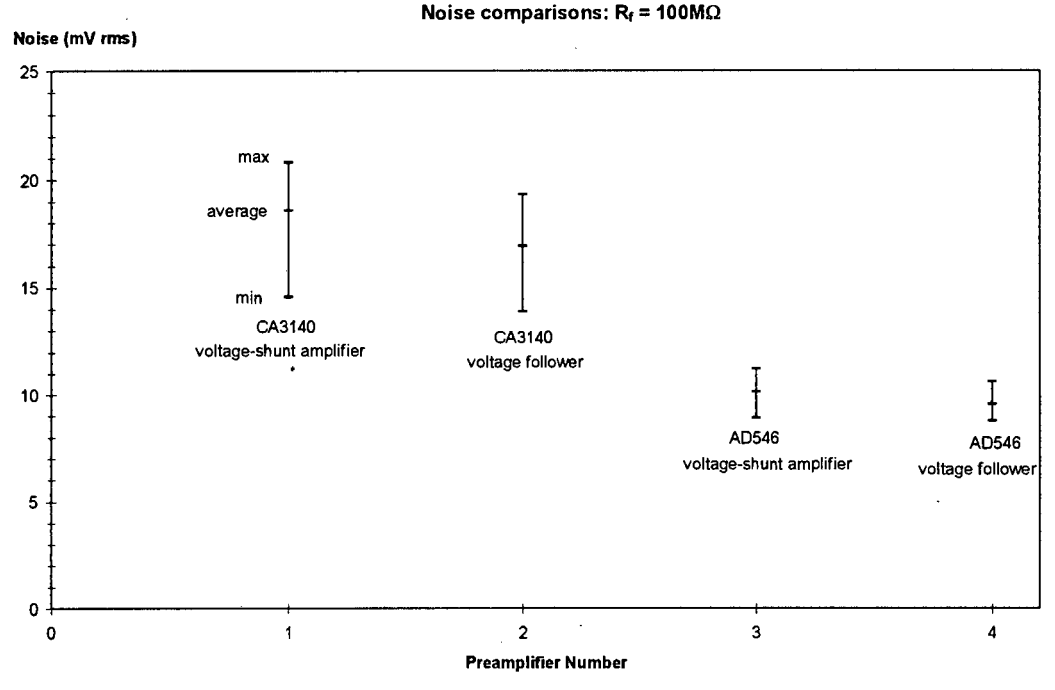

Fig.7.6 Noise comparisons of Table 7.5

Practical considerations

In some applications, it may be necessary to mount the preamplifier circuit some distance away from the electric field mill. The cable that carries the signal from the field mill stator to the preamplifier input will necessarily add some input capacitance. If a voltage-shunt amplifier circuit is used, the input terminals of the preamplifier are held at the same potential, so that the input capacitance is short-circuited. For this reason, Rossi [11] recommends that the voltage-shunt amplifier circuit should be used.

In his electric field mill designs, Chubb mounts the preamplifier inside the field mill casing, so that only a very short cable from stator to preamplifier is needed. Chubb uses the voltage follower configuration in his instruments since the input capacitance of the preamplifier is not a significant problem, and because the voltage follower circuit is, for him, "easier to understand" [17]. While this is not a strong scientific argument, it would seem to support the theory that there is little difference in terms of noise performance between the voltage follower and voltage-shunt amplifier configurations.

7.1.2.3 Conclusions

In general, the measured results agree well with the theoretical values for output noise. The results show little significant difference between the voltage-shunt amplifier and voltage follower configurations for a given op-amp type. However, the noise measured for both configurations is lower for the AD546 op-amp than for the CA3140 op-amp. Thus it would seem that the choice of a high quality op-amp is more important than the choice of op-amp configuration. The questions that we set out to address may now be answered:

1. There is little difference in performance between the voltage-shunt amplifier and voltage follower circuits. If a long cable run from field mill to preamplifier is necessary, then the voltage-shunt amplifier circuit is preferable.

2. A high-quality electrometer op-amp is critical for accurate measurements.

7.1.3 Preamplifier circuit-board layout

A very important consideration in the measurement of low-level current signals is the effect of leakage currents at the preamplifier. The use of guarding techniques is essential to realising the ultra-low current measurement accuracies obtainable with high-quality electrometer op-amps such as the AD546 [5]. Leakage currents may reach the input terminal of the voltage-shunt amplifier across the surface of the printed circut board (PCB). Two copper tracks spaced 1mm apart and running parallel for 25mm on the surface of a PCB have a leakage resistance of approximately $10^{11}\Omega$ [6]. This means that if one of the tracks is carrying the supply voltage of +15V, and the other track is the preamplifier input (at approximately ground potential), then a leakage current of about 150pA will enter the preamplifier input. If the PCB surface is contaminated with dust, or small solder particles, then the leakage current will increase. The critical regions of the preamplifier input are shown in the diagram below:

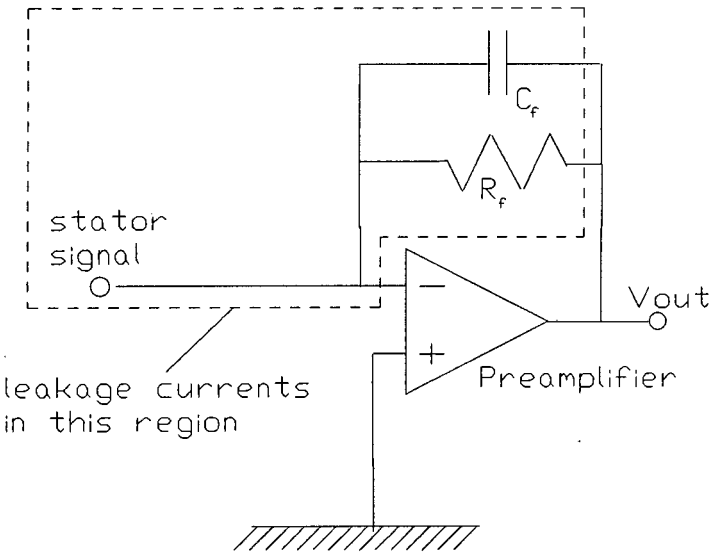

Fig. 7.7 Preamplifier circuit showing the region that is sensitive to leakage currents

7.1.3.1 Guarding of sensitive conductors

Guarding is achieved by applying a guard potential to the outside of the insulation surrounding the sensitive region, driven from a low-impedance source. The guard potential must be the same as the potential of the sensitive input conductor which it is to guard. In this case, the guard track must surround the inverting input track on both sides of the PCB [5]. This is shown in the diagram below:

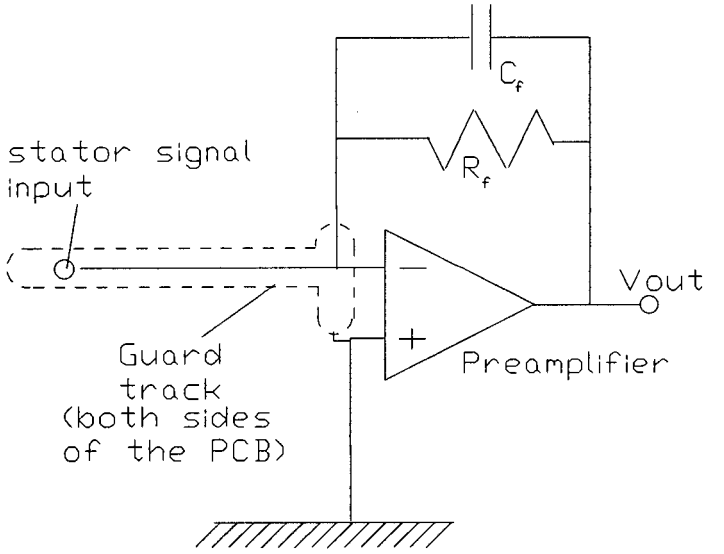

Fig. 7. 8 Preamplifier circuit showing guard track
The guard track is connected to the non-inverting input, which is at the same potential as the inverting input.

7.1.3.2 Teflon op-amp socket

The best performance is achieved with a Teflon socket for the op-amp, as this minimises leakage currents at the op-amp pins [5]. As Teflon sockets were not readily available, a home-made Teflon IC socket was constructed. Bob Pease recommends using a home-made socket, either made out of Teflon or else made without any insulating material at all [24]. Steel pins were cannibalised from an ordinary plastic IC socket, and inserted into holes drilled in a small piece of Teflon. This is not advisable if large quantities of sockets are required, but for this thesis it was the most practical way of obtaining a Teflon IC socket!

7.1.4 Input protection

In any electrostatic measurement system, it is necessary to provide some input protection for the sensitive preamplifier. The high voltages used in the electrostatic environment may cause high transient voltages at the preamplifier inputs, especially if a fault condition occurs. Where field mills are used outdoors to measure thundercloud electric fields, input protection is essential. In this case extreme input protection methods using zener diodes and neon breakdown tubes may be necessary [18].

For this thesis, it was felt that a pair of clamping diodes placed across the op-amp inputs would provide sufficient protection. In preliminary experiments with the field mill, input protection was not used, and on several occasions power to the circuit was switched off, with the field mill still underneath the energised 5kV source. After such events, the preamplifier op-amp was often 'blown", and produced no output voltage. Clamping diodes across the op-amp inputs solved this problem. Low-leakage diodes are recommended, and they should be shielded from light, to prevent photocurrents from being generated [19]. The IN4148 small-signal diodes used in the circuit below were not found to introduce significant noise. However, the currents being measured for this thesis were not below 100pA. If greater sensitivity is required, then gallium phosphide diodes are preferable to silicon diodes [25]. In this thesis, the preamplifier was enclosed in a metal box, so that the clamping diodes were shielded from light. The preamplifier circuit with clamping diodes is shown below:

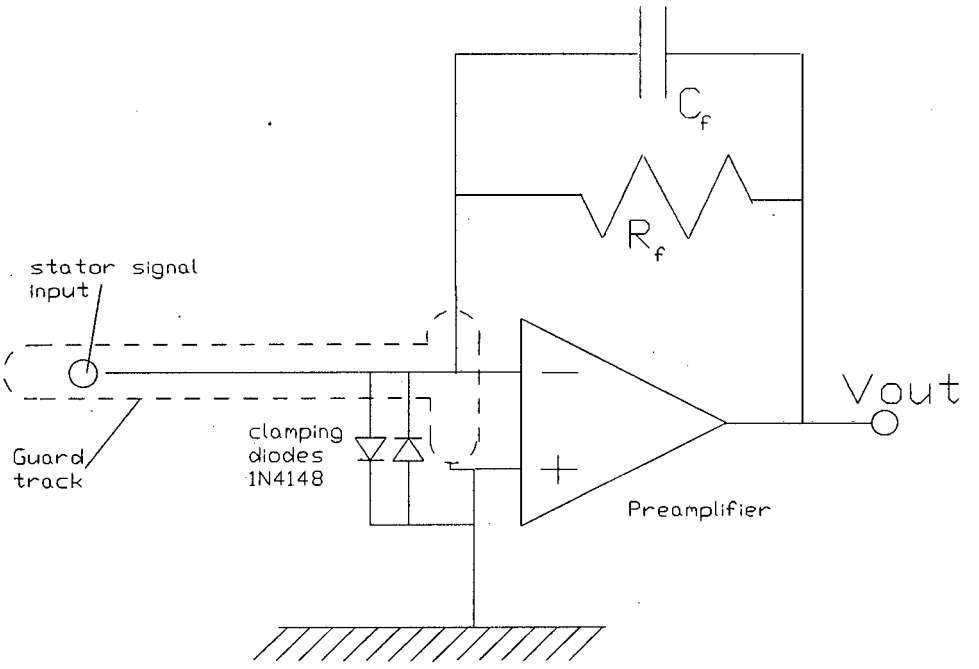

Note: the clamping diodes are connected between the inverting and non-inverting op-amp terminals.

Fig.7.9 Clamping diodes used for input protection of preamplifier

7.2 Bucking Voltage

As discussed in Chapter 3.7.1, it is necessary to provide some method for nulling (or 'bucking") the spurious electric field signal (caused by contact potential differences which are modulated by the spinning rotor).

7.2.1 Methods of Nulling the Spurious Electric Field Signal

There are three commonly-used ways to apply a bucking voltage, V_{buck} in order to null out the spurious electric field signal. These three methods are shown in the diagram below:

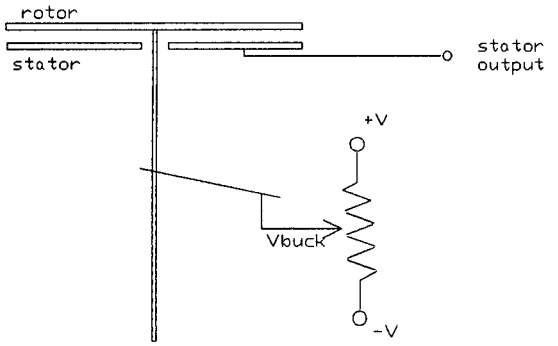

(a) V_{buck} applied to the rotor

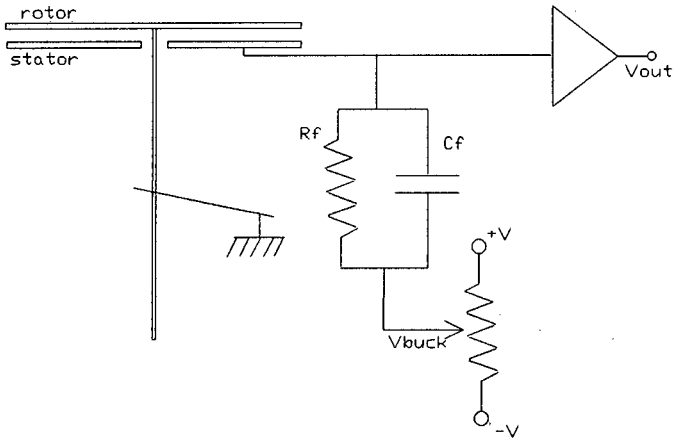

(b) V_{buck} applied to the stator, with a voltage follower preamplifier

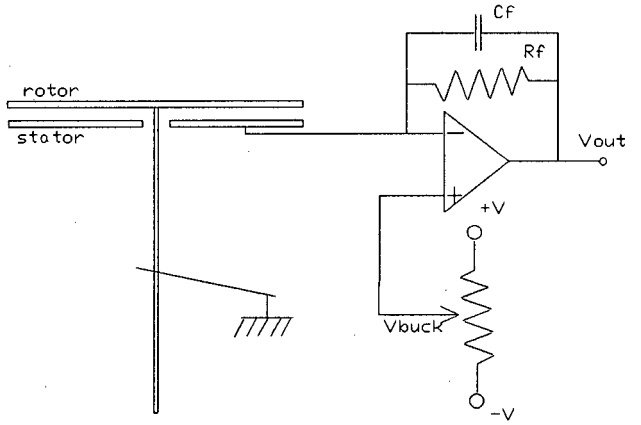

(c) V_{buck} applied to the stator, with a voltage-shunt amplifier preamplifier

Fig.7.10 Different arrangements to buck out the spurious electric field signal

In Fig.7.10 (a) the bucking voltage is applied to the spinning rotor. This method was used by Cross [7], Layton [8] and Secker [9]. The advantage of this method is that it does not add a DC offset to the preamplifier output. In Fig.7.10 (b) and (c) the bucking voltage is indirectly applied to the stator. This has the same effect as applying the bucking voltage to the rotor, but it also adds a DC offset to the output of the preamplifier. The circuit of Fig.7.10 (b) was used by Clark [10]. The circuit in Fig.7.10 (c) is a more recent development in the literature, and has been used by Rossi [11]. All three of the above methods for nulling the spurious signal were tested with the field mill. The first method was awkward to implement, since applying V_{buck} to the rotor meant that the ball bearings had to be isolated from ground (to prevent the rotor from being grounded through the bearings). This was accomplished by inserting thin insulators between the aluminium case of the field mill (grounded) and the aluminium cross pieces in which the bearings were mounted. Thus the bearings were isolated from ground, and so a bucking voltage could be applied to the rotor through the "earthing" brush. All three methods were found to be just as effective for nulling the spurious signal with zero applied field. The oscilloscope traces below show the field mill signal measured at the output of the preamplifier with zero applied field. The first trace, Fig.7.11 (a) shows the preamplifier output with no nulling of the spurious signal. The spurious signal is clearly seen as an electric field signal in phase with the reference signal. The magnitude of this spurious signal corresponds to an external electric field of +60V/m.

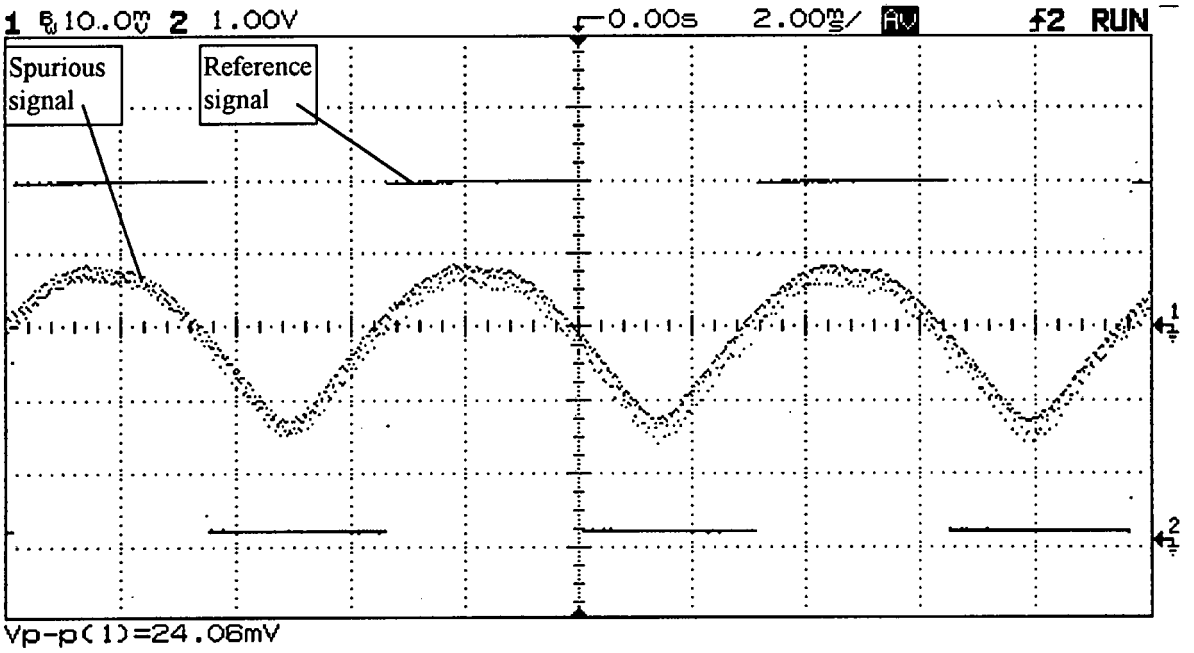

Fig.7.11(a) Spurious electric field signal at preamplifier output

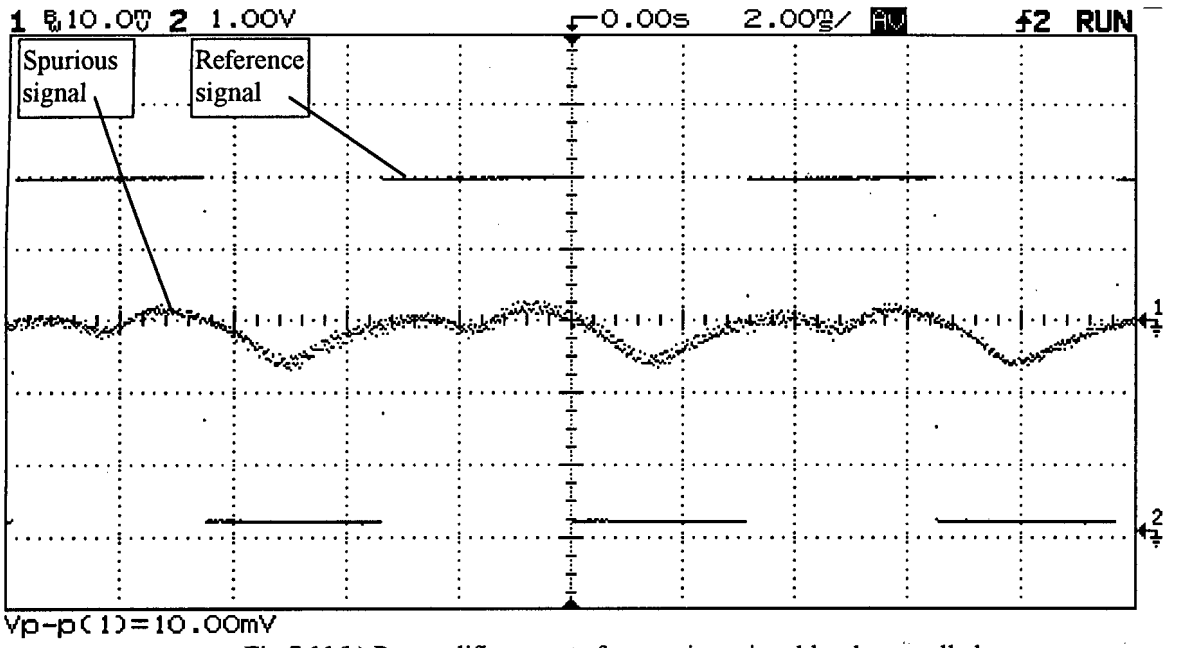

Fig.7.11(b) Preamplifier ouput after spurious signal has been nulled

In Fig.7.11(b), the preamplifier ouput is shown after nulling the spurious signal (by setting V_{buck} = -73mV in this case). This reduced the electric field reading to 0V/m. These oscilloscope traces show both the action of the bucking voltage, V_{buck}, and also its important role in the electric field measurement circuit. It is also evident that perfect cancellation of the spurious signal is not possible. This is due mainly to small mechanical asymmetries (for example, the rotor and stator may not be exactly parallel). Rossi notes that contact potentials between two metal surfaces may vary between different regions of the surfaces [11]. This means that the contact potentials may vary between the different vanes, although this is considered to be only a second-order effect.

Although perfect cancellation of the spurious signal is not possible, the bucking voltage, V_{buck}, allows the spurious signal to be sufficiently reduced for greatly-improved accuracy of electric field measurement.

7.2.2 Removing the DC Offset Introduced by the Bucking Voltage

The problem of DC offset introduced by the bucking voltage is shown by the PSpice simulation below. (See Appendix C for the PSpice source code). The bucking voltage is increased in 5mV steps from -10mV to +15mV, and the magnitude of the spurious signal is successively decreased (until the last step, when the bucking voltage overshoots, so that the spurious signal increases again). The output signal is shown for a sinusoidal stator signal (the "spurious signal") at frequency f=160Hz. It can be seen that when V_{buck} = +10mV, the sinusoidal signal (spurious signal) is completely nulled, and also there is a DC offset of the output signal. The DC offset has the same level as V_{buck}.

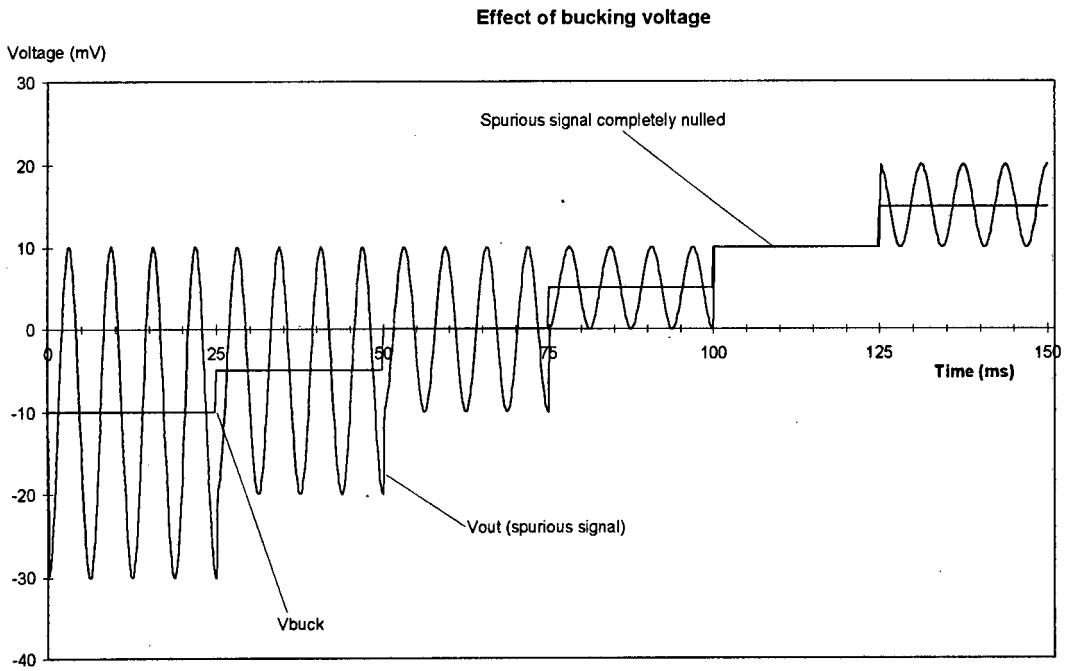

Fig.7.12 PSpice simulation showing the effect of varying V_{buck} to null the spurious signal

Steps must be taken to remove this DC offset, since it may cause non-linearities in following amplifier stages. This is shown in the diagram below:

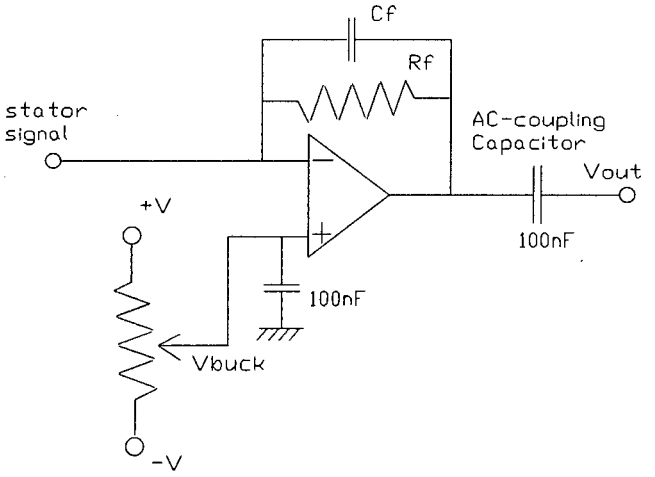

(a) The simplest method, (used by Rossi [11]) is to AC-couple the preamplifier output to the following stages. However, this means that the DC component of the stator signal due to ion currents is lost.

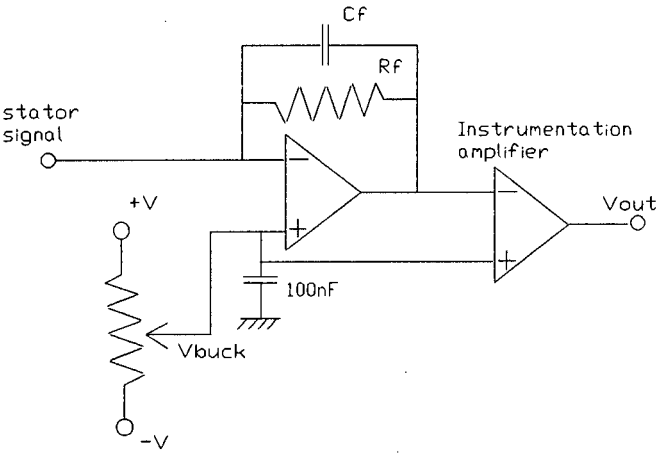

(b) This method is described in the Analog Devices application notes [5].
An instrumentation amplifier is used to subtract the DC offset from the stator signal, so that any DC signal due to ion currents is preserved. A suitable instrumentation amplifier is the AD620.

Fig.7.13 Methods for removing the DC offset introduced by V_{buck}

Both methods (a) and (b) for removing the DC offset voltage were tested, and found to be effective. It was decided to implement method (b), where the offset is removed using an instrumentation amplifier. This was necessary since the DC component of the stator signal was to be used to measure the ion current.

Error due to common-mode signal

One factor that must be considered when using the circuit of Fig.7.13(b) is the error introduced by the common-mode signal, V_{buck}, since this dc voltage may be as large as 100mV. Rossi [11] notes that contact potentials of up to 100mV may exist between two metal surfaces. Experience with the field mill thesis showed that the required bucking voltage, V_{buck}, ranged from 50mV to 100mV. The specifications for the AD620 give the common-mode rejection ratio as 100dB at the gain used in the circuit. If we assume that the dc output voltage of the preamplifier due to ion current is 250μV (for ion current density J = 10nA/m^2) and the dc bucking voltage V_{buck} = 100mV, then the error due to the common-mode signal = -100dB x 100mV = 1μV. This is considered to be sufficiently low that it will not introduce significant error into the ion current density readings.

7.3 Reference signals

Reference signals are necessary in the field mill system if synchronous detection is to be used.

7.3.1 Reference signal generation

The reference signal is generated by the reference rotor as it passes through the slotted optical switch mounted on the inside of the field mill casing. A circuit diagram for the reference signal recovery circuit is shown below:

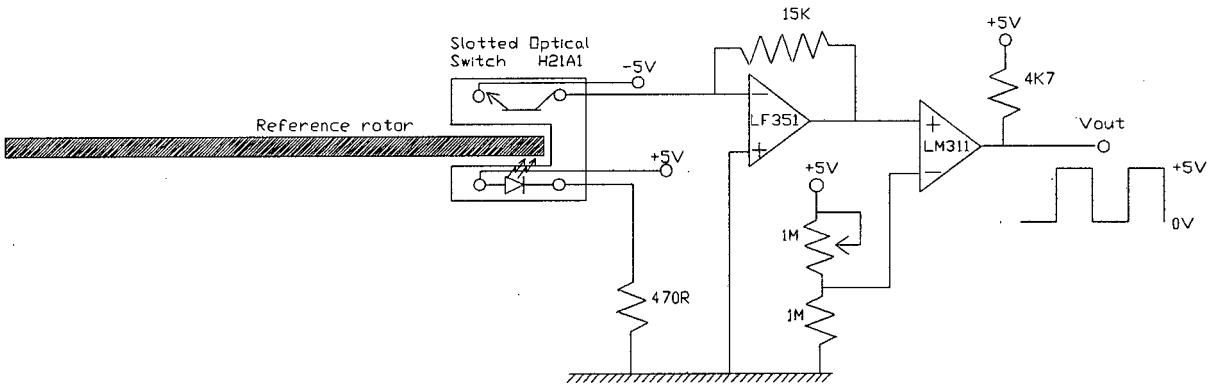

Fig.7.14 Circuit diagram of the reference signal recovery circuit

In the diagram above, the slotted optical switch outputs a square wave signal as the rotor blades spin through the slot. The LF351 op-amp is used to amplify this signal, and the LM311 comparator converts it into a square wave alternating between 0V and +5V. This signal is then fed to the reference input of the synchronous detector.

The circuit shown above is similar to that used in a BSc. thesis by Wheeler [21].

7.3.2 Phase shifter

It is common in systems using synchronous detection to use a phase shifter which enables the phase of the reference signal to be adjusted in relation to the phase of the sensed signal. The use of a phase shift circuit was investigated for solving two problems:

1. If there is some small phase mis-alignment between the reference and sensed signal, it is inconvenient to stop the field mill, adjust the position of the reference rotor, and then run the field mill again, and re-check the phase alignment. It would be more convenient if the phase alignment could be adjusted whilst running the field mill.

2. If quadrature detection is to be used for the ion current density measurements, then a second reference signal is required, which is at 90^0 to the reference signal used for electric field measurement. This means that either a second reference rotor is required, or else a 90^o phase shifter is required.

A phase shift circuit was designed and built, based on the Sanky Phase Shifter [12]. A circuit diagram is given below:

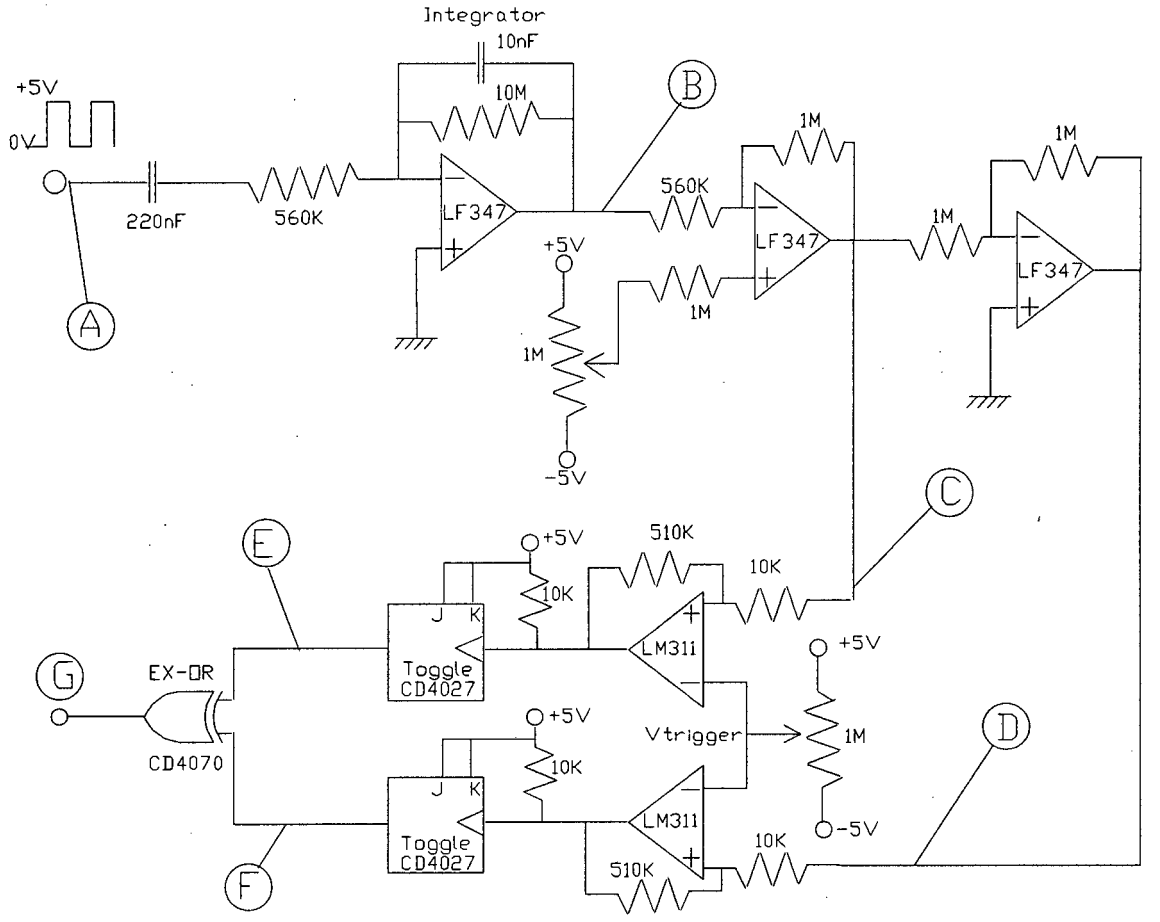

Fig.7.15 Circuit diagram of phase shifter

In the diagram above, the phase shift may be varied by varying $V_{trigger}$. The waveforms for the phase shift circuit are shown in the following diagrams:

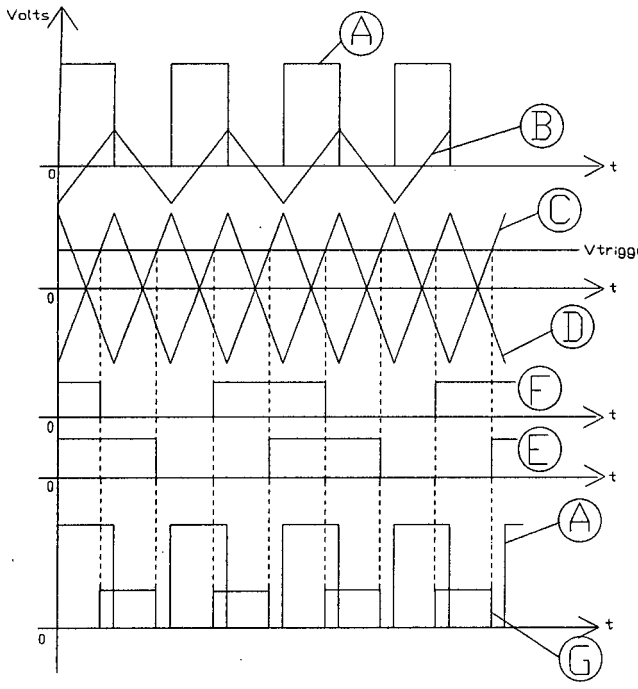

(a) The incoming square wave A is converted to a triangular wave B by the integrator.

(b) The triangular wave is amplified and inverted, so that there are now 2 triangular waves, C and D, which are in anti-phase.

(c) Each of the two triangular waves drives a comparator, which then drives a toggle, to produce the square waves E and F.

(d) The square waves E and F drive the inputs of an EXOR gate, so producing the square wave G. It can be seen that G has the same frequency as A, but is shifted in phase. Note: the amplitudes of E, F and G should all be the same as A, but they are shown smaller for clarity.

Fig.7.16 Waveforms showing the operation of the phase shift circuit of Fig.7.15

The phase shifter as shown above was built and tested, and found to give smooth phase shifts from 0° to almost 180° at a frequency of 150Hz. The phase shifter functioned as required at a fixed frequency. However, this design of phase shifter is frequency-dependent (the relative phase shift between signals A and G changes as the frequency changes). This drawback was not immediately apparent from the paper by Sankaranarayanan, in which a similar circuit is described [12]. The reason for the change in phase shift with frequency is explained in the diagram below:

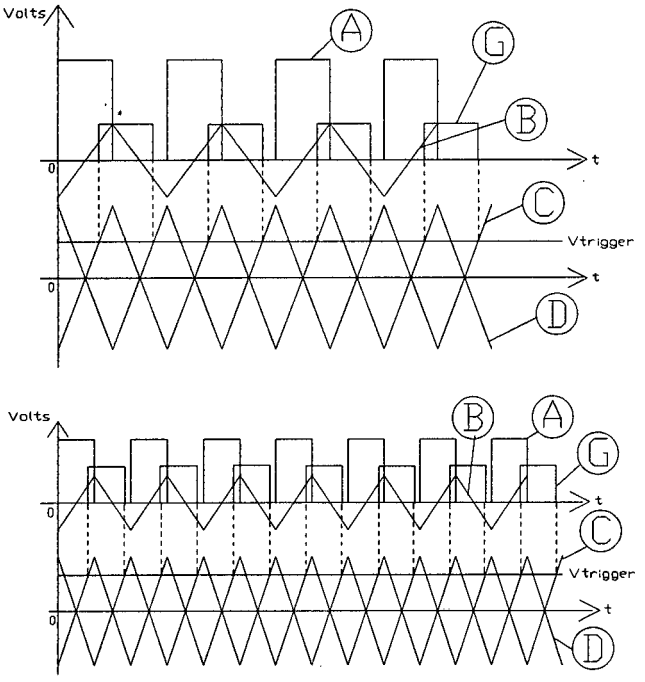

(a) Phase shift A-G = 126°. Here the phase shift is the same as shown in Fig.7.16

(b) Phase shift A-G = 128°. Here the frequency is increased. The integration time is reduced so that the triangular waveforms B, C and D are reduced in amplitude. However, the trigger level $V_{trigger}$ remains constant, and so triggering occurs further up the rising edges of the waves C and D. Thus the phase shift is increased relative to the phase shift in (a).

Fig.7.17 Change of phase shift with frequency

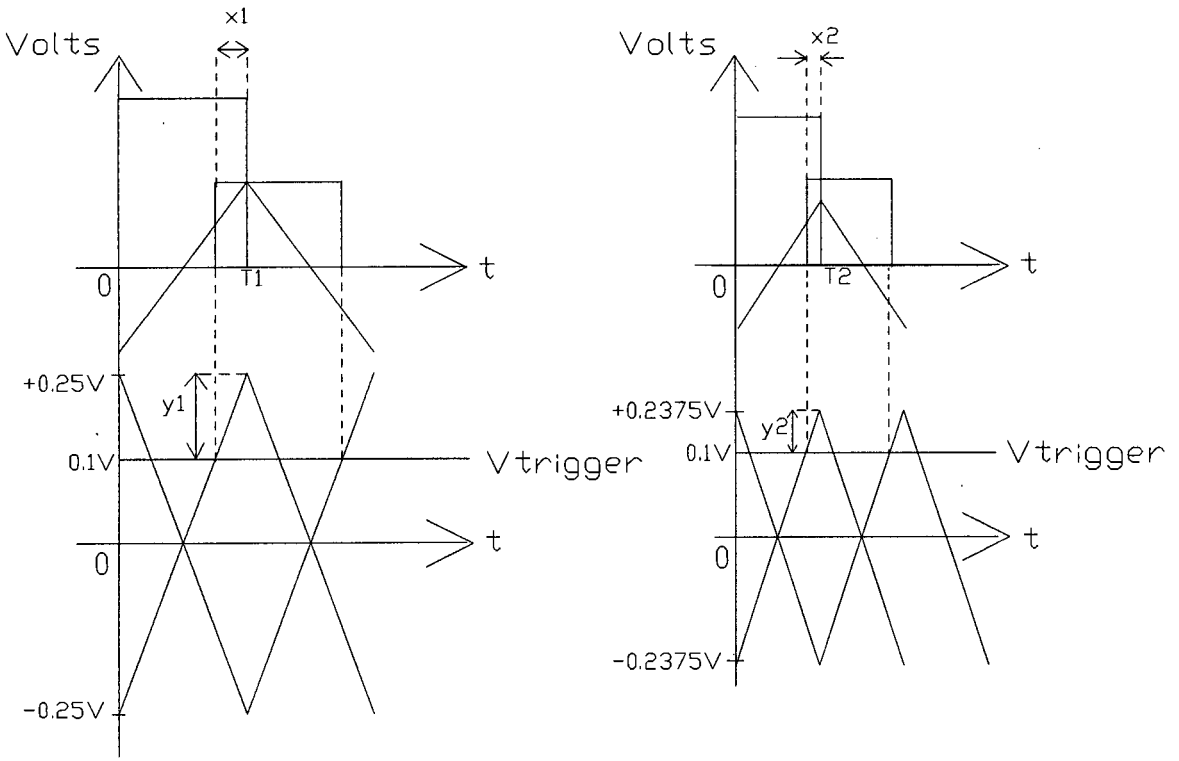

(a) Frequency f_1 (b) Frequency f_2

Fig.7.18 Diagram showing change in phase-shift with frequency in more detail (enlarged version of Fig.7.17)

In Fig.7.18(a) above, we assume $V_{trigger} = 0.1V$, $f_1 = 1Hz$, $T_1 = 0.5$seconds, slope of integrator = 1V/second.
=> $y1 = 0.25V - V_{trigger} = 0.15V$ => x1 = y1/slope = 0.15seconds
=> phase shift (1) = $180°(1 - 0.15/T_1) = 126°$.

In Fig.7.18(b), assume $V_{trigger} = 0.1V$, $f_2 = 1.05f_1 = 1.05Hz$, $T_2 = 0.95T_1 = 0.475s$, slope of integrator = 1V/s.
=> $y2 = 0.2375V - V_{trigger} = 0.1375V$ => x1 = y2/slope = 0.1375seconds
=> phase shift (2) = $180°(1-0.1375/T_2) = 128°$.

The change in phase shift with frequency observed with the phase shift circuit is illustrated by the oscilloscope traces below. The traces show the output of the phase shifter when driven by the field mill reference signal. Note that the two signals have been scaled slightly differently in amplitude, and given a small vertical offset, so that they may be clearly distinguished. The only important feature to note on these traces is the phase shift between the two signals.

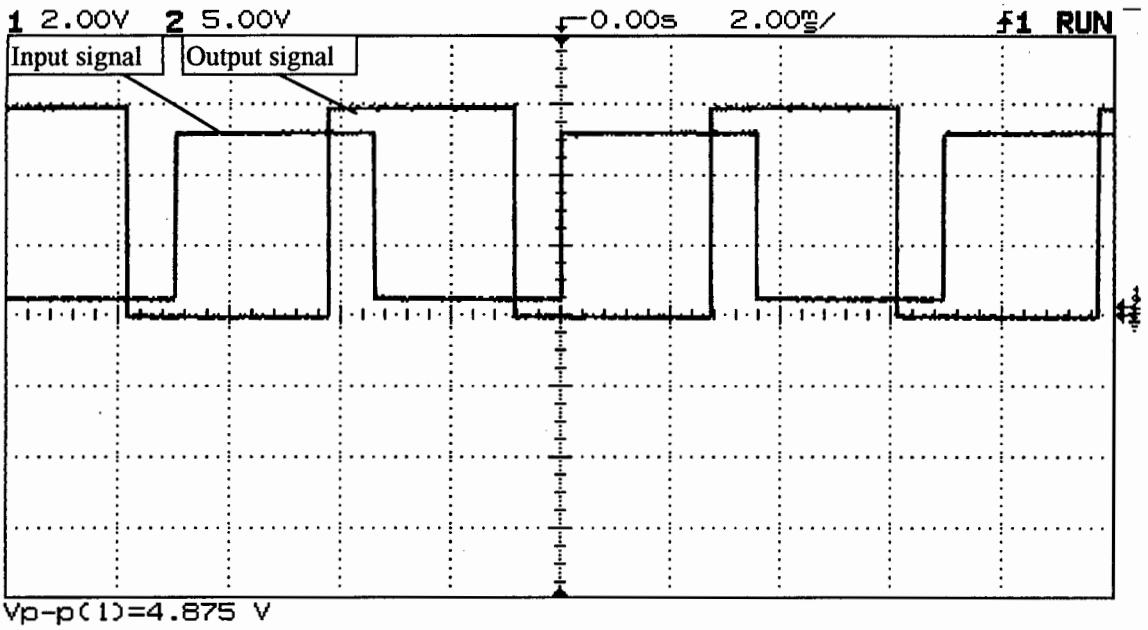

Fig.7.19(a) Oscilloscope trace showing the shifted and unshifted reference signals f=143Hz Φ=139°

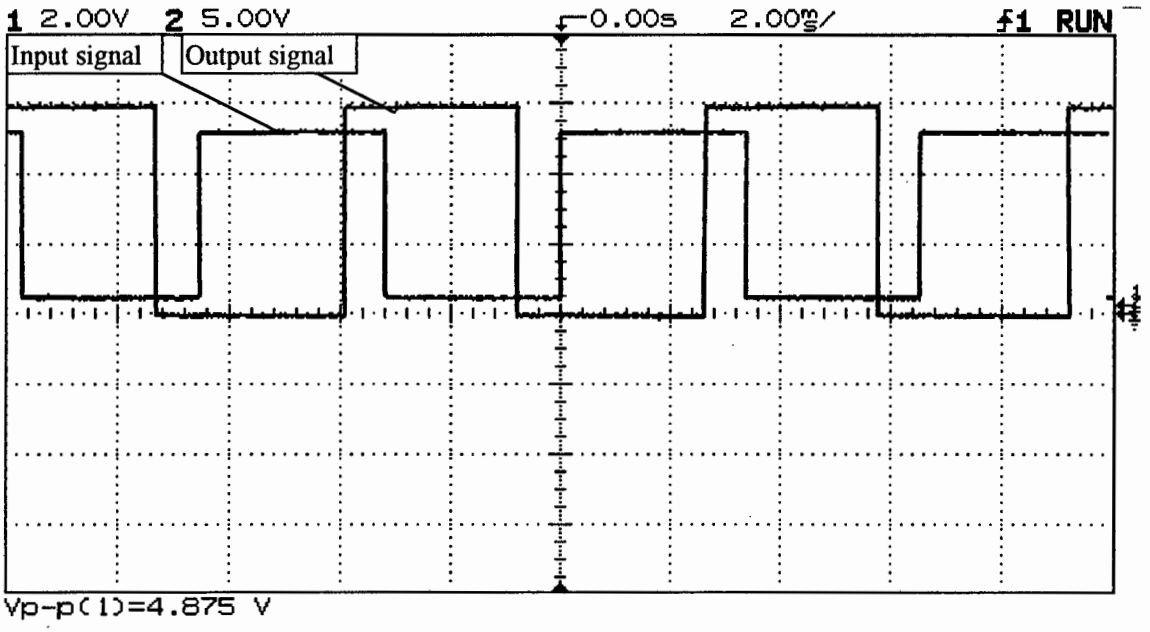

Fig.7.19(b) Oscilloscope trace showing shifted and unshifted reference signals f=153Hz Φ=144°

Thus it can be seen that the phase shifter circuit will introduce significant phase-shift errors if the frequency changes by more than, say, 2%. The small tape recorder motor used for the field mill could only keep the modulating frequency constant to +/-5%, so that the change of phase-shift with frequency posed a serious problem. This problem was evident in trial runs with the field mill. Phase shift circuits which are capable of keeping constant phase shift over a range of frequencies are described by Faulkner [13] and Lee [14]. However, these circuits are more elaborate, and it was felt that for this thesis it would be sufficient simply to adjust the position of the reference rotor by hand until the reference and sensed signals were in-phase. In order to align the reference and sensed signals, both signals were displayed simultaneously on a dual-trace oscilloscope. The phase was adjusted by adjusting the position of the reference rotor until the signals were visually in-phase. This simple method has also been used by Currie [15] to ensure correct phase alignment.

Another consideration is the 90° phase shifter that is required to produce a 90° reference signal for ion current detection. It was felt that with the frequency-dependence of the phase shift circuit, it would be more practical to mount a second reference rotor on the field mill shaft, and adjust it to be 90° out-of-phase with the first reference rotor. (Rather than using a 90° phase-shift circuit to produce a 90° reference signal from the first reference signal). This method ensured that the phase difference between the two reference rotors was constant no matter what the modulating frequency.

Conclusions

Due to problems with frequency-dependence, the phase shifter cicuit was not used in the final field mill system. Instead, reference signals (both in phase and quadrature) were taken directly from the optical switches through which the reference rotors pass. The development of a phase-shift circuit that is frequency-independent would be an improvement to the electric field mill, and should be one of the areas for further work.

7.4 Synchronous detector

7.4.1 Basic Synchronous Detector Design

The synchronous detector (phase-sensitive detector) was designed using the AD630 balanced modulator / demodulator from Analog Devices. The AD630 is intended for use in precision instrumentation and signal processing applications, which require wide dynamic range. When used as a synchronous demodulator, the AD630 is capable of recovering a signal from 100dB of interfering noise. The AD630 is optimised for frequencies up to 1kHz.

The basic mode of operation of the AD630 consists of two fixed-gain stages of opposite sign which are inserted into the signal path under the control of a sensitive voltage comparator. When the circuit is switched between the inverting and non-inverting gain (+2 and -2), demodulation occurs. A block diagram of the circuit is shown below:

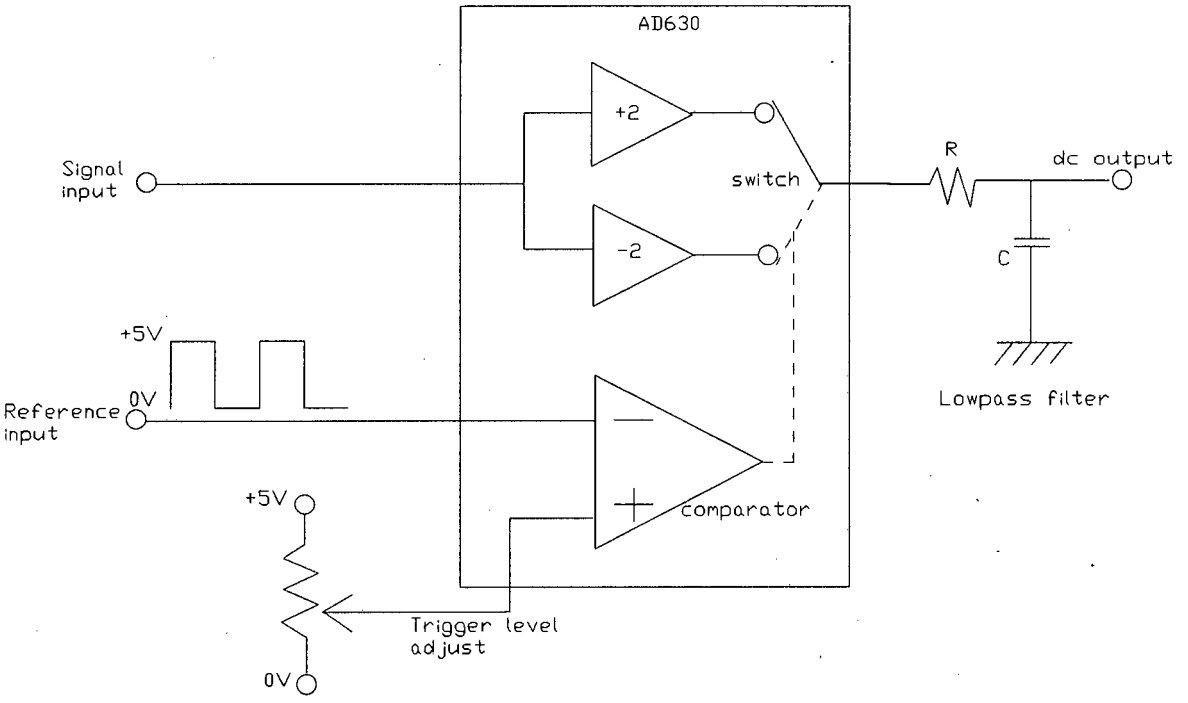

Fig. 7.20 AD630 Balanced modulator/demodulator used as a synchronous detector

As shown in the diagram above, the synchronous detector output is filtered with a first-order lowpass filter to remove high-frequency products (introduced by the operation of the mixer). The final output is a dc voltage proportional to the amplitude of the signal input to the synchronous detector. The amplitude of the output signal is also dependent on the relative phase shift between the reference and input signals.

7.4.2 Lowpass Filter at the Synchronous Detector Output

The choice of the R and C values for the lowpass filter is a trade-off between noise and response time. The response time of the synchronous detector output is $\tau = RC$. This means that for a given value of RC, a time period of 5RC should be allowed for the settling of transients, after a step change in the applied electric field, before taking a reading. Thus as RC is increased, so the harmonic noise (introduced by demodulation) is reduced, but the response time becomes slower. The field mill was operated under zero-applied field conditions, and the noise level at the lowpass filter output was measured for various values of the resistor R, with C=10μF . Each noise measurement represents the average of 100 consecutive readings of ac voltage in a bandwidth of 3Hz to 300kHz taken with a true-rms multimeter (HP 34401A). The graph below shows the output noise (expressed as electric field noise in V/m) for different values of time constant $\tau = RC$.

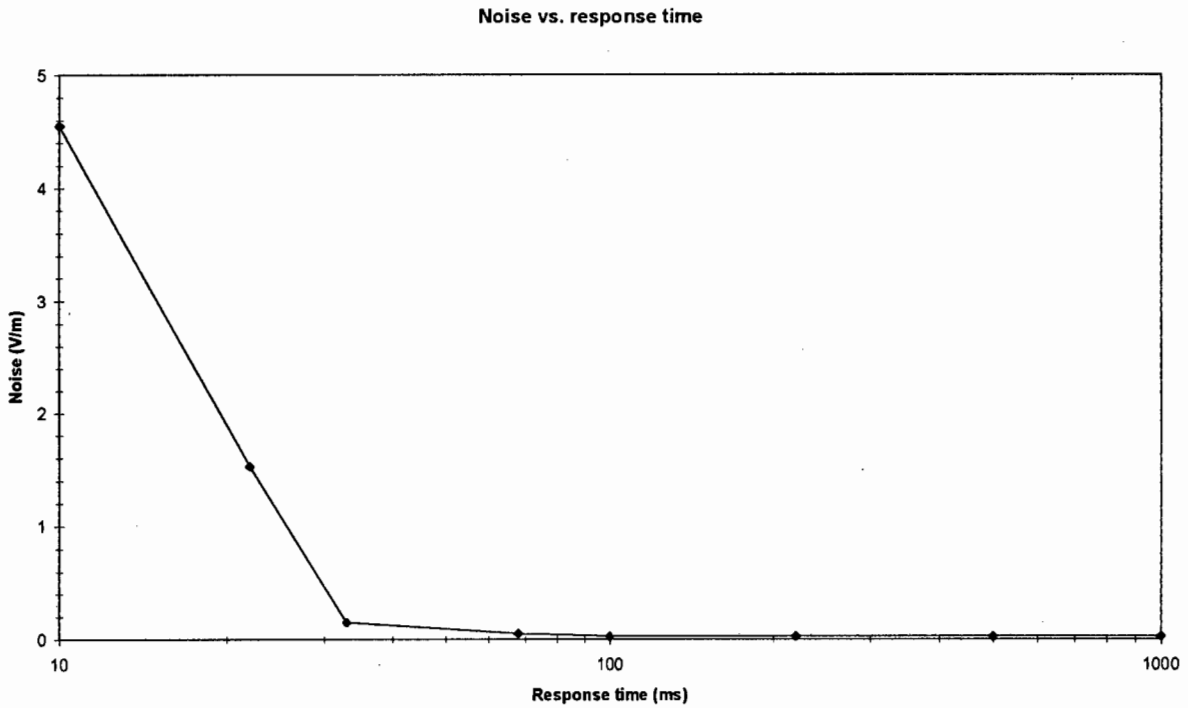

Fig.7.21 Noise vs. response time of the lowpass filter at the synchronous detector output

From the above graph, it would appear that provided the RC time constant is chosen to be about 33ms (for example, with R=33kΩ and C=1μF), then the electric field noise will be reduced to an acceptable level, and that further increasing the RC value will give very little improvement in noise, but will increase the response time. The minimum detectable signal in an electrostatic field is about 10V/m, so that a time constant of 33ms should give sufficient noise rejection.

Note: these noise measurements only consider the noise introduced by the field mill system itself. The characteristics of the measurand must also be taken into account. In our case we are measuring both electric field strength and ion current density. Are these quantities stable and time-invariant, or are there fluctuations with time that need to be averaged-out? This is discussed on the following page.

When making measurements of electric field strength underneath a corona needle where significant ion concentrations are found, slow fluctuations in the electric field readings were observed. The graph below shows the drift in the electric field output signal for two cases: electrostatic field (no ions) and ionised electric field (high ion concentration).

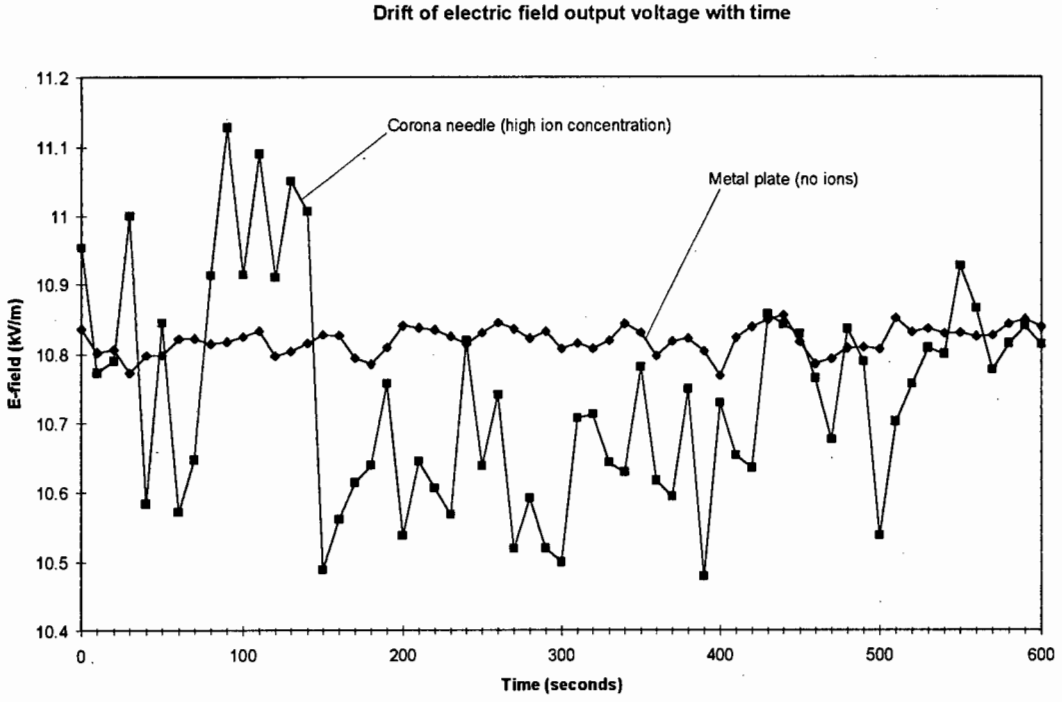

Fig.7.22 Drift of electric field output signal (after synchronous detection)

The graph above shows the drift of the electric field signal after the lowpass filter of the synchronous detector. The lowpass filter in this case had a time constant of 1 second. The electric field signal measured with the flat metal plate electrode (no ions) shows little fluctuation (about 0.5%). The electric field signal measured with the corona needle shows much larger fluctuations with time (about 5%). The fluctuations are caused by charged ion clouds drifting over the field mill sensing surface, so altering the electric field. It was necessary to increase the RC time constant to 1 second, in order to reduce the fluctuations to the levels shown in the graph above. (With a time constant of 33ms, the fluctuations were too large for accurate measurements). A time constant of 1 second was found to be a reasonable compromise between noise and response time.

Note: in general, it will be up to the user of the instrument to decide on the length of the time constant, taking into account the characteristic fluctuations in the signal being measured. The fluctuations will depend on the particular measurement situation. However, the time constant should not be reduced below 33ms.

7.5 Quadrature Method for Simultaneous Measurement of Electric Field and Ion Current Density

The principles of this method have already been described as Method II in Chapter 5. This method requires two synchronous detectors. The reference signal to the first synchronous detector is in phase with the electric field signal, and the reference signal to the second 90° out of phase. These two references were generated using two reference rotors on the field mill shaft, (90° out of phase from each other).

7.5.1 Preamplifier used before Quadrature Detection

It is desirable to choose the feedback of the preamplifier to be resistive ($\omega RC << 1$), so that the ion current component is favoured over the electric field component. This is necessary because both signals lie at exactly the same frequency, and also because the electric field signal is expected to be very much larger than the ion current signal. (This has already been discussed in Chapter 5). In this case the equations for the peak voltages of the preamplifier signal components are:

$V_e\,(max) = 2f\varepsilon_o EAR$ = peak output voltage due to electric field..... **(7.7)**

$V_j\,(max) = {}^1/_2\, V_j\,(pk\text{-}pk) = {}^1/_2\, JAR$ = peak output voltage due to ion current density.. **(7.8)**

$V_j\,(dc) = {}^1/_2\, JAR$ = dc component of ion current density signal..... **(7.9)**

where: ε_o = permittivity [F/m]
f = modulating frequency [Hz]
E = electric field strength [V/m]
A = maximum exposed stator area [m^2]
R = feedback resistance of preamplifier [Ω]
J = ion current density [A/m^2]

A PSpice program was written to simulate the two components $v_e(t)$ and $v_j(t)$ of the preamplifier output voltage as the rotor spins. The preamplifier circuit is as shown below:

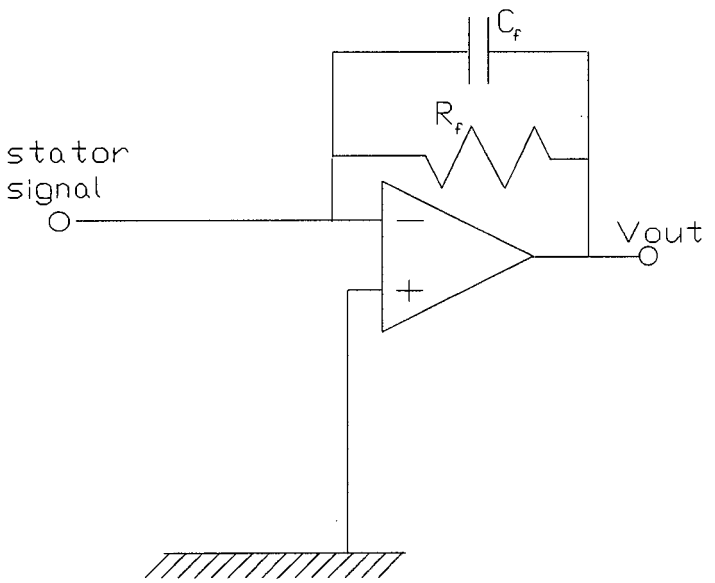

Fig.7.23 Circuit used for PSpice simulation

$R_f = 10M\Omega$ $C_f = 10pF$ f=160Hz
$\omega RC = 0.1 << 1$

Stator area: $A = 0.0025m^2$

Assume: $JA = 1nA$
$2f\varepsilon_o EA = 1nA$
(for purposes of illustration)

The PSpice source code is documented in Appendix C. The PSpice output is shown below:

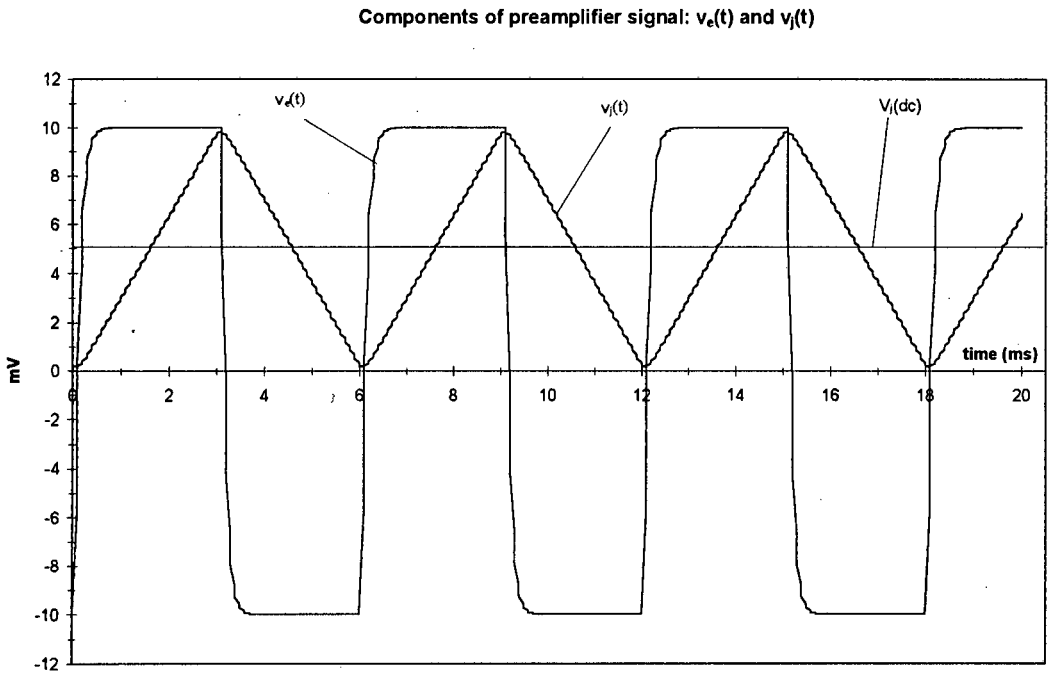

Fig.7.24 Preamplifier output showing components $v_e(t)$ and $v_j(t)$

Notes

1. In the plot above, JA = 1nA, and $2f\varepsilon_o EA$ = 1nA, whereas in practical situations we expect: JA ~ 250pA and $2f\varepsilon_o EA$ ~ 75nA, so that in the above plot, $v_j(t)$ has been shown magnified by a factor of about 300 (with respect to $v_e(t)$), for clarity.

2. The quadrature (90°) phase shift between $v_j(t)$ and $v_e(t)$ is clearly seen.

3. The dc component of the ion current $V_j(dc)$ = 5mV can also be seen.

7.5.2 Crosstalk in the Quadrature Detection Method

Due to the small magnitude of the ion current signal relative to the electric field signal, any crosstalk between the input channels to the synchronous detector will cause significant errors in the ion current density readings. If the two channels are exactly in quadrature (90° out of phase), then perfect phase-sensitive detection will occur, and the electric field and ion current components of the preamplifier signal may be separated out. However, it is difficult to achieve perfect quadrature phase shift between the two reference signals. The calculations below illustrate the problems caused by crosstalk due to a phase mis-alignment of 1° = 0.0175 radians between the two reference signals. (For example, the references might be 89° out of phase instead of 90°). Calculations are given for both preamplifier configuratons ($\omega RC << 1$) and ($\omega RC >> 1$) to illustrate the two cases. For these calculations, assume:

$A=0.0025m^2$ **E**=10kV/m **J**=1000nA/m^2 f=160Hz Φ = phase error =1°

For the two preamplifier cases: 1. ($\omega RC << 1$) choose R=10MΩ, and C=10pF
2. ($\omega RC >> 1$) choose R=100MΩ, and C=47pF

Table 7.6 Effects of crosstalk between electric field and ion current channels

	($\omega RC << 1$)		($\omega RC >> 1$)	
	Equation	Value	Equation	Value
V_e(max)	$2f\varepsilon_o EAR$	708mV	$\frac{\varepsilon_o EA}{2C}$	2.35V
V_j(max)	$^1/_2JAR$	125mV	$\frac{4JA}{\pi^2\omega C}$	21.4mV
V_i(dc)	$^1/_2JAR$	125mV	$^1/_2JAR$	125mV
Crosstalk	V_e(max) sinΦ	12.4mV	V_e(max) sinΦ	41.1mV
Crosstalk as % of V_i(max)	Crosstalk/V_i(max) %	99.2 %	Crosstalk/V_i(max) %	192 %

The table above shows that for a phase error of only 1°, there is significant crosstalk. Also the point is made that for quadrature detection it is preferable to use a preamplifier with $\omega RC << 1$ (feedback mainly resistive) so that the ion current component V_j(max) is maximised, and is independent of frequency. Even with this arrangement, the crosstalk is still severe.

Let us assume that we do use a preamplifier with $\omega RC << 1$. The equation $V_e(max) = 2f\varepsilon_o EAR$ (7.7) suggests that by decreasing the modulating frequency f sufficiently, it might be possible to reduce the crosstalk in the ion current channel to manageable levels. (The ion current signal is independent of frequency, and so should be unaffected by frequency changes). An experiment was set up to investigate this possibility.

7.5.3 Experiment to Investigate the Feasibility of Quadrature Detection

The field mill was set up with the rotor flush with the ground plate of a parallel-plate calibration box, as described in Chapter 3.7. Values for both electric field and ion current density were measured at different motor speeds (different values of modulating frequency). This was repeated for two different electric field and ion current source arrangements:

(a) Top electrode = flat metal plate, applied voltage = 5kV. No significant ion current.
(b) Top electrode = corona needle, applied voltage = 5kV. Significant ion current.

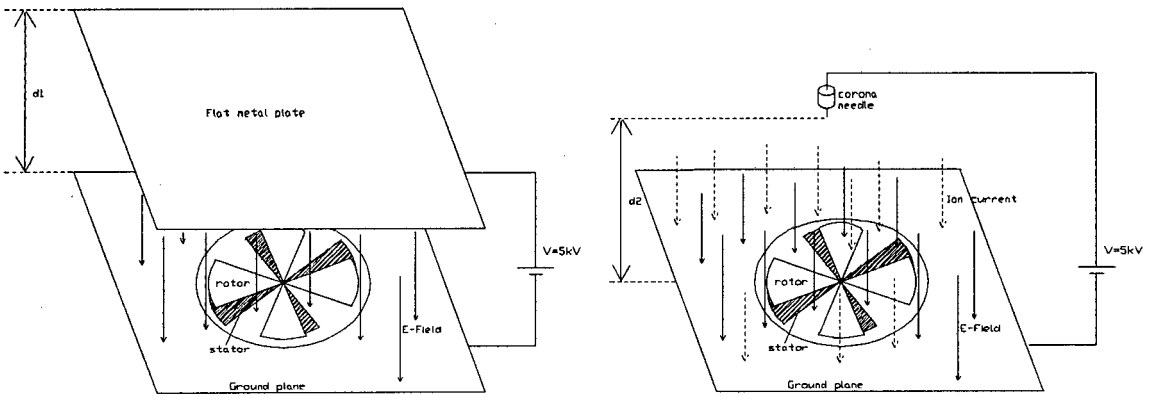

(a) Electric field only (no ions) (b) Electric field and ion currents

Fig.7.25 Arrangement for producing electric field and ion currents

Note: the height of the flat metal plate (d1=200mm) is different to the height of the corona needle above the ground plane (d2=180mm). This is due to the fact that the corona needle produces a smaller electric field than the metal plate, for a given height above the ground plane. It was desired to keep the electric field strengths approximately the same order of magnitude, so that the magnitude of the crosstalk would be reasonably comparable in the two configurations.

The circuit diagram of the amplifier is shown below:

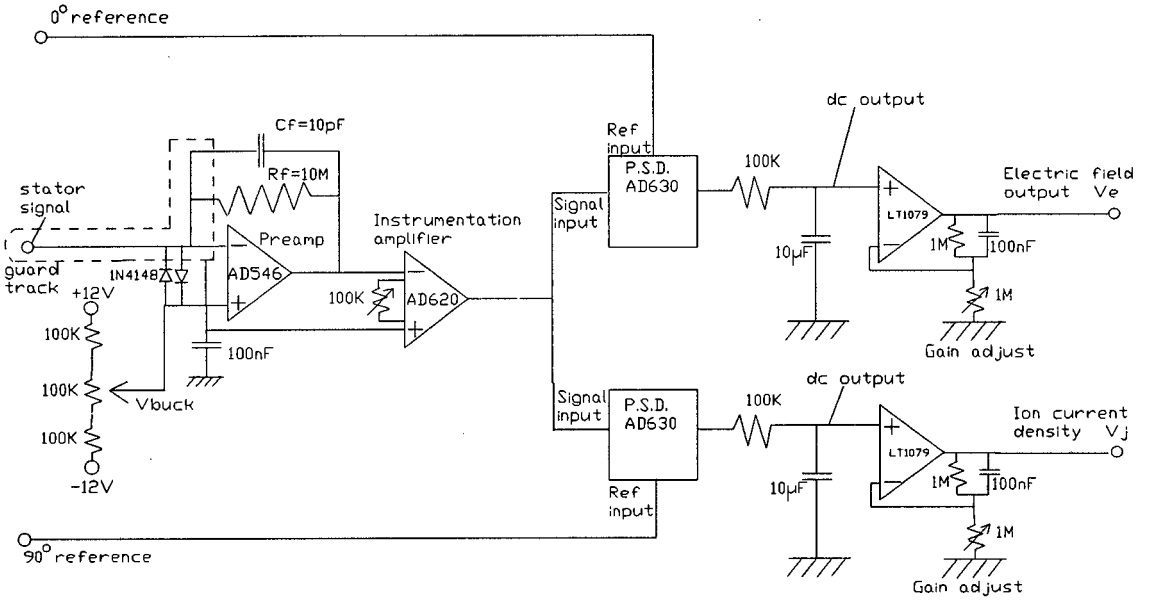

Fig.7.26 Amplifier circuitry for the quadrature detection method

The circuit shown above was constructed on double-sided PC board, and housed in a grounded metal box. +12V and -12V voltage regulators mounted on the circuit board were used to reduce 50Hz mains interference. The preamplifier uses feedback components such that $\omega RC<<1$, so the theoretical preamplifier output should have components:

$V_e(max) = 2f\varepsilon_o EAR_f$ = peak output voltage due to electric field..... (7.7)

$V_j(max) = {}^1/_2\, V_j(pk\text{-}pk) = {}^1/_2\, JAR_f$ = peak output voltage due to ion current density (7.8)

$V_j(dc) = {}^1/_2\, JAR_f$ = dc component of ion current density signal..... (7.9)

The oscilloscope trace below shows the preamplifier output with an applied electric field of 10kV/m.

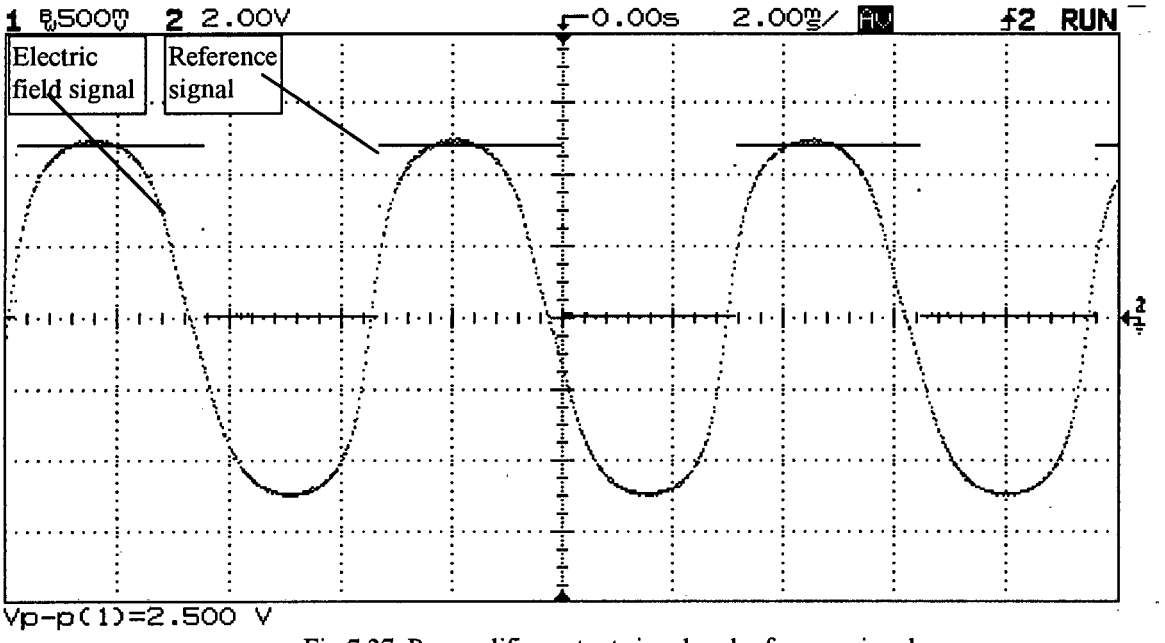

Fig.7.27 Preamplifier output signal and reference signal

The oscilloscope trace above shows the output of the preamplifier with the flat metal plate electrode (here the only signal component is $v_e(t)$ since there are no ions present). However, the oscilloscope trace taken with the corona needle is not visibly different from the above trace. This is due to the low amplitude of $v_j(t)$ compared to $v_e(t)$.

At the output of the phase-sensitive detector the magnitude of the electric field signal should be frequency-dependent, while the magnitude of the ion current density reading should remain constant with frequency. Synchronous detection should separate the components $V_e(max)$ and $V_j(max)$, and reject $V_j(dc)$.

The output values V_e and V_j, (being the output values for electric field and ion current density), were measured after phase-sensitive detection and some amplification. Before taking any readings, the bucking voltage, V_{buck}, was used to null the field mill output under zero-applied-field conditions. The two reference signals at 0° and 90° were taken directly from the two reference rotors mounted on the shaft (no phase shifter was used). The graphs below show the ouput values of V_e and V_j measured at different modulating frequencies (frequency was altered by changing the motor speed). Due to the poor motor response, it was difficult to maintain a constant frequency to better than +/-5Hz, so there is some scatter in the readings. Moreover, the graph of Fig.7.29 (corona needle electrode) shows that in the presence of ions, the electric field values exhibit considerably more scatter than with the flat metal plate electrode. This is due to the drift of charged ion clouds in the air between the corona needle, and the ground plane. As the frequency of modulation is increased, so the electric field reading increases, as expected. The ion current density reading should theoretically remain constant with frequency, but increases due to crosstalk from the electric field channel. At frequencies below about 40Hz, the crosstalk from the electric field channel becomes negligible, and a dc offset voltage is observed in the V_j curve with the corona needle (this is the signal V_j which we are trying to extract) . No dc offset is observed on the V_j curve with the flat metal plate electrode since there are no ions present.

Note: the curves V_e and V_j have different scales. (V_j is shown magnified with respect to V_e).

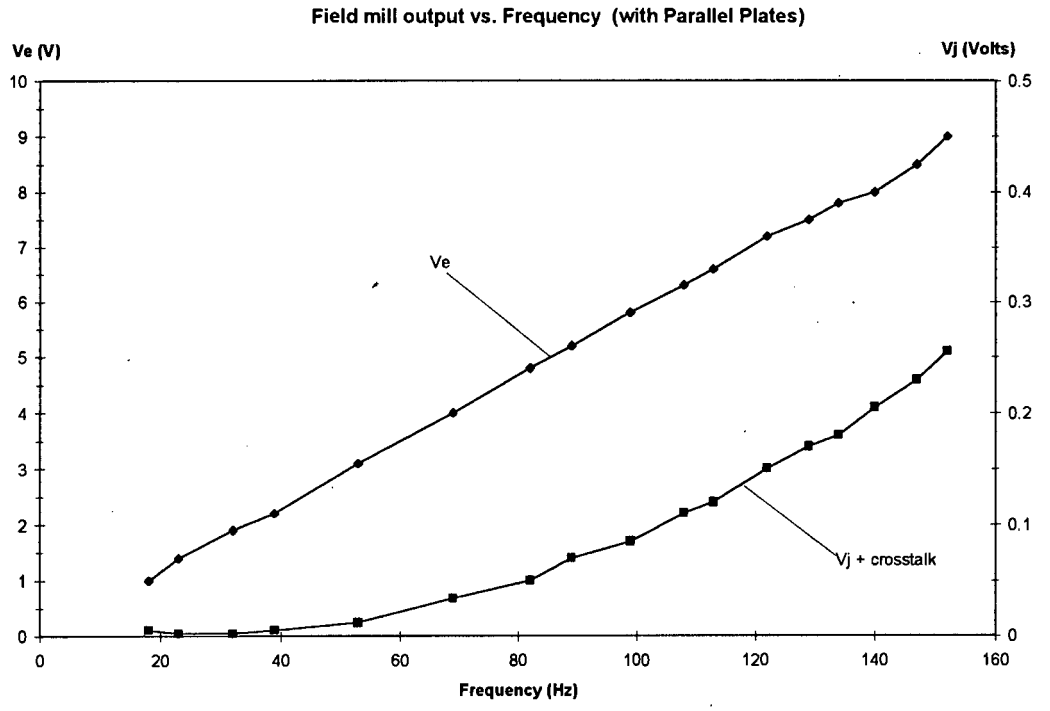

Fig.7.28 Electric field and ion current density measurements with flat metal plate electrode (no ions)

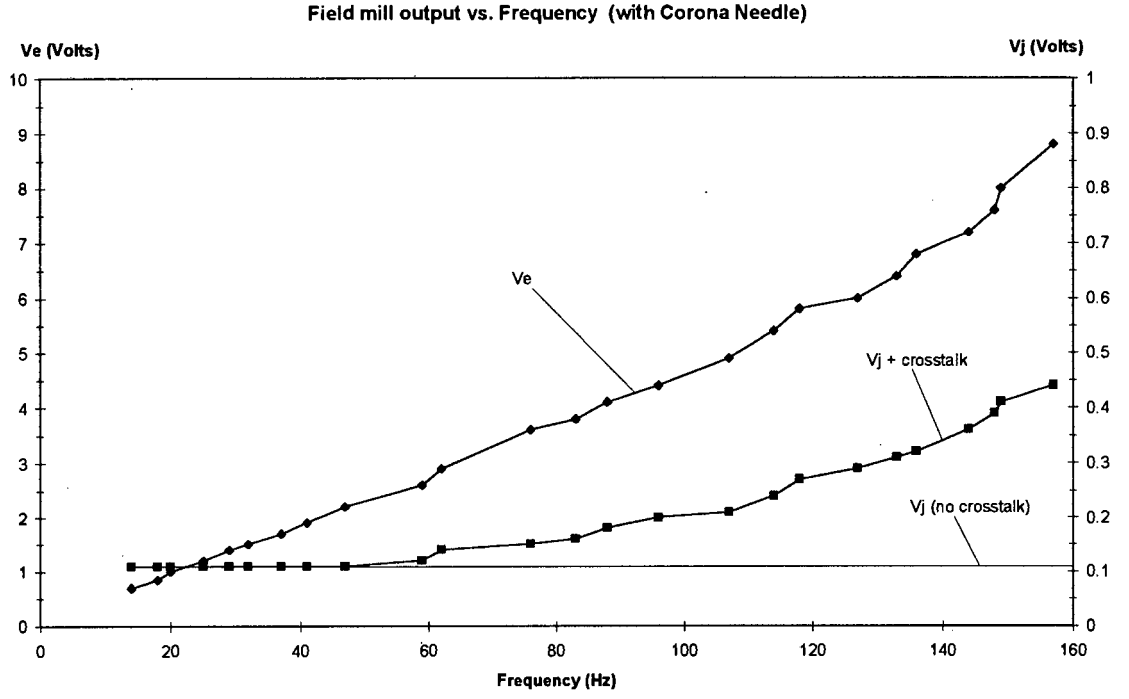

Fig.7.29 Electric field and ion current density measurements with corona needle electrode (ions present)

Discussion

From the graphs above, it would seem possible that the ion current density could be read by running the field mill at low frequency (say 40Hz), to reduce the crosstalk to a reasonable level. Operating at such low frequency is undesirable, as the noise rejection of the synchronous detector is now being compromised, (the frequency is now too low to allow 50Hz interference to be attenuated). Also, a fluctuation of say, 5Hz, in frequency now produces a 12.5% change in frequency, instead of the 3% change at 150Hz. This introduces errors since the crosstalk, although reasonably small, is non-zero, and frequency-dependent. Even if the crosstalk is removed, the magnitude of the output signal due to ion currents (V_j) is very small compared to the magnitude of the electric field output (V_e), so that V_j will need considerably more amplification. Finally, calibration of the ion current density channel will present difficulties, since the "current injection" calibration method (see Chapter 4) cannot easily be used in the synchronous detector system. Although Sheahen [16] used quadrature detection for the ion current density measurements, he was measuring ion currents in the upper atmosphere which are several orders of magnitude higher than the ion currents to be measured for this thesis.

Numerical analysis may possibly improve the results, but this would be tedious and require much data processing for measurements taken over several days or longer.

7.5.4 Conclusion

The main problem with the quadrature detection method is that the electric field component of the field mill signal is very much larger than the ion current component. This is the major source of interference in the ion current measurements, and the interference is not easily removed, since it lies at the same frequency. From these results we see that quadrature detection is not feasible in terms of the requirements for this thesis.

7.6 Final electronic circuit design

The final electronic design uses the lowpass filter method for the detection of ion current density. (This has been discussed as Method III in Chapter 5).

7.6.1 Preamplifier

The preamplifier uses feedback with $\omega RC >> 1$ (mainly capacitive feedback). This gives rise to the following equations at the preamplifier output:

$$V_e(\max) = \frac{\varepsilon_o EA}{2C} \quad \text{..... (7.10)}$$

$$V_j(\max) = \frac{1}{2}V_j(pk\text{-}pk) = \frac{4JA}{\pi^2 \omega C} \quad \text{..... (7.11)}$$

$$V_j(dc) = {}^1/_2\, JAR \quad \text{..... (7.12)}$$

where: ε_o = permittivity [F/m]
f = modulating frequency [Hz]
E = electric field strength [V/m]
A = maximum exposed stator area [m^2]
R = feedback resistance of preamplifier [Ω]
J = ion current density [A/m^2]

A PSpice program was written to simulate the two components $v_e(t)$ and $v_j(t)$ of the preamplifier output voltage as the rotor spins. The simulated preamplifier circuit is as shown below:

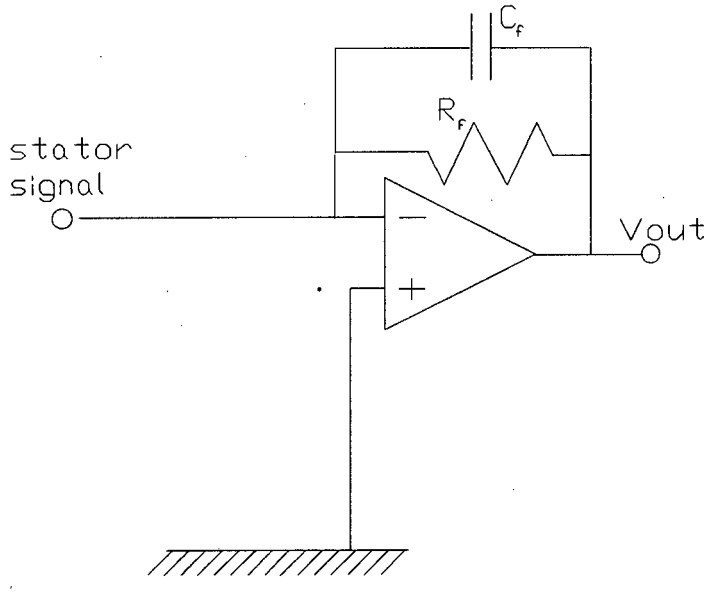

Fig.7.30 Circuit used for PSpice simulation

R_f = 50MΩ C_f = 100pF f=160Hz
ωRC = 5 >> 1

Stator area: A = $0.0025m^2$

Assume: JA = 1nA
$2f\varepsilon_o EA$ = 1nA
(for purposes of illustration)

The PSpice source code is documented in Appendix C. The PSpice output is shown below:

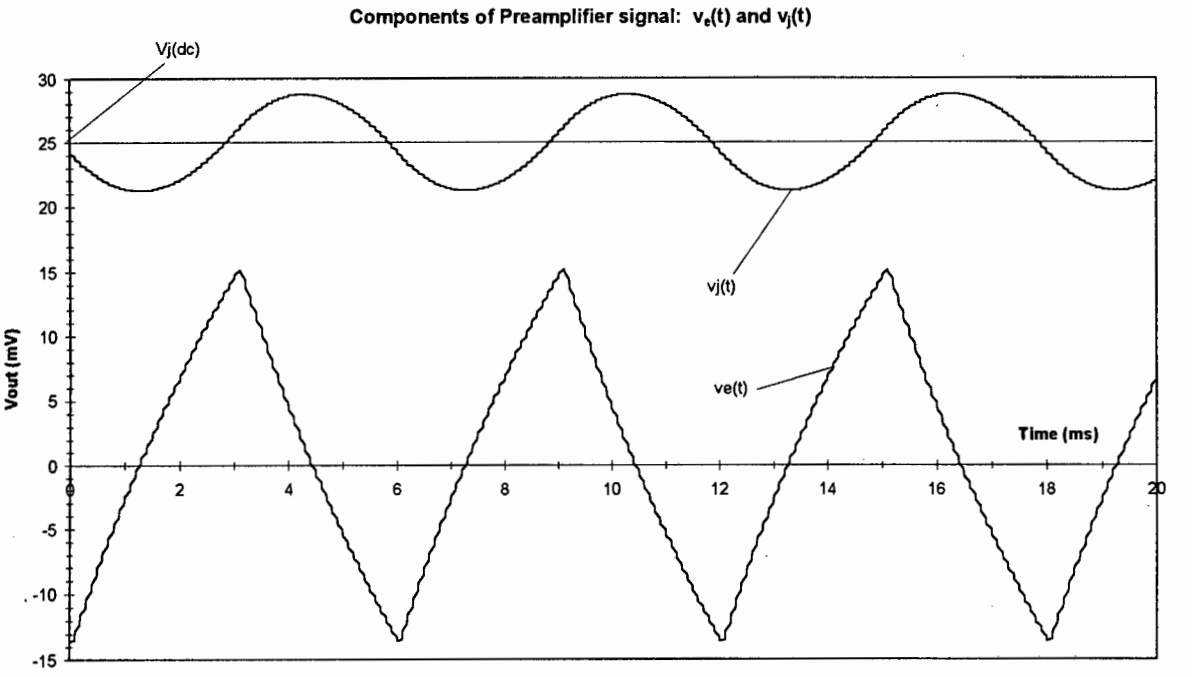

Fig.7.31 Preamplifier output signal: Electric field component = $v_e(t)$ Ion current = $v_j(t)$

Notes 1. In the plot above, JA = 1nA, and $2f\varepsilon_o EA$ = 1nA, whereas in practical situations, we expect: JA ~ 250pA and $2f\varepsilon_o EA$ ~ 75nA, so that in the above plot, $v_j(t)$ has been shown magnified by a factor of about 300 (with respect to $v_e(t)$), for clarity.

2. The quadrature (90°) phase relationship between $v_j(t)$ and $v_e(t)$ is clearly seen.

3. The dc component in the ion current $V_j(dc)$ = 25mV can also be seen.

The oscilloscope trace below shows the output of the preamplifier, in an applied electrostatic field of 10kV/m. Due to the small size of the ion current component $v_j(t)$ compared with the electric field component $v_e(t)$, there is little visible change in the oscilloscope trace if the field mill is placed in an ionised electric field.

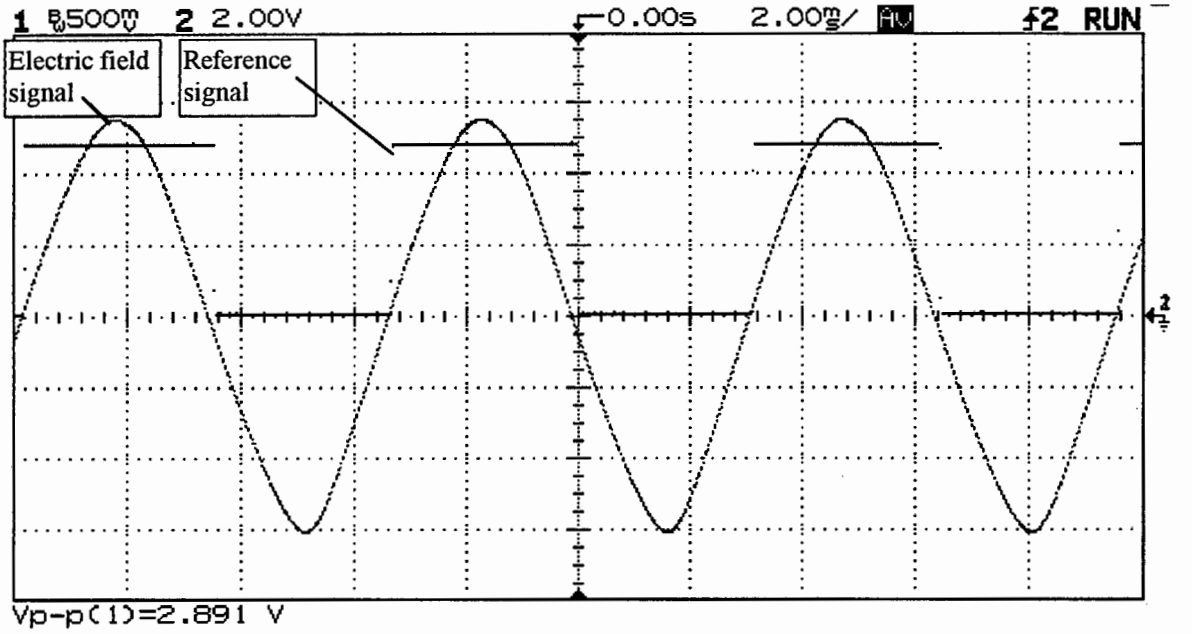

Fig.7.32 Preamplifier output with an applied electric field of 10kV/m

7.6.2 Synchronous detector

The synchronous detector is used to detect the electric field component $v_e(t)$ and reject the ion current component $v_j(t)$ (since the signals are in quadrature). The synchronous detector uses a reference signal taken directly from the slotted optical switch as the reference rotor spins through it. No phase shifter is used. The synchronous detector has exactly the same design as that used for the quadrature detection circuit of Fig.7.26.

7.6.3 Lowpass Filter

The lowpass filter is used to separate $V_j(dc)$, which is the dc component of the ion current signal. A fourth-order Butterworth lowpass filter was designed, with a cut-off frequency of 0.16 Hz. The filter was a Sallen-and-Key active filter using two opamps. This filter was found to be satisfactory in reducing fluctuations in the ion current signal, although for calibration purposes some signal averaging was required after the filter. The circuit diagram of the filter is shown below:

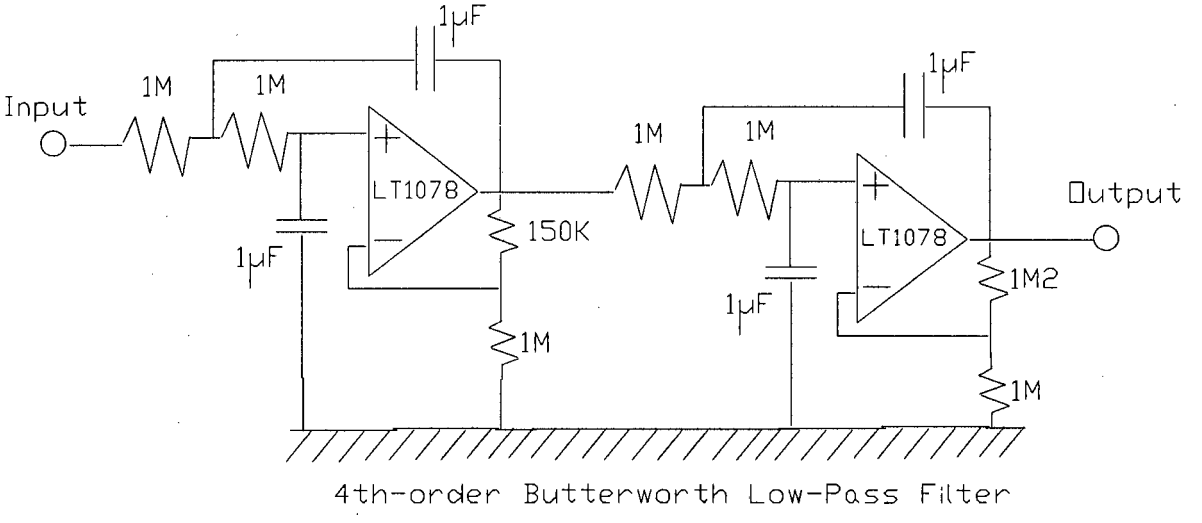

Fig.7.33 Sallen-and-Key lowpass filter

The graph below shows the slow drift in the ion current density output signal, due to fluctuations in the number of ions arriving at the stator. This is the final output signal after the lowpass filter. A lowpass filter with an even sharper cut-off would have further reduced the fluctuations, but it was felt that any further averaging required could be accomplished more easily by taking many readings, and averaging them numerically. Also, it was felt that the response time should not be further reduced. The response time $\tau = 2.5$ seconds, so that it is necesary to wait for $5\tau = 12$ seconds after a step-change in ion current before taking readings.

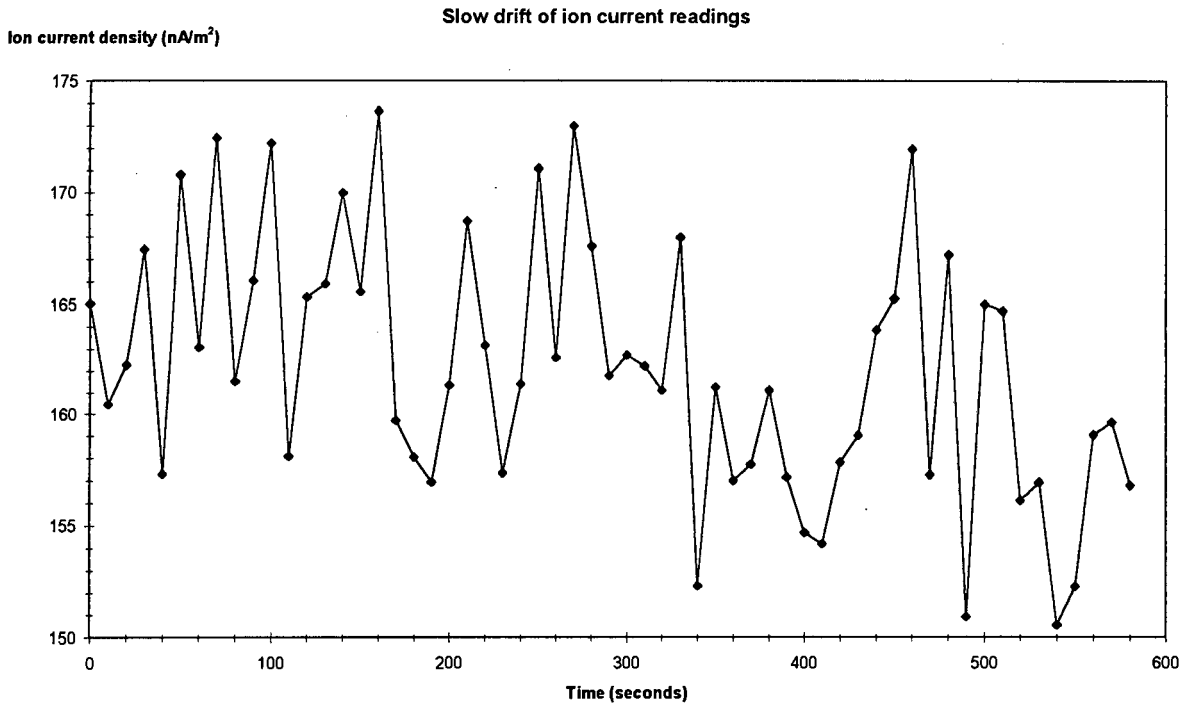

Fig.7.34 Slow variations in ion current density output signal

The graph above shows an average output signal of 162 nA/m^2, with fluctuations of +/-12 nA/m^2. This represents a fluctuation of +/-7% in the ion current readings. It is noted in the literature that even under conditions of steady corona generation, the ion current signal may exhibit considerable variability due to movement of space charge. In outdoor measurements, fluctuations in ion current density as high as +/- 50% of the average value have been recorded [22]. For calibration purposes, it is necessary to use numerical averaging of the output. Fluctuations in ion current density values are an unavoidable problem [20].

7.6.3 Amplifier circuit diagram

The final electronic circuit for the field mill amplifier is shown below. The circuit was constructed on double-sided PC board, and enclosed in a grounded metal box. The circuit includes its own +12V and -12V voltage regulators mounted on the circuit board.

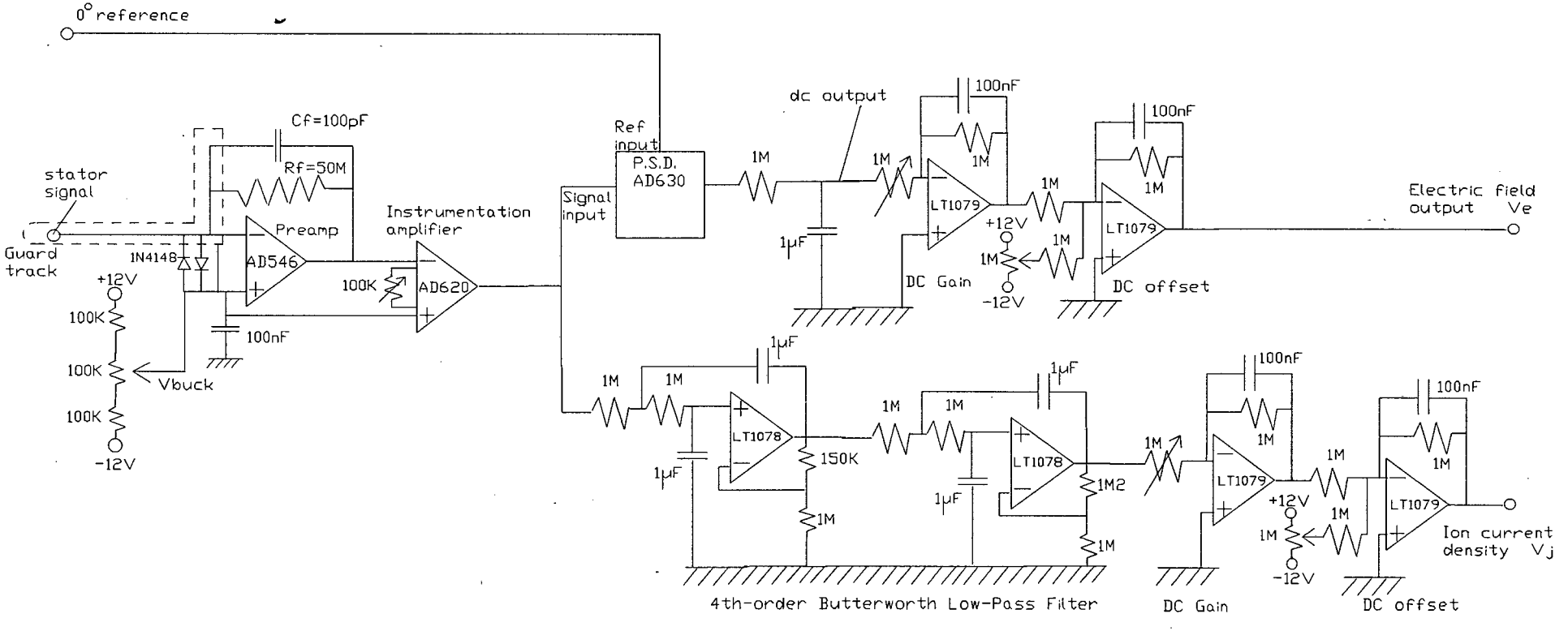

Fig.7.35 Circuit diagram of electric field mill circuitry

7.6.4 Zero-drift of the field mill output

7.6.4.1 Zero-drift of electric field measurements

The zero-drift of the electric field output over a 5-hour period is shown in the graph below. For this experiment, a gold wire earthing brush was used, and the field mill operated under zero-electric field conditions.

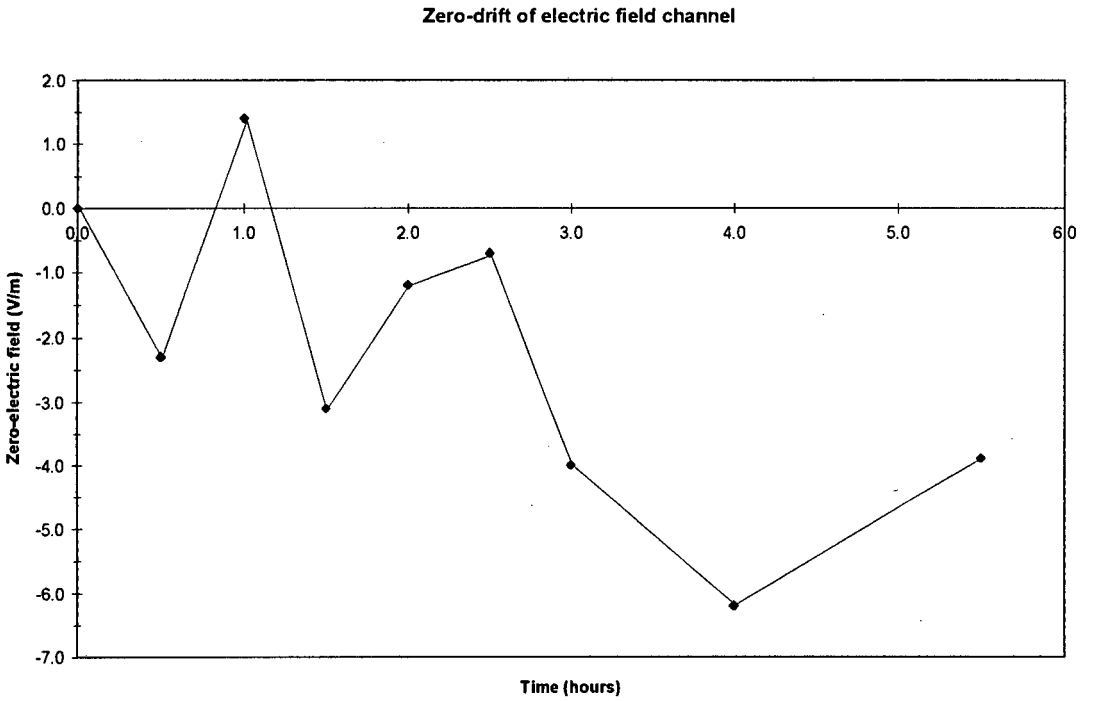

Fig.7.36 Zero-drift of electric field channel over a 5-hour period

From the graph above, the zero-drift of the electric field channel is approximately 7V/m over a 5-hour period. Note that the zero-drift of the electric field channel is due mainly to the variation in contact potential difference as the earthing brush rubs on the metal shaft of the field mill. This means that over a long period of time, as oxidation of the brush increases, so the value of the zero-electric-field reading will change. Thus, the zero-drift of the electric field channel should be characterised over a long time period.

The term "electric field channel" used above means "the output signal of the field mill which corresponds to the electric field".

7.6.4.2 Zero-drift of ion current density measurements

The ion current density varies as a function of humidity, corona needle voltage, surface condition of the corona needle, and other factors. Furthermore, the magnitude of the contact potential difference does not affect the ion current readings, since the contact potential produces an alternating signal at the preamplifier input, while the ion current signal is a dc signal. Thus the ion current channel is independent of the state of oxidation of the earthing brush. Any long-term drift in the ion current channel is predominantly due to fluctuations in the ion current density in the air, and so is not part of the field mill characteristics per se. It was decided that the drift of the ion current readings over a long time period was not a meaningful indication of the field mill performance. Instead, measurements of the zero-drift of the ion current density channel over a short time-period are presented here.

The zero-drift of the ion current density was measured for:

(a) Wilson Plate (plate diameter = 80mm)
(b) Electric field mill (stator diameter = 80mm)

The graph below shows the zero-drift of the ion current density channel over a short time period of 10 minutes:

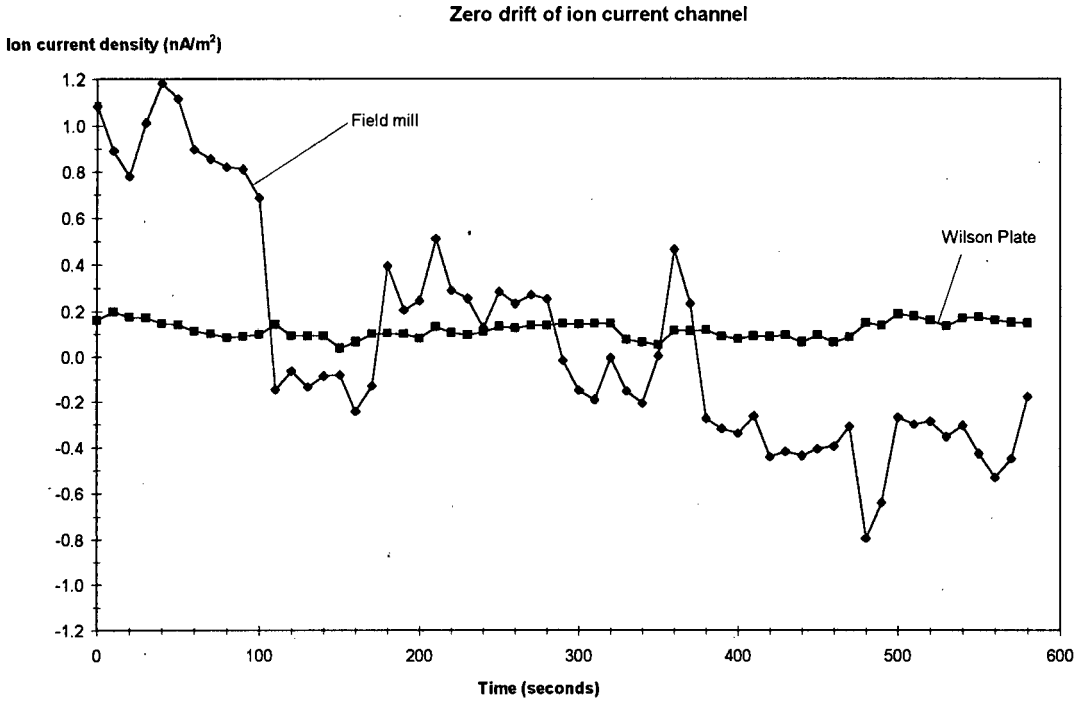

Fig.7.37 Zero-drift of ion current density measurments for Wilson Plate and Field Mill

The graph above shows that the electric field mill readings of ion current density have greater zero-drift than those taken with the Wilson Plate. The chief cause of this problem is that the stator of the field mill has a smaller surface area than the Wilson Plate. This means that in order to calibrate the field mill readings in terms of ion current per unit area, the field mill output must be amplified with respect to the Wilson Plate output. Thus the zero-drift of the field mill system is also amplified with respect to the zero-drift of the Wilson Plate system.

Zero-drift of Wilson Plate readings = +/- 0.2nA/m^2
Zero-drift of field mill ion current readings = +/- 1.2nA/m^2

Note: the zero-drift of the ion current channel is measured with no ion source (ie no ions present), and so fluctuations in the readings due to ion current variation in the air, and movement of space charge are avoided. The zero-drift therefore measures the drift of the electronic circuitry itself. The field mill zero-drift of +/- 1.2nA/m^2 is small compared to the ion current density fluctuations under a corona needle (see Fig.7.34 which shows fluctuations of +/-12nA/m^2). Thus it would appear that the major sources of error in the ion current readings are fluctuation of the ion current density in the air, and movement of space charge (rather than the noise and drift of the electronic circuitry).

The term "ion current channel" used above means "the output of the field mill which corresponds to the ion current reading".

7.6.4 Effect of variations in motor speed

For this thesis, no attempt was made to impose fine control upon the speed of the motor. The 12V DC motor that was used was not a high quality motor, so that intermittent variations in speed occurred. It was therefore necessary to determine the range of motor speeds tolerated by the field mill before significant errors were introduced into the readings. The field mill was run at different motor speeds, and the modulation frequency recorded using a digital frequency counter attached to the reference signal channel. At each frequency, the electric field reading was recorded in an electrostatic field. (The ion current density channel, being at dc, is independent of the modulating frequency). The results of the experiment are shown in the graph below:

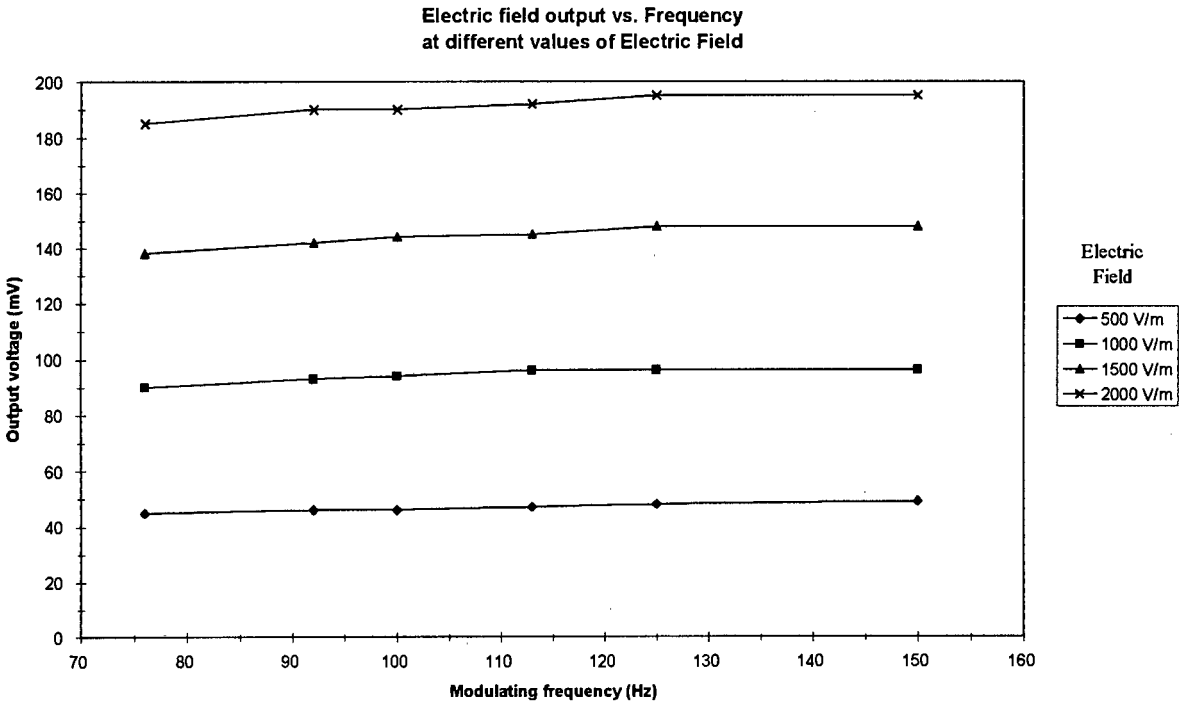

Fig.7.38 Variation of electric field output with modulation frequency

The effect that is being measured here is the error introduced when the factor ωRC is no longer >> 1. This occurs as the modulation frequency drops. The graph above shows that for less than 1% attenuation in the electric field output, the frequency should be kept above 125 Hz. The nominal operating frequency is 150Hz. This means that a drop in motor speed of up to 17% will be tolerated by the field mill circuitry. This is an important factor to consider if it is necessary to run the field mill from battery power over long time periods.

Note: in the above experiment, the field mill output was allowed 30 seconds to settle at each frequency setting before taking a reading. Transient changes in motor speed have not been investigated. Rather it has been assumed that any variation in motor speed will take place gradually, (due, for instance, to a gradual increase in friction as the earthing brush rubs on the shaft, or due to power supply batteries slowly discharging).

7.7 References

[1] Horowitz, P. Hill, W.
"The Art of Electronics"
Cambridge University Press 1989
Chapter 7

[2] Franklin, G. Hatley, T.
"Don't eyeball noise"
Electronic Design
Vol. 24 Nov 22, 1973 pg. 184 - 187

[3] Pallas-Areny, R. Vargas, M.
"The seemingly paradoxical noise behaviour of some active circuits"
IEEE Trans. Instrument. & Meas.
Vol. 43 October 1994 pg. 764 - 767

[4] Dostal, J.
"Operational Amplifiers"
Elsevier 1981
Chapter 12 - "Noise"

[5] AD515 Data Sheet
"Amplifier Reference Manual 1992",
Analog Devices, Chapter 2

[6] Kester, W.
"High Impedance, Low Current Applications"
"Amplifier Applications Guide 1992",
Analog Devices

[7] Cross, A.S.
"Two electrostatic field meters"
British Journal of Applied Physics
Vol. S2 1953 pg. S47 - S50

[8] Layton, R O'Dell, K.
"Student field mill"
American Journal of Physics
Vol.43 No.11 1975 pg.942-943

[9] Secker, P.E.
"The use of field mill instruments for charge density and voltage measurement"
Inst. Physics Conference Series
Vol. 27 1975 pg. 173 - 181

[10] Clark, J.F.
"Airborne measurement of atmospheric potential gradient"
J. of Geophysical Research
Vol. 62 December 1957 pg. 617 - 628

[11] Rossi, F.
"Contact potential measurement: The preamplifier"
Rev. Sci. Instruments
Vol. 63 No.7 1992 pg.3744-3751

[12] Sankaranarayanan, P.E.
"Sanky continuous phase shifter for square waves"
International J. of Electronics
Vol.35 No.6 1973 pg.745-749

[13] Faulkner, E. Carter, S.
"Accurate broadband square-to-triangle converter"
Electronics Letters
Vol.13 No.13 1977 pg.381-382

[14] Lee, S.M. Kwun, S.I.
"Digital frequency tripling circuit for third harmonic detection by lock-in amplifiers"
Review of Scientific Instruments
Vol. 65 No.4 1994 pg.971-973

[15] Currie, D.R. Kreielsheimer, K.S.
"A double field mill for the measurement of potential gradients in the atmosphere"
J. of Atmospheric and Terrestrial Physics
Vol. 19 1960 pg. 126 - 135

[16] Sheahen, T.P.
"Model of response of an electric field mill operating during suborbital flight"
Review of Scientific Instruments
Vol. 45 February 1974 pg. 171 - 177

[17] Chubb, J.N.
Private communication to M.Sellars
March 1995
See Appendix D

[18] Winn, W.P.
"Aircraft measurement of electric field: self-calibration"
J. Geophysical Research
Vol. 98 (D4) (1993) pg. 7351 - 7365

[19] AD549 Data Sheet
"Amplifier Reference Manual 1992",
Analog Devices, Chapter 2

[20] "IEEE Guide for the Measurement of DC Electric-field and Ion Related Quantities
IEEE Standard 1227-1990

[21] Wheeler, A.J.
"Development of an Instrument for the Simultaneous Measurement of Electric Field Strength and Ion Current Density"
BSc. Thesis, 1987
Dept. of Electrical Engineering, UCT

[22] Comber, M.G. Kotter, R.
"Experimental evaluation of instruments for measuring DC transmission line electric fields and ion currents"
IEEE Trans. Power Apparatus & Systems
Vol.102 No.11 1983

[23] Beardwood, C.J.
Private communication to M.Sellars
July 1995

[24] Pease, R.A.
"What's all this Femtoampere Stuff, Anyhow?"
Electronic Design September 2, 1993
pg.85-89

[25] Miles, R.
"Supersensitive measurement demands critical input design"
Electronics September 27, 1979
pg.145-149

8. Calibration of the Electric Field Mill

8.1 Electric field measurement

8.1.1 Agreement of measured electric field values with theoretical values

The theoretical value for the peak alternating signal measured after the preamplifer is (as in Eqn.7.10):

$$V_e(max) = \varepsilon_o EA/2C = {}^1/_2\, V_e(peak\text{-}peak) \quad \textbf{(8.1)}$$

where: ε_o = permittivity [F/m]
E = electric field magnitude [V/m]
A = maximum exposed stator area [m^2]
C = feedback capacitance of preamplifier [F]

If we choose C=100pF, and A=$2.5 \times 10^{-3} m^2$ then we expect to measure V_e(peak-peak) = 0.22mV per V/m of electric field strength **E**. To check on the agreement between theory and practice, the following experiment was conducted.

The field mill was placed in an electrostatic field (using two parallel plates), and the peak-peak value of the signal at the preamplifier output was measured on the oscilloscope, for different values of electric field **E**. The results are plotted in the graph below:

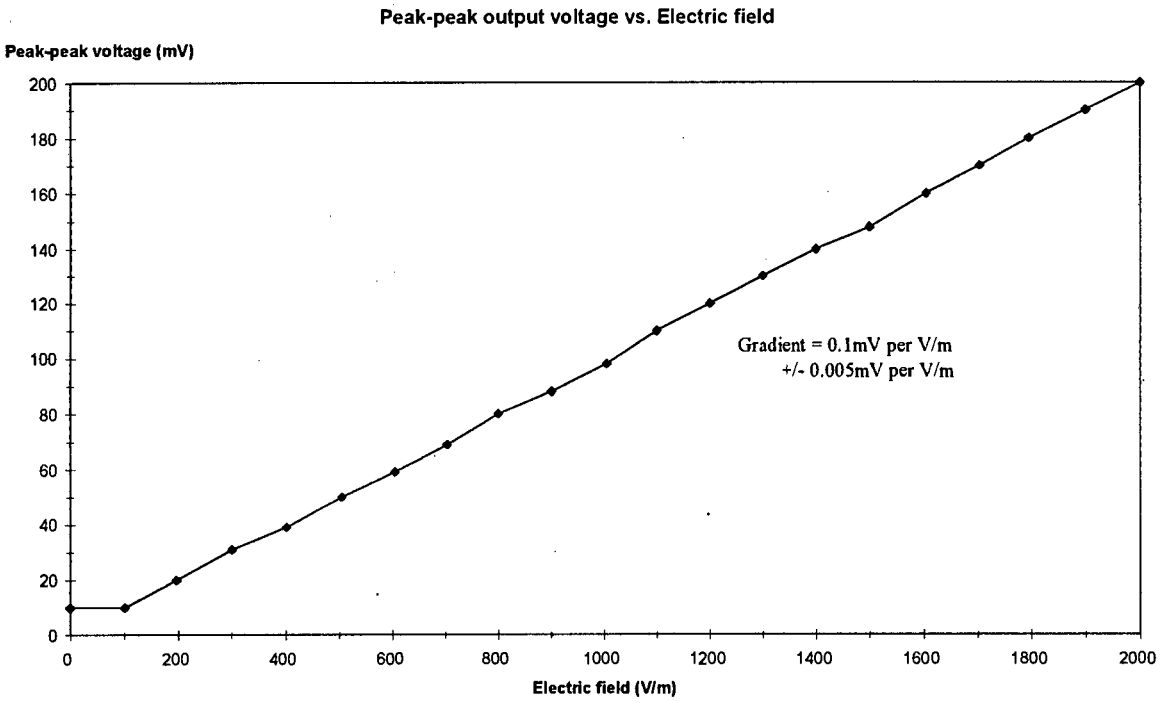

Fig.8.1 Peak-peak output voltage after preamplifier in electrostatic field

The gradient of the above graph is 0.1mV per V/m +/- 0.005mV per V/m. The measured output is lower than the calculated value. In this case the reduction factor is 2.2. It is postulated that this is due to the field mill stator not being exactly flush with the ground plane, but being recessed behind it, as described in Chapter 6.2.6. The above results were discussed with Chubb [1], and he suggested that the reduction factor of approximately 2 was a sensible figure. He also said that although it would be possible to calculate exactly what the reduction factor should be using 3-D computer modelling, it would be better just to calibrate-out this factor. This underscores the necessity for calibration of the electric field mill.

8.1.2 Electric field calibration

The electric field calibration is fairly straight-forward, since it involves the measurement of the electric field between two parallel plates, as described in Chapter 3.7. (This is an electrostatic field, so there are no ions present). It is usual to calibrate the electric field readings in a purely electrostatic field, since in an ionised field the electric field is both difficult to calculate and may vary with time due to ion fluctuation [4]. The dimensions of the parallel plates were:

length = breadth	l = 500mm
field mill aperture diameter	D = 100mm
distance between plates	d = 200mm

Note: these dimensions are smaller than the recommendations outlined in Chapter 3.7 for the size of the parallel plates. A much larger parallel-plate apparatus was set up, having plates of size 1500mm x 1500mm, and the field mill output was measured for various electric field values. There was no measurable difference between the results obtained using the large parallel-plate setup, and using the small parallel-plate setup. Furthermore, the large parallel-plates required a large area of floor space in the laboratory, and so it was not possible to keep them set up for very long. It was decided that, for the purposes of this thesis, the use of the smaller calibration plates would provide sufficient accuracy. The minimum requirement for the plate size (discused in Chapter 3.7) that length $l > 2d$, is satisfied. An estimate of the calibration error introduced due to the parallel-plates being too small is 5%.

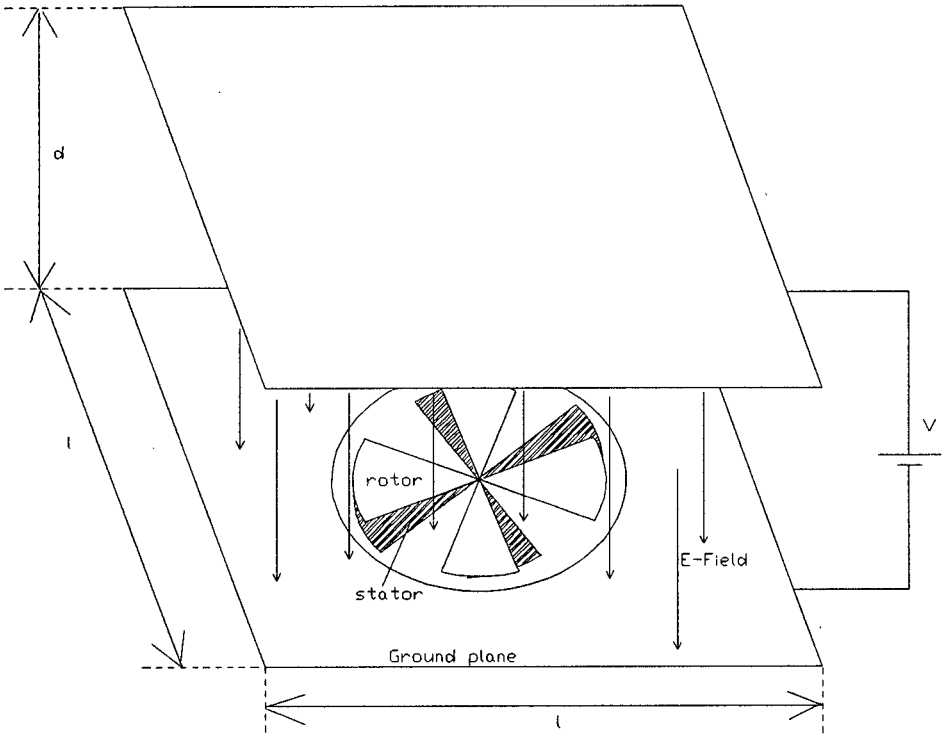

Fig.8.2 Parallel-plate calibration of field mill

The following graphs show the output of the electric field mill for different values of applied electric field **E**. Note that the electronic circuitry has a very wide dynamic range of 0 to 25 kV/m. The results have been presented in two different graphs so that the linearity at the more sensitive end of the scale may be appreciated.

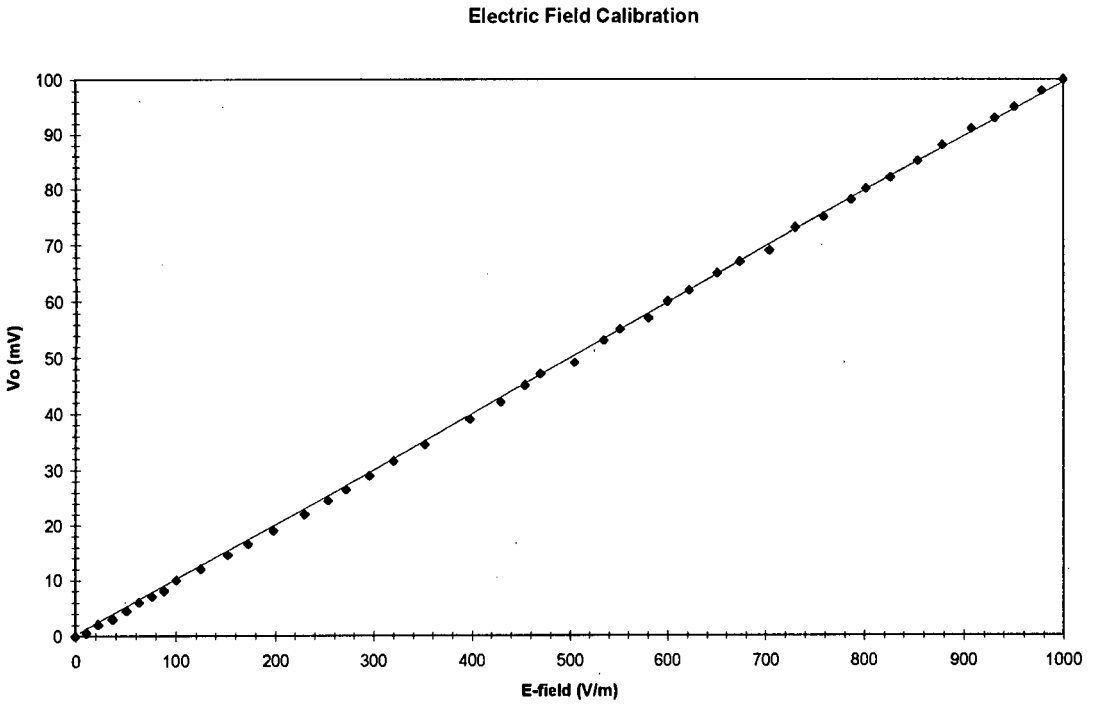

Fig.8.3 Electric field calibration for the sensitive range (0 to 1000 V/m)

In the graph above, slope = 0.1mV per V/m (+/- 0.004mV per V/m). Uncertainty in slope = 4%.

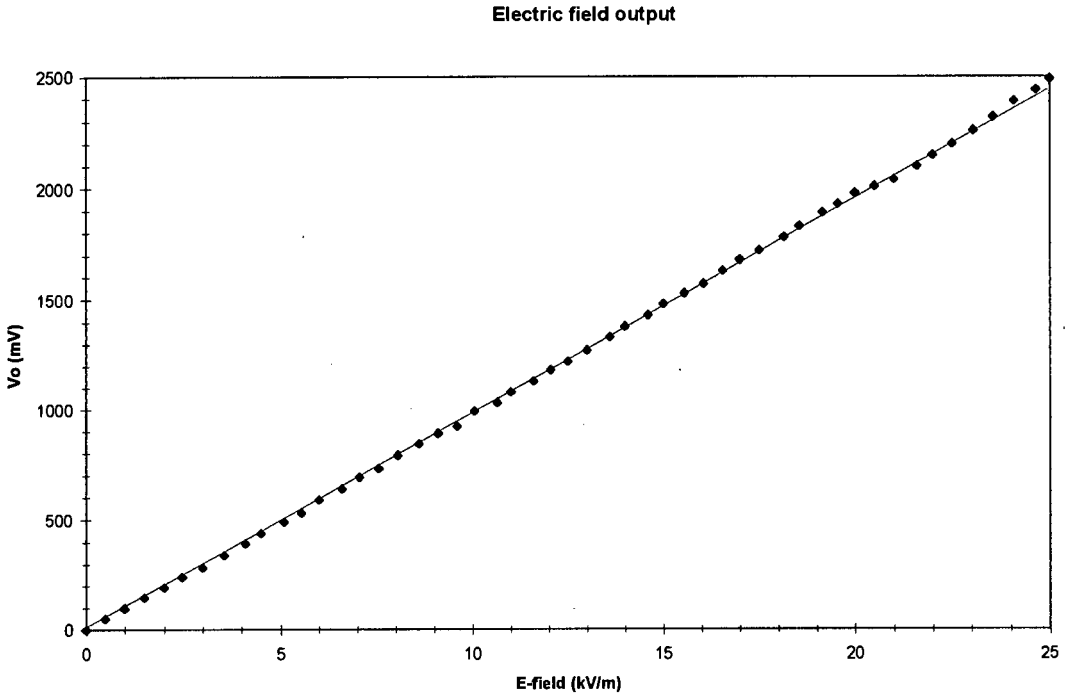

Fig.8.4 Electric field calibration (0 - 25kV/m)

In the graph above, slope = 0.1mV per V/m (+/- 0.004 mV per V/m). Uncertainty in slope = 4%.

8.1.3 Uncertainties in the Electric Field Measurement

The equation for the calibrated electric field output is:

$$V_e = K_1 K_2 V/d \quad \text{..... (8.2)}$$

where: K_1 = slope of graph in Fig.8.3 [V per V/m]
K_2 = factor due to small size of plates [no units]
V = applied DC voltage [V]
d = distance between plates [m]

We are interested in the relative uncertainty in V_e which comes about as a result of the relative uncertainties in the measured values of K_1 , K_2 , V and d. Since these are all small, we may expand equation (8.2) by use of a Taylor's Series, retaining only first-order terms and dropping all higher terms, obtaining:

$$dV_e = \frac{\partial V_e}{\partial K_1} dK_1 + \frac{\partial V_e}{\partial K_2} dK_2 + \frac{\partial V_e}{\partial V} dV + \frac{\partial V_e}{\partial d} dd$$

$$\frac{dV_e}{V_e} = \frac{(K_2 V/d)}{V_e} dK_1 + \frac{(K_1 V/d)}{V_e} dK_2 + \frac{(K_1 K_2/d)}{V_e} dV - \frac{(K_1 K_2 V/d^2)}{V_e} dd$$

$$\frac{dV_e}{V_e} = \frac{dK_1}{K_1} + \frac{dK_2}{K_2} + \frac{dV}{V} - \frac{dd}{d}$$

We see then that the quantity on the left is made up of a linear combination of the quantities on the right. Moreover the latter are all random variables which are statistically independent. Using these facts we can thus say that [5]:

(relative uncertainty in V_e)^2 = (relative uncertainty in K_1)^2 + (relative uncertainty in K_2)^2
+ (relative uncertainty in V)^2 + (relative uncertainty in d)^2 ..... **(8.3)**

This agrees with the IEEE Standard [2], which states that the total uncertainty in the measurement is the square root of the sum of the individual uncertainties squared. The individual uncertainties are:

K_1 ..... Uncertainty = 4%
K_2 ..... Uncertainty = 5%
V ..... Uncertainty = 5%
d ..... Uncertainty = 1%

The applied DC voltage, V, was measured with a Fluke 80K-40 High Voltage Probe, and the reading displayed on a digital multimeter, with an uncertainty of 5%. The distance, d, between the parallel plates was measured with an uncertainty of 1%.

Electric Field Measurement: TOTAL UNCERTAINTY = 8% of measured value

Note: these uncertainties are applicable in an electrostatic field (which is time invariant). As such they represent the uncertainties in the electric field mill instrument itself. In an ionised electric field, however, movement of space charge in the air will cause fluctuations of the electric field readings. These fluctuations depend on many factors, including corona voltage, wind speed, and humidity. This means that the fluctuations will be different for different environments, and so are not considered to be part of the uncertainty due to the field mill itself. For the measurements made under a corona needle in the laboratory, the fluctuations were approximately +/-5% of the measured electric field value (see Section 7.4.2).

8.2 Ion current density calibration

8.2.1 Calibration of preamplifier circuitry

The first requirement in calibrating the ion current density measurement system, is to calibrate the preamplifier circuitry. This is carried out using the current injection method described in Chapter 4.2. A circuit diagram is shown below:

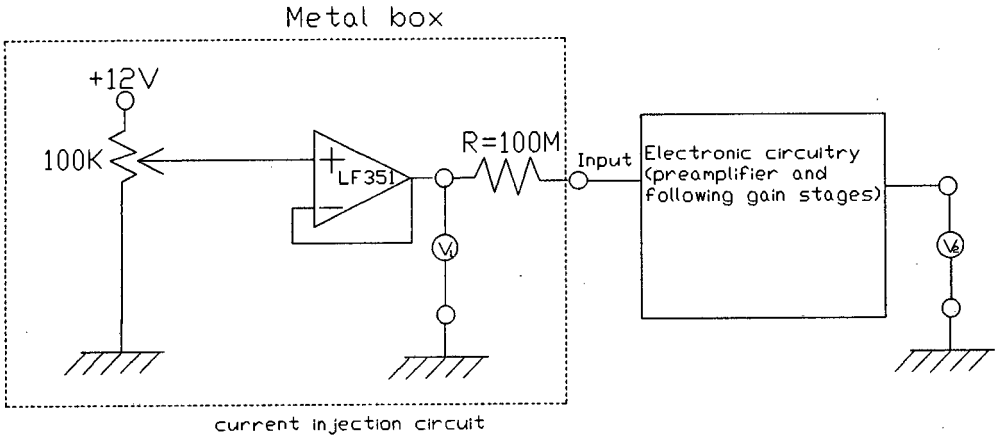

Fig.8.5 Current injection circuit for calibrating the preamplifier

The circuit above was enclosed in a grounded metal box, and coaxial cables were used to connect the current injection circuit to the voltmeters and to the preamplifier input. The current injection circuit included a pair of 12V voltage regulators to remove both 50Hz ripple and errors due to loading effects of other electronic circuits on the supply rails. The current-setting resistor R (nominally 100MΩ) was measured with the HP multimeter in-circuit, and found to have a resistance of 101MΩ (+/- 0.5MΩ).

The injected current $I = V_1/R$. (This is because the input to the preamplifier is a virtual earth).

The gain of the preamplifier = $V_2/I = V_2R/V_1$ [ohms].

The results of measurements taken of the gain for different values of injected current are shown in the graph below:

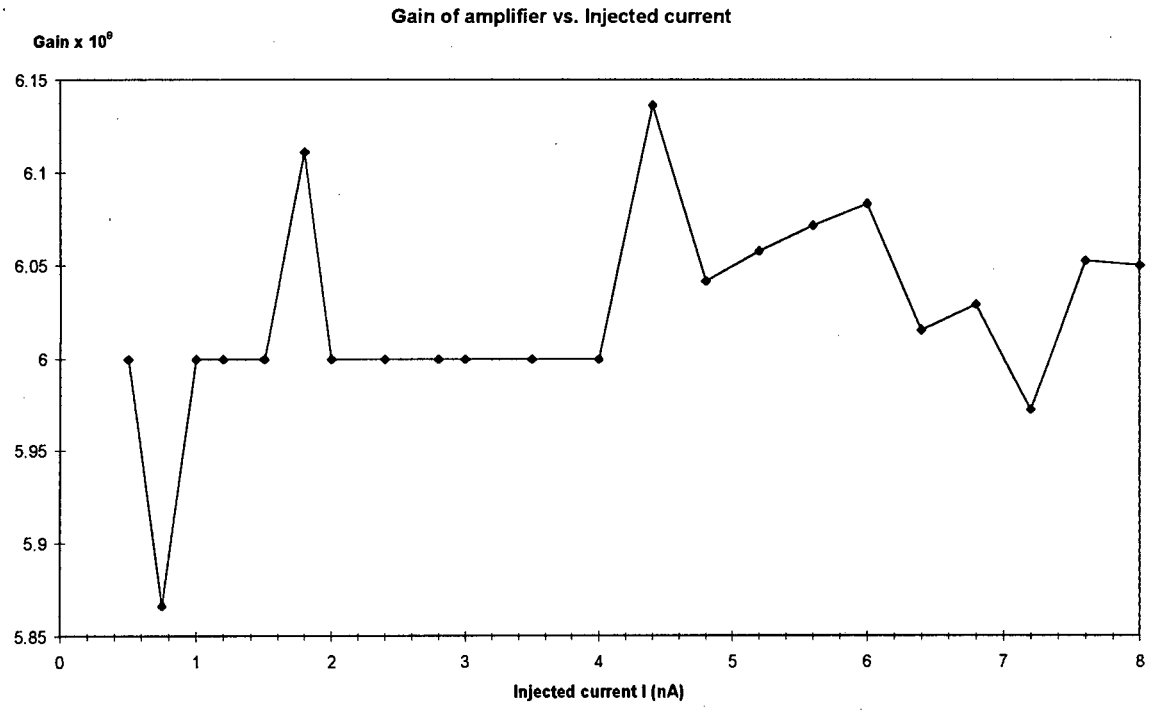

Fig.8.6 Plot of amplifier gain vs. injected current

From the graph above, it can be seen that over the range of injected currents from 0.5nA up to 8nA, the gain of the amplifier (preamplifier and following gain stages) is measured to be 6.0×10^8 ohms.

The total uncertainty in the value for the gain is 3.5%. The total uncertainty includes uncertainty in the measurement of resistor R, and voltages V_1 and V_2.

8.2.2 Effective surface area of the stator

The maximum exposed surface area of the stator is $0.0024m^2$. Since the exposed stator area is continuously changing, the average value of the exposed area will be half of the maximum area:

$$A_{av} = {}^1/_2 A_{max} \quad \text{..... (8.4)}$$

From this simplistic calculation, we might expect the effective ion-collecting area of the stator to be $0.0012m^2$. However, the effective surface area of the stator when considering ion currents is not easily calculated. This is because of the presence of the grounded rotor above the stator plate, which will inevitably attenuate the ion current that reaches the stator. This is due to some of the ions being attracted towards the rotor by fringing fields. The only way to calibrate the ion current measurements is to compare the field mill readings with the readings taken with a Wilson Plate, using the same amplifier circuitry. A correction factor can then be found to give the effective stator surface area of the field mill. An experiment was set up in which ion current density measurements were taken beneath a corona needle with:

1. Wilson Plate — A_{max} = maximum exposed area = $0.005m^2$.
2. Electric field mill — A_{max} = maximum exposed area = $0.0024m^2$. $A_{av} = {}^1/_2 A_{max} = 0.0012m^2$.

From the simplistic calculation of Eqn.8.4, we would expect the ion current readings from the Wilson Plate to be approximately 4 times larger than those from the field mill. The Wilson Plate and field mill stator were of the same diameter (D=80mm), so that errors due to fringing field effects would affect both pickup surfaces in the same way. Both instruments were mounted flush with the ground plane. The measurements were repeated for a number of different heights of the corona needle above the ground plane. The experimental setup is shown in the diagram below:

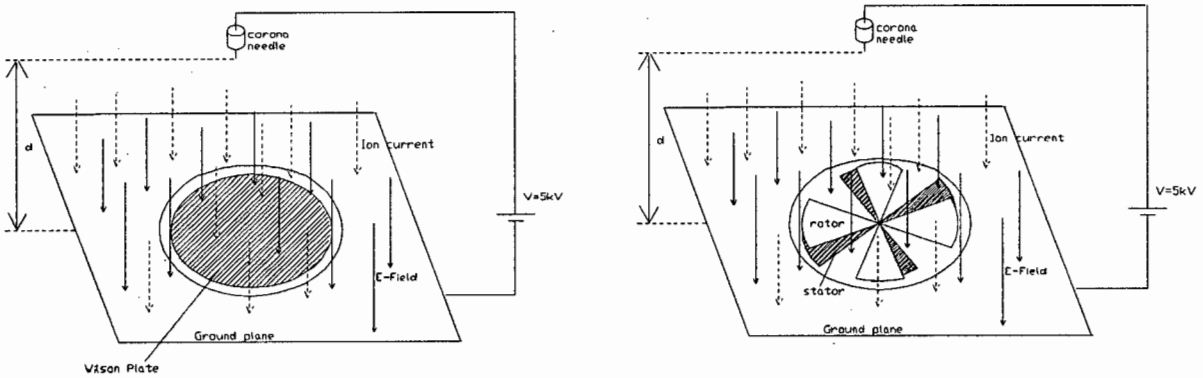

(a) Wilson Plate mounted flush with ground plane

(b) Field mill mounted flush with ground plane

Fig.8.7 Experiment to determine the effective surface area of the stator for ion collection

Note: the surface area of the ion-collecting surface is taken to extend to the middle of the gap between the Wilson Plate (or stator) and the guard band [2]. This introduces an uncertainty of 10% in the value for the surface area (the uncertainty in the width of the gap is 2mm).

At each height, d, of the corona needle above the ground plane, measurements of ion current density were made using first the Wilson Plate, as in Fig.8.7(a), and then using the field mill, as in Fig.8.7(b). The results of the measurements are displayed in the graph below. Each point on the graph represents the average of 100 consecutive readings obtained using the HP 34401A multimeter.

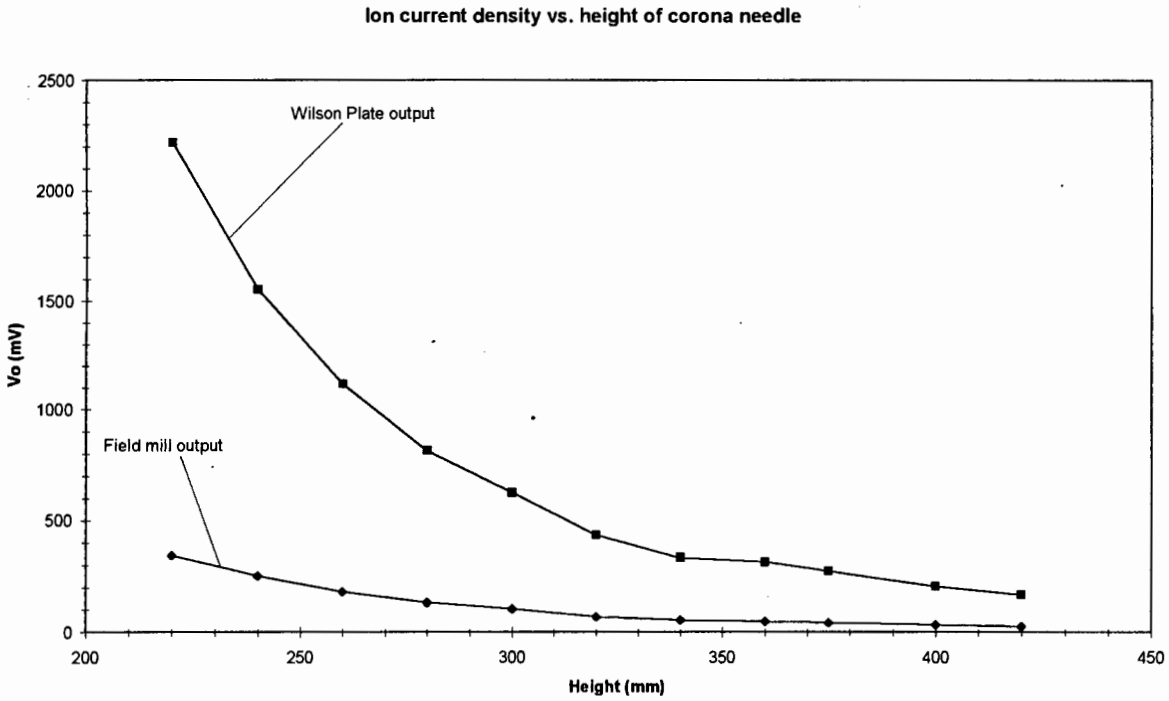

Fig.8.8 Graph showing output voltage of both the field mill and Wilson Plate for different heights of the corona needle above the ground plane

As the height of the corona needle above the ground plane increases, so the ion current density decreases. However, the ratio of the Wilson Plate reading to the field mill reading remains constant at a value of 6.3 +/- 0.3. Since we know the surface area of the Wilson Plate, we may now calibrate the field mill output directly in terms of ion current density [nA/m^2]. The graph below shows the same values as Fig.8.8, but the measurements are given in terms of ion current density. Thus we expect the readings from both the Wilson Plate and the electric field mill to agree.

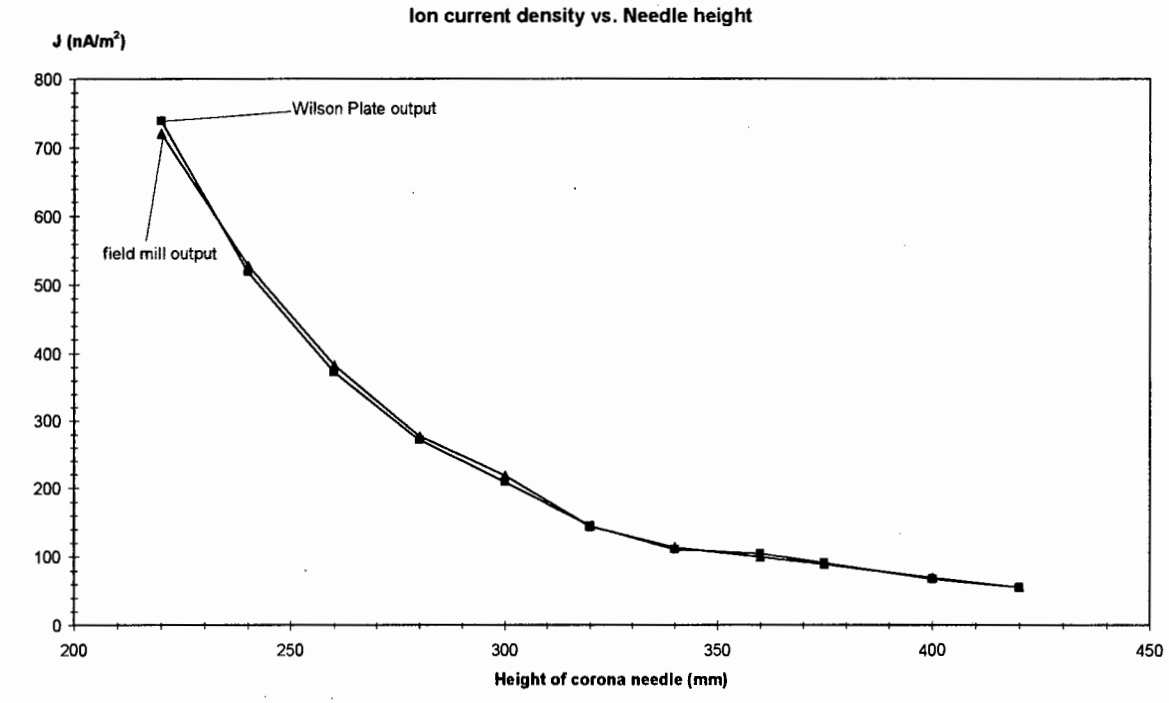

Fig.8.9 Agreement of ion current density readings from Wilson Plate and field mill

The above graph shows that, after calibration, the field mill output readings agree with the readings taken with the Wilson Plate, over the range of ion current densities measured. It is interesting to note that the measured correction factor of 6.3 is not very much different from the value of 4.17 calculated using Eqn.8.4. This would seem to indicate that the presence of the rotor above the stator does attenuate the ion current signal, but that the attenuation is not great enough to prevent measurement of the ion current.

8.2.3 Effective surface area of the Wilson Plate

The effective surface area of the Wilson Plate is assumed to be taken as simply the exposed surface area. However, it is noted that errors may occur if the Wilson Plate is not closely surrounded by a grounded guard band (also known as a guard electrode). The use of a grounded guard band is illustrated in Chapter 4.1. An experiment was set up to investigate the nature and magnitude of such errors.

Three different Wilson Plates were used:

(a) Radius = 18mm (no guard band)
(b) Radius = 18mm (grounded guard band)
(c) Radius = 40mm (grounded guard band)

For each of the three Wilson Plates, the ion current density was measured for a corona needle at various heights above the ground plane. The field mill amplifier circuit was used to measure the Wilson Plate output signal. The setup is shown in the diagram below:

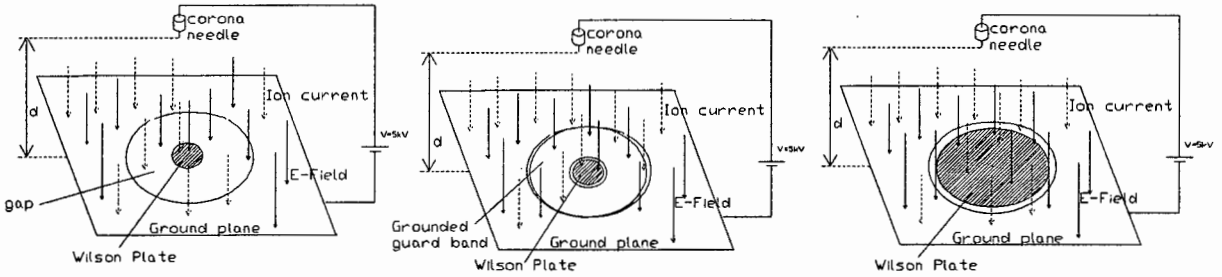

(a) Small plate, no guard band (b) Small plate, with guard band (c) Large plate, with guard band

Fig.8.10 Experiment to investigate effect of Wilson Plate guard band

The large plate fills the aperture in the ground plane, so that effectively it also has a grounded guard band. (The inner edge of the ground plane aperture acts as a guard band). The results of the experiments are shown in the graph below:

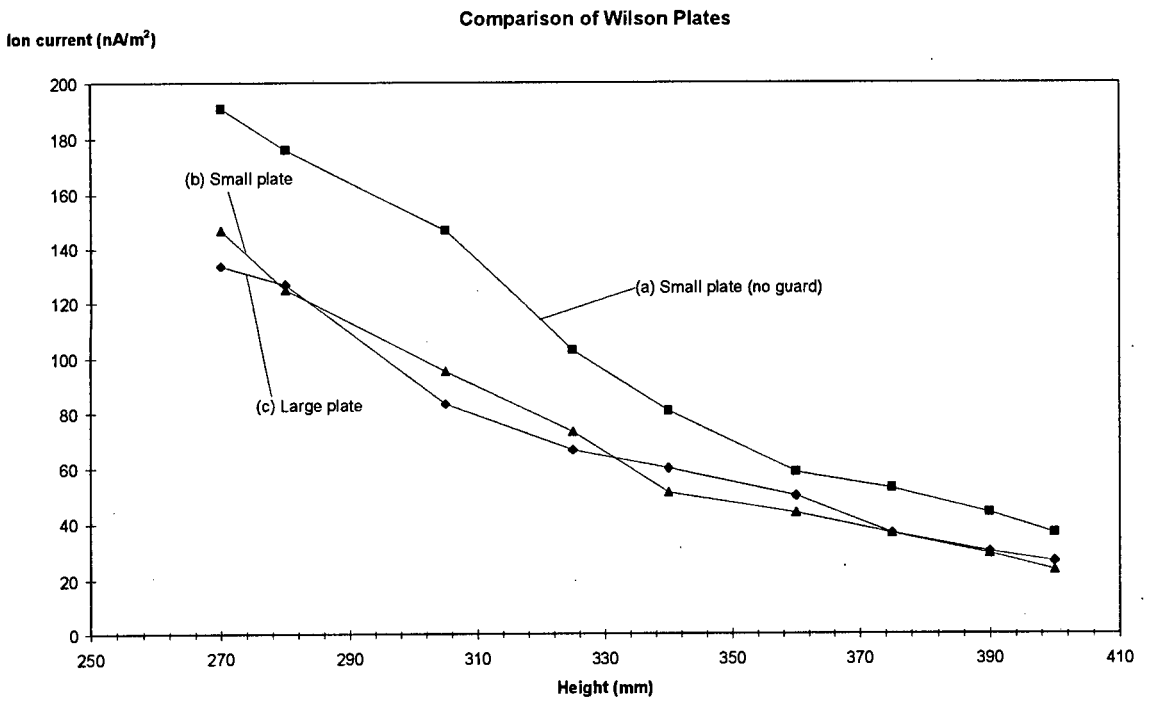

Fig.8.11 Comparison of ion current density measurements made with different Wilson Plates

The graph above shows that the Wilson Plates (b) and (c), which both have grounded guard bands give ion current density readings which agree reasonably well, considering the errors due to ion fluctuation. However, the Wilson Plate (a), (which has no guard band), gives an increased reading. The observed ion current in the Wilson Plate without guard band (a) is about 50% higher than for (b) and (c). Similar findings are reported in [2] and [3]. This shows that in making any ion current density measurements, it is important that the pickup surface is surrounded by a grounded guard band. In the case of the field mill, the stator is surrounded by the grounded field mill casing, (and also the stator almost fills the aperture in the ground plane). This means that the field mill effectively has its own grounded guard band.

Conclusion

The error introduced by using a Wilson Plate (or field mill) without a grounded guard band is substantial.

8.2.4 Uncertainties in the Ion Current Density Measurements

The equation for the ion current density output is:

$$V_j = JA_{stator}G \quad [\text{Volts}] \qquad \textbf{(8.5)}$$

where: G = Gain of amplifier [ohms]
J = Ion current density [nA/m^2]
A_{av} = Average surface area of stator [m^2]

However, we have no way of obtaining a known ion current density **J** with which to calibrate the readings (as discussed in Chapter 4.2). Nor do we have an accurate expression for the *effective* average area of the stator. The best that we can do then is to compare the field mill readings with the readings taken with a Wilson Plate, and use the proportionality constant measured in Section 8.2.2 to calibrate the field mill readings. In this case, the equation for the ion current density output becomes:

$$v_j = K_3AG \quad [\text{Volts per nA/m}^2] \qquad \textbf{(8.6)}$$

where:	K_3 = Ratio of electric field signal to Wilson Plate signal	[no units]
	A = Surface area of Wilson Plate	[m^2]
	G = Gain of amplifier	[ohms]

As measured in Section 8.2.2: $K_3 = 1/6.3$
$A = 0.005$ m^2
$G = 6.0 \times 10^8$

Therefore: $v_j = 0.476$mV per nA/m^2.

Thus we now have a calibrated value (v_j), which we use in all ion current density measurements. To work out the magnitude of the ion current density, J, we divide the measured output voltage (V_j) by the value v_j. Therefore:

$$J = \text{ion current density} = V_j/v_j \qquad \textbf{(8.7)}$$

The terms in Eqn.8.6 are statistically independent (see pg.111). Using this fact, we can say that [5]:

$$(\text{relative uncertainty in } v_j)^2 = (\text{relative uncertainty in } K_3)^2 + (\text{relative uncertainty in A})^2 + (\text{relative uncertainty in G})^2 \qquad \textbf{(8.8)}$$

This agrees with the IEEE Standard [2], which states that the total uncertainty in the measurement is the square root of the sum of the individual uncertainties squared. The indivdual uncertainties are:

K_3 ..... Uncertainty = 5%
A ..... Uncertainty = 10%
G ..... Uncertainty = 3.5%

Ion Current Density Measurement: TOTAL UNCERTAINTY = 12% of measured value

Note: these uncertainties represent the uncertainties in the electric field mill instrument itself. In an ionised electric field, however, movement of space charge in the air will cause fluctuations of the ion current density readings. These fluctuations depend on many factors, including corona voltage, wind speed, and humidity. This means that the fluctuations will be different for different environments, and so are not considered to be part of the uncertainty due to the field mill itself. For the measurements made under a corona needle in the laboratory, the fluctuations were approximately +/-7% of the measured ion current density value. According to a published report, even under conditions of steady corona generation, the ion current readings may exhibit considerable variation. Fluctuations as high as 50% of the average ion current density reading have been recorded [4].

8.3 Performance Specifications of the Electric Field Mill

8.3.1 Electric field measurements

The table below shows the specifications for the electric field measurement channel of the field mill.

Table 8.1 Specifications for the electric field channel of the electric field mill

Specification		Notes
Calibrated Range *	0 V/m to 25kV/m	
Calibration factor	V_o = 0.1mV per 1V/m	Multiply V_o (mV) by 10 to read electric field strength in V/m
Resolution	10 V/m	Minimum signal detectable = 10V/m
Zero drift	7V/m	Measured over 5 hours
Accuracy (electrostatic field)	+/- 8% of reading (for **E** > 100 V/m)	Below 100V/m, accuracy = +/- 7V/m
Modulating frequency range	Frequency > 125Hz	Nominal frequency =150Hz
Settling time	5 seconds	Allow 5 seconds for output to settle

* The calibrated range begins at 0V/m for short-term measurements, but in any long-term investigation, zero-drift sets the lower range limit at 7V/m. The upper limit of the range is dictated by corona breakdown between the stator and rotor plates, which only occurs for electric field values in excess of 100kV/m. The field mill has been tested in electric fields of up to 75kV/m, and found to function correctly.

8.3.2 Ion current density measurements

The table below shows the specifications for the ion current density measurement channel of the field mill.

Table 8.2 Specifications for the ion current density channel of the electric field mill

Specification		Notes
Calibrated Range *	0 to 1000 nA/m^2	
Calibration factor	V_o = 0.476mV per 1nA/m^2	Multiply V_o (mV) by 2.1 to read ion current density in nA/m^2
Resolution	20 nA/m^2	Minimum signal detectable = 20 nA/m^2, due to ion current fluctuation. This depends on the characteristics of the ion environment
Zero drift	+/- 1.5 nA/m^2	Short-term zero-drift
Accuracy	+/- 12% of reading (for **J** > 100 nA/m^2)	Below 100 nA/m^2, accuracy = +/- 20 nA/m^2
Settling time	12 seconds	Allow 12 seconds for output to settle

* The calibrated range has its lower limit set by zero drift of 1.5nA/m^2. The upper limit is difficult to define, but the field mill has been tested in ionised electric fields with ion current densities of up to 5000 nA/m^2, and found to function correctly.

8.4 References

[1] Chubb, J.
Private communication to M.Sellars
February 1995

[2] IEEE Standard 1227-1990
IEEE Guide for the Measurement of DC Electric-Field Strength and Ion Related Quantities
December 1990

[3] McKnight, R. Kotter, F.
Misakian, M.
"Measurement of Ion Current Density at Ground Level in the vicinity of HVDC transmission lines"
IEEE Trans. Power Apparatus & Systems
Vol.102 April 1983 pg.934-941

[4] Comber, M. Kotter, R.
"Experimental evaluation of instruments for measuring DC transmission line electric fields and ion currents"
IEEE Trans. Power Apparatus & Systems
Vol.102 No,11 1983 pg.3549-3557

[5] Whittle, R.
"Experimental Physics for Scientists"
Chapman & Hall, 1973
Chapter 1, "Errors of Observation"

9. Measurements made with the Electric Field Mill

9.1 Measurements under HVDC transmission lines

Ideally, measurements should be made under an operating HVDC line with the electric field mill in order to ascertain whether it functions correctly in a real measurement situation. Unfortunately, there are no HVDC transmission lines conveniently near to Cape Town. The Cahora-Bassa HVDC line is due to become operational only in 1997. ESKOM in Johannesburg do have a HVDC test line, but due to both time and financial constraints it was not possible to travel up to Johannesburg to make measurements there. This would be one area for further work on the field mill project.

The next-best to making measurements under an operating line is to build a scale model of an HVDC transmission line. This has been done by Johnson and Zafanella [1], who report that a scale model HVDC line is very useful for testing instrumentation such as field mills and Wilson Plates. Again, time and financial constraints made the construction of a scale model HVDC line impractical.

It was decided instead to produce in the laboratory a similar range of electric field and ion current density conditions to those that may be expected under an operating HVDC transmission line. To date, no work has been done on the measurement of electric fields and ion currents under the Cahora-Bassa HVDC line, so that no data is available [5]. The graph below shows some measurements made by Maruvada under a +/- 900kV HVDC transmission line [2]. These values give an indication of the electric field and ion current density range that we expect to measure under an operating HVDC line. The graph shows values of electric field and ion current density measured at ground level at different distances from the point directly beneath the transmission line conductor bundle.

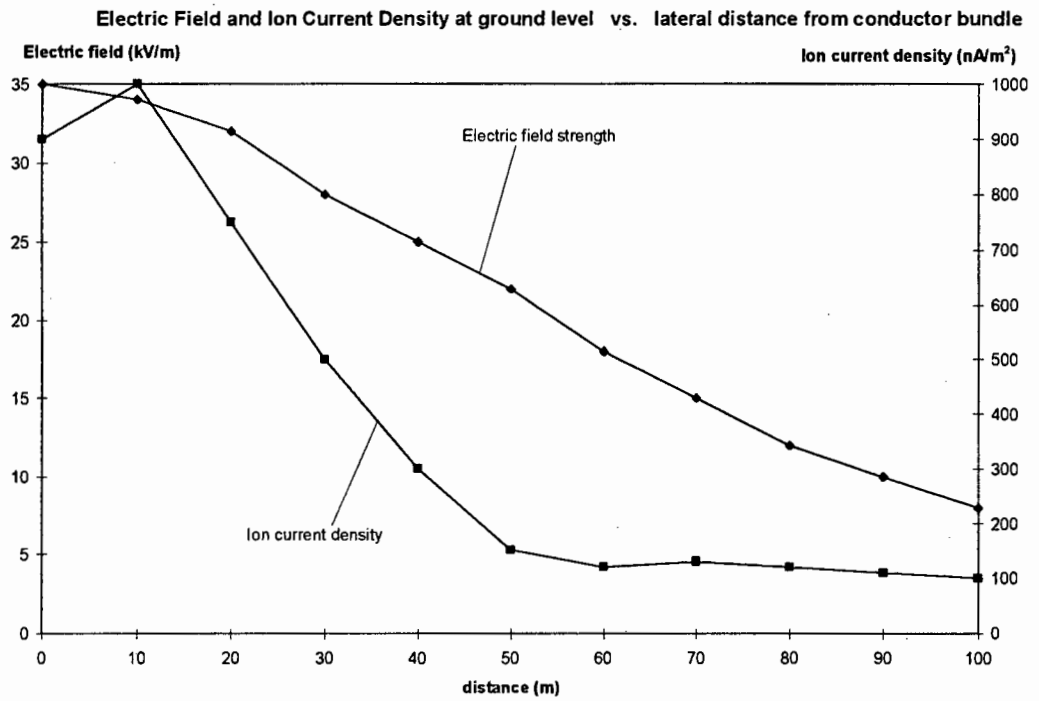

Fig.9.1 Electric field and ion current density values measured beneath an operating HVDC line

9.2 Measurements in a simulated HVDC transmission line environment

The range of electric field and ion current density values shown in Fig.9.1 was used to produce a simulated HVDC transmission line environment. The electric fields and ion currents were produced using a corona needle with a high DC voltage applied to it.

9.2.1 Measurements with the Electric Field Mill

The electric field mill was used to make measurements underneath a corona needle at a voltage of 5.8kV. The height of the needle above the ground plane was varied, and at each height, readings of the electric field and ion current density were made. Each point represents the average of 100 consecutive readings taken using the HP34401A digital multimeter. The results are plotted in the graph below:

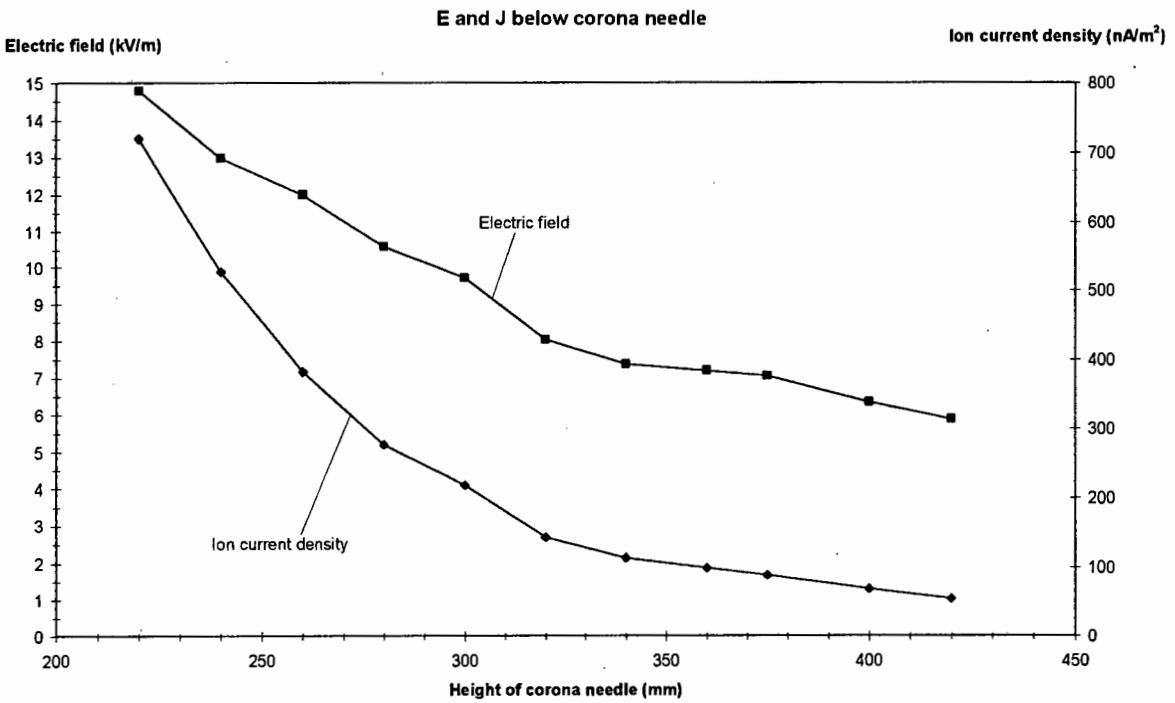

Fig.9.2 Measurements made with the field mill underneath a corona needle

As can be seen in the graph above, as the corona needle is moved higher above the ground plane, so both the electric field and ion current density decrease. This experiment covered the range of electric field and ion current density values that are expected to be measured at ground level under HVDC transmission lines. Typical values would be [3]:

Electric field $\mathbf{E} = 10$ kV/m
Ion current density $\mathbf{J} = 400$ nA/m^2

Note It was considered more convenient to take many readings of the field mill output for each position of the corona needle and average them digitally, rather than use a lowpass filter with a very slow response time (Eg. 100 seconds).

9.2.2 Comparison of results with independent measurements

The results shown in Fig.9.2 are comparable with measurements made by Dr. Beardwood (Dept. of Physiology, UCT Medical School) using an identical high voltage source and corona needle [4]. In order to measure ion current density, he used a gold-plated Wilson Plate (mounted flush with the ground plane) and a Keithley Electrometer with a gain of 10^{10}. Dr. Beardwood did not make measurements of the electric field strength. There were a number of differences between Dr. Beardwood's experimental setup and the experimental setup used for this thesis. These included:

1. Size of the ground plane.
2. Size of the ground plane aperture.
3. Dimensions of the walls of the test cage.

Therefore, it is not expected that Dr. Beardwood's measurements should agree exactly with those shown in the graph of Fig.9.2. The measurements recorded by Dr. Beardwood are shown in the table below:

Table 9.1 Measurements of ion current density in a similar experimental setup [23]

Height of corona needle above the ground plane (mm)	Ion current density (nA/m^2)
320	230
390	42.5

From this table, it can be seen that Dr. Beardwood's results show reasonable agreement with those of Fig.9.2.

9.2.3 Interest in the Electric Field Mill project shown by ESKOM

In April 1995, Mr. Britten from Technology Research & Investigations (ESKOM, Johannesburg) examined the field mill developed for this thesis. He said in a later discussion that ESKOM would be able to make good use of the field mill to quantify the electrical phenomena under the Cahora-Bassa HVDC line [5].

9.3 Conclusions

Ideally, tests should be made under an operating HVDC line in order to determine whether or not the field mill functions correctly. However, the HVDC electrical environment has been simulated in the laboratory, and the field mill functioned correctly over the range of values of electric field strength and ion current density in this simulated environment. Furthermore, the measurements made in the simulated environment agree reasonably well with measurements made in a very similar electrical environment by an independent researcher (Dr. Beardwood), who used a different measuring instrument.

This gives us confidence both that the field mill will function correctly over the range of electric field and ion current density values expected, and also that the results obtained are reasonably accurate.

9.4 References

[1] Johnson, G.B. Zaffanella, L.E.
"Study of electric field and ion effects on HVDC lines"
DOE Report DOE/RA/50153-T1
October 1984

[2] Maruvada, P.S.
"Corona-generated space charge environment in the vicinity of HVDC transmission lines"
IEEE Trans. Electrical Insulation
Vol. 17 No. 2 April 1982
pg. 125 - 130

[3] IEEE Std. 1227-1990
"IEEE Guide for Measurement of DC Electric Field Strength and Ion Related Quantities"
IEEE 1990

[4] Beardwood, C.J.
Private Communication to M.Sellars
July 1995

[5] Britten, A.C. (ESKOM)
Private Communication to M.Sellars
1995

10. Conclusions

1. An electric field mill has been constructed which is capable of measuring:

   Electric fields from 0 to 25 kV/m, with an accuracy of +/- 8%.
   Ion current densities from 0 to 1000 nA/m^2 with an accuracy of +/-12%.

2. The required resolutions of:

100 V/m	(electric field)
100 nA/m^2	(ion current density)

   have been met and improved upon.

3. The electric field mill has been tested in a simulated HVDC environment having electric field and ion current density values similar to those observed under HVDC transmission lines. The field mill was found to perform correctly over the full range of electric field and ion current density values tested.

4. No attempt has been made to control the speed of the motor accurately, and this may result in errors if the field mill is to be operated over periods greater than 24 hours.

5. A phase shift circuit that is independent of frequency is needed.

6. No attempt has been made to make the field mill resistant to water, ice or insects. This means that operation outdoors is not possible except for short periods in fair weather.

7. If suitably weatherproofed, the field mill will be a useful instrument for medical researchers studying biological effects under HVDC transmission lines.

8. The field mill will be useful for measurements of the electrical environment of the Cahora-Bassa HVDC transmission line when it becomes operational in 1997.

11. Recommendations

The following recommendations are made for continuing the work done in this thesis:

1. Motor speed control should be implemented. A high quality DC motor should be used, together with a closed-loop control system. This will allow the field mill to operate continuously for long periods without errors in the measurements caused by variations in the motor speed.

2. An electronic phase shift circuit that is independent of frequency should be developed and used in the field mill system.

3. The physical design of the field mill should be modified to render it completely weatherproof.

4. The field mill should be incorporated into a fully-automated data-collection system, controlled by a computer. This would allow continuous monitoring of electric fields and ion current densities over long time periods.

5. The field mill should be used to make measurements under the Cahora-Bassa HVDC transmission line when the line becomes operational in 1997.

Appendix A -- Field Mill Literature Survey

The following survey lists all articles describing rotating vane electric field mills found in a thorough literature search.

Reference number	Year	Ground contact	Rotor vanes	Stator vanes	Rotor-stator gap	Material for vanes	Stator insulators	Frequency Hz	Input impedance	Sensitivity V/m	F.S.D. V/m
1	1933	*	Sector	Circular	*	*	*	120	C	*	*
2	1936	*	Lemniscate	Sector	*	*	*	120	R	*	50
3	1940	*	Sector	Sector	*	Brass	*	240	R	1000	
4	1948	Bush + Slip ring	Sector	Sector	3mm	Steel	Polystyrene	500	C	*	500
5	1950	Phosphor-bronze strip	Circular holes	Circular	*	Brass	*	1200	C	3	20
6	1953	Leaf spring	Sector	Sector	3mm	Stainless steel	*	100	C	20	1000
7	1954	Graphite bush	Sector	Sector	1.5mm	Brass	*	120	C	40	400
8(a)	1955	Phosphor-bronze strip	Circular holes	Circular	1mm	Nickel plated	Tufnol	500	C	2.5	25
8(b)	1955	Carbon brush	Sector	Sector	3mm	Chrome plated	Tufnol	330	C	1	75
9	1957	*	Sector	Sector	*	*	*	500	C	1	10
10	1958	Carbon and brass brush	Sector	Sector	*	Stainless steel	*	*	C	1	10 000
11	1960	*	Sector	Sector	4mm	Nickel plated	*	25	C	*	100
12	1963	Mercury cup	Sector	Circular	*	Brass	*	1000	R	*	*
13	1965	Silver slipring Silver graphite	Sector	Sector	18mm	Chrome plated	Nylon	40	R	1	100
14	1965	*	Circular holes	Circular	*	Gold plated	Nylon Kel-F	417 1250	C C	*	100
15	1967	*	Sector	Sector	*	*	*	200	C	*	300

Reference number	Year	Ground contact	Rotor vanes	Stator vanes	Rotor-stator gap	Material for vanes	Stator insulators	Frequency Hz	Input impedance	Sensitivity V/m	F.S.D. V/m
16	1974	Brushes on armature	Sector	Sector	*	Gold plated	*	1300	R	4	40
17	1975	*	Sector	Sector	*	*	*	400	C	1	100
18	1983	*	Sector	Lemniscate	*	*	*	180	C		100
19	1988	*	Circular holes	Circular	*	Stainless steel	*	127	C	100	10 000
20	1989	*	Sector	Sector	*	Stainless steel	*	*	C	*	100
21	1990	Gold wire	Sector	Sector	*	Gold plated	*	200	C	1	100
22	1992	Brass-nickel brushes	Sector	Sector	*	Al	Rubber	167	R	0.5	300
23	1993	Slipring, bushes	Sector	Sector	*	Stainless steel	*	50	C	*	25 000
24	1994	Mercury rotating contact	Sector	Circular	8mm	Stainless steel	Kel-F	85	C	3.7	30 000
**	1995	Gold wire	Sector	Sector	1.5mm	Stainless steel	Teflon	150	C	10	25 000

* Details not specified.
** Electric Field Mill built for this MSc. thesis.

References (Appendix A)

[1] Harnwell, G.P. Van Voorhis, S.N.
"An electrostatic generating voltmeter"
Review of Scientific Instruments
Vol. 4 October 1933 pg. 540 - 541

[2] Van Atta Northrup
"Round Hill electrostatic generator"
Physics Review
Vol. 49 1936 pg. 761 - 776

[3] Trump, J.G. Safford, F.J.
"Generating voltmeter for pressure-insulated high voltage sources"
Review of Scientific Instruments
Vol. 11 February 1940 pg. 54 - 56

[4] Waddel, R.C.
"An electric field meter for use on airplanes"
Review of Scientific Instruments
Vol. 19 January 1948 pg. 31 - 35

[5] Malan, D.J. Schonland, B.F.J.
"An electrostatic fluxmeter of short response-time"
Proc. Phys. Society
Vol. 63 1950 pg. 402 - 408

[6] Cross, A.S.
"Two electrostatic field meters"
British Journal of Applied Physics
Vol. S2 1953 pg. S47 - S50

[7] Smith, L.G.
"An electric field meter with extended frequency range"
Review of Scientific Instruments
Vol. 25 May 1954 pg. 510 - 513

[8] Mapleson, W.W. Whitlock, W.S.
"Apparatus for the accurate and continuous measurement of the earth's electric field"
J. of Atmospheric and Terrestrial Physics
Vol. 7 1955 pg. 61 - 72

[9] Clark, J.F.
"Airborne measurement of atmospheric potential gradient"
J. of Geophysical Research
Vol. 62 December 1957 pg. 617 - 628

[10] Smiddy, M. Chalmers, J.A.
"The double field mill"
J. of Atmospheric and Terrestrial Physics
Vol. 12 1958 pg. 206 - 210

[11] Currie, D.R. Kreielsheimer, K.S.
"A double field mill for the measurement of potential gradients in the atmosphere"
J. of Atmospheric and Terrestrial Physics
Vol. 19 1960 pg. 126 - 135

[12] Malan, D.J.
"Physics of Lightning"
The English Universities Press 1963
Chapter 5.5

[13] Gathman, S.G. Anderson, R.V.
"Improved field meter for electrostatic measurements"
Review of Scientific Instruments
Vol. 36 (1965) pg. 1490 - 1493

[14] Wildman, P.J.L.
"A device for measuring electric field in the presence of ionisation"
J. of Atmospheric and Terrestrial Physics
Vol. 27 1965 pg. 417 - 423

[15] Lane-Smith, D.R.
"A new design of sign-discriminating field mill"
J. of Atmospheric and Terrestrial Physics
Vol. 29 1967 pg. 687 - 699

[16] Sheahen, T.P.
"Model of response of an electric field mill operating during suborbital flight"
Review of Scientific Instruments
Vol. 45 February 1974 pg. 171 - 177

[17] Secker, P.E.
"The use of field mill instruments for charge density and voltage measurement"
Inst. Physics Conference Series
Vol. 27 1975 pg. 173 - 181

[18] Maruvada, P.S. Dallaire, R.D.
Pedneault, R.
"Development of field-mill instruments for ground-level and above-ground electric field measurement under HVDC transmission lines"
IEEE Trans. Power Apparatus & Systems
Vol. 102March 1983 pg. 738 - 744

[19] Castle, G.S.P Inculet, I.I.
Lundquist, S. Cumming, J.B.
"Measurement of the particle space charge in the outlet of an electrostatic precipitator using an electric field mill"
IEEE Trans. Industry Applications
Vol. 24 July/Aug. 1988 pg. 702 - 706

[20] Kessler, E. (Ed.)
Chapter 8: "Techniques for measuring electrical parameters of thunderstorms"
Instruments and Techniques for Thunderstorm Observation and Analysis
University of Oklahoma Press
1989

[21] Chubb, J.N.
"Two new designs of "field mill" type fieldmeters not requiring earthing of rotating chopper"
IEEE Trans. Industry Applications
Vol. 26 (1990) pg. 1178 - 1181

[22] Yeboah-Amankwah, D. V. d. Made, P.
"Sign discriminating field mill"
J. of Atmospheric and Terrestrial Physics
Vol. 54 1992 pg. 851 - 861

[23] Winn, W.P.
"Aircraft measurement of electric field: self-calibration"
J. Geophysical Research
Vol. 98 (D4) (1993) pg. 7351 - 7365

[24] Stewart, M.
"Electric Field Measuring System"
United States Patent No. 05315232
1994

Appendix B -- Turbo C++ Program used in Section 6.2.1.2

Note The source code listing below includes only the section of code that calculates the stator areas. The code for displaying the graphics has been omitted.

```
//*********************************************************************//
// Turbo C++ Program to calculate the exposed area of the stator as the rotor spins.  //
// Author: Malcolm Sellars, Electrical Engineering, UCT          (1995)      //
//*********************************************************************//

const long double pi      = 3.14159;
const max_pts             = 1000;
const step                = 1;
long double area[max_pts][4];

void main (void)
{
 long double theta, x, dx, x2, d, l, R, area1, area2, area3, start, stop;
  int i, j, k;
  start = -pi/4;
 stop  = +pi/4;
 x=start;
 dx = (stop - start)/((long double)max_pts);
 l = 1/(2*(sin(pi/8)));
 R = l+0.5;                    // R =Stator Plate radius (sector and lemniscate vanes)
 for (i=0; i<max_pts; i+=step)  // Circular stator plates have radius r=0.5
  { if (x<=0) x2=x+pi/4;
    else x2=x-pi/4;
    d    = l*sin(x2/2);                    // Distance between centre of circular stator
                                           //   plate and centre of circular rotor hole

    theta = 2*acos(fabsl(d*2));
    area1 = pi - theta + sin(theta);       // Circular Stator Plates
    area2 = (1 - (fabsl(x))/stop)*R*R*pi/2; // Sector Stator Vanes
    area3 = (1+cos(x*4))*R*R/2;            // Bernoulli Lemniscate Vanes
    area[i][0] = x;
    area[i][1] = area1;
    area[i][2] = area2;
    area[i][3] = area3;
    x += dx;
  }
 display ();
}
```

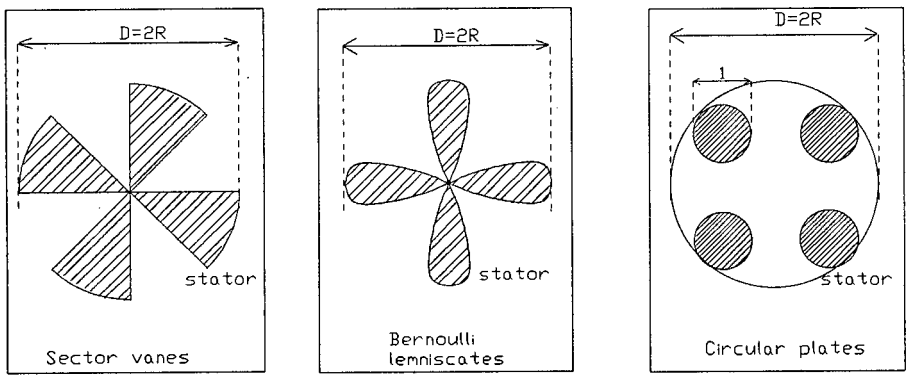

Fig.B-1 Diagram showing stator dimensions used in the program above

Appendix C -- PSpice Source Code

Contents

Theoretical noise calculations (Section 7.1.2.1)

***** Theoretical noise claculations *******

```
.subckt opamp non inv out
 ** Model of CA 3140 opamp **
 Cin    non  inv  4pF
 egain  out  0    (non, inv) 100000
.ends

** Noise generator : 100nV/(sqrt(Hz)) **
Rn1     n1  0  16.56mohm
Vsen1   n1  0  DC  0
Hn1     5   0  Vsen1  100

** Noise generator : 0.01pA/(sqrt(Hz)) **
Rn2     n2  0  16.56Kohm
Vsen2   n2  0  DC  0
Fn2     3   0  Vsen2  0.01

X1      5  3  4  opamp
Cf      4  3  47pF
Rf      4  3  10MEGohm
Igen    3  0  AC 1nA

.AC DEC 10  1Hz  10KHz
.NOISE V(4)  Igen  100
.PRINT NOISE (ONOISE)
.END
```

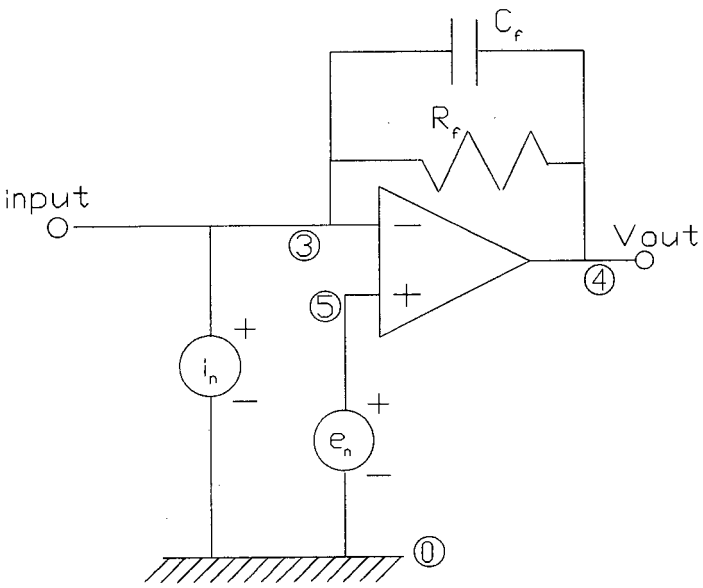

Fig.C1 Circuit diagram for PSpice noise simulation

Bucking voltage for nulling spurious signal (Section 7.2.2)

```
***** Model spurious signal and bucking voltage *******
.subckt opamp non inv out
 Rin    non inv 1Gohm
 egain  out  0   (non, inv) 100000
.ends

***** Variable capacitor simulates rotor-stator capacitance *****
.subckt  yx   1 2 3 4 5
 ecopy  3 6 poly(2) (1,2) (4,5) 0 0 0 0 1
 fout   4 5 vsen 1
 Rin    1 2 1Gohm
 vsen   0 6 0
.ends

X2      b1 3 4 opamp
C1      b1 0 100nF
Rf      4 3  10MEGohm
Vc      2 0  10mV          ***** Contact potential difference *****

***** Bucking voltage = Vb *****
Vb      b1 0  PWL  (0,-10mV,25ms,-10mV,25.1ms,-5mV,50ms,-5mV,50.1ms,0mV,
          + 75ms,0mV,75.1ms,5mV,100ms,5mV,100.1ms,10mV,125ms,10mV,
          + 125.1ms,15mV,150ms,15mV)

X1      a1 0  a3 2 3 yx
Cref    a3 0  100pF
Vsig a1 0  SIN (0 1V 160Hz)        ***** Controls variable capacitor *****
Rsig a1 0  10Kohm

.TRAN 0.2ms 150ms 0ms 0.2ms
.PRINT TRAN V(4)
.END
```

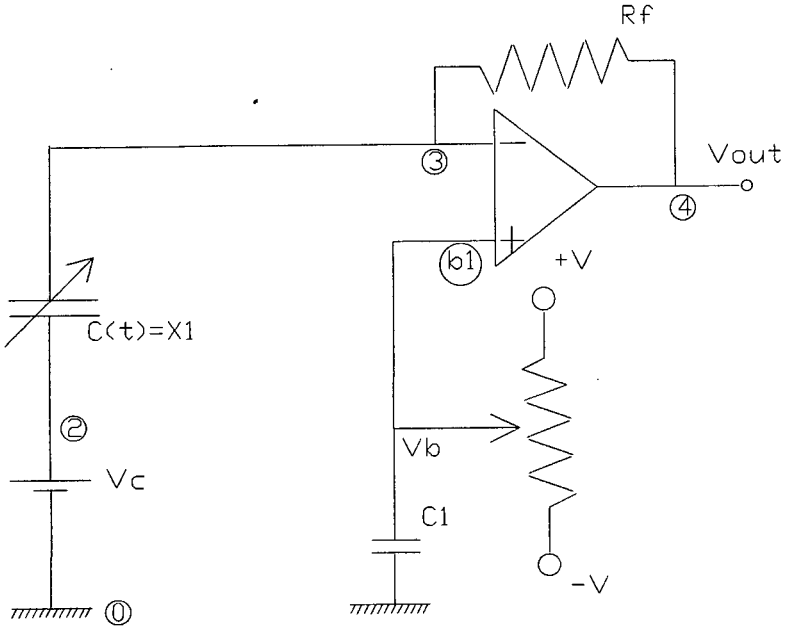

Fig.C2 PSpice circuit for modelling of the spurious signal and bucking voltage

Preamplifier output signal for quadrature detection (Section 7.5.1)

```
***** Theoretical preamplifier output signal   ωRC << 1  *****
***** Quadrature detection                                *****

.subckt  opamp non inv out
 Cin     non  inv  4pF
 Rin     non  inv  1E12ohm
 egain   out  0    (non, inv) 100000
.ends

***** Ion current signal *****
X1  0  2  4  opamp
Ci1 2  4  10pF
Ri1 2  4  10MEGohm
Is1  2  0  PULSE (0nA,+1nA, 0, 2.95ms, 2.95ms, 0.05ms, 6ms)

***** Electric field signal *****
X2  0  2b  4b opamp
Ci2 2b 4b  10pF
Ri2 2b 4b  10MEGohm
Is2  2b 0  PULSE (-1nA,+1nA, 0, 0, 0, 3ms, 6ms)

.TRAN 0.05ms 200ms 180ms 0.05ms
.PRINT TRAN V(4) V(4b)
.END
```

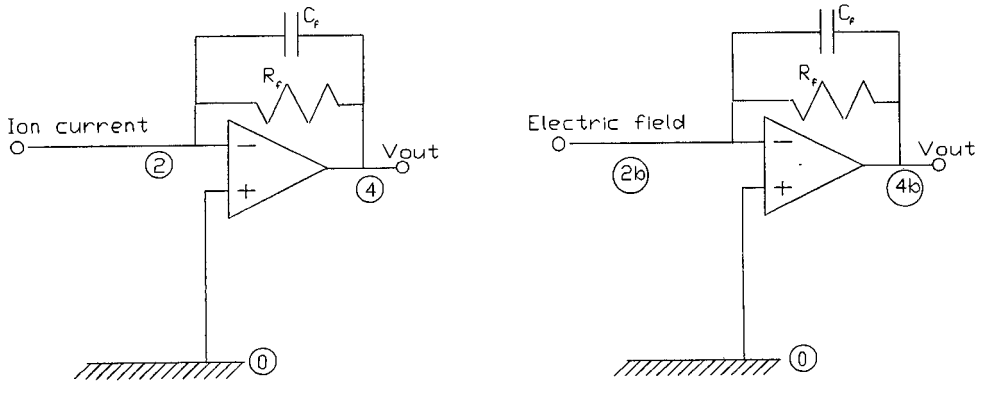

Fig.C3 PSpice circuit for preamplifier output simulation

Preamplifier output signal for final circuit. (Section 7.6)

```
***** Theoretical preamplifier output signal    ωRC >> 1  *****
***** Final field mill circuit                             *****
.subckt  opamp non inv out
 Cin     non  inv  4pF
 Rin     non  inv  1E12ohm
 egain   out  0    (non, inv) 100000
.ends

***** Ion current signal *****
X1  0  2  4  opamp
Ci1 2  4  100pF
Ri1 2  4  50MEGohm
Is1  2  0  PULSE (0nA,+1nA, 0, 2.95ms, 2.95ms, 0.05ms, 6ms)

***** Electric field signal *****
X2  0  2b  4b opamp
Ci2 2b 4b  100pF
Ri2 2b 4b  50MEGohm
Is2  2b 0  PULSE (-1nA,+1nA, 0, 0, 0, 3ms, 6ms)

.TRAN 0.05ms 200ms 180ms 0.05ms
.PRINT TRAN V(4) V(4b)
.END
```

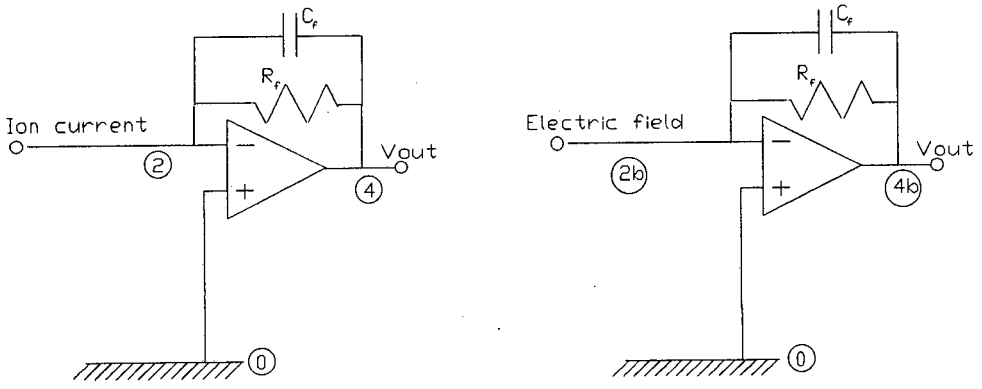

Fig.C4 PSpice circuit for preamplifier output simulation

Appendix D -- Private Communications

Contents Page

Malcolm Sellars
Dept. of Electrical Engineering
University of Cape Town
Rondebosch 7700
Cape Town
South Africa
Email: msellars@eleceng.uct.ac.za

23 January 1995

Dr. Nguyen
IREQ
Varennes, Quebec
CANADA

Dear Dr. Nguyen

REF **"An Exposure Chamber for Studies on Human Perception of DC Electric Fields and Ions"**
IEEE Trans. Power Delivery Vol.9 (4) October 1994

I am studying for my MSc. in electrical engineering at the University of Cape Town, (South Africa), and my thesis project is to build an electric field mill for the simultaneous measurement of electric field and ion current density. I am working on a prototype field mill similar to that described by Dr. Maruvada in references [1], [2].

In your recent paper of October 1994 (above), I note that you do not use a field mill that measures both electric field and ion current density simultaneously, but rather use a field mill for the electric field and a Wilson Plate for the ion current density measurements. Could you tell me why you choose to measure these quantities with separate instruments, rather than with a single field mill that can measure both simultaneously? I would be very interested to find out if there were any practical difficulties encountered with the field mill described by Dr. Maruvada in his earlier papers.

References

[1] "Mesure des champs electriques et des courants ioniques dessous les lignes de transport aux tres hautes tensions continues"
Dallaire, R.D. Maruvada, P.S.
Conference Canadienne sur les Communications et l'Energie, Montreal
October 1978 pg.336-340

[2] "Development of field mill instruments for ground-level and above-ground electric field measurement under HVDC transmission lines"
Dallaire, R.D. Maruvada, P.S. Pedneault, R.
IEEE Trans. Power Apparatus & Systems Vol.102 (3) 1983 pg.738-744

Yours faithfully,
Malcolm Sellars

Return-Path: duc@ireq.hydro.qc.ca
To: msellars@eleceng.uct.ac.za
Subject: Field-mill for simultaneous meas. elec. field and ion current

Unless you have problem with space the use of field-mill and Wilson Plate is more economic in terms of design and maintenance. We develop only one prototype of field-mill for both measurements and the cost is close twice the price of field-mill+Wilson Plate. For single field-mill, data processing is much more complicated, insulation is more delicate and also you have to know the position of the rotor. In summary single field-mill is very challenging in term of design and construction but not economically justified.

Dr Nguyen Duc Hai (IREQ)
duc@ireq.hydro.qc.ca

Malcolm Sellars
Dept. of Electrical Engineering
University of Cape Town
Rondebosch 7700
Cape Town
SOUTH AFRICA

FAX: 27 - 21 - 6503465
Email: msellars@eleceng.uct.ac.za

March 1995

Dr. John Chubb
John Chubb Instrumentation
Unit 30 Lansdown Industrial Estate
Gloucester Rd., Cheltenham, Gloucester

Dear Dr. Chubb

Electric field mill

I am a MSc. student in the Dept. of Electrical Engineering, University of Cape Town. My Msc. project is an electric field mill for the simultaneous measurement of d.c. electric field strength and ion current density in the ground plane. The required sensitivities are:

E-field	10 V/m
Ion current density	10 nA/m^2

I am working on a prototype field mill of the "standard field mill" type discussed in your paper [1]. My field mill has an earthed rotor (sector vanes) spinning in front of a stator (sector vanes) from which the signal is sensed. The relevant specifications are:

Stator diameter	80 mm
Shaft material	silver steel
Rotor and stator	aluminium
Earthing brush	phosphor-bronze
Chopping frequency	150 Hz
Calibrating plates	500mm x 500mm square plates

So far I have been working on the electric field strength measurements only. There are some observations I have made so far that I would be very grateful for your comments on:

1. I am experimenting with different rotor-stator gaps from 1mm to 5mm. I notice that as the gap becomes small, so the spurious signal (possibly due to contact potentials) increases. This is with zero applied field. In your paper [2], you suggest that the rotor and stator should be kept reasonably well separated to reduce this effect. Does this however mean that the sensitivity is reduced? If so, is this simply a factor that must be calibrated out when making measurements?

2. I have noticed that the depth that the stator is recessed behind the ground plane has quite a large effect on the magnitude of the E-field signal. As the stator is moved up closer to the ground plane, so the magnitude of the E-field signal increases. In your paper [3], you suggest that in some designs it may be necessary to reduce the depth of recession to reduce the E-field perturbation. Does the depth of recession introduce a significant loss factor into the measurements? If so, do you just calibrate it out, or can you calculate what the loss should be?

The reason I mention these two points is that my experimental measurements to date are lower than those predicted by the equations by a factor of between 1.5 and 2. Is it possible that the recession depth and rotor-stator gap could be factors causing this discrepancy? (There may well be some systematic error in my measurement circuit).

3. Is there a specific reason why you choose to use a voltage follower configuration (as in (a) below) rather than placing the impedance inside the feedback loop (b)?

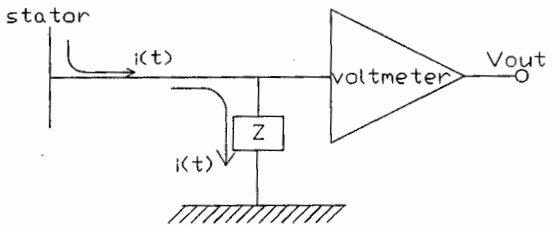

(a) Voltage follower

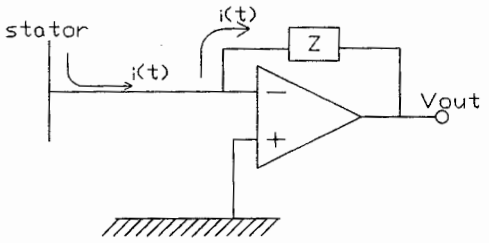

(b) Charge amplifier

4. In your papers [1,2] you advise the use of cantilever spring wires of a selected precious metal alloy resting directly on the motor shaft for earthing the rotor. Could you be more specific about the material for the spring wires. I am using phosphor-bronze at present because a small piece was available. Can you suggest a reasonably inexpensive material? I have noticed that as soon as the earthing brush starts to wear and a track of oxide develops on its surface, the brush starts to vibrate, and the noise on the output signal increases dramatically. At present this condition develops within about 20 minutes of continuous operation, so that I am forced to keep removing the brush and cleaning off the oxide deposit.

I have mounted two reference rotors (sector vanes) lower down on the field mill shaft to provide in-phase and quadrature reference signals. I hope to use synchronous detection to separate the E-field and ion current density signals, which should be in quadrature.

The application is for ground plane measurements in the environment of high voltage d.c. power lines. However, the environment is to be simulated, as the measurements are to made in an exposure cage for rats. This means that considerations such as rain or dirt are not important at this stage. As an MSc. student, I am working on a limited budget, so that gold plating of sensing surfaces is not feasible.

I appreciate the valuable information given in your papers. Thankyou very much for your help.

Yours faithfully
Malcolm Sellars

References

[1] "Two new designs of "Field Mill" type fieldmeters not requiring earthing of rotating chopper"
Chubb J.N.
IEEE Trans. Industry Applications Vol.26 1990 pg.1178 - 1181

[2] "The performance capabilities of electrostatic fieldmeters"
Chubb J.N.
S.E.E Conference, Nice October 1986

[3] "The calibration of electrostatic fieldmeters and the interpretation of their observations"
Chubb J.N.
Institute Phys. Conf. Series No. 85
Electrostatics '87 pg. 261 - 266

John Chubb Instrumentation
Unit 30, Lansdown Industrial Estate
Gloucester Rd.
Cheltenham, Gloucester
GL51 8PL England
Tel. (01242) 573347
Fax. (01242) 251388

28 March 1995

Malcolm Sellars
Dept. of Electrical Engineering, UCT
Rondebosch 7700
Cape Town, South Africa

Dear Mr. Sellars,

Many thanks for your letter and the description and information about the electrostatic fieldmeter you are building. I hope the following comments will be helpful.

1. The sensitivity will not depend too much on the rotor/stator gap until the gap starts to get comparable to the widths of the chopper/sensing sectors. The fieldmeter we built for use in wet and dirty environments had a case diameter of about 100mm and I think the rotor sensing spacing was about 5mm with only 2 sectors. For all our fieldmeters we gold plate all surfaces around the sensing region. This avoids electrochemical voltages due to corrosion - if you think of batteries then if you have say a battery voltage of 0.1V between your rotor and sensing surface and a gap of 5mm you have a local field around $20Vm^{-1}$! It would be wise to keep a constant gap by reducing the end float on the motor bearings. Gold plating is not very expensive - but how about a stainless steel or a nickel plate?

2. The further the sensing surface is back from the sensing aperture the more will the external field be attenuated. To reduce perturbation in the calibration situation and to keep sensitivity as high as easily possible it is good to have the plane of the rotor close to the plane of the sensing aperture. It would be feasible to calculate the attenuation BUT this requires 3D computer modelling and I think it best just to calibrate this out - you need to do that anyway at the end of the day as it is not likely that you can feel confident in the modelling to as good accuracy as you can calibrate. The factor between 1.5 and 2 you mention seems quite sensible reduction factors. Your calibration plates are on the small side - what separation gap are you using? You know the recommendations in my Electrostatics '87 paper.

3. We use the voltage follower configuration to have a suitably high input resistance and (for me) it is a simpler configuration to understand (!). We use between 47-100M for slower chopping speed instruments (150-200Hz) and perhaps 22M for our high speed fieldmeters. We do not use very high gain for the first stage so having very high feedback resistor values would risk poor frequency response with local stray capacitance.

4. We found phosphor bronze very unsatisfactory and with quite high noise levels. We did try rhodium plated phosphor bronze - that was fine for about a day, but was bad as soon as the plating wore through! We use a hard gold alloy wire about $^1/_2$mm diameter with 5-10gram spring pressure. These last up to 3-4 months of continuous operation. (We have used the gold wire used for ear rings and this was OK). We have now moved over most instruments to our 'back-to-back' fieldmeter configuration as described in the IEEE paper. The best performance is no better than you get with good earthing brushes but with appropriate hardware configuration we get good performance (noise around $1Vm^{-1}$ from a 50mm case diameter instrument) with long term stability and easy achievement of fast response where needed. With our JCI 140 we get 3ms response time from a simple battery powered instrument with a low frequency noise around $20Vm^{-1}$.

As regards application: where I use fieldmeters to measure atmospheric electric fields I mount the fieldmeter above earth 1-2m pointing down from a slender pole/frame mounting. This is using the fieldmeter as a potential probe and gives enhanced sensitivity. E = V/d where d is the fieldmeter body diameter and V the local potential before the fieldmeter was introduced (see my Electrostatics '87 paper). This reduces the need to make the instrument able to work in direct rain and avoids possible ground blown dust. It also avoids the need for a large ground plane.

I will be interested to hear further of your progress - and good luck!
With best wishes,
Yours sincerely,
John N. Chubb

Appendix E -- Photographs of the Electric Field Mill

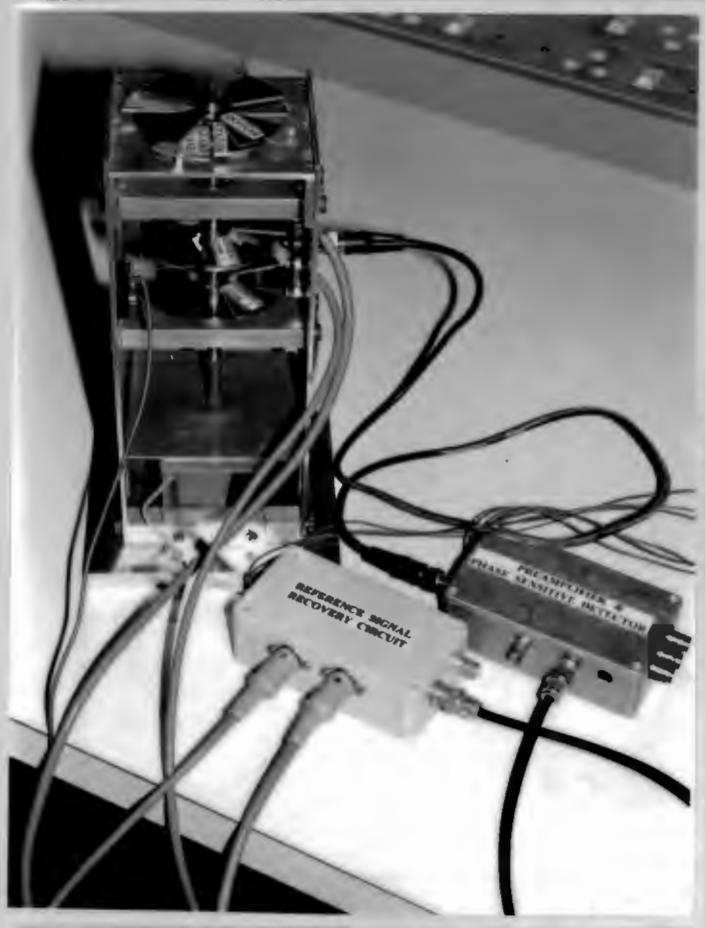

Fig.E1 Electric field mill system
This photograph shows the field mill and the electronic circuit modules. Note the metal box used for the preamplifier and phase sensitive detector circuitry. All signal cables are shielded. See Fig.6.1 on pg.46.

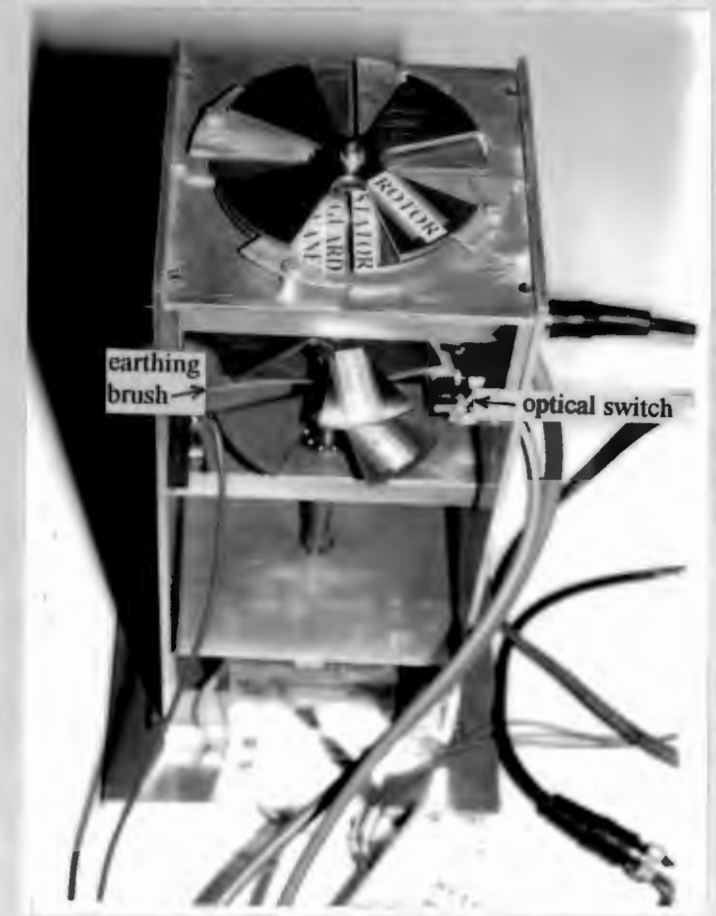

Fig.E2 Electric field mill
The rotor, stator and grounded guard vanes of the field mill are shown. The gold wire earthing brush is also visible. The two reference rotors and the slotted optical switches through which they pass are also shown.
See Fig.6.1 on pg.46.

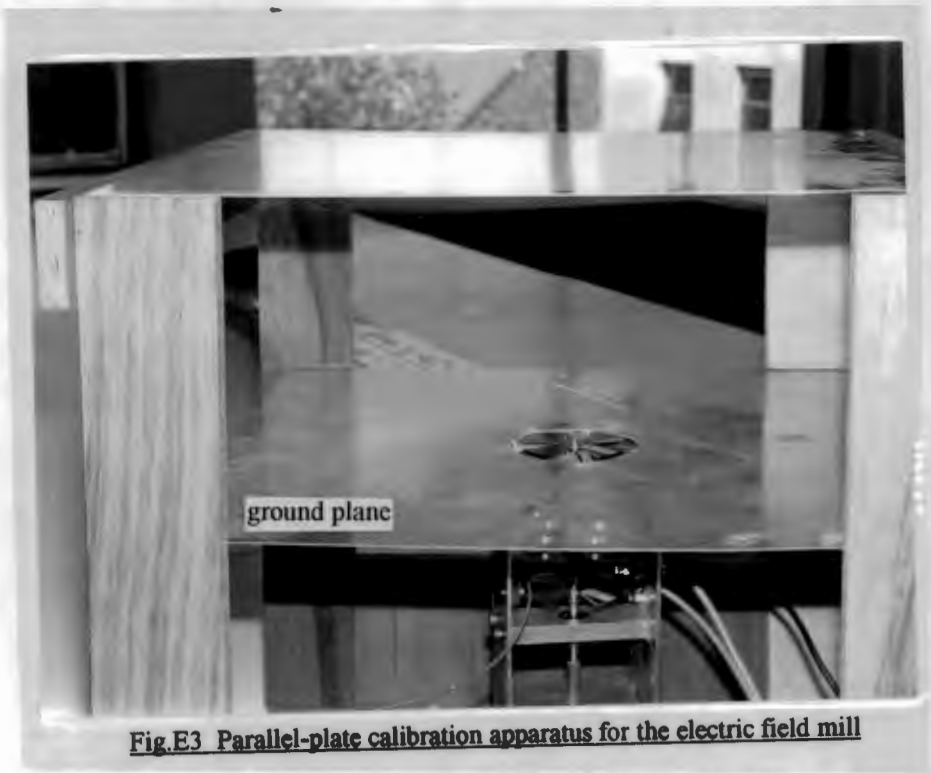

Fig.E3 Parallel-plate calibration apparatus for the electric field mill

In the photograph above, the rotor and stator of the field mill are located in the aperture of the ground plane. (The ground plane is the lower metal plate, and is at ground potential). The upper plate is the high voltage electrode, and will have a known voltage applied to it, in order to generate a uniform electric field in-between the parallel plates. See Fig.8.2 on pg.109.